Spine: 5.5 mm

ISSN : 0003-2778

Scopus
Indexed

JOURNAL OF THE ANATOMICAL SOCIETY OF INDIA

An International Journal

An Official Publication of Anatomical Society of India

Full text online at **https://journals.lww.com/joai**
Submit articles online at **https://review.jow.medknow.com/jasi**

Editor-in-Chief
Dr. Vishram Singh

Wolters Kluwer

Medknow

Journal of The Anatomical Society of India • Volume 74 • Issue 2 • April-June 2025 • Pages 89-196

Volume 74 • Issue 2 • April-June 2025

Journal of the Anatomical Society of India

Print ISSN: 0003-2778

GENERAL INFORMATION

About the Journal

Journal of the Anatomical Society of India (ISSN: Print 0003-2778) is peer-reviewed journal. The journal is owned and run by Anatomical Society of India. The journal publishes research articles related to all aspects of Anatomy and allied medical/surgical sciences. Pre-Publication Peer Review and Post-Publication Peer Review Online Manuscript Submission System Selection of articles on the basis of MRS system Eminent academicians across the globe as the Editorial board members Electronic Table of Contents alerts Available in both online and print form. The journal is published quarterly in the months of January, April, July and October.

Scope of the Journal

The aim of the *Journal of the Anatomical Society of India* is to enhance and upgrade the research work in the field of anatomy and allied clinical subjects. It provides an integrative forum for anatomists across the globe to exchange their knowledge and views. It also helps to promote communication among fellow academicians and researchers worldwide. The Journal is devoted to publish recent original research work and recent advances in the field of Anatomical Sciences and allied clinical subjects. It provides an opportunity to academicians to disseminate their knowledge that is directly relevant to all domains of health sciences.

The Editorial Board comprises of academicians across the globe.

JASI is indexed in Scopus, available in Science Direct.

Abstracting and Indexing Information

The journal is registered with the following abstracting partners:

Baidu Scholar, CNKI (China National Knowledge Infrastructure), EBSCO Publishing's Electronic Databases, Ex Libris – Primo Central, Google Scholar, Hinari, Infotrieve, Netherlands ISSN center, ProQuest, TdNet, Wanfang Data

The journal is indexed with, or included in, the following:

SCOPUS, Science Citation Index Expanded, IndMed, MedInd, Scimago Journal Ranking, Emerging Sources Citation Index.

Impact Factor® as reported in the 2024 Journal Citation Reports® (Clarivate Analytics, 2025): 0.2

Information for Authors

Article processing and publication charges will be communicated by the editorial office. All manuscripts must be submitted online at https://review.jow.medknow.com/jasi.

Subscription Information

A subscription to JASI comprises 4 issues. Prices include postage. Annual Subscription Rate for non-members-

Annual Subscription Rate for non-members

	India	Outside India
Institutional	INR 15000	USD 1200
Individual	INR 7,500	USD 800

The Journal of Anatomical Society of India (ISSN: 0003-2778) is published quarterly **Subscriptions** are accepted on a prepaid basis only and are entered on a calendar year basis. Issues are sent by standard mail Priority rates are available upon request.

Information to Members/Subscribers

All members and existing subscribers of the Anatomical Society of India are requested to send their membership/existing subscription fee for the current year to the Treasurer of the Society on the following address: Prof (Dr.) Punit Manik, Treasurer, ASI, Department of Anatomy, KGMU, Lucknow - 226003. Email: punitamanik@yahoo.co.in. All payments should be made through an account payee bank draft drawn in favor of the **Treasurer, Anatomical Society of India,** payable at **Lucknow** only, preferably for **Allahabad Bank, Medical College Branch, Lucknow.** Outstation cheques/drafts must include INR 70 extra as bank collection charges.

All complaints regarding non-receipt of journal issues should be addressed to the Editor-in-Chief, JASI at editorjasi@gmail.com. The new subscribers may, please contact wkhlrpmedknow_subscriptions@wolterskluwer.com.

Requests of any general information like travel concession forms, venue of next annual conference, etc. should be addressed to the General Secretary of the Anatomical Society of India.

For mode of payment and other details, please visit www.medknow.com/subscribe.asp

Claims for missing issues will be serviced at no charge if received within 60 days of the cover date for domestic subscribers, and 3 months for subscribers outside India. Duplicate copies cannot be sent to replace issues not delivered because of failure to notify publisher of change of address. The journal is published and distributed by Wolters Kluwer India Pvt. Ltd. Copies are sent to subscribers directly from the publisher's address. It is illegal to acquire copies from any other source. If a copy is received for personal use as a member of the association/society, one cannot resale or give-away the copy for commercial or library use.

The copies of the journal to the subscribers are sent by ordinary post. The editorial board, association or publisher will not be responsible for non receipt of copies. If any subscriber wishes to receive the copies by registered post or courier, kindly contact the publisher's office. If a copy returns due to incomplete, incorrect or changed address of a subscriber on two consecutive occasions, the names of such subscribers will be deleted from the mailing list of the journal. Providing complete, correct and up-to-date address is the responsibility of the subscriber.

Nonmembers: Please send change of address information to subscriptions@medknow.com.

Advertising Policies

The journal accepts display and classified advertising. Frequency discounts and special positions are available. Inquiries about advertising should be sent to Wolters Kluwer India Pvt. Ltd, advertise@medknow. com.

The journal reserves the right to reject any advertisement considered unsuitable according to the set policies of the journal.

The appearance of advertising or product information in the various sections in the journal does not constitute an endorsement or approval by the journal and/or its publisher of the quality or value of the said product or of claims made for it by its manufacturer.

Disclaimer

The information and opinions presented in the Journal reflect the views of the authors and not of the Journal or its Editorial Board or the Publisher. Publication does not constitute endorsement by the journal. Neither the JASI nor its publishers nor anyone else involved in creating, producing or delivering the JASI or the materials contained therein, assumes any liability or responsibility for the accuracy, completeness, or usefulness of any information provided in the JASI, nor shall they be liable for any direct, indirect, incidental, special, consequential or punitive damages arising out of the use of the JASI. The JASI, nor its publishers, nor any other party involved in the preparation of material contained in the JASI represents or warrants that the information contained herein is in every respect accurate or complete, and they are not responsible for any errors or omissions or for the results obtained from the use of such material. Readers are encouraged to confirm the information contained herein with other sources.

Addresses

Editorial Office

Dr. Vishram Singh, Editor-in-Chief, JASI
B5/3 Hahnemann Enclave, Plot No. 40, Sector 6, Dwarka Phase – 2,
New Delhi - 110 075, India.
Email: editorjasi@gmail.com

Published by

Wolters Kluwer India Pvt. Ltd.,
Fourth Floor, East Wing, Marisoft III, Marisoft Premises,
Part of Software Technology Park, S. No. 15, Vadgaon Sheri,
Kalyani Nagar, Pune – 411 014, Maharashtra, India.
Website: www.medknow.com

Printed at

Nikeda Art Printers Pvt. Ltd.,
Building No. C/3 - 14,15,16, Shree Balaji Complex, Vehele Road,
Village Bhatale, Taluka Bhiwandi, District Thane - 421302, India.

Journal of the Anatomical Society of India

Print ISSN: 0003-2778

EDITORIAL BOARD

Journal of the Anatomical Society of India

Volume 74 | Issue 2 | April-June 2025

CONTENTS

The Anatomical Basis of Cerebral Stroke: Leveraging Artificial Intelligence for Enhanced Detection and Diagnosis

Introduction

A stroke, also known as a cerebral stroke, is a medical condition in which blood supply to the brain is interrupted or blocked, leading to its cell death. This can lead to long-term disabilities and even death.

Cerebral stroke remains a leading cause of mortality and long-term disability worldwide, affecting approximately 15 million people annually and representing a critical public health challenge.[1] Immediate intervention is critical, as delays in treatment exacerbate neuronal loss and worsen clinical outcomes.[2] Advances in artificial intelligence (AI) have revolutionized stroke care by enabling rapid, precise anatomical analysis of cerebrovascular pathology, from vascular occlusion patterns to penumbral viability.[3,4] This integration of neuroanatomical expertise and computational power promises to transform diagnostic paradigms, offering personalized treatment strategies grounded in real-time imaging analytics.

Anatomical Basis of Cerebral Stroke

Vascular architecture and vulnerability

The cerebral vasculature's complex anatomy determines both stroke susceptibility and clinical presentation. The brain receives blood supply through two main systems: the anterior circulation (carotid arteries) supplying approximately 80% of cerebral tissue and the posterior circulation (vertebrobasilar system) serving the brainstem, cerebellum, and posterior cerebral regions.[3] This anatomical arrangement creates distinct vulnerability patterns, with middle cerebral artery (MCA) territory strokes being the most common due to the vessel's direct continuation from the internal carotid artery and its extensive cortical distribution.

Types of Stroke and Their Anatomical Impact

The cerebral strokes are broadly classified into two types.

Ischemic stroke (85% of cases)

The various causes of ischemic stroke are:

- Thrombotic stroke: Caused by blood clot (thrombus) and occurs in large vessels (carotid, MCA). It creates well-demarcated infarct zones in the areas supplied by these vessels affecting cortical and subcortical structures
- Embolic stroke: Occurs when a blood clot formed elsewhere in the body travels through the bloodstream to lodge elsewhere in a blood vessel of brain. Typically affects cortical areas first, creating wedge-shaped infarcts pointing toward the ventricles. Multiple small infarcts may occur simultaneously
- Lacunar stroke: A type of ischemic stroke which affects small penetrating arteries (100–400 micrometers), creating small, deep infarcts in basal ganglia, thalamus, brainstem. This type of stroke is anatomically distinct from cortical strokes. It occurs due to hyperfusion as in shock and cerebral venous thrombosis.

Hemorrhagic stroke (15% of cases)

The various causes of hemorrhagic stroke are:

- Intracerebral hemorrhage: Occurs due to rupture of blood vessel inside the brain, following head trauma, high blood pressure, etc. It is most common in basal ganglia, thalamus, brainstem, and cerebellum, creating a mass effect with displacement of surrounding structures
- Subarachnoid hemorrhage: Occurs due to bleeding in subarachnoid space, due to rupture of aneurysms. Here, blood accumulates in cerebrospinal fluid spaces around the brain surface, causing vasospasm affecting multiple vascular territories and may lead to secondary ischemic changes.

The circle of Willis provides crucial collateral circulation during vascular compromise. However, anatomical variants occur in up to 50% of individuals, significantly affecting stroke risk and severity.[4] Understanding these variations is essential for predicting clinical outcomes and planning therapeutic interventions.

Cellular and tissue-level changes

Stroke involves complex cellular changes triggered by cerebral hypoperfusion. The ischemic core, where blood flow drops below 10–12 mL/100 g/min, undergoes irreversible neuronal death within minutes through energy failure and excitotoxicity. Surrounding this core lies the ischemic penumbra, a region of reduced perfusion (12–20 mL/100g/min) where neurons remain viable but functionally impaired.[5] This penumbral tissue represents the therapeutic target for acute interventions, as its salvage can significantly improve clinical outcomes.

The anatomical distribution of gray and white matter creates differential vulnerability patterns. Gray matter, with its high metabolic demands and dense neuronal populations, shows earlier ischemic changes. White matter, consisting primarily of myelinated axons, demonstrates a greater resistance to hypoxia but suffers delayed deterioration through Wallerian degeneration when disconnected from neuronal cell bodies.

Regional anatomical correlations

Different brain regions exhibit varying susceptibility to ischemic injury based on their vascular supply and

metabolic demands. The hippocampus, with its high energy requirements and end-arterial blood supply, shows vulnerability, explaining the memory deficits often observed in posterior circulation strokes. Similarly, the watershed zones between major arterial territories become critically important during systemic hypotension, creating characteristic bilateral cortical or subcortical infarction patterns.

The basal ganglia and thalamus, supplied by small perforating arteries, are common sites for lacunar strokes. These regions' compact fiber arrangement means that small lesions can produce disproportionately severe clinical deficits, particularly affecting motor and sensory pathways coursing through the internal capsule.

Artificial Intelligence (AI) in Stroke Detection: Anatomical Foundations

Imaging-based pattern recognition

AI's application in stroke detection leverages the technology's superior pattern recognition capabilities to identify subtle anatomical changes that may escape human observation. Modern AI algorithms analyze multiple imaging parameters simultaneously, including tissue density variations, perfusion patterns, and structural deformations that reflect underlying anatomical pathology.[6]

In computed tomography (CT) imaging, AI systems detect early ischemic changes by recognizing loss of gray–white matter differentiation, subtle hypodensity, and the Alberta Stroke Program Early CT Score regions. These anatomical markers, often imperceptible in the crucial 1st hours after symptom onset, become identifiable through AI's ability to process subtle Hounsfield unit variations across 1000 of pixels simultaneously.

Magnetic resonance (MR) imaging provides a richer anatomical information for AI analysis. Diffusion-weighted imaging reveals cellular-level changes through restricted water movement in ischemic tissue, while perfusion studies demonstrate hemodynamic alterations in anatomically defined vascular territories. AI algorithms ability to integrate these multimodal datasets to create comprehensive anatomical maps of stroke pathology.[7]

Vascular territory analysis

One of the AI's most significant contributions lies in automated vascular territory analysis. Traditional stroke assessment relies on clinicians' ability to correlate clinical findings with anatomical knowledge of cerebral vascular territories. AI systems can instantaneously map infarct locations to specific arterial distributions, predict clinical deficits based on anatomical involvement, and estimate tissue at risk in real time.[8]

This anatomical precision enables more targeted therapeutic decisions. For instance, AI can differentiate between strokes affecting eloquent cortical areas versus those limited to subcortical white matter, informing decisions about aggressive interventional approaches versus conservative management.

Collateral circulation assessment

AI's ability to analyze complex vascular anatomy extends to collateral circulation assessment, a critical factor in stroke outcomes. By analyzing CT angiography or MR perfusion data, AI algorithms can quantify collateral flow patterns, predict penumbral viability, and estimate the time window for successful intervention.[9] This anatomically based assessment moves beyond simple time-based treatment protocols toward personalized medicine approaches.

Clinical Implications and Future Directions

Enhanced diagnostic accuracy

AI's integration into stroke care has demonstrated remarkable improvements in diagnostic accuracy. Studies show that AI systems can detect large vessel occlusions with sensitivity and specificity exceeding 90%, often identifying strokes missed by initial clinical assessment.[10] This enhanced detection capability, grounded in sophisticated anatomical analysis, translates directly into improved patient outcomes through earlier intervention.

The technology's ability to process imaging data within minutes of acquisition enables real-time decision support, particularly valuable in emergency settings where rapid triage is essential. AI systems can automatically alert stroke teams, predict clinical severity based on anatomical involvement, and recommend appropriate treatment pathways.

Personalized treatment approaches

Understanding individual anatomical variations through AI analysis enables increasingly personalized treatment strategies. Rather than applying uniform protocols, clinicians can tailor interventions based on specific anatomical findings, collateral circulation patterns, and predicted tissue outcomes. This precision medicine approach represents a fundamental shift from time-based treatment windows toward biology-based decision-making.

Challenges and limitations

Despite significant advances, AI implementation in stroke care faces several challenges. Algorithm training requires vast, diverse datasets representing various anatomical variants and pathological presentations. Ensuring AI systems perform reliably across different populations, imaging protocols, and clinical settings remains an ongoing challenge requiring continuous validation and refinement. However, overreliance on AI risks the diagnostic complacency, a challenge addressed through hybrid human-AI workflows that prioritize clinician oversight in complex cases.[2]

Conclusion

The intersection of anatomical understanding and AI represents a transformative approach to cerebral stroke detection and management. By leveraging detailed knowledge of cerebrovascular anatomy, AI systems can identify subtle pathological changes, predict clinical outcomes, and guide therapeutic decisions with unprecedented precision. As these technologies continue to evolve, they promise to enhance the speed and accuracy of stroke diagnosis, ultimately improving outcomes for millions of patients worldwide. The future of stroke care lies in this synergistic combination of anatomical expertise and computational power, offering hope for more effective treatments and better patient outcomes.

Vishram Singh, Krishna Chaitanya Reddy[1], Rashi Singh[2], Gaurav Singh[3]

Department of Anatomy, Kasturba Medical College, Mangalore, Manipal Academy of Higher Education, Manipal, Karnakataka, [2]Department of Pediatric and Preventive Dentistry, Santosh Dental College and Hospital, Ghaziabad, [3]Clinical Editor, British Medical Journal (BMJ), Noida, NCR Delhi, Uttar Pradesh, India, [1]Department of Anatomy, Faculty of Medicine, MAHSA University, Selangor, Malaysia

Address for correspondence: *Prof. Vishram Singh, B5/3 Hahnemann Enclave, Plot No. 40, Sector 6, Dwarka Phase – 2, New Delhi - 110 075, India.*
E-mail: drvishramsingh@gmail.com

References

1. Feigin VL, Stark BA, Johnson CO. Global, regional, and national burden of stroke and its risk factors, 1990-2019: A systematic analysis for the Global Burden of Disease Study 2019. Lancet Neurol 2021;20:795-820.
2. Tailor KG, Rishi P, Harioudh SK, Medhi B, Motagi MV. Anatomical variations of the circle of Willis – A systematic review. Int J Pharm Clin Res 2024;16:506-14.
3. Desai SM, Rocha M, Jovin TG, Jadhav AP. Time is brain – Requantified. Stroke 2019;50:34-7.
4. Zarrinkoob L, Ambarki K, Wåhlin A, Birgander R, Eklund A, Malm J. Blood flow distribution in cerebral arteries. J Cereb Blood Flow Metab 2015;35:648-54.
5. Astrup J, Siesjö BK, Symon L. Thresholds in cerebral ischemia – The ischemic penumbra. Stroke 1981;12:723-5.
6. Soun JE, Chow DS, Nagamine M, Takhtawala RS, Filippi CG, Yu W, *et al.* Artificial intelligence and acute stroke imaging. Am J Neuroradiol 2021;42:2-11.
7. Ginat DT. Analysis of head CT scans flagged by deep learning software for acute intracranial hemorrhage. Neuroradiology 2020;62:335-40.
8. Gautam A, Rosen C. The neuroanatomy of stroke: A systematic review and meta-analysis of associations between stroke anatomy and cognitive function. Neuropsychol Rev 2022;32:699-712.
9. Menon BK, Campbell BC, Levi C, Goyal M. Role of imaging in current acute ischemic stroke workflow for endovascular therapy. Stroke 2015;46:1453-61.
10. Barreira CM, Bouslama M, Lim J. Aladin study: Automated large artery occlusion detection in stroke imaging study – A diagnostic accuracy study. Stroke 2022;53:3636-44.

Article Info

Received: 11 June 2025
Accepted: 15 June 2025
Available online: 30 June 2025

Access this article online	
Quick Response Code:	**Website:** https://journals.lww.com/joai
	DOI: 10.4103/jasi.jasi_102_25

How to cite this article: Singh V, Reddy KC, Singh R, Singh G. The anatomical basis of cerebral stroke: Leveraging artificial intelligence for enhanced detection and diagnosis. J Anat Soc India 2025;74:89-91.

Original Article

Biochemical and Histological Analyses of Taurine's Therapeutic Triad: Antidiabetic, Antioxidant, and Anti-inflammatory Effects in Alloxan-induced Diabetic Rats

Engy F. Risha[1], Fatma M. Abdelhamid[1], Walaa F. Awadin[2], Dalia Mahmoud Abdelmonem Elsherbini[3,4], Rasha Hamed Al-Serwi[5], Donia Elsaid Fathi Zaghamir[6,7], Ehab Kamal Ali[8], Dania S Waggas[9], Mohamed El-Sherbiny[10], Mamdouh Eldesoqui[4,10]

[1]Clinical Pathology Department, [2]Pathology Department, Faculty of Veterinary Medicine, Mansoura University, Mansoura, [4]Department of Anatomy, Faculty of Medicine, Mansoura University, Mansoura, [7]Department of Pediatric Nursing, Faculty of Nursing, Port Said University, Port Said, [8]Department of Anatomy and Embryology, Faculty of Medicine, Al- Azhar University, New Damietta, Egypt, [3]Department of Clinical Laboratory Sciences, College of Applied Medical Sciences, Jouf University, Sakaka, [5]Department of Basic Dental Sciences, College of Dentistry, Princess Nourah bint Abdulrahman University, Riyadh, [6]College of Nursing, Prince Sattam bin Abdulaziz University, Al-Kharj, [9]Pathological Sciences Department, Fakeeh College for Medical Sciences, Jeddah, [10]Department of Basic Medical Sciences, College of Medicine, AlMaarefa University, Diriyah, Saudi Arabia

Abstract

Background: Diabetes mellitus poses a significant health challenge worldwide. Oxidative stress, altered lipid profile, and inflammation are linked to diabetic complications. **Objective:** This work aimed to assess the effects of taurine (TAU) in alloxan (ALX)-induced diabetes in rats, evaluating its antihyperglycemic, antidyslipidemic, antioxidant, and anti-inflammatory effects. In addition, evaluating the effect of TAU on hepatic, renal, and cardiac complications. **Materials and Methods:** Fifty rats were divided into four groups, control, TAU, ALX, and ALX + TAU. At the end of the experiment, blood and tissue were collected and subjected to serum glucose, insulin, lipid profile, liver enzyme, creatinine, urea detection, oxidative-antioxidant parameters evaluation, inflammatory, anti-inflammatory cytokines detection, and histological evaluation. **Results:** Experimental results demonstrated that TAU effectively mitigated hyperglycemia, dyslipidemia, oxidative stress, and inflammatory conditions induced by ALX. TAU treatment improved serum glucose and insulin levels, restored lipid profiles, enhanced antioxidant enzyme activities, and reduced lipid peroxidation. In addition, TAU ameliorated hepatic and renal function alterations preserved histological architecture in the pancreas, liver, kidney, and heart tissues, and modulated inflammatory responses by diminishing the inflammatory mediators interleukin-6 (IL-6) and tumor necrosis factor-α while augmenting the anti-inflammatory mediator IL-10. **Conclusions:** TAU exerts a therapeutic effect on ALX-induced hepatic, renal, and cardiac diabetic complications by lowering blood glucose levels, augmenting insulin secretion, ameliorating dyslipidemia, preserving the oxidative-redox balance, and boosting antioxidant activity. TAU has also an anti-inflammatory impact.

Keywords: *Alloxan, hepatoprotective, oxidative stress, renal functions, taurine*

Introduction

Noncommunicable diseases, including diabetes, are becoming a greater threat to all countries, irrespective of their current stage of development.[1] Diabetes is defined by abnormal elevation of blood sugar levels during fasting or after meals, resulting from insufficient insulin production or impaired insulin function, leading to disruptions in the metabolism of proteins and fats.[2]

Alloxan (ALX) is a water-soluble, unstable chemical molecule with a structure like that of glucose, which potentially damages the pancreatic β-cells, causing hyperglycemia due to the generation of reactive oxygen species (ROS).[3-5] Beta cells (β-cells) have limited ability to counteract oxidative stress, increasing their vulnerability. In diabetes, ROS are linked to inflammation conditions during the early stages of the disease.[6]

The development of diabetic complications is related to the oxidative stress, which is one of the key factors in the emergence of complications, affecting both the microvascular circulation and the cardiovascular system.[7] The inequality between the formation and elimination of ROS results in oxidative stress. Numerous pathophysiological processes, which

Article Info

Received: 11 January 2025
Revised: 28 January 2025
Accepted: 24 May 2025
Available online: 30 June 2025

Address for correspondence: *Dr. Dalia Mahmoud Abdelmonem Elsherbini,*
Department of Clinical Laboratory Sciences, College of Applied Medical Sciences, Jouf University, Sakaka, Saudi Arabia.
Department of Anatomy, Faculty of Medicine, Mansoura University, Mansoura, Egypt.
E-mail: dmelsherbini@ju.edu.sa

How to cite this article: Risha EF, Abdelhamid FM, Awadin WF, Elsherbini DM, Al-Serwi RH, Zaghamir DE, *et al.* Biochemical and histological analyses of taurine's therapeutic triad: Antidiabetic, antioxidant, and anti-inflammatory effects in alloxan-induced diabetic rats. J Anat Soc India 2025;74:92-103.

Access this article online

Website: https://journals.lww.com/joai
DOI: 10.4103/jasi.jasi_9_25
Quick Response Code:

eventually result in cell death, can be activated when tissues are subjected to oxidative stress.[8,9]

The disturbance of the antioxidant defense mechanism is not only notable in diabetic complications; previous research has also indicated a link between diabetes and significant changes in serum lipid and lipoprotein profiles, along with an increased risk of cardiac diseases.[10] Correcting oxidative stress and restoring the balance between ROS-derived oxidant state and antioxidants to reduce complications in diabetic patients, therapeutic assistance is needed to achieve antioxidant effects, improve dyslipidemia, and provide anti-inflammatory benefits to successfully reduce diabetic complications.

Previous research has demonstrated significant changes in the serum levels of numerous amino acids and their metabolites in diabetic patients.[11-14] Taurine (TAU) (2-aminoethane-sulfonic acid) is a sulfur-containing amino acid that is not involved in protein formation; hence, it is the most prevalent free amino acid in mammalian tissues, except for the human liver.[15] TAU is a conditionally essential amino acid found in the body in its free form. TAU in mammals is formed in the pancreas via the cysteine sulfonic acid pathway. Its therapeutic effects are primarily exerted through its antioxidative and anti-inflammatory properties.[16]

Due to its endogenous synthesis, TAU is well tolerated in clinical use as it is not linked to signs of toxicity or drug dependence. Recent animal and human studies on animal and human have drawn the attention of scientists, highlighting its potential utility in clinical nutrition and as a potential pharmaconutrient.[17,18] TAU has a significant part in body detoxification by enhancing the cholesterol catabolism and lowering the absorption of dietetic cholesterol.[19] TAU significantly contributes to glucose homeostasis; nevertheless, the precise molecular processes underlying this function remain unidentified. TAU influences glucose homeostasis through two established mechanisms: (i) Through its impact on β-cell insulin secretion. (ii) By disrupting the insulin signaling pathway and subsequent postreceptor processes.[20] TAU supplementation protects the pancreatic β cell and preserves normal secretory granule function.[21] In 2015, research shown that TAU supplementation in mice might enhance brain insulin receptors, a potential protective benefit against illnesses.[22] TAU has the potential to enhance overall health by slowing down cellular aging, reducing mitochondrial dysfunction, and ameliorate DNA damage.[23,24]

TAU deficiency is linked to diabetic complications. Little researches studied the relationship between plasma TAU levels with diabetic retinopathy (DR), neuropathy (DN), and nephropathy,[20] but the mechanisms implicated in the role of TAU in mitigating these complications not sufficiently elaborated. This work aimed to assess the effects of TAU administration in ALX-induced diabetes in rats, evaluating its antihyperglycemic, anti-dyslipidemic, antioxidant, and anti-inflammatory effects. In addition, evaluating the effect of TAU on hepatic, renal, and cardiac complications.

Materials and Methods

Chemicals

ALX (2,4,5,6-tetraoxypyrimidine; 2,4,5,6-pyrimidinetetrone) was obtained from Sigma-Aldrich Co, UK. TAU was purchased from Sigma Chemical, Co. Ltd. (St. Louis, MO, USA).

Sample size calculation

The (G*Power, Düsseldorf, Germany) program for Windows (version 3.1.9.7) was used to compute the sample size according to the procedures specified.[25] Following the previous study of Aziz *et al*.,[26] the means for four groups (control, TAU, ALX, ALX + TAU) would be (48.60, 49.24, 70.73, and 53.20) for alanine aminotransferases (ALT), (163.17, 177.67, 288.50, and 212.02) for aspartate aminotransferases (AST), (38.37, 38.73, 60.47, and 50.84) for urea, and (0.80, 0.90, 1.35 and 1.00) for creatinine. Considering the S_{pooled} (common standard deviation [SD]), 3.96 for ALT, 2.92 for AST, 2.00 for urea, and 0.07 for creatinine, the effect size (f) would be 2.27 for ALT, 16.60 for AST, 4.64 for urea, and 2.96 for creatinine. According to these assumptions, sample sizes for ALT, AST, urea, and creatinine of 12, 8, 8, and 8, respectively, achieve 95% power at an alpha level of 5%, considering the smallest effect size (2.27) with sample sizes of 3 per group in a one-way analysis of variance (ANOVA) design with four groups. Using the *F*-test with a significance level of 0.05, the total sample of 12 achieves a power of 95%. In accordance with Foda *et al*.,[27] we assumed ten rats per group except the diabetic group (ALX) 20 rats.

Experimental animal

Fifty adult male rats (weighing 200–250 g) were acquired from the laboratory animals. For acclimatization, the rats were fed on the standard laboratory conditions for 2 weeks with a 10/14 h light/dark cycle with unlimited access to food and water.

Induction of diabetes

The rats were made diabetic after an overnight fast by administering subcutaneous injections of ALX monohydrate (120 mg/kg) in acetate buffer (pH 4.5).[28] The damage of β-cells by ALX results in increased insulin release. To address acute hypoglycemia, the rats were provided with a 10% sucrose solution for 48 h. After diabetes induction by 5 days, blood samples were taken from the tips of the tails and used to assess the levels of glucose using a glucometer. Rats are considered diabetic

when blood glucose levels ≥300 mg/dl (16.7 mmol/l).[29,30] The rats were housed in an environment with a 12/12 dark-light cycle at a temperature of 21ºC ± 3°C. Throughout the experiment, all animals had unrestricted access to food and water.

Experimental design

The rats were randomly divided into four groups:

- Group 1: Control group - Ten rats received neither ALX nor TAU, only 1 ml intraperitoneal (IP) saline as a vehicle. No mortality occurred
- Group 2: TAU group - Ten rats received TAU only (100 mg/kg/day) dissolved in saline via IP injection.[31,32] No mortality occurred
- Group 3: ALX group - Twenty rats were administered a single IP injection of ALX at 120 mg/kg body weight in citrate buffer (pH 4.5).[4,33] Six rats died during the study
- Group 4, the ALX + TAU post-treatment group, 10 rats received TAU (100 mg/kg/day) dissolved in saline through IP injection (as in Group 2) starting from the 4th day after ALX injection (as in group 3) for 21 days. Three rats died during the experimental period.

Sample collection

Rats in each group were blood-sampled every 3 days from the lateral vein of the tail, with 100 μL of blood collected for plasma glucose measurement.

At the end of the experiment, the rats were euthanized under light ether anesthesia, then blood was collected by puncturing the left ventricle, and then the blood samples were gathered in regular centrifuge tubes and left in an inclined position for 20 min at room temperature. They were then refrigerated to inhibit glycolysis. Following this, the samples were centrifuged at 3000 rpm for 10 min, meticulously separated, collected, and preserved in Eppendorf tubes at −20°C for subsequent biochemical analysis. Pancreases were excised immediately, and part of each pancreas was homogenized and stored at −80°C for the analysis of oxidative and antioxidant parameters. The other part of the pancreas, liver, heart, and kidney specimens were fixed in 10% buffered formalin for histological assessments.

Evaluation of biochemical parameters

The serum levels of ALT and AST (Randox, UK), total protein (Stanbio Laboratory, USA), and albumin (Stanbio Laboratory, USA) were measured using a spectrophotometric method as per standard protocols provided.[34] The albumin-globulin ratio (AGR) was calculated using the formula AGR = albumin/(total protein-albumin) using the Omni calculator online site for calculation https://www.omnicalculator.com/health/albumin-globulin-ratio. Furthermore, urea, creatinine, triglycerides (TG), high-density lipoprotein (HDL), and total cholesterol (CHO) levels were determined using standard kits obtained. Blood glucose levels were assessed using the glucose oxidase-phenol amino phenazone method through an enzymatic colorimetric approach.[35] Enzyme-linked immunosorbent assay (ELISA) was utilized for the quantitative measurement of insulin using commercially available kits.[36]

Evaluation of oxidative stress and antioxidant status

To prepare the pancreatic tissue for analysis, we first thoroughly rinsed it with a chilled saltwater solution (ice-cold saline). Then, we took half a gram of each sample and ground it up in a cold phosphate buffer solution with a neutral pH (7.4) using specialized glass tubes and a motor-powered grinder. The resulting mixture (homogenate) was spun in a centrifuge (Centrikon H-401 centrifuge) at 4000 revolutions per minute (rpm) for 15 min at a cold temperature (4°C). The clear liquid remaining on top after spinning (supernatant) was separated into smaller portions and stored at a very cold temperature (−80°C) for further testing related to oxidative stress and antioxidant enzymes.

A spectrophotometer (Photometer 5010, Photometer, BM Co. Germany) was used to determine the levels of GPX, Malondialdehyde (MDA), and NO in the tissue homogenate. For CAT activity, we followed a method developed by Aebi. This method involves measuring how much the concentration of hydrogen peroxide (H_2O_2) decreases at a specific wavelength of light (240 nm).[37] Ellman's reagent (DTNB) was used to measure the GSH levels.[38] To measure GPX activity, we tracked a change in light absorption. We used a specific substrate called CDNB (1-chloro-2,4-dinitrobenzene) that gets linked to a molecule called reduced glutathione. We monitored how much light this combination absorbs at a wavelength of 340 nm. This method follows a protocol established by Habig *et al*.[39] TBARS levels (MDA concentration) were quantified according to Ohkawa *et al*.[40] Superoxide dismutase (SOD) levels were measured as U/g tissue using an enzymatic colorimetric method based on Nishikimi *et al*.'s procedure.[41] The total antioxidant capacity (TAC) in serum was determined following Koracevic *et al*.'s method,[42] where the residual H_2O_2 from the reaction of antioxidants with exogenous H_2O_2 is measured calorimetrically.

Estimation of serum cytokines

The levels of tumor necrosis factor-α (TNF-α), interleukin-6 (IL-6), and IL-10 in the blood serum were measured using commercially available test kits designed for ELISA (Invitrogen Co. USA).

Histopathological studies

Small pieces of tissue from the liver, pancreas, kidneys, and heart of each rat were preserved in 10% buffered

formalin overnight. Then, the tissues were encased in paraffin. Very thin slices (4 micrometers thick) were cut from the paraffin-embedded tissues and stained with Hematoxylin and Eosin. A special microscope (binocular light microscope from Olympus) was used to examine these stained slices for any damage or changes in the tissues. To avoid bias, the examination was done without knowing which sample belonged to which animal. Images of the stained tissues were captured using a digital camera (Canon, 5 megapixels, 3.2 × zoom).

Statistical analysis

GraphPad Prism (version 9.0.0) and IBM SPSS Statistics for Windows, version 20.0 (IBM Corp., Armonk, N.Y., USA) were used to analyze the data statistically for each measurement, we calculated the average value (mean) and the variability around that average (SD). The ANOVA and *post hoc* Tukey statistical test were used to detect and compare any significant differences between the average values of different groups; significance was considered with a $P < 0.05$.

Results

Effect of taurine on serum glucose, insulin, and lipid profile

Regarding the serum level of glucose, the results obtained revealed a significant increase in the ALX group compared with all other investigated groups, on the other hand, the glucose level significantly decreased in the ALX + TAU group when compared to the diabetic group. Moreover, the experimentally induced diabetic group showed a significant decrease in the measured insulin level compared to control and other experimental groups [Table 1]. Regarding the lipid profile (CHO, TG, and HDL), the diabetic rats showed a significant increase in both CHO and TG levels, with a significant decrease in HDL levels compared with all studied groups. Interestingly, TAU treatment in diabetic animals largely reverses these negative changes [Table 1].

Effect of taurine on liver enzymes

Results revealed that the serum liver enzymes (ALT and AST) were notably elevated in the experimentally diabetic animals (ALX group) as contrasted with the control and other experimental groups. Despite signs of improvement, however, these liver enzymes were increased significantly in the diabetic treated group with TAU compared with the control one [Figure 1].

Effect of taurine on serum protein

Besides the hepatic enzyme level disturbance, we found that the serum biochemical parameters revealed a significant decrease in the total protein level in the TAU group compared to all studied groups, but interestingly, in ALX and ALX + TAU groups, the total protein level significantly declined compared by control rats, meanwhile insignificantly changes in the albumin level between all experimental groups. The TAU group had significantly lower levels of globulin and a lower A/G ratio compared to both the control and ALX groups [Table 2].

Effect of taurine on renal parameters

Rats with ALX-induced diabetes showed significantly higher levels of urea and creatinine compared to the control and TAU-treated groups. Importantly, the TAU-treated group had no significant difference in these kidney function markers compared to the healthy control group. In addition, the results revealed a significant rise in creatinine levels in the ALX + TAU group when compared to the control group [Table 2].

Table 1: Serum level of glucose, insulin, cholesterol, triglycerides, and high-density lipoproteins

Groups	Glucose	Insulin	Cholesterol	TG	HDL
Control	120.76±0.17	10.32±0.43	125.76±2.57	71.50±3.86	40.60±2.71
TAU	121.50±2.78	11.60±0.32	120.5±2.78	70.25±5.05	41.30±0.87
Alloxan	200.50±6.79**	4.58±0.46**	202±9.62**	134.75±2.63**	27.25±1.68**
Alloxan + TAU	137.75±7.13$^{\#\#}$	7.62±1.15*,$^{\#\#}$	153.25±5.28$^{\#\#}$	82.25±3.89$^{\#\#}$	34.50±1.32$^{\#}$

**P <0.01 significance against the control group and $^{\#}P$<0.05, $^{\#\#}P$<0.01 significance against the ALX group. TAU: Taurine treatment, TG: Triglycerides, HDL: High density lipoprotein

Table 2: Serum level of total protein, albumin, globulin, urea, and creatinine

Groups	Total protein (g/dL)	Albumin (g/dL)	Globulin (g/dL)	A/G ratio	Urea (mg/dL)	Creatinine (mg/dL)
Control	7.39±0.17	4.20±0.13	3.19±0.28	1.31±0.28	55.46±3.91	0.47±0.02
TAU	7.53±0.23	4.31±0.12	3.22±0.30	1.33±0.30	53.25±3.26	0.41±0.02
Alloxan	5.25±0.16*	3.67±0.12*	1.58±0.26*	2.32±0.26*	85.47±2.39*	1.38±0.05*
Alloxan + TAU	6.10±0.42$^{\#}$	4±0.45	2.1±0.52$^{\#}$	1.9±0.52	61.67±2.96	0.62±0.02$^{\#}$

*Significance against the control group and $^{\#}$Significance against the Alloxan group. TAU: Taurine treatment, A/G: Albumin-to-globulin

Effect of taurine on antioxidant system and lipid peroxidation

The results indicate a notable decrease ($P < 0.05$) in antioxidant enzymes such as GSH, GPX, catalase, SOD, and TAC in ALX diabetic group compared to the control group. In addition, levels of peroxidation markers MDA and NO were notably higher in the ALX-treated group in comparison to the control group. Conversely, TAUtreatment group resulted in a significantly higher level of the antioxidant enzyme SOD in the pancreas compared to all other groups in the experiment, but other parameters showed non-significant change. In addition, the ALX + TAU group showed a significant increase in the antioxidant markers GSH, CAT, SOD, GPx, and TAC and a decrease in MDA and NO when compared to the ALX group. These changes in the oxidant/antioxidant system still significantly changed when compared with the control rats except for MDA, which showed nonsignificant increase [Table 3].

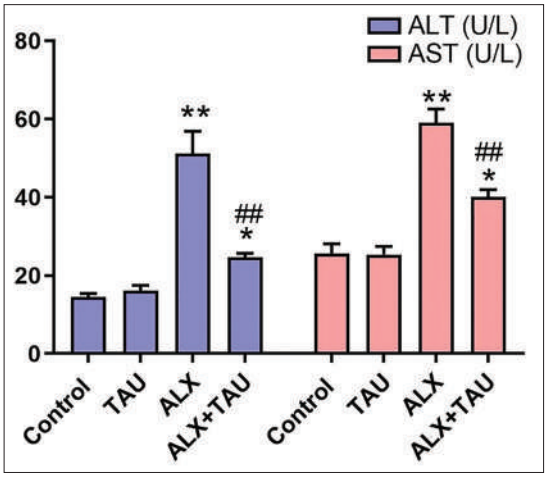

Figure 1: Serum alanine aminotransferases and aspartate aminotransferases in the studied groups. *P<0.05, **P<0.01 significance against the control group and ##P<0.01 significance against the Alloxan group. TAU: Taurine, ALX: Alloxan, ALT: Alanine aminotransferases, AST: Aspartate aminotransferases

Effect of taurine on the serum tumor necrosis factor-α, interleukin-6 and interleukin-10

Rats with ALX-induced diabetes had significantly higher levels of TNF-α and IL-6, and lower levels of IL-10, compared to the control, TAU, and ALX + TAU groups. While TAU treatment in the ALX + TAU group improved these inflammatory markers, TNF-α and IL-6 remained significantly elevated, and IL-10 remained lower, compared to the healthy control group [Figure 2].

Histopathological results

The histology of the pancreas from control and TAU-fed rats exhibited a normal arrangement of Islets of Langerhans of various sizes scattered throughout the exocrine tissue with no visible lesions. In contrast, the pancreas of diabetic rats showed significant degeneration, necrosis, and shrinkage of the Islets of Langerhans with severe vacuolization of the exocrine tissue. Perivascular and perductal fibrosis, in addition to ductal epithelial hyperplasia, was also noted. In diabetic rats that received TAU, the exocrine and endocrine components of the pancreas retained normal histology [Figure 3].

Microscopic examination of the liver from control rats and rats [Figures 4a and b] fed on TAU [Figures 4c and d] revealed sinusoidal cords of hepatocytes with a central vein

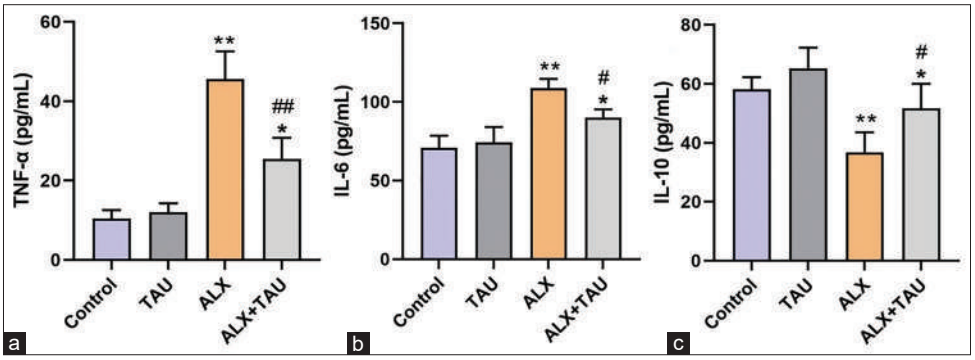

Figure 2: Serum tumor necrosis factorα (a), interleukin6 (IL6) (b), and IL10 (c) in the studied groups. *P<0.05, **P<0.01 significance against the control group and #P<0.05, ##P<0.01 significance against the Alloxan group. TAU: Taurine, ALX: Alloxan

Table 3: Oxidant and antioxidant systems in pancreatic tissue homogenate

Groups	MDA (nmol/mL)	Nitric oxide (µmol/L)	SOD (U/mL)	Catalase (U/g)	GSH (mg/g)	GPX (U/mg)	TAC (µmol/L)
Control	15.46±2.44	3.11±0.44*	276.38±5.80	61.32±6.25	7.87±0.47	8.32±0.59	1±0.04
TAU	15.65±0.82	3.52±0.28	303.9±2.25	50.14±2.53	8.21±0.59	7.39±0.35	1.10±0.06
Alloxan	54.50±7.29*	10.62±0.66*	195.20±2.65*	28.45±2.7*	3.65±0.31*	3.04±0.36*	0.52±0.03*
Alloxan + TAU	18.92±2.70#	5.67±0.45*,#	240.5±4.52*,#	43.65±3.02*,#	6.27±0.47*,#	5.19±0.22*,#	0.80±0.05*,#

*Significance against the control group and #Significance against the Alloxan group. TAU: Taurine treatment, GSH: Glutathione, GPX: Glutathione peroxidase, TAC: Total antioxidant capacity, SOD: Superoxide dismutase, MDA: Malondialdehyde

and portal tracts. The portal tracts exhibited a portal triad consisting of a portal vein, hepatic artery, and bile duct. However, histological examination of the liver of diabetic rats revealed diffuse hydropic degeneration of the hepatocytes and mononuclear cells (MNCs) infiltration in portal areas [Figures 4e and f]. Meanwhile, liver from diabetic rats fed on TAU [Figures 4g and h] brought back the cellular arrangement around the central vein with normal-shaped hepatocytes.

Histological examination of the kidneys of control rats showed no visible lesions, with renal corpuscles appearing as normal dense rounded structures; the glomeruli were surrounded by narrow Bowman's spaces. Moreover, sections from rats that received only TAU were like control rats except for the presence of tubular casts. Histological examination of the kidney of diabetic rats revealed degeneration of the glomeruli with wider Bowman's spaces, mild vacuolation of the tissues, focal MNCs aggregation in the interstitial tissue, and mild perivascular edema. Kidneys from diabetic rats who received TAU showed mild perivascular fibrosis with few MNC infiltration [Figure 5].

Microscopic examination of the heart from control and TAU-fed rats revealed a normal histological picture. Cardiomyocytes showed single, oval, and centrally located nuclei with regularly arranged cardiac myofibers. However, the hearts of diabetic rats revealed marked vacuolations in cross and longitudinal cardiac myofibers, congestion, edema, and few MNCs infiltration. Meanwhile, hearts from diabetic rats treated with TAU retained normal histological appearance [Figure 6].

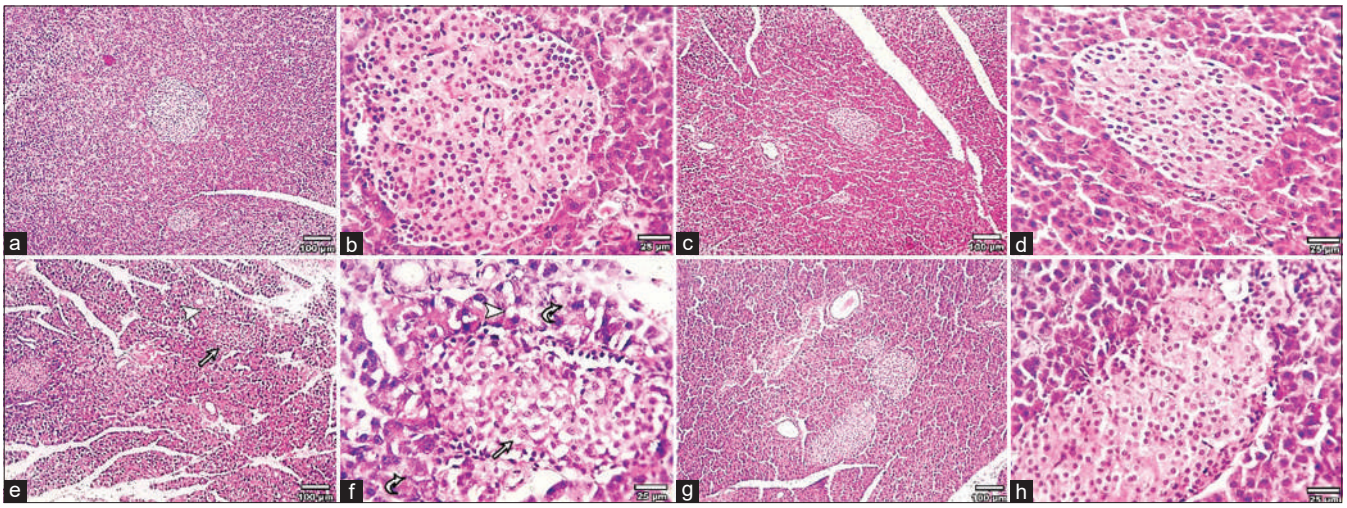

Figure 3: Photomicrographs of the pancreas show: normal acini and Islets in the control group (a and b) and taurine (TAU) group (c and d), while Alloxan (ALX) group (e and f) show vacuolations (arrowhead) necrosis (curved arrow) and shrinkage in exocrine acini, vacuolations in most cells of Islet (arrow), normal acini and Islets in ALX + TAU group (g and h). Magnifications X:100 bar 100 and X:400 bar 25

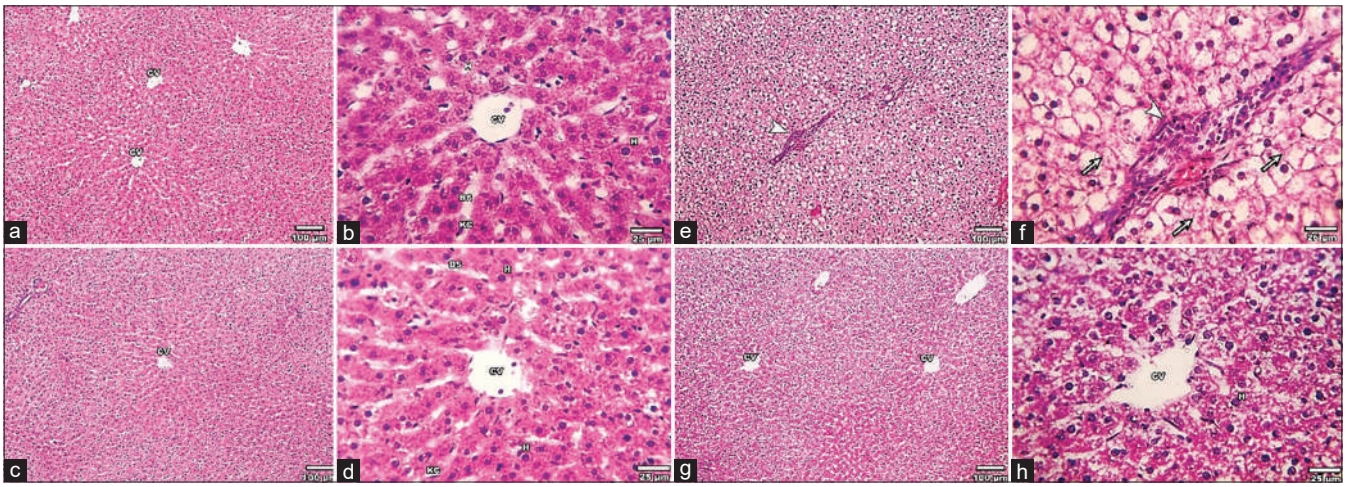

Figure 4: Microscopic examination of the liver from control rats (a and b) and rats fed on taurine (TAU) (c and d) revealed normal sinusoidal cords of hepatocytes with central vein and portal tracts. Diabetic rats revealed diffuse hydropic degeneration of the hepatocytes (arrow), occluded sinusoids, and mononuclear cells infiltration (arrowhead) in portal areas (e and f). Meanwhile, liver from diabetic rats fed on TAU brought back the cellular arrangement around the central vein with normal-shaped hepatocytes (g and h). CV: Central vein, BS: Blood sinusoid, H: Hepatocyte, KC: Kupffer cell.Magnifications X:100 bar 100 and X:400 bar 25

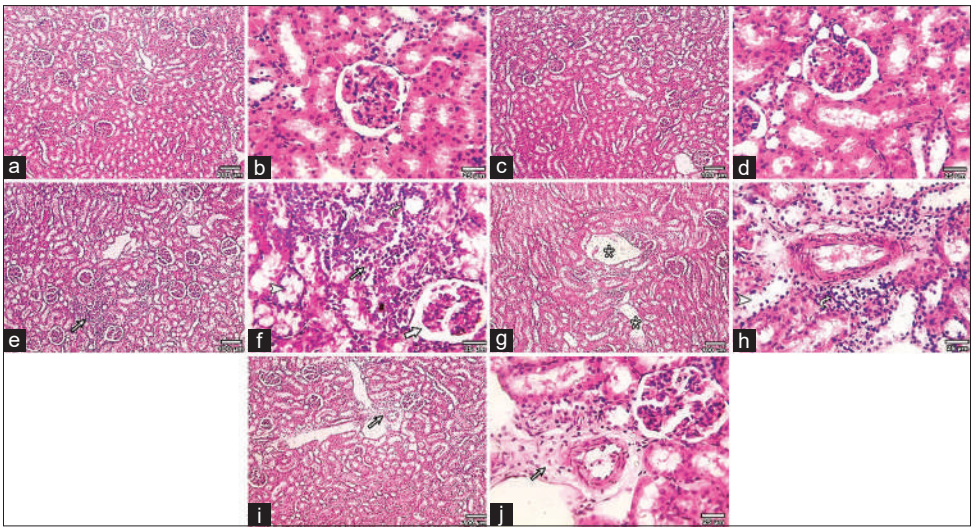

Figure 5: Photomicrographs of kidneys show: Normal glomeruli and tubules in control (a and b) and taurine (TAU) (c and d) groups, photos from Alloxan (ALX) group (e-h) showed focal aggregation of mononuclear cells (MNCs) in interstitium (thin arrow) and shrunken glomerular tuft (thick arrow), hydropic degeneration in tubular epithelium (arrowheads) in, dilated lymphatics (*) and perivascular MNCs infiltration (curved arrow). ALX + TAU group (i and j) showed perivascular fibrosis with few MNC infiltration (arrow). Magnifications X:100 bar 100 and X:400 bar 25

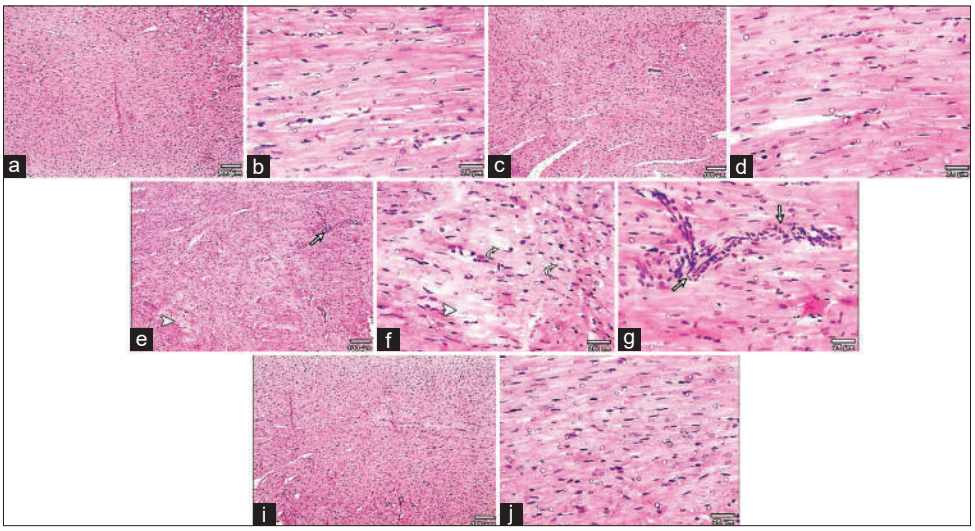

Figure 6: Photomicrographs of the heart show: a normal histological picture of cardiomyocytes with minimal interstitial space control (a and b) and taurine (TAU) (c and d) groups, hydropic degeneration (arrowhead), vacuolation (curved arrow) of cardiac myofibers and few mononuclear cells infiltration (arrow) in Alloxan (ALX) group (e-g), retained normal histological in ALX + TAU group (i and j). Magnifications X:100 bar 100 and X:400 bar 25

Discussion

In the current study, we examined the hypoglycemic effect of TAU and its beneficial impact on oxidative damage under diabetic conditions. Based on the findings, our study suggests that the amino acid TAU exhibits significant antidiabetic activity.

ALX and streptozotocin (STZ) are commonly used as diabetogenic agents to evaluate antidiabetic properties.[43] ALX is utilized more frequently due to their affordability and accessibility compared to STZ.[44]

TAU is extensively utilized in beverages,[45] infant formula,[46] and other products due to its excellent safety profile. Depletion of TAU can result in various pathological conditions such as cardiomyopathy,[47] renal dysfunction,[48] and pancreatic β cell dysfunction.[49]

Results in the current study showed that ALX induced a marked increase in blood glucose and a decrease in serum insulin with marked degeneration, necrosis, and shrinkage of the pancreatic islets. Studies reported that ALX-induced alterations in the pancreatic function and structure are owed to its cytotoxic effect on β cells, resulting in cell vacuolation, suppression of insulin secretion, and cellular apoptosis.[4,50-53]

In our experiment, TAU markedly decreased serum glucose and increased serum insulin levels in ALX-induced diabetic rats, as well as protecting pancreatic β cells. TAU improves

hyperglycemia through diminished glucose absorption from the gastrointestinal tract,[54] accelerated utilization by peripheral tissues,[33] increases the sensitivity to insulin through upregulation of insulin receptor substrate one phosphorylation,[55,56] enhanced insulin production,[57,58] re-established the function of the damaged pancreatic islet,[59] and prevent islet cell apoptosis.[60] Meanwhile, others reported unchanged blood glucose levels in TAU-treated diabetic rats,[61] this difference may be due to the mode of TAU administration, which plays a vital role in its absorption and effectiveness.[62]

Persistent hyperglycemia and hyperlipidemia are significant features of diabetes. Prolonged hyperglycemias are linked to changes in the levels of fats in the blood, as well as variations in serum enzymes and overall body weight.[63] The present study reported that ALX-induced dyslipidemia, hypertriglyceridemia, hypercholesterolemia, and decreased HDL, which was also reported in many studies.[64-69] LDL-cholesterol can be easily glycated, interacts with oxidizing agents, and turned into oxidized LDL, which induces macrophage recruitment, resulting in foam cells.[70] Moreover, diabetic rats exhibited increased oxidative stress lipid peroxidation and decreased antioxidant defense and TAC. Similar results were reported.[33,62,66,69,71-73]

The present results confirmed that TAU ameliorated the dyslipidemia induced by ALX in diabetic rats, similar results were also reported.[69,74-80] On the other hand, it restores the oxidant/antioxidant state by decreasing the lipid peroxidation and enhancing the antioxidant enzymatic activity and TAC, which is in accordance with earlier studies.[62,69,76,80] TAU maintains a functioning electron transport chain, free radical scavenging, inhibits ROS generation, stimulates antioxidant enzyme production, and enhances the adaption to cellular stress.[81-83]

TAU modulated the inflammatory process associated with hyperglycemia, dyslipidemia, and oxidative stress associated with ALX-induced diabetes. TAU decreased NFkβ nuclear translocation and activation,[69] reduced inflammation, neutrophil accumulation, proinflammatory cytokine,[84] decreased the level of IL-6 and TNF-α.[80,85] TAU not only decreases the inflammatory mediators but also enhances the anti-inflammatory activity. The present study reported that TAU increased the IL-10, which was also reported.[53,86] TAU inhibited M1 macrophage polarization, and inflammatory mediators production,[87] and stimulated M2 macrophage polarization.[88]

ALX-induced hyperglycemia, hyperinsulinemia, dyslipidemia, oxidative stress, and inflammation contributed to diabetic complications.[72] These causes were proved in our work by elevated liver enzymes, serum urea, creatinine, decreased TP, and the histopathological findings. Adeyi *et al*. reported various degrees of degeneration observed in the hepatocytes, renal glomeruli, and cardiomyocytes in ALX-induced diabetic rats.[50]

Several studies reported ALX-induced diabetic complications including hepatic complications,[33,72,77,89-93] renal complications,[62,72,94,95] and cardiac complications.[69,96]

Our study found that TAUtreatment significantly improved liver and kidney function and restored the normal tissue structure (histological architecture) in the liver, kidney, and heart of diabetic rats. These findings support the potential of TAU to prevent the worsening of diabetes and its associated complications, including in both type 1 and type 2 diabetes mellitus.[23,27,97]

The hepatoprotective effect of TAU was attributed to that TAU inhibits steatosis by decreasing the TGs and cholesterol levels,[97,98] inhibits lipogenesis by downregulating sterol regulating element binding protein and its target genes,[78,98] improve the antioxidant state,[99,100] enhance the antioxidant activity by prevent degradation of Nrf2 and subsequent downstream HO-1,[101] downregulate Bax, caspases, and upregulate Bcl2 thus inhibiting the apoptotic pathway.[102] Moreover, TAU reduces the hepatic expression of inflammatory markers[103] and upregulates the anti-inflammatory IL-10 and adiponectin.[104]

Animal models, either STZ or ALX-induced diabetes, were used to study the protective effect of TAU against diabetic-induced renal injury. TAU exerted its nephroprotective effect through its hypoglycemic, antioxidant, and protective effects. TAU improves the dyslipidemic state and decreases the level of oxidative stress.[76] The TAU nephroprotective effect is attributed to the decreased activity of NADPH oxidase in the kidney,[62] modulates the expression of TGF-β and extracellular matrix remodeling,[76,105] moreover, TAU has anti-inflammatory activity through modulation of proinflammatory cytokines as IL-6, IL-1 β, and TNF-α.[62] TAU improves glomerular hyperpermeability and proteinuria through modulation of VEGF and nephrin in the podocytes[106] and decreases podocyte apoptosis,[107] TAU prevents renal apoptosis by downregulating caspase three and Bax/Bcl-2 ratio through activation of Akt signaling.[108]

The present study showed that TAU treatment alleviated the histological alterations of ALX-induced diabetes (congestion, edema, and inflammatory infiltrations. These results are in accordance with Das *et al*.[69] TAU deficiency is associated with cardiac atrophy and remodeling,[109] the cardioprotective effect of TAU is attributed to its glucose-lowering effect through increasing insulin secretion and sensitivity, antioxidant, antihyperlipidemic, and anti-inflammatory actions.[69,110] Defective vasorelaxation is a main predisposing factor for cardiovascular complications,[111] TAU-induced vasodilatation through the opening of potassium channels[112] or osmoregulatory effect[113] controlling diuresis and natriuresis through regulation of vasopressin.[114] In addition, TAU induces a SIRT-1 deacetylating effect on P53,

thus promoting its inhibition and suppressing apoptosis.[115] TAU inhibited cardiac inflammation through the reduction of IL-6and TNF-α and modulation of Janus kinase 2 and signal transducer and activator 3 of transcription (STAT3) signaling pathway.[116]

Conclusions

TAU has a therapeutic effect against ALX-induced hepatic, renal, and cardiac diabetic complications through its hypoglycemic effect, enhancing insulin secretion, improving dyslipidemia, maintaining the oxidative-redox state through minimizing oxidative stress, and enhancing antioxidant activity. TAU has an anti-inflammatory effect through the reduction of inflammatory mediators IL-6 and TNF-α and increasing the anti-inflammatory IL-10.

Ethics statement

Experiments were performed according to the international ethical standards and ARRIVE guidelines following the U.K. Animals (Scientific Procedures) Act, and National Institutes of Health guide for the care and use of Laboratory animals. The local Administrative Panel on Laboratory Animal Care Committee, code number MU-ACUC (VM.R.24.02.152), authorized all experimental protocols, which followed Mansoura University's Animal Care and Use Guidelines.

Acknowledgments

This research was Supported by Princess Nourah bint Abdulrahman University Researchers Supporting Project number (PNURSP2025R199), Princess Nourah bint Abdulrahman University, Riyadh, Saudi Arabia and by the Researchers Supporting program, AlMaarefa University, Diriyah, Saudi Arabia. The work supported by Prince Sattam bin Abulaziz University project number (PSAU/2024/R/1446).

Financial support and sponsorship

This research was funded by Princess Nourah bint Abdulrahman University Researchers Supporting Project number (PNURSP2025R199), Princess Nourah bint Abdulrahman University, Riyadh, Saudi Arabia and by the Researchers Supporting program, AlMaarefa University, Diriyah, Saudi Arabia. The work supported via funding from Prince Sattam bin Abulaziz University project number (PSAU/2024/R/1446).

Conflicts of interest

There are no conflicts of interest.

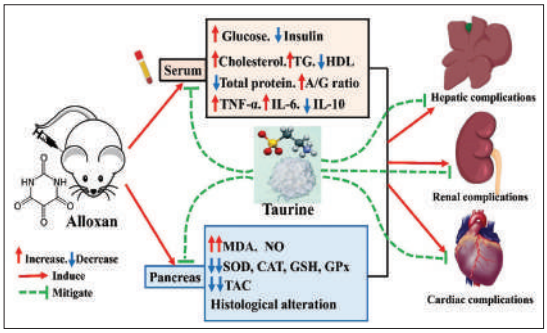

Graphical Abstract

References

1. Animaw W, Seyoum Y. Increasing prevalence of diabetes mellitus in a developing country and its related factors. PLoS One 2017;12:e0187670.
2. Sperling MA. Pediatric Endocrinology. Saunders: Philadelphia, PA, USA,: Elsevier Health Sciences; 2014.
3. Sun JE, Ao ZH, Lu ZM, Xu HY, Zhang XM, Dou WF, *et al.* Antihyperglycemic and antilipidperoxidative effects of dry matter of culture broth of *Inonotus obliquus* in submerged culture on normal and alloxan-diabetes mice. J Ethnopharmacol 2008;118:7-13.
4. Verma L, Singour PK, Chaurasiya PK, Rajak H, Pawar RS, Patil UK. Effect of ethanolic extract of *Cassia occidentalis* Linn for the management of alloxan-induced diabetic rats. Pharmacognosy Res 2010;2:132-7.
5. Middha SK, Usha T, Basistha BC, Goyal AK. Amelioration of antioxidant potential, toxicity, and antihyperglycemic activity of *Hippophae salicifolia* D don leaf extracts in alloxan-induced diabetic rats. 3 Biotech 2019;9:308.
6. Leenders F, Groen N, de Graaf N, Engelse MA, Rabelink TJ, de Koning EJ, *et al.* Oxidative stress leads to β-Cell dysfunction through loss of β-cell identity. Front Immunol 2021;12:690379.
7. Giacco F, Brownlee M. Oxidative stress and diabetic complications. Circ Res 2010;107:1058-70.
8. Fakhruddin S, Alanazi W, Jackson KE. Diabetesinduced reactive oxygen species: mechanism of their generation and role in renal injury. J Diabetes Res 2017; 2017:8379327, 30 pages.
9. Raza MA, Malik MS, Azam M. Impact of natural antioxidants on biological systems. Lahore Garrison Univ J Life Sci 2020;4:139-62.
10. Ansar S, Koska J, Reaven PD. Postprandial hyperlipidemia, endothelial dysfunction and cardiovascular risk: Focus on incretins. Cardiovasc Diabetol 2011;10:61.
11. De Luca G, Calpona PR, Caponetti A, Romano G, Di Benedetto A, Cucinotta D, *et al.* Taurine and osmoregulation: Platelet taurine content, uptake, and release in type 2 diabetic patients. Metabolism 2001;50:60-4.
12. Vangipurapu J, Stancáková A, Smith U, Kuusisto J, Laakso M. Nine amino acids are associated with decreased insulin secretion and elevated glucose levels in a 7.4-Year follow-up study of 5,181 Finnish Men. Diabetes 2019;68:1353-8.
13. Yoneshiro T, Wang Q, Tajima K, Matsushita M, Maki H, Igarashi K, *et al.* BCAA catabolism in brown fat controls energy homeostasis through SLC25A44. Nature 2019;572:614-9.
14. Bao L, Wu B, Yang C, Xu X, Shi Z, Jiang D. Targeted metabolomics analysis of serum amino acids in T2DM patients. Diabetes Metab Syndr Obes 2024;17:203-12.
15. Barle H, Ahlman B, Nyberg B, Andersson K, Essén P, Wernerman J. The concentrations of free amino acids in human liver tissue obtained during laparoscopic surgery. Clin Physiol 1996;16:217-27.
16. Sarkar P, Basak P, Ghosh S, Kundu M, Sil PC. Prophylactic role of taurine and its derivatives against diabetes mellitus and its related complications. Food Chem Toxicol 2017;110:109-21.

17. Jong CJ, Sandal P, Schaffer SW. The role of taurine in mitochondria health: More than just an antioxidant. Molecules 2021;26:4913.
18. Joseph G, Varughese A, Daniel A. Determination of total proteinogenic amino acids and taurine by pre-column derivatization and UHPLC: Single laboratory validation, first action official methodSM 2019.09. J AOAC Int 2021;104:431-46.
19. Heibashy M. Hypolipidimia effect of taurine and L-carnine on rats fed a high cholesterol diet. J Union Arab Biol Cairo 2000;14:11-23.
20. Sak D, Erdenen F, Müderrisoglu C, Altunoglu E, Sozer V, Gungel H, *et al.* The Relationship between plasma taurine levels and diabetic complications in patients with type 2 diabetes mellitus. Biomolecules 2019;9:96.
21. Chang KJ. Effect of taurine and βalanine on morphological changes of pancreas in streptozotocininduced rats. In: Taurine 4: Taurine and Excitable Tissues. Boston, MA: Springer US; 2002. p. 5717.
22. El Idrissi A, Sidime F, Tantawy O, Obeysekera D, Wisidagama D, Tariq S, *et al*, editors. Taurine supplementation induces hyperinsulinemia and neuronal hyperexcitability. Taurine 9. Springer Nature Switzerland; 2015.
23. Chen W, Guo J, Zhang Y, Zhang J. The beneficial effects of taurine in preventing metabolic syndrome. Food Funct 2016;7:1849-63.
24. Singh P, Gollapalli K, Mangiola S, Schranner D, Yusuf MA, Chamoli M, *et al.* Taurine deficiency as a driver of aging. Science 2023;380:eabn9257.
25. Kang H. Sample size determination and power analysis using the G*Power software. J Educ Eval Health Prof 2021;18:17.
26. Aziz MM, Majid A, Al-Fartosi KG. Effect of Taurine on liver and kidney functions of Diabetic female rats. Res J Pharm Technol 2020;13:4826-8.
27. Foda DS, Farrag EK, Metwally NS, Maghraby AS, Farrag AR, Rawi SM. Protective and therapeutic impact of taurine on some biochemical, immunological and histological parameters in diabetic rats. J Appl Pharm Sci 2016;6:045-054.
28. Fernandes NP, Lagishetty CV, Panda VS, Naik SR. An experimental evaluation of the antidiabetic and antilipidemic properties of a standardized *Momordica charantia* fruit extract. BMC Complement Altern Med 2007;7:29.
29. Haidara MA, Mikhailidis DP, Rateb MA, Ahmed ZA, Yassin HZ, Ibrahim IM, *et al.* Evaluation of the effect of oxidative stress and Vitamin E supplementation on renal function in rats with streptozotocin-induced type 1 diabetes. J Diabetes Complications 2009;23:130-6.
30. Shi Y, Wan X, Shao N, Ye R, Zhang N, Zhang Y. Protective and anti-angiopathy effects of ginsenoside Re against diabetes mellitus via the activation of p38 MAPK, ERK1/2 and JNK signaling. Mol Med Rep 2016;14:4849-56.
31. Gomez R, Caletti G, Arbo BD, Hoefel AL, Schneider R Jr., Hansen AW, *et al*. Acute intraperitoneal administration of taurine decreases the glycemia and reduces food intake in type 1 diabetic rats. Biomed Pharmacother 2018;103:1028-34.
32. Barbiera A, Sorrentino S, Fard D, Lepore E, Sica G, Dobrowolny G, *et al.* Taurine administration counteracts aging-associated impingement of skeletal muscle regeneration by reducing inflammation and oxidative stress. Antioxidants (Basel) 2022;11:1016.
33. Rashid K, Das J, Sil PC. Taurine ameliorate alloxan induced oxidative stress and intrinsic apoptotic pathway in the hepatic tissue of diabetic rats. Food Chem Toxicol 2013;51:317-29.
34. Duran AO, Inanc M, Karaca H, Dogan I, Berk V, Bozkurt O, *et al.* Albumin-globulin ratio for prediction of long-term mortality in lung adenocarcinoma patients. Asian Pac J Cancer Prev 2014;15:6449-53.
35. Thomas L, Labor U. Enzymatic kinetic colorimetric test (GOD-PAP). Biocon Diagnostics. Hecke 1992;8:34516.
36. Chevenne D, Letailleur A, Trivin F, Porquet D. Effect of hemolysis on the concentration of insulin in serum determined by RIA and IRMA. Clin Chem 1998;44:354-6.
37. Aebi H. Catalase *in vitro*. Methods in enzymology 1984;105:121-6.
38. Beutler E, Duron O, Kelly BM. Improved method for the determination of blood glutathione. J Lab Clin Med 1963;61:882-8.
39. Habig WH, Pabst MJ, Jakoby WB. Glutathione S-transferases. The first enzymatic step in mercapturic acid formation. J Biol Chem 1974;249:7130-9.
40. Ohkawa H, Ohishi N, Yagi K. Assay for lipid peroxides in animal tissues by thiobarbituric acid reaction. Anal Biochem 1979;95:351-8.
41. Nishikimi M, Appaji N, Yagi K. The occurrence of superoxide anion in the reaction of reduced phenazine methosulfate and molecular oxygen. Biochem Biophys Res Commun 1972;46:849-54.
42. Koracevic D, Koracevic G, Djordjevic V, Andrejevic S, Cosic V. Method for the measurement of antioxidant activity in human fluids. J Clin Pathol 2001;54:356-61.
43. Fajarwati I, Solihin DD, Wresdiyati T, Batubara I. Self-recovery in diabetic sprague dawley rats induced by intraperitoneal alloxan and streptozotocin. Heliyon 2023;9:e15533.
44. Federiuk IF, Casey HM, Quinn MJ, Wood MD, Ward WK. Induction of type-1 diabetes mellitus in laboratory rats by use of alloxan: Route of administration, pitfalls, and insulin treatment. Comp Med 2004;54:252-7.
45. Jagim AR, Harty PS, Barakat AR, Erickson JL, Carvalho V, Khurelbaatar C, *et al.* Prevalence and amounts of common ingredients found in energy drinks and shots. Nutrients 2022;14:314.
46. Almeida CC, Mendonça Pereira BF, Leandro KC, Costa MP, Spisso BF, Conte-Junior CA. Bioactive compounds in infant formula and their effects on infant nutrition and health: A systematic literature review. Int J Food Sci 2021;2021:8850080.
47. Zulli A. Taurine in cardiovascular disease. Curr Opin Clin Nutr Metab Care 2011;14:57-60.
48. Yamori Y, Taguchi T, Hamada A, Kunimasa K, Mori H, Mori M. Taurine in health and diseases: Consistent evidence from experimental and epidemiological studies. J Biomed Sci 2010;17 Suppl 1:S6.
49. L'Amoreaux WJ, Cuttitta C, Santora A, Blaize JF, Tachjadi J, El Idrissi A. Taurine regulates insulin release from pancreatic beta cell lines. J Biomed Sci 2010;17 Suppl 1:S11.
50. Adeyi AO, Idowu BA, Mafiana CF, Oluwalana SA, Ajayi OL, Akinloye OA. Rat model of food-induced non-obese-type 2 diabetes mellitus: Comparative pathophysiology and histopathology. Int J Physiol Pathophysiol Pharmacol 2012;4:51-8.
51. El-Esawy B, Alghamdy A, El Askary A, Elsayed E. Histopathological evaluation of the pancreas following administration of paricalcitol in alloxan-induced diabetic Wistar rats. World J Pharm Pharm Sci 2016;5:189-98.
52. Mostafa AM, Serwah AH, Mohamed WS, Mohamed KM. Effects of some antidiabetic medicinal plants on pancreas and liver of diabetic Albino rats. Egypt J Hosp Med 2018;50:156-68.
53. Ibrahim RM, Abdelhafez HM, El-Shamy SA, Eid FA, Mashaal A. Arabic gum ameliorates systemic modulation in Alloxan

monohydrate-induced diabetic rats. Sci Rep 2023;13:5005.
54. Tsuchiya Y, Kawamata K. Effects of taurine on plasma glucose concentration and active glucose transport in the small intestine. Anim Sci J 2017;88:1763-7.
55. Arany E, Strutt B, Romanus P, Remacle C, Reusens B, Hill DJ. Taurine supplement in early life altered islet morphology, decreased insulitis and delayed the onset of diabetes in non-obese diabetic mice. Diabetologia 2004;47:1831-7.
56. Wu N, Lu Y, He B, Zhang Y, Lin J, Zhao S, *et al*. Taurine prevents free fatty acid-induced hepatic insulin resistance in association with inhibiting JNK1 activation and improving insulin signaling *in vivo*. Diabetes Res Clin Pract 2010;90:288-96.
57. Lin S, Wu G, Zhao D, Han J, Yang Q, Feng Y, *et al.* Taurine increases insulin expression in STZ-treated rat islet cells *in vitro*. Adv Exp Med Biol 2017;975:319-28.
58. Vettorazzi JF, Ribeiro RA, Santos-Silva JC, Borck PC, Batista TM, Nardelli TR, *et al.* Taurine supplementation increases K (ATP) channel protein content, improving Ca2+handling and insulin secretion in islets from malnourished mice fed on a high-fat diet. Amino Acids 2014;46:2123-36.
59. Şahin D. Possible Relationship Between Diabetes Mellitus and Alzheimer Disease. Tıp Fakültesi Klinikleri Dergisi 2018;1:112
60. Zhao D, Zhang X, Bian Y, Meng L, Wu Y, Ma Y, *et al.* Taurine reduces apoptosis mediated by endoplasmic reticulum stress in islet β-cells induced by high-fat and -glucose diets. Food Chem Toxicol 2023;175:113700.
61. Li F, Obrosova IG, Abatan O, Tian D, Larkin D, Stuenkel EL, *et al.* Taurine replacement attenuates hyperalgesia and abnormal calcium signaling in sensory neurons of STZ-D rats. Am J Physiol Endocrinol Metab 2005;288:E29-36.
62. Winiarska K, Szymanski K, Gorniak P, Dudziak M, Bryla J. Hypoglycaemic, antioxidative and nephroprotective effects of taurine in alloxan diabetic rabbits. Biochimie 2009;91:261-70.
63. Kumar S, Kumar V, Prakash O. Antidiabetic, hypolipidemic and histopathological analysis of *Dillenia indica* (L.) leaves extract on alloxan induced diabetic rats. Asian Pac J Trop Med 2011;4:347-52.
64. Sharma S, Dwivedi S, Swarup D. Hypoglycaemic and hypolipidemic effects of *Cinnamomum tamala* Nees leaves. Indian J Exp Biol 1996;34:372-4.
65. Banda M, Nyirenda J, Muzandu K, Sijumbila G, Mudenda S. Antihyperglycemic and antihyperlipidemic effects of aqueous extracts of *Lannea edulis* in alloxan-induced diabetic rats. Front Pharmacol 2018;9:1099.
66. Yin P, Wang Y, Yang L, Sui J, Liu Y. Hypoglycemic effects in alloxan-induced diabetic rats of the phenolic extract from mongolian oak cups enriched in ellagic acid, kaempferol and their derivatives. Molecules 2018;23:1046.
67. Asif M, Saleem M, Yousaf S, Saadullah M, Zafar M, Khan RU, *et al*. Antidiabetic activity of aqueous extract of *Sigesbeckia orientalis* (St. Paul's Wort) in alloxan-induced diabetes model. Braz J Pharm Sci 2019;55:e18408.
68. Singh H, Singh R, Kaur S, Arora R, Mannan R, Buttar HS, *et al.* Protective role of *Phyllanthus fraternus* in alloxan-induced diabetes in rats. J Ayurveda Integr Med 2020;11:391-8.
69. Das J, Vasan V, Sil PC. Taurine exerts hypoglycemic effect in alloxan-induced diabetic rats, improves insulin-mediated glucose transport signaling pathway in heart and ameliorates cardiac oxidative stress and apoptosis. Toxicol Appl Pharmacol 2012;258:296-308.
70. Al Hroob AM, Abukhalil MH, Alghonmeen RD, Mahmoud AM. Ginger alleviates hyperglycemia-induced oxidative stress, inflammation and apoptosis and protects rats against diabetic nephropathy. Biomed Pharmacother 2018;106:381-9.
71. El-Shenawy NS, Abdel-Nabi IM. Hypoglycemic effect of *Cleome droserifolia* ethanolic leaf extract in experimental diabetes, and on non-enzymatic antioxidant, glycogen, thyroid hormone and insulin levels. Diabetol Croat 2006;35:15-22.
72. Ben Salem M, Ben Abdallah Kolsi R, Dhouibi R, Ksouda K, Charfi S, Yaich M, *et al.* Protective effects of *Cynara scolymus* leaves extract on metabolic disorders and oxidative stress in alloxan-diabetic rats. BMC Complement Altern Med 2017;17:328.
73. Adeosun A, Asejeje F, Ighodaro O, Oluwole B, Akinloye O. Hypoglycemic, antidyslipidemic, and antioxidant activities of methanol extract of *Struchium sparganophora* leaves in alloxan-induced oxidative stress-mediated diabetes in rats. Futur J Pharm Sci 2020;6:1-7.
74. Nakaya Y, Minami A, Harada N, Sakamoto S, Niwa Y, Ohnaka M. Taurine improves insulin sensitivity in the Otsuka long-evans tokushima fatty rat, a model of spontaneous type 2 diabetes. Am J Clin Nutr 2000;71:54-8.
75. Nishimura N, Yamamoto T, Ota T. Taurine feeding inhibits bile acid absorption from the ileum in rats fed a high cholesterol and high fat diet. Adv Exp Med Biol 2009;643:285-91.
76. Pandya KG, Budhram R, Clark GJ, Lau-Cam CA. Taurine can enhance the protective actions of metformin against diabetes-induced alterations adversely affecting renal function. Adv Exp Med Biol 2015;803:227-50.
77. Kim KS, Oh DH, Kim JY, Lee BG, You JS, Chang KJ, *et al.* Taurine ameliorates hyperglycemia and dyslipidemia by reducing insulin resistance and leptin level in Otsuka Long-Evans Tokushima fatty (OLETF) rats with long-term diabetes. Exp Mol Med 2012;44:665-73.
78. Miyata M, Funaki A, Fukuhara C, Sumiya Y, Sugiura Y. Taurine attenuates hepatic steatosis in a genetic model of fatty liver disease. J Toxicol Sci 2020;45:87-94.
79. Rais N, Parveen K, Ahmad R, Siddiqui WA, Nadeem A, Ved A. Sallyl cysteine and taurine revert peripheral metabolic and lipid profile in noninsulindependent diabetes mellitus animals: Combination versus monotherapy. Braz J Pharm Sci 2022;58: e201183.
80. ElBanna AH, Osman AS, Hossny A, ElBanna H, Abo El-Ela FI. Dose-dependent effects of taurine against testicular damage in a streptozotocin-induced type 1 diabetes mellitus rat model. Int J Immunopathol Pharmacol 2023;37:3946320231172745.
81. Surai PF. Vitagenes in Avian Biology and Poultry Health. Wageningen, Netherlands: Wageningen Academic Publishers; 2020.
82. Surai P, Kochish I, Kidd M. Taurine in poultry nutrition. Anim Feed Sci Technol 2020;260:114339.
83. Baliou S, Adamaki M, Ioannou P, Pappa A, Panayiotidis MI, Spandidos DA, *et al*. Protective role of taurine against oxidative stress (Review). Mol Med Rep 2021;24:1-19.
84. Sobrido-Cameán D, Fernández-López B, Pereiro N, Lafuente A, Rodicio MC, Barreiro-Iglesias A. Taurine promotes axonal regeneration after a complete spinal cord injury in lampreys. J Neurotrauma 2020;37:899-903.
85. Giri SN, Gurujeyalakshmi G, Wang Y. Suppression of bleomycin-induced increased production of nitric oxide and NF-kB activation by treatment with taurine and niacin. Adv Exp Med Biol 2000;483:545-61.
86. Zhu FL, Huang T, Lv ZL, Liang G, Yao Z, Lan LC, *et al.* Taurine regulates the expression of interleukin -17/10 and intestinal flora and protects the liver and intestinal mucosa in a nonalcoholic fatty liver disease rat model. Diabetes Metab Syndr Obes 2024;17:675-89.

87. Murakami S. The physiological and pathophysiological roles of taurine in adipose tissue in relation to obesity. Life Sci 2017;186:80-6.
88. Lopez-Escalera S, Lund ML, Hermes GD, Choi BS, Sakamoto K, Wellejus A. *In vitro* screening for probiotic properties of *Lactobacillus* and *Bifidobacterium* strains in assays relevant for non-alcoholic fatty liver disease prevention. Nutrients 2023;15:2361.
89. Ashish B, Swapnil G, Baldi A. Hypoglycemic effect of polyherbal formulation in alloxan induced diabetic rats. Pharmacologyonline 2011;3:764-73.
90. Ashraf MM, Abdel Hamid AS, Waleed SM, Khaled MM. Effects of some antidiabetic medicinal plants on pancreas and liver of diabetic albino rats. Egypt J Hospital Med 2013;50:156-68.
91. Lucchesi AN, Cassettari LL, Spadella CT. Alloxan-induced diabetes causes morphological and ultrastructural changes in rat liver that resemble the natural history of chronic fatty liver disease in humans. J Diabetes Res 2015;2015:494578.
92. Markkas N, Govindharajalu M. Protective effect of *Mollugo cerviana* extract on liver markers in alloxan induced diabetic rats. J Phytopharmacol 2018;20:60.
93. Suputri N, Azmijah A, Bijanti R, Putra MM. Effects of onion extract on hepar histopatology in alloxan-induced diabetic *Rattus norvegicus*. Medico Legal Updates 2020;20:383-390.
94. Sekiou O, Boumendjel M, Taibi F, Tichati L, Boumendjel A, Messarah M. Nephroprotective effect of *Artemisia herba* alba aqueous extract in alloxan-induced diabetic rats. J Tradit Complement Med 2021;11:53-61.
95. Delfita R, Dahelmi D, Tjong D, Suhatri S. Effect of *Enhydra fluctuans* on kidney function in alloxan-induced diabetic rats. Open Access Maced J Med Sci 2021;9:1187-94.
96. Kaplan JL, Stern JA, Fascetti AJ, Larsen JA, Skolnik H, Peddle GD, *et al.* Taurine deficiency and dilated cardiomyopathy in golden retrievers fed commercial diets. PLoS One 2018;13:e0209112.
97. McCarty MF. Supplementation with phycocyanobilin, citrulline, taurine, and supranutritional doses of folic acid and biotin-potential for preventing or slowing the progression of diabetic complications. Healthcare (Basel) 2017;5:15.
98. Tang R, Yang Q, Lin S, Feng Y, Yang J, Lv Q, *et al.* Preventive or curative administration of taurine regulates lipid metabolism in the liver of rats with alcoholic liver disease. Adv Exp Med Biol 2019;1155:119-31.
99. Goc Z, Kapusta E, Formicki G, Martiniaková M, Omelka R. Effect of taurine on ethanol-induced oxidative stress in mouse liver and kidney. Chin J Physiol 2019;62:148-56.
100. Murakami S, Ono A, Kawasaki A, Takenaga T, Ito T. Taurine attenuates the development of hepatic steatosis through the inhibition of oxidative stress in a model of nonalcoholic fatty liver disease *in vivo* and *in vitro*. Amino Acids 2018;50:1279-88.
101. Kim W, Kim HU, Lee HN, Kim SH, Kim C, Cha YN, *et al.* Taurine chloramine stimulates efferocytosis through upregulation of Nrf2-mediated heme oxygenase-1 expression in murine macrophages: Possible involvement of carbon monoxide. Antioxid Redox Signal 2015;23:163-77.
102. Wu G, Yang J, Lv H, Jing W, Zhou J, Feng Y, *et al.* Taurine prevents ethanol-induced apoptosis mediated by mitochondrial or death receptor pathways in liver cells. Amino Acids 2018;50:863-75.
103. Qiu T, Pei P, Yao X, Jiang L, Wei S, Wang Z, *et al.* Taurine attenuates arsenic-induced pyroptosis and nonalcoholic steatohepatitis by inhibiting the autophagic-inflammasomal pathway. Cell Death Dis 2018;9:946.
104. Abd Elwahab AH, Ramadan BK, Schaalan MF, Tolba AM. A novel role of SIRT1/FGF-21 in taurine protection against cafeteria diet-induced steatohepatitis in rats. Cell Physiol Biochem 2017;43:644-59.
105. Higo S, Miyata S, Jiang QY, Kitazawa R, Kitazawa S, Kasuga M. Taurine administration after appearance of proteinuria retards progression of diabetic nephropathy in rats. Kobe J Med Sci 2008;54:E35-45.
106. Koh JH, Lee ES, Hyun M, Kim HM, Choi YJ, Lee EY, *et al.* Taurine alleviates the progression of diabetic nephropathy in type 2 diabetic rat model. Int J Endocrinol 2014;2014:397307.
107. Zhang R, Wang X, Gao Q, Jiang H, Zhang S, Lu M, *et al.* Taurine supplementation reverses diabetes-induced podocytes injury via modulation of the CSE/TRPC6 axis and improvement of mitochondrial function. Nephron 2020;144:84-95.
108. Li S, Wang D, Zhang M, Zhang C, Piao F. Taurine ameliorates apoptosis via AKT pathway in the kidney of diabetic rats. Adv Exp Med Biol 2022;1370:227-33.
109. Pansani MC, Azevedo PS, Rafacho BP, Minicucci MF, Chiuso-Minicucci F, Zorzella-Pezavento SG, *et al.* Atrophic cardiac remodeling induced by taurine deficiency in Wistar rats. PLoS One 2012;7:e41439.
110. Das J, Ghosh S, Sil PC. Taurine and cardiac oxidative stress in diabetes. Diabetes. Academic Press: Elsevier; 2020. p. 36172
111. Lusis AJ. Atherosclerosis. Nature 2000;407:233-41.
112. Niu LG, Zhang MS, Liu Y, Xue WX, Liu DB, Zhang J, *et al.* Vasorelaxant effect of taurine is diminished by tetraethylammonium in rat isolated arteries. Eur J Pharmacol 2008;580:169-74.
113. Alfieri RR, Cavazzoni A, Petronini PG, Bonelli MA, Caccamo AE, Borghetti AF, *et al.* Compatible osmolytes modulate the response of porcine endothelial cells to hypertonicity and protect them from apoptosis. J Physiol 2002;540:499-508.
114. Li W, Yang J, Lyu Q, Wu G, Lin S, Yang Q, *et al.* Taurine attenuates isoproterenol-induced H9c2 cardiomyocytes hypertrophy by improving antioxidative ability and inhibiting calpain-1-mediated apoptosis. Mol Cell Biochem 2020;469:119-32.
115. Liu J, Ai Y, Niu X, Shang F, Li Z, Liu H, *et al.* Taurine protects against cardiac dysfunction induced by pressure overload through SIRT1-p53 activation. Chem Biol Interact 2020;317:108972.
116. Hou X, Sun G, Guo L, Gong Z, Han Y, Bai X. Cardioprotective effect of taurine and β-alanine against cardiac disease in myocardial ischemia and reperfusion-induced rats. Electron J Biotechnol 2020;45:46-52.

Original Article

Comparative Study of Prenatal Diagnosis by Karyotype and Microarray in Cases of Balanced Translocation Carriers of Parents and Finding in Fetuses

Brijesh Kumar, Meenu Singh, Rakesh Kumar Verma[1], Navneet Kumar[1]

Department of Biotechnology, IILM College of Engineering and Technology, Greater Noida, [1]Department of Anatomy, King George Medical University, Lucknow, Uttar Pradesh, India

Abstract

Background: The prenatal diagnosis was carried out to analyze the results providing scientific clinical guidance for prenatal screening. Furthermore, analysis of women in progressive maternal stage helped in finding out the chromosomal abnormalities in the form of translocations. Hence, the objective of the study was to analyze the correlation between clinical indication and chromosomal patterns for translocations in high-risk pregnancies. **Materials and Methods:** A total of 200 women between 21 and 41 years of age who underwent prenatal diagnosis were selected for the study. At the gestation age of 9–20 weeks, they underwent genetic counseling as well. The samples (chorionic villus sampling and amniotic fluid) were collected after consideration of high-risk factor with informed consent. The karyotyping and fluorescent in situ hybridization (FISH) were performed to find out the any chromosomal translocation and to confirm the type of translocation (balanced and unbalanced) microarray technique was used. **Results:** Results indicated that 5 out of 200 cases were reported for balanced translocation, in which one case was reported for balanced translocation between chromosomes 13 and 22 in karyotype while the FISH and microarray results were normal. In the second case, a translocation between chromosomes 13 and 20 was found, the FISH was normal and the microarray showed arr20q11.2(29,835,035-30,117,285) x3 with a variant of uncertain significance. The third case was reported for translocation between chromosomes 13 and 15, the fourth case was reported for balanced translocation between chromosomes 3 and 9, whereas the fifth case was reported for balanced translocation between chromosomes 2 and 20. **Conclusions:** To be concluded, 2.5% of women were recorded for balanced translocation 3 out of 5 translocation cases indicated the balanced translocation to be coming from the parents either mother or father. Clinical indications after karyotype results showed translocations in all cases which were transferred from parents, but in two cases, the balanced translocation was observed for the first time, and it is called *de novo*. In this case, the parent did not contribute to the balanced translocation, and it may be due to abnormal gametogenesis.

Keywords: *Fetus, karyotype analysis, prenatal diagnosis, prenatal screening*

Introduction

Prenatal diagnosis is a type of testing to detect the genetic as well as other pathophysiological conditions in an unborn fetus or embryo. The practice was first performed using karyotype analysis of cultured amniotic cells by Steele and Breg in 1966.[1] The technique of chromosome banding was confirmed by Craig and Bickmore in 1993.[2] The main aim of such prenatal diagnosis is to detect the birth defects if any, such as neural tube defects, chromosomal abnormalities (change in number and structure), genetic diseases, and other pathological conditions associated with the fetus. Amniotic fluid and chorionic villus are the main source of samples for prenatal diagnosis. On the other hand, product of conception is another source of sample for testing the abnormality associated with the fetus to rule out the reason behind the recurrent miscarriage to normal parents. Approximately 2.5% of infants are born with congenital anomalies, which accounted for 8%–15% of perinatal deaths and 13%–16% of mortality in India.[3] Moreover, chromosomal abnormalities found in infants can be structural or numerical. The numerical chromosomal abnormalities may be associated with sex chromosome or autosomes (monosomies, trisomies, diploidy, triploidy, tetraploidy, etc.) and

How to cite this article: Kumar B, Singh M, Verma RK, Kumar N. Comparative study of prenatal diagnosis by karyotype and microarray in cases of balanced translocation carriers of parents and finding in fetuses. J Anat Soc India 2025;74:104-9.

Article Info

Received: 20 October 2022
Revised: 21 May 2025
Accepted: 23 May 2025
Available online: 30 June 2025

Address for correspondence:
Brijesh Kumar,
IILM College of Engineering and Technology, Greater Noida, Uttar Pradesh, India.
E-mail: brijlpl@gmail.com

Access this article online

Website: https://journals.lww.com/joai

DOI: 10.4103/jasi.jasi_147_22

Quick Response Code:

structural abnormalities comprise addition, deletion, translocation, inversion, insertion, etc., Studies show the rate of point mutation is slightly higher in sperms of older fathers, whereas the risk for trisomies significantly increases with advanced maternal age.[4] Other than that, principal indications for prenatal diagnosis are advanced maternal age (>35 years or older at the time of delivery), previous child with *de novo* chromosomal aneuploidy, presence of structural chromosome abnormality in either of the parents, family history of a genetic disorder that may be diagnosed or ruled out by biochemical or DNA analysis, family history of an X-linked disorder, risk of neural tube defects, abnormal maternal serum screening, and ultrasound examination.[4-7] Prenatal diagnosis is important for screening of congenital malformations or disorders and other genetic diseases which may also help to understand the prognosis of the disease and treatment options if any. If this is untreatable, then medical termination process is an option that may be advised by the clinician. Hence, the prenatal cytogenetic studies help to screen the chromosomal abnormalities using karyotyping and fluorescent *in situ* hybridization (FISH) with available probes (13, 18, 21, X, Y, etc.) and microarray from amniotic fluid, chorionic villus samples, and blood samples.

Since genetic diseases are not curable, testing can offer early prevention and increased surveillance.[8] The population of India has diverse ethnicity at the level of cultural, religious, and social background. Due to diverse ethnicity in India, some communities have a very high load of genetic variation and particular disorders.[9]

This happens because of consanguineous marriages between close relatives in certain communities, high birth rate, poor diagnostic facilities, and lack of expertise in genetic counseling.[10,11]

The main objective of this study was to find chromosomal abnormalities in amniotic fluid and chorionic villus sampling (CVS) from high-risk pregnancies, to analyze the abnormal chromosomal pattern in the fetus with respect to their parents, and to increase the knowledge and scope to simplify accurate genetic diagnosis of unborn fetuses.

Materials and Methods

Sample selection

After confirmation of pregnancies, subsequent counseling was done to obtain preliminary data of patient like indication and family medical history and relevant medical information. After considering high-risk pregnancy, written consent was obtained from patients. CVS samples were collected at a gestation age of 10–12 weeks, and amniotic fluids were collected at 16–18 weeks. The CVS and amniotic fluids were used for the cell culture for karyotyping and FISH. For karyotyping, the chromosomes were isolated from metaphase of the cell. To get metaphase, amniotic cells and CVS must go under mitosis cell division process. Metaphase is the stage of cell cycle in which the chromosomes assume their characteristic condensed and discrete shape.

Sample preparation

Subsequent processing of samples involved tissue culturing, harvesting, slide preparation to obtain metaphase, and Giemsa-Trypsin-Giemsa (GTG) banding. After final preparation of slide, the karyotype was done to analyze the results. In the current study, the standard method for karyotyping (GTG banding method) was used in which for normal cell lines 20 karyotypes were counted, whereas for mosaic cell lines, 50 karyotypes were counted to confirm the mosaicism. The trypsin was used to digest the protein (heterochromatin and euchromatin) following staining in which the slides were stained with Giemsa. Moreover, when chromosome banding is performed by this method, it gives pattern of light and dark bands, and this allows the identification of abnormalities in the number or morphology of chromosomes.[12] Furthermore, analysis was performed using an automated karyotype system using the light microscope with ×10 to ×100.

Interphase Fluorescence *in situ* hybridization (I-FISH)

The amniotic and chorionic cells were used for interphase FISH. A set of FISH probes for chromosomes 13, 18, 21 and X, Y (VYSIS Aneuvysion Probe Kit) were used for screening.[12]

Chromosome analysis

A standard karyotype with good banding resolution of 350–450 band level was achieved for the study.[13] Nomenclature for chromosomal aberration that is numerical or structural was done by the International System for Human Cytogenomic Nomenclature (ISCN) method.[14,15] After subsequent analysis compilation of comprehensive data, it was correlated with the referral risk factors. Analysis of FISH slides for aneuploidy was done by the standard pattern of the FISH probe. Blood samples from the couples were also cultured in PB Max media for karyotype. ISCN 2016 has been used as a reference for karyotyping.

Chromosomal microarray

Chromosomal microarray was performed on prenatal samples (amniotic fluid and chorionic villus) using CytoScan 750K Array microarray chip. The arrays used included the loss of heterozygosity determination and detection of uniparental isodisomy. Analysis was done using the Chromosome Analysis Suite software [Figure 1].

Results and Discussion

In the present study, 200 cases were analyzed by karyotype as well as by FISH simultaneously. In this analysis, 31 cases were identified as abnormal by karyotype and 19 cases were found abnormal by FISH [Figure 2]. In karyotype study; eleven cases for trisomy (9 cases for trisomy 21 , one case for trisomy 13 and one case for trisomy 18), three cases for

monosomy X, two cases for chromosome inversion 9, two cases for chromosome inversion Y, two cases of abnormal mosaic (one for 25% cell tetraploid & 75% cells normal, and other for 12% cells trisomy 21 & 88% cells normal 21), four cases for balanced translocation (Chromosome 13 & 22, in which mother is carrier and another for Chromosome 3 & 9, in which father is carrier, Chromosome 13 & 20, in which mother is carrier, Chromosome 2 & 12, in which fetus is effected), one case for triploidy, one case for Robertsonian translocation (Chromosome 13 & 15) and one case for chromosome 15ps+ , one case for chromosome tetrasomy 9p, one case for Klinefelter syndrome , one case for super female with 21ps+ , one case for inversion chromosome 8 were found [Figure 3].

In the FISH study, 11 cases were found of trisomy, 3 cases of monosomy X, 2 cases of abnormal mosaic and 1 case of triploidy, 1 case of Klinefelter, 1 case of super female with 21ps+ were found. The comparative studies of selected cases for abnormalities are listed in Table 1.

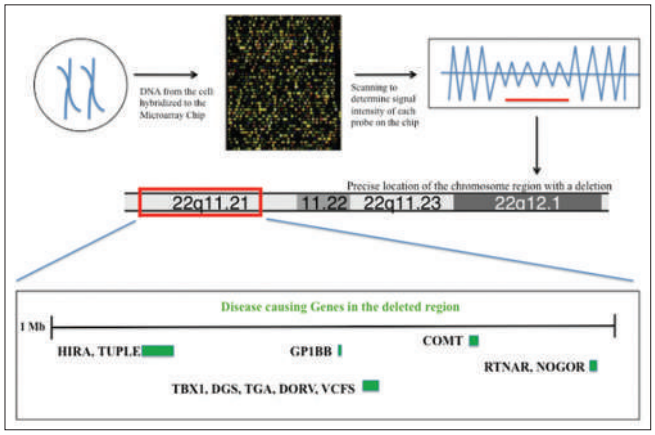

Figure 1: Microarray technique

The comparative analyses of cases of balanced translocation confirmed from karyotype, FISH, and microarray are listed in Table 2.

The balanced translocation was reported in 5 samples out of 200 and the women with this translocation ranged between the age of 27 and 35 years. The karyotype confirmed abnormalities for all five cases while the samples were found normal in FISH. The microarray of samples showed the normal copy number profile for case#17 (age 35 years), and on the other hand, case#64 (age 30 years), case# 81 (age 33), and case#184 (age 30) were reported for balanced translocation while case#181 (age 27 years) was reported as a variant of uncertain significance (arr 20q11.2 (29,835,035-30,117,285) x3) (human genome build: hg19). Moreover, case#17, 64, and 181 were reported to be inherited. Case#81 (age 33 years) and case# 184 (age 30 years) suggested that the parent karyotype was normal, but the child was carrying the balanced translocation and hence it is called *de novo.*

A total of five cases were reported for balanced translocation, of which three cases were inherited while two cases were observed as *de novo* where parent karyotype was normal. Chromosomal abnormality is one of the major causes of recurrent abortions; however, genetic testing is routinely suggested after two or three consecutive abortions. The presence or absence of genomic imbalance, when confirmed early using high-resolution genetic analysis like CMA, can avoid trauma and distress in couples. Conventional karyotyping is informative for microscopic genomic imbalance but also has its own limitations that we cannot get information about the microdeletions and microduplications. Hence, we recommend including chromosomal microarray even for the first pregnancy loss to rule out cryptic translocation or submicroscopic deletions and duplications.

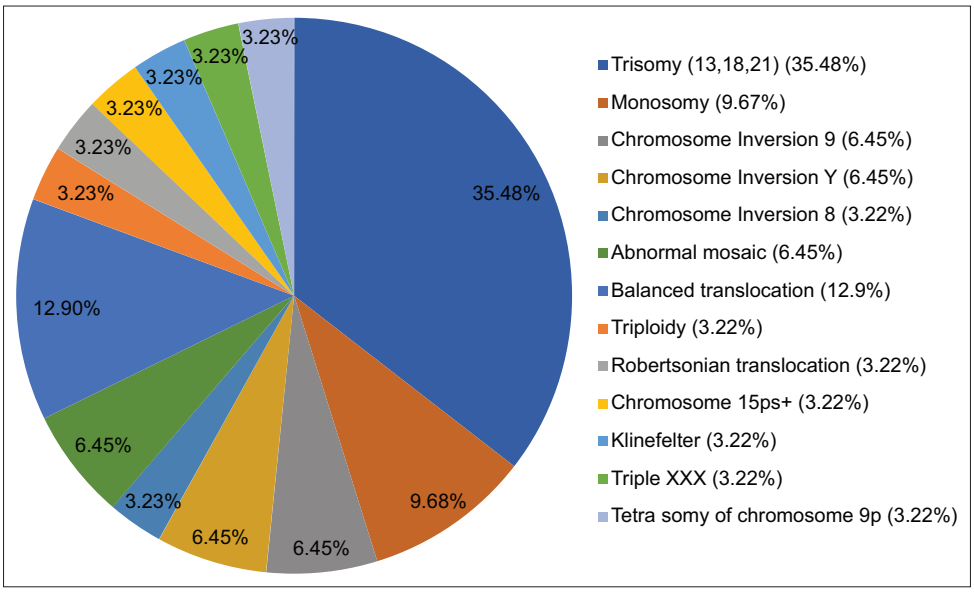

Figure 2: Distribution of chromosomal abnormalities by karyotype

The chromosomal microarray is reported to be a reliable and comprehensive technique with higher success rates for detecting genomic imbalance in products of conception.[16,17]

Previous studies showed that deletions were generally detected more frequently than duplications which were associated with less severe phenotype and were therefore less likely to be referred in postnatal setting.[18,19]

There were dozens of *de novo* and rare inherited copy number variants identified to be associated with autism through large-scale genome-wide studies involving more than thousands of families of primarily European ancestry.[20-22] The most common variants were the 16p11.2 deletion and duplication, the 7q11.23 duplication, the 15q11-q13 duplication, the 1q21.1 duplication, the 3q29 deletion, the 22q11.2 deletion and duplication, and the deletion at 2p16.3 (Pitt-Hopkins-like syndrome 2).[22] These variants together accounted for approximately 4% of autism spectrum disorder (ASD) cases.[22,23] A few studies have also looked into the variants related to ASD or developmental delay in Chinese populations, with 11-19% detection rate for pathogenic variants.[24-29] The comparative analysis of our findings with another researcher is provided in Table 3. The present study shows less percentage of chromosomal abnormality in comparison to another researcher [Table 3], as here in this study, only balanced translocation cases have been considered inherited from parent to fetus and

Table 1: Comparative studies of karyotype and fluorescent *in situ* hybridization

Types of abnormalities	Methods	
	Karyotype (31 cases)	FISH (19 cases)
Trisomy		
Trisomy 21	9 (abnormal)	9 (abnormal)
Trisomy 18	1 (abnormal)	1 (abnormal)
Trisomy 13	1 (abnormal)	1 (abnormal)
Monosomy X	3 (abnormal)	3 (abnormal)
Chromosome inversion 9	2 (abnormal)	2(normal)
Chromosome inversion Y	2 (abnormal)	2 (normal)
Chromosome inversion 8	1 (abnormal)	1 (normal)
Abnormal mosaic	2 (abnormal)	2 (abnormal)
Balanced translocation	4 (abnormal)	4 (normal)
Triploidy	1 (abnormal)	1 (abnormal)
Robertsonian translocation	1 (abnormal)	1 (normal)
Chromosome 15ps+	1 (abnormal)	1 (normal)
Klinefelter	1 (abnormal)	1 (abnormal)
Triple XXX with 21ps+	1 (abnormal)	1 (abnormal)
Tetrasomy of chromosome 9p	1 (abnormal)	1 (normal)

FISH: Fluorescent *in situ* hybridization

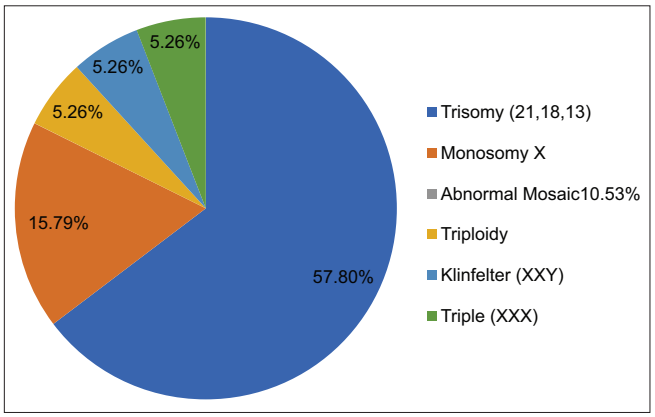

Figure 3: Distribution of chromosomal abnormalities by fluorescent *in situ* hybridization

Table 2: Comparative studies of karyotype, fluorescent *in situ* hybridization, and microarray for balanced chromosomal abnormality

Case number	Age (years)	Test performed	Type of sample	Karyotype	FISH	Microarray	Interpretation	Clinical indications
17	35	Karyotype + FISH + CMA	CVS	Abnormal	Normal	Normal copy number profile by array	Balanced translocation (13 and 22)	Mother carrier of balanced translocation (13 and 22) (inherited)
64	30	Karyotype + FISH + CMA	CVS	Abnormal	Normal	Normal copy number profile by array	Translocation between chromosomes 3 and 9	Father carrier for balanced translocation (inherited)
81	33	Karyotype + FISH	Amniotic fluid	Abnormal	Normal	Normal copy number profile by array	Robertsonian carrier between chromosomes 13 and 15	Abnormal maternal serum screening parent karyotype was normal (*de novo*)
181	27	Karyotype + FISH + CMA	CVS	Abnormal	Normal	Arr 20q11.2 (29,835,035–30,117,285) × 3 variant of uncertain significance	Balanced translocation chromosomes 13 and 20	Mother have balanced translocation chromosomes 13 and 20 (inherited)
184	30	Karyotype + FISH + CMA	Amniotic fluid	Abnormal	Normal	Normal copy number profile by array	Balanced translocation chromosomes 2 and 12	Abnormal Maternal serum screening parent karyotype was normal (*de novo*)

FISH: Fluorescent *in situ* hybridization, CMA: Chromosomal microarray analysis, CVS: Chorionic villus sampling

Table 3: Comparative analysis of cytogenetic balanced chromosomal abnormality

Author	Year	Population	Study type	Chromosomal abnormality (%)
Petrosky and Borgaonkar[30]	1984	UK	6q translocations	48.28
Choi *et al*.[31]	2014	Korea	Autosomal trisomy	43-54
Polipalli *et al*.[32]	2016	North India	Robertsonian translocation	10.6
Pandey *et al*.[33]	2017	North India	Robertsonian translocation	4.7
Li *et al*.[34]	2017	China	Abnormal karyotype	27.72
Shi *et al*.[35]	2019	China	Balanced translocations	22.5
Present study	2022	North India	Balanced translocation	2.5

de novo cases which are first time observed in fetus due to abnormal gametogenesis.

In view of the consecutive abnormal pregnancies mentioned in this study, we strongly recommend prenatal diagnosis for all individuals with balanced chromosome rearrangement. With the development of preimplantation genetic diagnosis for chromosomal rearrangement, new data concerning segregation modes in female translocation carriers are emerging. *In vitro* fertilization with preimplantation genetic diagnosis is currently being offered to carriers of balanced translocations increasing their chances of conceiving and decreasing the probability of miscarriages.

Conclusions

Overall, this study involving 200 prenatal cases who underwent prenatal diagnosis using karyotyping, FISH, and microarray analysis aimed at understanding the relative role/importance of various techniques involved in prenatal diagnosis and discovering the pattern/s of genetic abnormalities. The study highlights the role of microarrays in identifying, confirming, and differentiating balanced and unbalanced translocations as discovered through karyotyping which remains the main technique for identifying balanced translocation. FISH is a supporting technique for faster identification of common aneuploidies in chromosomes 13, 18, and 21 and sex chromosomes. The study presents another evidence of the relative distribution of various aneuploidies. Further studies involving quantitative fluorescent polymerase chain reaction, exome, and genome sequencing can add more insights for prenatal diagnosis. Identification of prenatal abnormalities and their further classification into inherited and *de novo* by comparing the results of parental genetic studies is helpful in-patient counseling and planning the course of actions for future pregnancies. Choices related to preimplantation genetic studies are also guided by the results of prenatal diagnosis in previous pregnancies including cases of pregnancy loss. There is a case for application of multiple technologies in prenatal diagnosis to address various prenatal conditions and offer options of clinicians and parents.

Limitations

The test results show the variability with standard error at 95% confidence level. Whether for the numerical chromosomal anomalies there are many techniques available, the structural chromosomal aberrations, rarely found, can raise different problems for a correct diagnosis and an accurate genetic counseling. Regarding the structural chromosomal anomalies, the most important aspect is about the viability of the fetus, depending on the chromosome(s) involved, the type of anomaly, and the size of the defect. For these cases, in some situations, additional investigations should be performed, as a more comprehensive molecular characterization is essential. The genetic investigations must be associated with ultrasound evaluation.

Acknowledgments

The authors are grateful to the Department of Biotechnology, IILM, Greater Noida, and Advanced Genomics Institute and Laboratory Medicine, New Delhi, for providing facility to complete the research work.

Financial support and sponsorship

Nil.

Conflicts of interest

There are no conflicts of interest.

References

1. Steele MW, Breg WR Jr. Chromosome analysis of human amniotic-fluid cells. Lancet 1996;1:383-5.
2. Craig JM, Bickmore WA. Chromosome bands – Flavours to savour. Bioessays 1993;15:349-54.
3. Ravikumara M, Bhat BV. Early neonatal mortality in an intramural birth cohort at a tertiary care hospital. Indian J Pediatr 1996;63:785-9.
4. Parker MJ, Budd JL, Draper ES, Young ID. Trisomy 13 and trisomy 18 in a defined population: Epidemiological, genetic and prenatal observations. Prenat Diagn 2003;23:856-60.
5. Bernard JP, Suarez B, Rambaud C, Muller F, Ville Y. Prenatal diagnosis of neural tube defect before 12 weeks' gestation: Direct and indirect ultrasonographic semeiology. Ultrasound Obstet Gynecol 1997;10:406-9.
6. Nicolaides KH. Screening for chromosomal defects. Ultrasound Obstet Gynecol 2003;21:313-21.
7. Moore JW, Binder GA, Berry R. Prenatal diagnosis of aneuploidy and deletion 22q11.2 in fetuses with ultrasound detection of cardiac defects. Am J Obstet Gynecol 2004;191:2068-73.
8. Purandarey H, Chakravarty A. Human Cytogenetics Techniques and Clinical Application. 1st ed. Delhi: Bhalani Publishing House; 2000. p. 85-117.
9. Adiga SK, Kalthur G, Kumar P, Girisha KM. Preimplantation diagnosis of genetic diseases. J Postgrad Med 2010;56:317-20.

10. Thompson MW, McInnes RR, Willard HF. Genetics in Medicine. 5th ed. Philadelphia: WB Saunders; 1991. p. 45-84.
11. Krishna U, Dafftary S. Pregnancy at risk: Current concepts Federation of Obstetric and Gynaecological Societies of India (FOGSI) 1993:pp. 157-66.
12. Jobanputra V, Sobrino A, Kinney A, Kline J, Warburton D. Multiplex interphase FISH as a screen for common aneuploidies in spontaneous abortions. Hum Reprod 2002;17:1166-70.
13. Karaoguz MY, Bal F, Yakut T, Ercelen NO, Ergun MA, Gokcen AB, *et al.* Cytogenetic results of amniocentesis materials: Incidence of abnormal karyotypes in the Turkish collaborative study. Genet Couns 2006;17:219-30.
14. Shaffer LG, Slovak ML, Campbell LJ. ISCN: An international system for human cytogenetic nomenclature. Journal of Histochemistry & Cytochemistry, 2009;57:991-3.
15. Shaffer LG, McGowan-Jordan J, Schmid M. (Eds.). ISCN 2013: an international system for human cytogenetic nomenclature Karger Medical and Scientific Publishers. 2013.
16. Levy B, Sigurjonsson S, Pettersen B, Maisenbacher MK, Hall MP, Demko Z. Genomic imbalance in products of conception: Single-nucleotide polymorphism chromosomal microarray analysis. Obstet Gynecol 2014;124:202-9.
17. Zhu X, Li J, Zhu Y, Wang W, Wu X, Yang Y, *et al*. Application of chromosomal microarray analysis in products of miscarriage. Mol Cytogenet 2018;11:44.
18. Park SJ, Jung EH, Ryu RS, Kang HW, Ko JM, Kim HJ, *et al.* Clinical implementation of whole-genome array CGH as a first-tier test in 5080 pre and postnatal cases. Mol Cytogenet 2011;4:12.
19. Turner DJ, Miretti M, Rajan D, Fiegler H, Carter NP, Blayney ML, *et al*. Germline rates of *de novo* meiotic deletions and duplications causing several genomic disorders. Nat Genet 2008;40:90-5.
20. Marshall CR, Noor A, Vincent JB, Lionel AC, Feuk L, Skaug J, *et al.* Structural variation of chromosomes in autism spectrum disorder. Am J Hum Genet 2008;82:477-88.
21. Pinto D, Pagnamenta AT, Klei L, Anney R, Merico D, Regan R, *et al.* Functional impact of global rare copy number variation in autism spectrum disorders. Nature 2010;466:368-72.
22. Sanders SJ, He X, Willsey AJ, Ercan-Sencicek AG, Samocha KE, Cicek AE, *et al*. Insights into autism spectrum dis-order genomic architecture and biology from 71 risk loci. Neuron 2015;87:1215-33.
23. Guo H, Peng Y, Hu Z, Li Y, Xun G, Ou J, *et al.* Genome-wide copy number variation analysis in a Chinese autism spectrum disorder cohort. Sci Rep 2017;7:44155.
24. Chan PY, Luk HM, Lee FM, Lo IF. Genetic profile and clinical application of chromosomal microarray in children with intellectual disability in Hong Kong. Hong Kong Med J 2018;24:451-9.
25. Chong WW, Lo IF, Lam ST, Wang CC, Luk HM, Leung TY, *et al.* Performance of chromosomal microarray for patients with intellectual disabilities/developmental delay, autism, and multiple congenital anomalies in a Chinese cohort. Mol Cytogenet 2014;7:34.
26. Gazzellone MJ, Zhou X, Lionel AC, Uddin M, Thiruvahindrapuram B, Liang S, *et al*. Copy number variation in Han Chinese individuals with autism spectrum disorder. J Neurodev Disord 2014;6:34.
27. Tao VQ, Chan KY, Chu YW, Mok GT, Tan TY, Yang W, *et al*. The clinical impact of chromosomal microarray on paediatric care in Hong Kong. PLoS One 2014;9:e109629.
28. Wang B, Ji T, Zhou X, Wang J, Wang X, Wang J, *et al*. CNV analysis in Chinese children of mental retardation highlights a sex differentiation in parental contribution to *de novo* and inherited mutational burdens. Sci Rep 2016;6:25954.
29. Franssen MT, Korevaar JC, van der Veen F, Leschot NJ, Bossuyt PM, Goddijn M. Reproductive outcome after chromosome analysis in couples with two or more miscarriages: Index [corrected]-control study. BMJ 2006;332:759-63.
30. Petrosky DL, Borgaonkar DS. Segregation analysis in reciprocal translocation carriers. Am J Med Genet 1984;19:137-59.
31. Choi TY, Lee HM, Park WK, Jeong SY, Moon HS. Spontaneous abortion and recurrent miscarriage: A comparison of cytogenetic diagnosis in 250 cases. Obstet Gynecol Sci 2014;57:518-25.
32. Polipalli SK, Karra VK, Jindal A, Puppala M, Singh P, Rawat K, *et al.* Cytogenetic analysis for suspected chromosomal abnormalities; a five years experience. J Clin Diagn Res 2016;10:C01-5.
33. Pandey P, Verma RK, Kumar N, Koonwar S. Autosomal trisomy: A cytogenetic study in Lucknow Region. J Anat Sci 2017;25:37-43.
34. Li L, Wang R, Yu Y, Xi Q, Liu M, Liu R. Chromosomal translocations detected by prenatal and postnatal genetic diagnosis: Our experience. Int J Clin Exp Med 2017;10:10928-35.
35. Shi Y, Ma J, Xue Y, Wang J, Yu B, Wang T. The assessment of combined karyotype analysis and chromosomal microarray in pregnant women of advanced maternal age: A multicenter study. Ann Transl Med 2019;7:318.

Original Article

The Protective Effect of Melatonin against Monosodium Glutamate-induced Hippocampal Injury: Focused on Regulating the Nrf2/Heme Oxygenase 1 and nuclear factor-kappa β/Tumor Necrosis Factor-α/Caspase 3 and Brain Derived Neurotrophic Factor Signaling Pathways in Rat Model

Maha M. Amer[1,2], Samah Mohammed Mahmoud Abozaid[3], Eman Ali Abd El-Meguid[4], Hanan S Seleem[5], Mohamed R. Abdel-Hamed[1,2]

[1]Department of Anatomy and Embryology Faculty of Medicine, Ain Shams University, Cairo, [3]Department of Human Anatomy and Embryology, Faculty of Medicine, Minia University, Minia, [4]Department of Anatomy and Embryology, Faculty of Medicine, Fayoum University, Fayoum, [5]Department of Histology and Cell Biology, Faculty of Medicine, Menoufia University, Shebin Elkoum-Menoufia, Egypt, [2]Department of Anatomy and Histology, College of Medicine, Qassim University, Buraydah, Saudi Arabia

Abstract

Background: Monosodium glutamate (MSG) is a fine white crystalline material. It is added to many numerous types of food as it improves the flavor of many processed products. However, a number of studies documented systemic detrimental effects. **Aims:** The current research investigated the histological and immunohistochemical changes that may develop in rat cornu ammonis (CA) 1, CA3 hippocampus, and dentate gyrus (DG) experimentally exposed to MSG and the possible neuroprotective role of melatonin. **Materials and Methods:** Thirty-two male albino rats were allocated randomly into four equal groups; the control group, melatonin-treated group, received IP injections of melatonin (6 mg/kg/day), MSG-treated group injected IP with MSG (4 mg/kg/day), and MSG + melatonin-treated group injected IP the aforementioned dose of MSG accompanied with melatonin for 14 days. The brains were carefully dissected and sectioned for the staining with hematoxylin and eosin, Cresyl violet, and immunohistochemical staining. **Results:** The data of the current research showed that IP administration of MSG decreased the number of pyramidal cell layers in CA1 and CA3 areas of the hippocampus due to neuronal cell death. In addition DG neurons revealed granular cells with shrunken cell bodies, deeply stained cytoplasm, and pyknotic nuclei with some areas of cellular loss. **Conclusion:** The current study's findings demonstrate the neuroprotective benefits of melatonin, a naturally occurring antioxidant that restores normal redox activity and improves cells regeneration.

Keywords: *Hippocampus, melatonin, monosodium glutamate, neurotoxicity*

Introduction

Monosodium glutamate (MSG) is a fine white crystalline material that resembles sugar and sodium chloride in appearance. It is added to many numerous types of food in varying amounts.[1] As it improves the flavor of many processed food by making them taste better. Nonetheless, a number of studies documented systemic detrimental effects.[2]

Inside the human body, MSG dissociates into sodium and glutamate ions. Glutamate is a nonessential amino acid and acts as an excitatory brain neurotransmitter.[3] It is found in high concentration in regions of the brain that is important in mediating cognition, such as the cerebral cortex, hippocampus, and striatum.[4] In addition, it plays a major role in synaptic plasticity, learning, and developmental processes[5] and is a precursor for the synthesis of glutathione.[6]

N-methyl D aspartate receptors are influenced by glutamate.[7] It plays significant roles in numerous brain activities, particularly memory, cognition, and learning.[8] However, elevated glutamic acid content due to dietary intake injures brain tissues.[9]

Yap *et al*.[3] also reported that excess brain glutamate content has been linked to several neurodegenerative disorders, including Alzheimer's, Parkinson's, and multiple sclerosis. These disorders are caused by long-term increases in oxidative stress triggered by excess glutamate levels.

Glutamate over-activates excitatory amino acid receptors with subsequent increased

How to cite this article: Amer MM, Abozaid SM, El-Meguid EA, Seleem HS, Abdel-Hamed MR. The protective effect of melatonin against monosodium glutamate-induced hippocampal injury: Focused on regulating the Nrf2/heme oxygenase 1 and nuclear factor-kappa β/tumor necrosis factor-α/caspase 3 and brain derived neurotrophic factor signaling pathways in rat model. J Anat Soc India 2025;74:110-23.

Article Info

Received: 26 October 2024
Revised: 31 January 2025
Accepted: 19 February 2025
Available online: 30 June 2025

Address for correspondence:
Dr. Samah Mohammed Mahmoud Abozaid, Department of Human Anatomy and Embryology, Faculty of Medicine, Minia University, Minia, Egypt.
E-mail: samah.abozaid@mu.edu.eg

Access this article online

Website: https://journals.lww.com/joai
DOI: 10.4103/jasi.jasi_172_24
Quick Response Code:

level of intracellular calcium, which triggers a cascade of enzymatic activities leading to neurotoxicity and cell death, particularly neurons of the hypothalamus and hippocampus.[10]

The hippocampus is a part of the limbic system. It is responsible for memory and learning.[11] The laminar organization is similar in all the fields of the hippocampus. The cornu ammonis (CA) regions are constructed of three clearly defined layers: polymorphic, pyramidal, and molecular layers (MLs).[12]

The pineal gland secretes a hormone called melatonin. In addition, melatonin has other numerous natural sources, such as cereals, ginger, olives, tomatoes, walnuts, pineapple, and legumes. Other sources of melatonin include blood lymphocytes, stomach, and retina.[13] The circadian rhythm of biological processes, including sleep and aging, is regulated by melatonin. It also operates the immunological and endocrine systems responses. According to Yu *et al*.,[14] it has anti-aging, antioxidant, anti-inflammatory, and anti-apoptotic properties.[15] According to Reiter *et al*.,[16] melatonin works by enabling cells to resist the harmful impact of free radicals. It has the ability to quickly cross blood–brain barrier, therefore its usefulness as an adjuvant in neurological issues.[17]

The current research was designated to evaluate the histological and immunohistochemical effects of IP administration MSG on the rat hippocampi and to demonstrate the possible neuroprotective effect produced by the concomitant administration of melatonin.

Materials and Methods

Animals

Thirty-two male albino rats (200–250 g) were obtained from animal house and housed in clean cages made of plastic material at 23°C–26°C and at normal light/dark cycle. The animals were nourished with standard diet and water *ad libitum*. The experiment protocol was approved by the ethical committee for animal handling for research work in Faculty of Medicine, Fayoum University (Approval No R556/2024) according to the international guidelines (Act 1986).

Tested compounds

1. MSG: 1 g of MSG in 1 mL of distilled water was dissolved using 99% pure white crystals that were acquired from DØBELLA Food and Beverage, Egypt
2. Melatonin (5 mg): Acquired from Puritan's Pride, located in the European Union. It came in the shape of tablets.

Design of an experiment

Rats were allocated randomly into four groups, with eight rats each:

1. The control group: for 14 days, rats received IP injections 0.1 mL of distilled water
2. Melatonin-treated group: for 14 days, rats received IP injections of melatonin (6 mg/kg/day) dissolved in 2.5% concentrated ethanol
3. MSG-treated group: for 14 days, rats were injected IP with MSG (4 mg/kg/day) dissolved in distilled water
4. MSG + melatonin-treated group: for 14 days, rats were injected IP the aforementioned dose of MSG accompanied with Melatonin.

Sampling

At the end of the experiment, all rats were decapitated under anesthesia, and the skulls were carefully dissected. The brains were carefully dissected for:

Measurements of oxidative stress parameters

Portions of brain tissues were subjected to homogenization in 20% w/v cold potassium phosphate buffer solution (0.01 M, pH 7.4), then centrifugated at 5,000 rpm for ten min at 4°C, to obtain supernatant used for estimation of:

- At 420 nm SOD activity was quantified colorimetrically
- Malondialdehyde (MDA) brain contents as an indices of lipid peroxidation was measured using thiobarbituric acid reacting substance which is displayed as equivalents of (MDA) using 1, 1, 3, 3-tetra methoxy propane as a reference.[18]

Histological studies

Brain tissues were carefully removed, parasagittal sections were cut, fixed in 4% formaldehyde solution for 24 h, dehydrated using a sequence of increasing alcohol concentrations, cleaned with xylene, and then embedded in blocks of paraffin. According to manufacturer guidelines, paraffin-embedded brain blocks were sectioned at a thickness of 4 μm, de-parafinized, and then mounted on glass slides for staining with hematoxylin and eosin (H and E) and cresyl violet.[19]

Immunohistochemical studies

Brains were cut in 4-μm thick sections then placed on positively charged glass, and then went through the de-parafinization and rehydration procedures. Afterwards they were incubated with trypsin followed by being washed with phosphate buffer saline (PBS). Blocking the nonspecific binding of endogenous peroxidase was done by adding Hydrogen peroxidase 3% solution and Ultra V Block.

Brain sections for a whole night were incubated with the primary antibody of rabbit polyclonal anti-glial fibrillary acidic protein (GFAP) antibody (Catalog NO. FNab03426, Wuhan Fine Biotech, Co. China, dilution 1:50) for diagnosis of gliosis, NRF2 antibody (Catalog No. A1244, Abclonal technology, dilution 1:50) as a cellular oxidant regulator, Heme Oxygenase 1 (HO-1) rabbit monoclonal antibody (Catalog No: A19062, Abclonal Technology, dilution 1:50) as antioxidant, rabbit polyclonal tumor necrosis

factor-α (TNF-α) (Catalog No: A11534, Abclonal Technology, dilution 1:100), NF-κB p65 polyclonal antibody (Catalog No. bs-20159R, Bios ANTIBODIES) as indicators of inflammation, rabbit polyclonal anti-caspase 3 (Catalog No. PA1-29157, Thermo Fisher Scientific Biotechnology, dilution 1:100) for the detection of apoptosis.[20]

Following that, wash the sample with PBS and then incubate it for 10 min with the secondary antibody and diaminobenzidine chromogen. Hematoxylin counterstain was applied to sections after they had been cleaned. The primary antibody was not added in the negative controls.

Results

Oxidative stress marker; malondialdehyde and SOD results

The MSG group's brain tissue content of MDA was significantly higher than those of the control groups (all $P < 0.0001$), and the MSG brain tissue concentration of SOD was significantly lower than those of the control groups (all $P < 0.0001$). On the other hand, these assessed markers were considerably improved (both $P < 0.05$) in MSG + melatonin group [Histogram 1a and b].

Histopathological results

Hematoxylin and eosin results

H and E parasagittal sections of the hippocampus proper and the dentate gyrus (DG) of the control group showed that the hippocampus proper was constituted of the CA with its sections, CA1, CA2, CA3, and CA4 zones. DG appeared as an opaque V shaped structure around CA4 region by its open portion. The DG's crest is the point where the supra-and infra-pyramidal blades merge [Figure 1a]. CA1, CA3 and DG were described in each studied group in the current research. Higher magnification of CA1 and CA3 regions in the control group revealed that each region was made up of three distinct layers: polymorphic layer (POL), pyramidal cell layer (PCL) and ML. The PCL of CA1 region is found to be made up of densely packed, uniformly distributed 3–4 compact rows of small pyramidal neurons with little neuropil in between. Each pyramidal cell had a single, rounded central large, vesicular nucleus with prominent nucleoli and scanty cytoplasm [Figure 1b]. However, that of CA3 [Figure 1c] area formed of numerous bigger pyramidal neurons.

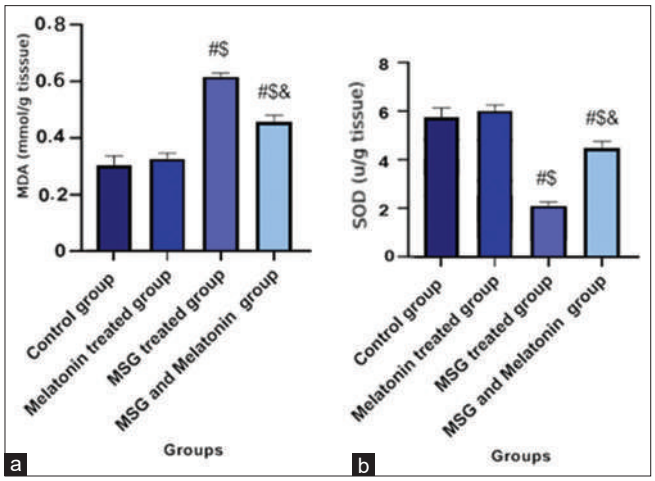

Histogram 1: (a) MDA (mmol/g tissue) and (b) SOD (U/G TISSUE) in the studied groups ($n = 8$). #versus C-group, $versus melatonin group, &versus Monosodium glutamate group, *$P < 0.05$ is significant. Using one-way ANOVA followed by Tukey-Kramer *post hoc* test

Each neuron had a big, vesicular, spherical nucleus with a noticeable nucleolus in the center. The nuclei of sparse neuroglial cells appeared with dark basophilic cytoplasm, tiny, spherical nuclei were noticed scattered on a pink neuropil background [Figure 1b and c]. The neuropil was composed of glial and neuronal cell processes.

The DG is composed of three layers: the POL, the granule cell layer (GCL), and the ML. Dense columns of tiny, spherical granular cells with vesicular nuclei and little interstitial tissue between neurons were diagnostic of the GCL [Figure 1d].

Melatonin-treated group sections revealed nearly similar normal histological structure of the hippocampus proper and the DG to the control group [Figure 2a-d].

In contrast to the control group, the MSG-treated group's hippocampal regions displayed clear histological alterations affecting CA and DG along with a dilatation in the ventricular lumen [Figure 3a]. The PCL in CA1 [Figure 3b] and CA3 [Figure 3c] revealed pyramidal neuron heterogenicity. The majority of small and big pyramidal neurons in PCL showed significant degeneration. The pyramidal neurons showed deeply pigmented pyknotic nuclei, and widely spaced, shrunken cell bodies with pericellular haloes were observed. In addition, clogged blood capillaries were seen. With their big, rounded vesicular nuclei and basophilic cytoplasm, a small number of pyramidal cells seemed to be more or less typical. Higher magnification of DG showed many dark shrunken granular cells with strongly stained basophilic cytoplasm and pyknotic nuclei. A few granular cells are surrounded by pericellular haloes with vacuolated cytoplasm and areas of cellular loss. Vacuolated neuropil also noticed [Figure 3d].

All of the aforementioned histological alterations that occurred in the MSG-treated group were ameliorated in the melatonin- and MSG-treated groups [Figure 4a]. With the exception of a few dispersed degenerated pyramidal neurons with reduced cell bodies, a small number of pyknotic nuclei, and perineural halos, the pyramidal neurons in CA areas seemed to be more or less normal, with basophilic cytoplasm and vesicular nuclei [Figure 4b and c]. The granular cells in DG improved maintaining their typical morphological look; basophilic cytoplasm and vesicular nuclei with a small number of cells encircled by pericellular haloes [Figure 4d].

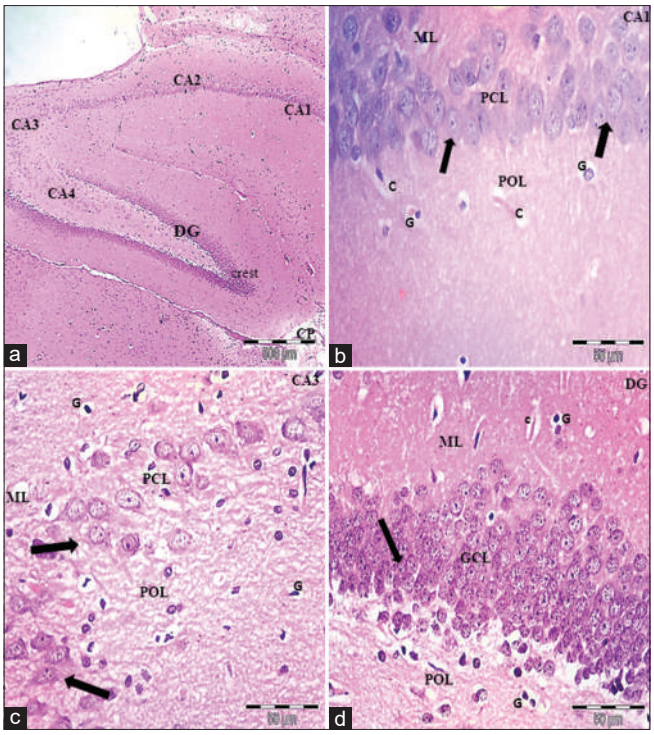

Figure 1: Representative photomicrographs of a parasagittal section of a control rat's hippocampus proper and dentate gyrus (DG). (a) The different areas of the hippocampus proper. The hippocampus is formed of; cornu ammonis (CA) and DG, The CA; CA1, CA2, CA3 and CA4 areas. While, DG a V-shaped structure, surrounding the CA4 area. The choroid plexus of the lateral ventricle can be observed. (b) A higher magnification of CA1 region showing three distinctive layers; molecular layer (ML), pyramidal cell layer (PCL), and polymorphic layer (POL). PCL showing closely packed small pyramidal neurons (thick arrows) with vesicular nuclei, prominent nucleoli, and scanty cytoplasm. (c) A higher magnification of CA3 region showing three layers; ML, PCL and POL. PCL showing the cell bodies of the large pyramidal neurons (thick arrows) with vesicular nuclei, prominent nucleoli, and scanty cytoplasm. (d) A higher magnification of the DG reveals well-defined three layers; ML, granule cell layer (GCL) and POL. The GCL reveals showing vesicular nuclei of the granular cells (thick arrows) arranged in dense columns. Notice the POL and ML display scattered glial cells (g) and normal blood capillaries (c). Scale bar of Figure 1 (a) 500 μm (H and E, ×40) and scale bar of Figure 1 (b-d) 50 μm (H and E, ×400). CA: Cornu ammonis, DG: Dentate gyrus, POL: Polymorphic layer, PCL: Pyramidal cell layer, GCL: Granule cell layer, ML: Molecular layer

Cresyl violet-staining results

Staining with cresyl violet showed both the control group [Figure 5a and b] and the melatonin-treated group [Figure 5c and d] CA1 and CA3 areas displayed the typical morphology of pyramidal cells, which are large conical cells with a clearly defined cell membrane, faintly stained cytoplasm, and a well-defined nucleus. On the other hand, the MSG-treated group displayed neurodegeneration and neuronal death in the form of deformed, shrunk pyramidal cells with uneven borders. In contrast to the other groups, the majority of neurons had dark cytoplasm and pyknotic heterochromatic nuclei that were difficult to distinguish [Figure 5e and f]. The group treated with MSG and melatonin exhibited a reduction in neurodegenerative histological findings, with the majority of pyramidal neurons retaining its normal appearance pattern and only a small number of shrunken degenerated neurons [Figure 5g and h].

Immunohistochemical results

Regarding GFAP immunostaining, astrocytes showed up as thin-processed, star-shaped cells. The control group [Figure 6a and b] and melatonin-treated group [Figure 6c and d] displayed normal distribution GFAP immunoreactivity with mild positive reaction in the astrocytes and their processes among the granular and pyramidal cells in GCL and PCL respectively, along with few scattered astrocytes in ML and POL. However, The MSG-treated group displayed strong GFAP immunoreactivity with numerous bigger astrocytes with thick multiple ramified processes if compared to control and Melatonin groups [Figure 6e and f]. In contrast, the MSG- and melatonin-treated group exhibited tiny astrocytes with short thin few processes when compared to MSG group [Figure 6g and h].

Regarding NRF-2 immunostaining, positive immunoreactivity appeared as brown cytoplasmic/nuclear expression. The control [Figure 7a] and melatonin-treated [Figure 7b] groups showed few sporadic pyramidal neurons with faint cytoplasmic NRF-2 immunoexpression. However, MSG-treated group exhibited numerous pyramidal neurons with strong cytoplasmic and nuclear immunoexpression [Figure 7c]. MSG- and melatonin-treated group revealed few pyramidal neurons with mild cytoplasmic and nuclear expression when compared to MSG group [Figure 7d].

Regarding HO-1 positive immunoreactivity appeared as brown cytoplasmic expression. The control [Figure 8a]

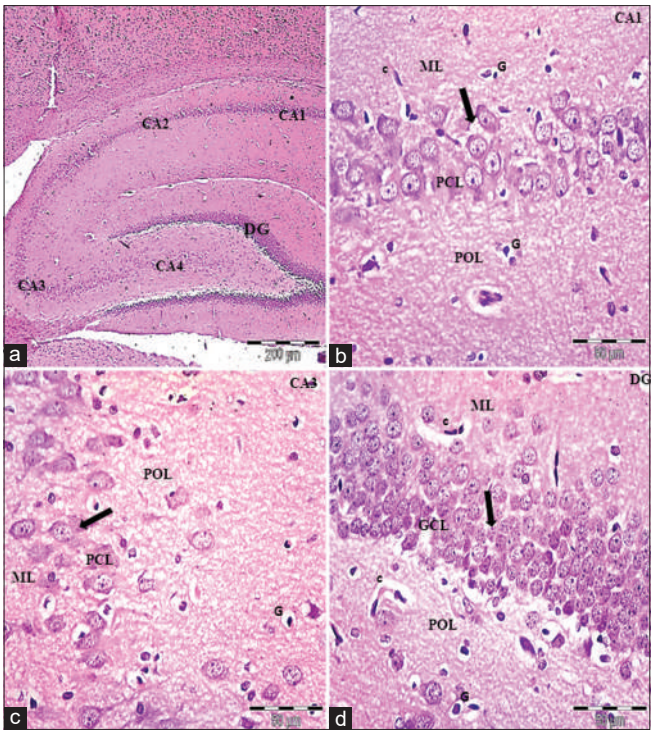

Figure 2: Representative photomicrographs of a parasagittal section of melatonin-treated group rat's hippocampus proper and dentate gyrus (DG). (a) The normal histological structure of the hippocampus proper formed of; cornu ammonis (CA) and DG, The CA; CA1, CA2, CA3 and CA4 areas. While, DG a V-shaped structure, surrounding the CA4 area. (b) A higher magnification of CA1 region showing three distinctive layers; molecular layer (ML), pyramidal cell layer (PCL), and polymorphic layer (POL). PCL showing closely packed small pyramidal neurons (thick arrows) with vesicular nuclei, prominent nucleoli, and scanty cytoplasm. (c) A higher magnification of CA3 region showing three layers; ML, PCL and POL. PCL showing the cell bodies of the large pyramidal neurons (thick arrows) with vesicular nuclei, prominent nucleoli, and scanty cytoplasm. (d) A higher magnification of the DG reveals well-defined three layers; ML, granule cell layer (GCL) and POL. The GCL reveals showing vesicular nuclei of the granular cells (thick arrows) arranged in dense columns. Notice the POL and ML display scattered glial cells (g) and normal blood capillaries (c). Scale bar of Figure 2 (a) 500 µm (H and E, ×40) and scale bar of Figure 2 (b-d) 50 µm (H and E, ×400). CA: Cornu ammonis, DG: Dentate gyrus, POL: Polymorphic layer, PCL: Pyramidal cell layer, GCL: Granule cell layer, ML: Molecular layer

and melatonin-treated [Figure 8b] groups exhibited few pyramidal neurons with faint cytoplasmic expression. However, MSG-treated group exhibited many pyramidal neurons with strong cytoplasmic immunoexpression [Figure 8c]. MSG- and melatonin-treated group revealed some pyramidal neurons with mild weak cytoplasmic expression when compared to MSG group [Figure 8d].

Regarding nuclear factor-kappa β (NF-kβ) immunostaining, positive immunoreactivity appeared as brown cytoplasmic/nuclear expression. The control [Figure 9a] and melatonin-treated [Figure 9b] groups exhibited faint cytoplasmic expression in some pyramidal neurons. However, MSG-treated group exhibited numerous pyramidal neurons with strong cytoplasmic and nuclear immunoexpression [Figure 9c]. MSG- and melatonin-treated group exhibited few pyramidal neurons with mild cytoplasmic and/or nuclear expression when compared to MSG group [Figure 9d].

Regarding TNF-α immunostaining, positive immunoreactivity appeared as brown cytoplasmic expression. The control [Figure 10a] and melatonin-treated [Figure 10b] groups showed a negative cytoplasmic expression in hippocampal pyramidal neurons. MSG-treated group exhibited many pyramidal neurons with strong positive cytoplasmic expression [Figure 10c]. MSG- and melatonin-treated group exhibited few pyramidal neurons with faint cytoplasmic expression when compared to MSG group [Figure 10d].

Regarding activated caspase-3, positive immunoreactivity appeared as brown cytoplasmic/nuclear expression. The control [Figure 11a] and melatonin-treated [Figure 11b] groups showed faint cytoplasmic expression in some pyramidal neurons. However, MSG-treated group exhibited numerous pyramidal neurons with strong cytoplasmic and/or nuclear immunoexpression [Figure 11c]. MSG- and melatonin-treated group exhibited some pyramidal neurons with moderate cytoplasmic expression when compared to MSG group [Figure 11d].

Regarding brain-derived neurotrophic factor (BDNF) immunostaining, positive immunoreactivity appeared as brown cytoplasmic expression. The control [Figure 12a] and melatonin-treated [Figure 12b] groups showed a positive cytoplasmic expression in numerous hippocampal pyramidal neurons. MSG-treated group showed decrease in BDNF immunoreactivity as many pyramidal neurons showed negative cytoplasmic immunoexpression. However, few neurons appeared with faint cytoplasmic immunoexpression

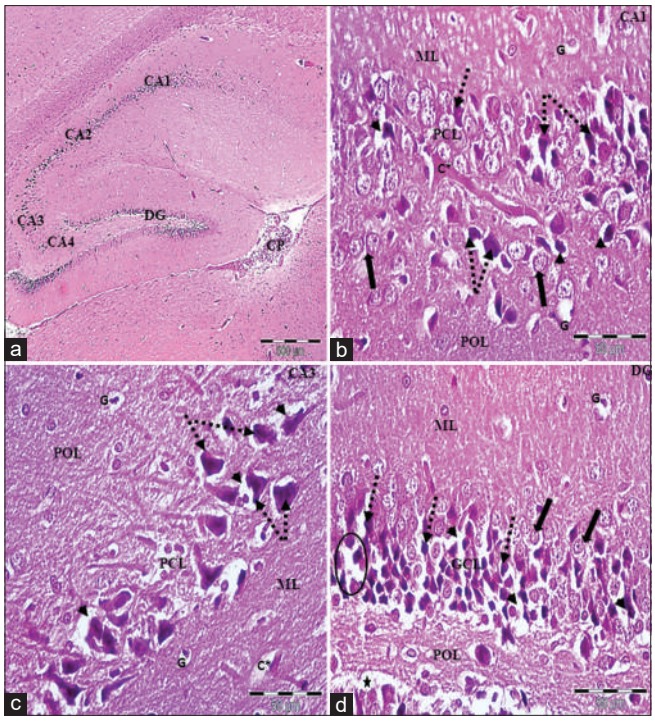

Figure 3: Representative photomicrographs of a parasagittal section of Monosodium glutamate treated group rat's hippocampus proper and dentate gyrus (DG). (a) Disruption of the normal histological structure of the hippocampus cornu ammonis (CA) and DG. The choroid plexus of the lateral ventricle can be noticed. (b) A higher magnification of CA1 region showing some degenerated neurons with shrunken cell bodies, pyknotic nuclei (dotted arrows) surrounded by pericellular halos (arrow heads), others more or less normal with central rounded vesicular nuclei (thick arrows). (c) A higher magnification of CA3 region showing shrunken widely separated most pyramidal cells with deeply stained cytoplasm and pyknotic nuclei (dotted arrows) surrounded by pericellular halos (arrow heads). (d) A higher magnification of the DG reveals most granular cells with shrunken cell bodies, deeply stained cytoplasm and pyknotic nuclei (dotted arrows), some cells surrounded by pericellular haloes (arrow heads), with some areas of cellular loss (circle), other granule cells appear more or less normal. Vacuolated neuropil could be observed (star). Notice the polymorphic layer and molecular layer display scattered glial cells (g) and congested blood capillaries (c*). Scale bar of Figure 3 (a) 500 μm (H and E, ×40) and scale bar of Figure 3 (b-d) 50 μm (H and E, ×400). CA: Cornu ammonis, DG: Dentate gyrus, POL: Polymorphic layer, PCL: Pyramidal cell layer, GCL: Granule cell layer, ML: Molecular layer

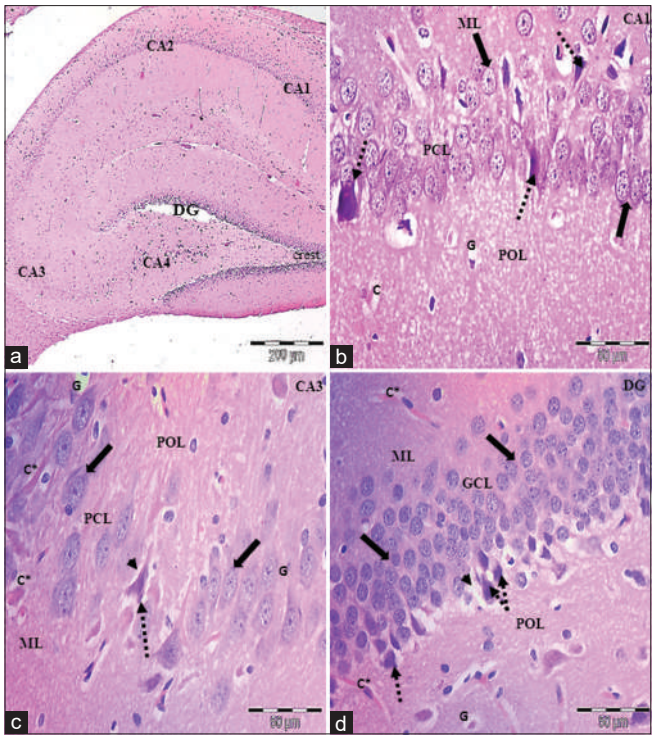

Figure 4: Representative photomicrographs of a parasagittal section of Monosodium glutamate and melatonin-treated group rat's hippocampus proper and dentate gyrus (DG). (a) Preservation of the normal histological structure of the hippocampus cornu ammonis (CA) and DG. (b) A higher magnification of CA1 region showing most of pyramidal neurons appearance more or less normal with basophilic cytoplasm and large central rounded vesicular nuclei (thick arrows). Notice few shrunken cells with pyknotic nuclei (dotted arrows). (c) A higher magnification of CA3 region showing widely separated pyramidal cells; few cells shrunken with deeply stained cytoplasm and pyknotic nuclei (dotted arrows) surrounded by pericellular halos (arrow heads), while others apparently normal (thick arrows). (d) A higher magnification of the DG reveals preserved most granular cells (thick arrows) with some shrunken granular cells with deeply stained cytoplasm and pyknotic nuclei (dotted arrows), some cells surrounded by pericellular haloes (arrow heads). Notice the polymorphic layer and molecular layer display scattered glial cells (g) and congested blood capillaries (c*). Scale bar of Figure 4 (a) 500 μm (H and E, ×40) and scale bar of Figure 4 (b-d) 50 μm (H and E, ×400). CA: Cornu ammonis, DG: Dentate gyrus, POL: Polymorphic layer, PCL: Pyramidal cell layer, GCL: Granule cell layer, ML: Molecular layer

[Figure 12c]. MSG- and melatonin-treated group exhibited restoration of BDNF mild cytoplasmic expression in few pyramidal neurons when compared to MSG group [Figure 12d].

Morphometric results

Histopathological scoring of degenerated pyramidal neurons

The morphometric analysis [Histogram 2a] indicated that there was insignificant difference in the number of the degenerated neurons between control group and melatonin-treated group ($P = 0.919$). In MSG group, there was a significant increase in the number of the degenerated neurons by comparison to the control and melatonin-treated groups (both $P < 0.0001$). The administration of melatonin in MSG and melatonin-treated group resulted in significant decrease in the number of the degenerated neurons if compared to MSG group ($P < 0.0001$) and significant increase by comparison to control and Melatonin groups ($P = 0.0015$, 0.0055 respectively).

The morphometric analysis to assess GFAP, NRF-2, HO-1 immunopositivity [Histogram 2b-d], NF-kβ, TNF-α AND activated caspase-3 [Histogram 3a-c] indicated that there was insignificant difference between control group and melatonin-treated group. MSG group showed a significant increase in immunoreactivity by comparison to both control and melatonin-treated groups. Administration of melatonin in MSG- and melatonin-treated group resulted in significant decrease in immunoreactivity by comparison to the MSG group and significant increase by comparison to control and Melatonin groups.

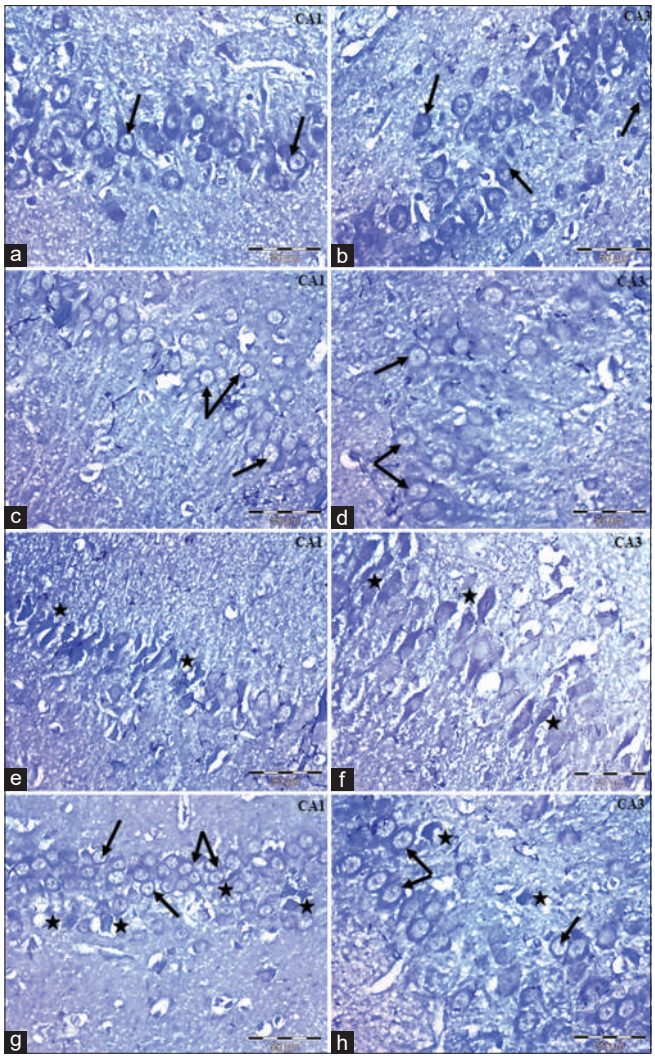

Figure 5: Representative photomicrographs of Cresyl violet stained sections of rat's Cornu ammonis (CA) 1 and CA3 hippocampal regions of all experimental groups. (a and b) CA1 and CA3 of the control group and (c and d) CA1 and CA3 of the melatonin-treated group display normal healthy pyramidal neurons with well-defined cell membrane, lightly colored cytoplasm and a well delineated nuclei (arrows). (e and f) CA1 and CA3 of the monosodium glutamate (MSG)-treated group showing distorted, shrunken pyramidal cells with irregular boundaries and a dark cytoplasm with indistinct pyknotic nuclei (stars). (g and h) CA1 and CA3 of the MSG and melatonin-treated group showing most of pyramidal neurons appear normal (arrows) with few shrunken degenerated neurons (stars). Scale bar: 50 μm (Cresyl violet staining, ×400). CA: Cornu ammonis

The morphometric analysis to assess BDNF immunopositivity [Histogram 3d] indicated that there was insignificant difference between control group and melatonin-treated group (P = 0.900). MSG group showed a significant decrease in BDNF immunoreactivity by comparison to both control and melatonin-treated groups (P < 0.0001). Administration of melatonin in MSG and melatonin-treated group significantly increased BDNF immunoreactivity by comparison to the MSG group (P = 0.0041) and significantly decrease BDNF immunoreactivity by comparison to control and Melatonin groups (P = 0.0002, 0.0005 respectively).

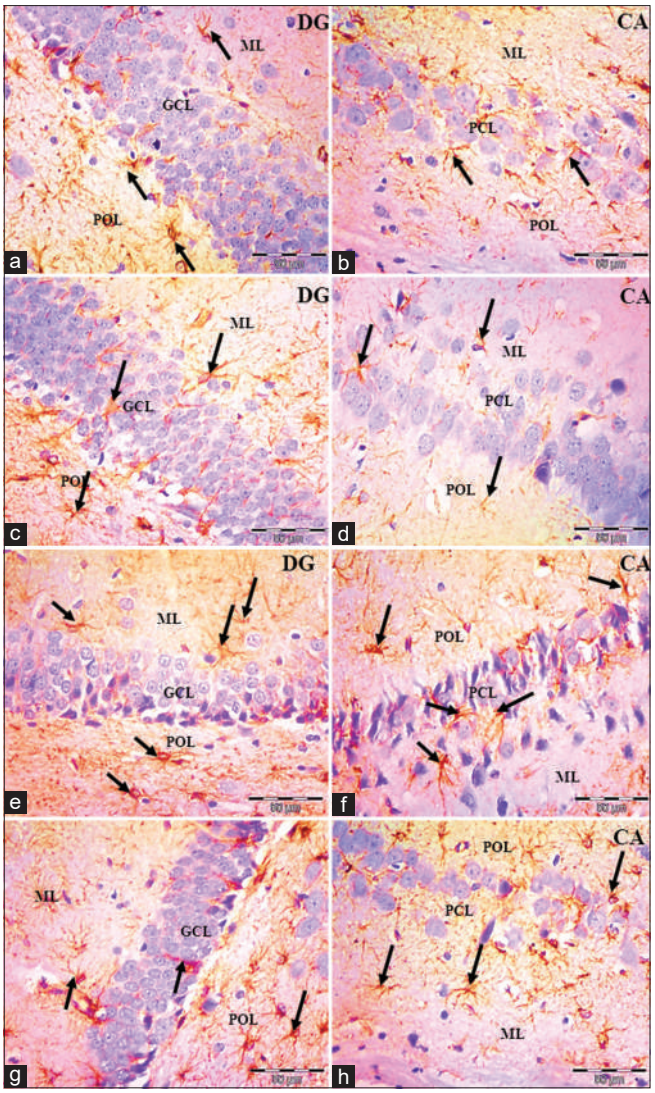

Figure 6: Representative photomicrographs of immunohistochemical staining of glial fibrillary acidic protein (GFAP) in the dentate gyrus and cornu ammonis of hippocampi of all experimental groups. (a and b) The control group exhibits few small-sized astrocytes with short thin few processes (arrows) among the granular and pyramidal cells in granule cell layer (GCL) and pyramidal cell layer (PCL), respectively, along with few dispersed astrocytes in molecular layer (ML) and polymorphic layer (POL). (c and d) The melatonin-treated group showing few small-sized astrocytes with short thin few processes (arrows) among the granular and pyramidal cells in GCL and PCL, respectively, along with few dispersed astrocytes in ML and POL. (e and f) The monosodium glutamate (MSG)-treated group reveals many larger astrocytes with thick multiple ramified processes (arrows) in ML, POL and among the granular and pyramidal cell bodies in GCL and PCL. (g and h) The MSG and melatonin-treated group reveals small astrocytes with short thin few processes (arrows) in ML and POL. Scale bar: 50 μm (GFAP immunostaining, ×400). CA: Cornu ammonis, DG: Dentate gyrus, POL: Polymorphic layer, PCL: Pyramidal cell layer, GCL: Granule cell layer, ML: Molecular layer

Discussion

The current research investigated the histological and immunohistochemical changes that may develop in rat CA1, CA3 hippocampus, and DG experimentally exposed to MSG and the possible neuroprotective role of melatonin.

MSG is one of the common food additives that have been first used by Asian population.[21] It activates the tongue's

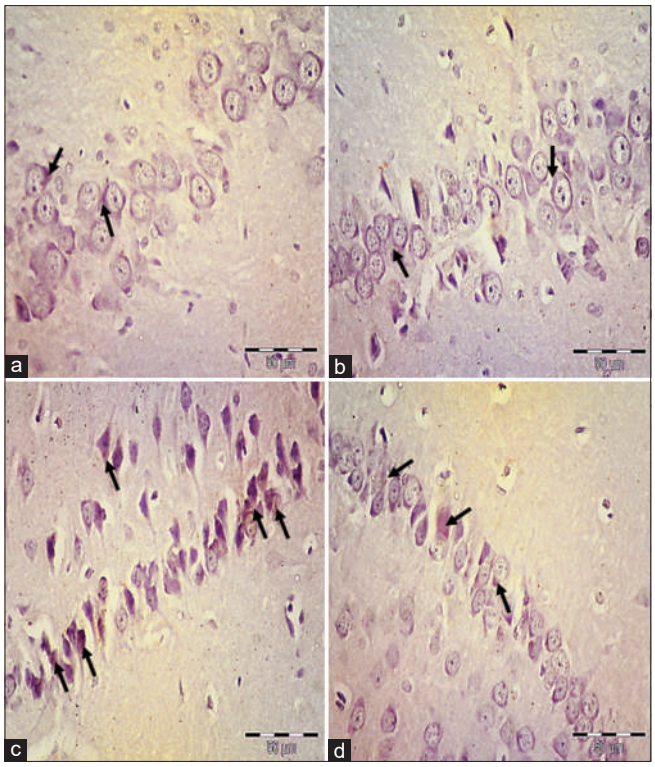

Figure 7: Representative photomicrographs of immunohistochemical staining of NRF-2 in hippocampi of all experimental groups. (a) The control group and (b) The melatonin-treated group exhibit few sporadic pyramidal neurons with faint cytoplasmic expression (arrows). (c) The monosodium glutamate (MSG)-treated group reveals many pyramidal neurons with strong cytoplasmic and nuclear immunoexpression (arrows). (d) The MSG- and melatonin-treated group reveals few pyramidal neurons with mild cytoplasmic and nuclear expression (arrows). Scale bar: 50 μm (NRF-2 immunostaining, ×400)

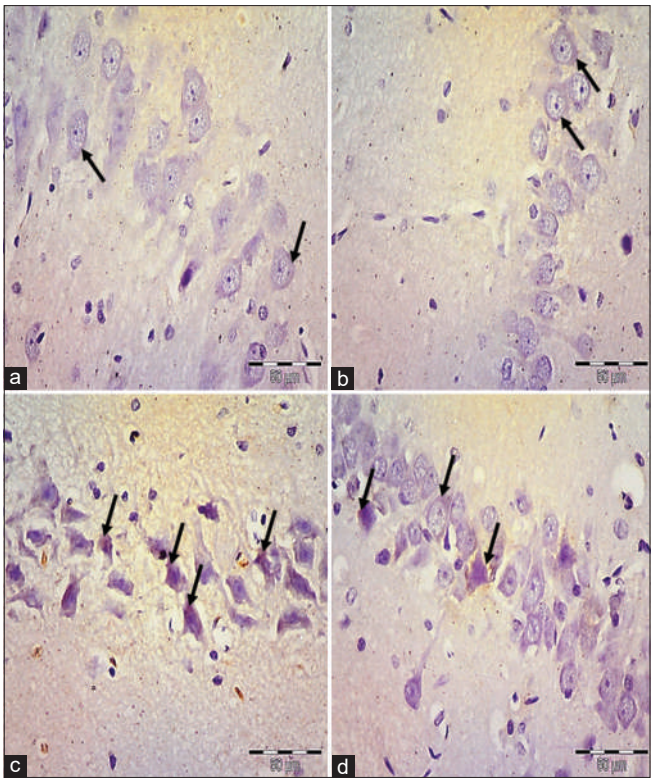

Figure 8: Representative photomicrographs of immunohistochemical staining of HO-1 in hippocampi of all experimental groups. (a) The control group and (b) The melatonin-treated group exhibit few pyramidal neurons with faint cytoplasmic expression (arrows). (c) The monosodium glutamate (MSG) treated group reveals many pyramidal neurons with strong cytoplasmic immunoexpression (arrows). (d) The MSG- and melatonin-treated group reveals some pyramidal neurons with mild cytoplasmic expression (arrows). Scale bar: 50 μm (HO-1 immunostaining, ×400)

TAS1R1-TAS1R3 receptors, which results in the production of the characteristic umami taste. Due of its characteristic flavor, MSG is being consumed more often across the whole world. Because the safety of MSG is controversial it ought to only be consumed in moderation and in accordance with the allowed dosages recommended by various organizations to avoid undesirable side effects.[22] Melatonin is a well-known antioxidant, anti-inflammatory, and anti-apoptotic agent.[23]

The findings of the current study demonstrated that IP injection of rat animal with MSG-induced excitotoxicity, which was evidenced by neuronal cells death and necrosis.

As MSG's dissociates into both glutamate and sodium ions inside the body, the extracellular glutamate levels rise considerably.[24] The increased extracellular glutamate hyperactivates the brain receptors with subsequent brain tissue injury.[25]

The brain tissues contain both excitatory neurons and inhibitory interneurons. They interact together to produce a functional brain equilibrium, preventing the occurrence of pathological events. Glutamate is an excitatory neurotransmitter that is involved in numerous normal physiological functions inside the central nervous system.[26]

Excess glutamate with subsequent hyperactivation of glutamate receptors results in disruption in the calcium homeostasis and sets a series of membrane, cytoplasmic, and nuclear events that ultimately cause excitotoxic neuronal damage.[27]

Hyperactivation of glutamate receptors in various brain regions, including cerebrum, cerebellum, and hippocampus, may lead to neuronal cell death.[26]

The current work found a significant increase in the MDA level in brain tissues and a significant decrease in SOD levels indicating oxidative stress in the brain following injection of MSG indicating alterations in the antioxidant status of brain tissues. These findings are in accordance with Farombi and Onyema,[28] who reported that IP administration of MSG has resulted in a marked increase in MDA in brain level and marked decrease in SOD brain level in rats.

MDA is widely determined by thiobarbituric reactive substances and is a determinant of oxidative stress. An increased tissues level of MDA results in affection of neuronal plasma membranes structure and function through changing its ions permeability properties.[29] As the

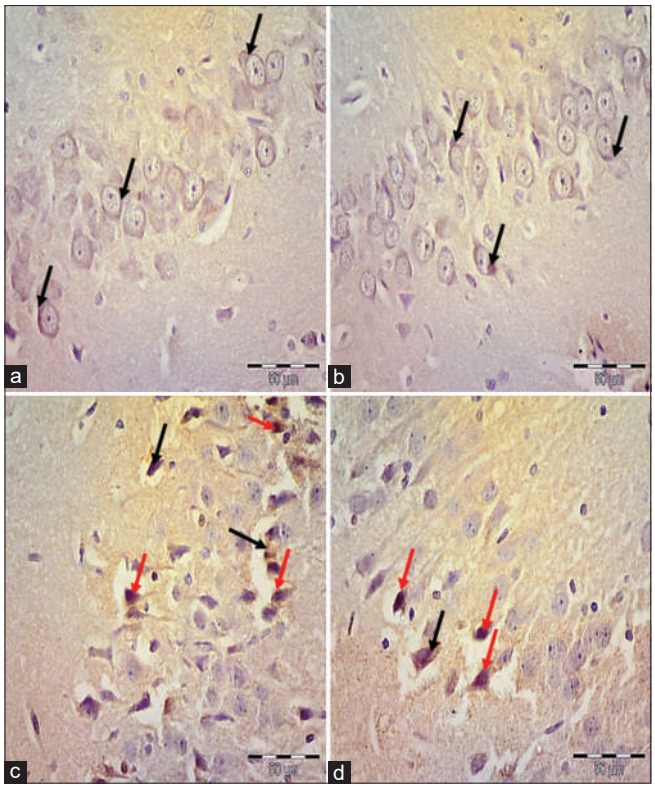

Figure 9: Representative photomicrographs of immunohistochemical staining of nuclear factor–kappa β (NF-kβ) in hippocampi of all experimental groups. (a) The control group and (b) The melatonin-treated group showing faint cytoplasmic expression in pyramidal neurons (arrows). (c) The monosodium glutamate (MSG) treated group showing many pyramidal neurons with strong cytoplasmic (black arrows) and nuclear immunoexpression (red arrows). (d) The MSG- and melatonin-treated group reveals few pyramidal neurons with cytoplasmic (black arrows) and nuclear expression (red arrows). Scale bar: 50 μm (NF-kβ immunostaining, ×400)

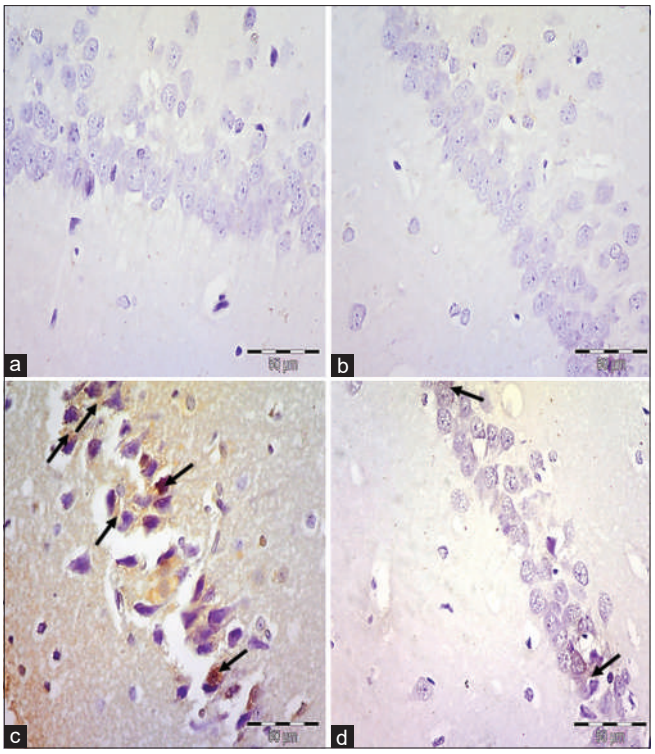

Figure 10: Representative photomicrographs of immunohistochemical staining of tumor necrosis factor-α (TNF-α) in hippocampi of all experimental groups. (a) The control group and (b) The melatonin-treated group showing negative cytoplasmic expression in pyramidal neurons. (c) The monosodium glutamate (MSG)-treated group showing many pyramidal neurons with strong cytoplasmic expression (black arrows). (d) The MSG- and melatonin-treated group reveals faint cytoplasmic expression in few pyramidal neurons (black arrows). Scale bar: 50 μm (TNF-α immunostaining, ×400)

central nervous system tissues consume a lot of oxygen, they have very high susceptibility to be damaged by free radicals with subsequent neuronal damage.[30] The reactive oxygen species (ROS) plays major role in MSG-induced neurotoxicity.[31]

The data of the current research showed that IP administration of MSG decreased the number of PCLs in CA1 and CA3 areas of the hippocampus due to neuronal cell death. In addition, most of the nerve cells were distorted in shape. In addition, DG neurons revealed granular cells with shrunken cell bodies, deeply stained cytoplasm and pyknotic nuclei with some areas of cellular loss.

These findings are in accordance with Onaolapo *et al*.[32] who reported an association between MSG administration and neuronal loss, inflammation, and cellular swelling. Furthermore, these findings are in accordance with Rycerz *et al*.,[33] who reported that MSG administration to rats in the postnatal week resulted in 11.5% hippocampal pyramidal neurons loss.

In the current research, a light microscopic analysis of hippocampal and DG sections stained with GFAP revealed few tiny astrocytes with short thin few processes in the melatonin and control groups while the MSG-treated group demonstrated many larger astrocytes with thick multiple ramifying processes. The MSG group treated with melatonin displayed small astrocytes with short thin few processes.

In the current research, MSG-induced increased GFAP. Astrogliosis is a hallmark of increased astrocyte activity as a result of CNS injury.[34] These results are in consistent with Gudiño- Gudiño-Cabrera *et al*.[35] who reported that administration of MSG-induced reactivity of astrocytes in the hippocampus, leading to neuronal apoptosis. Also previous data indicated that MSG administration-induced hypertrophy of astrocytes and microglial cells in the hippocampus.[35]

In addition Martínez-Contreras *et al*.[36] stated that astrocytes and microglia cells are highly susceptible to neuro-excitotoxic effects of MSG administration. Hazzaa *et al*.[37] confirmed that MSG leads to hypertrophy of astrocytes and enhancement of their number, which was accompanied with elevation in GFAP expression, and accordingly inducing neurotoxicity.

As astrocytes express glutamate receptors and play an important role in glutamate homeostasis and the reuptake of

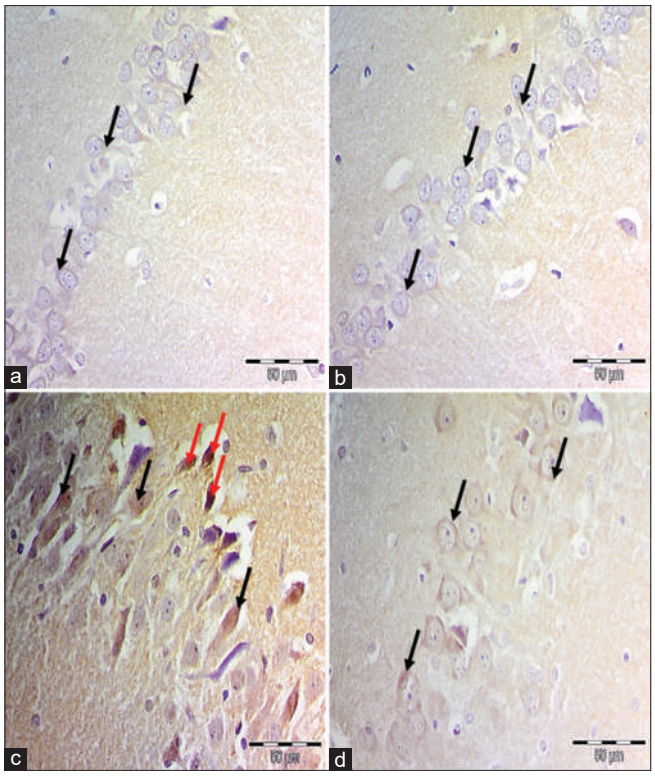

Figure 11: Representative photomicrographs of immunohistochemical staining of activated caspase-3 in hippocampi of all experimental groups. (a) The control group and (b) the melatonin-treated group showing faint cytoplasmic expression in pyramidal neurons (arrows). (c) The monosodium glutamate (MSG) treated group showing many pyramidal neurons with strong cytoplasmic (black arrows) and nuclear immunoexpression (red arrows). (d) The MSG and melatonin-treated group reveals pyramidal neurons with moderate cytoplasmic expression (black arrows). Scale bar: 50 μm (activated caspase-3 immunostaining, ×400)

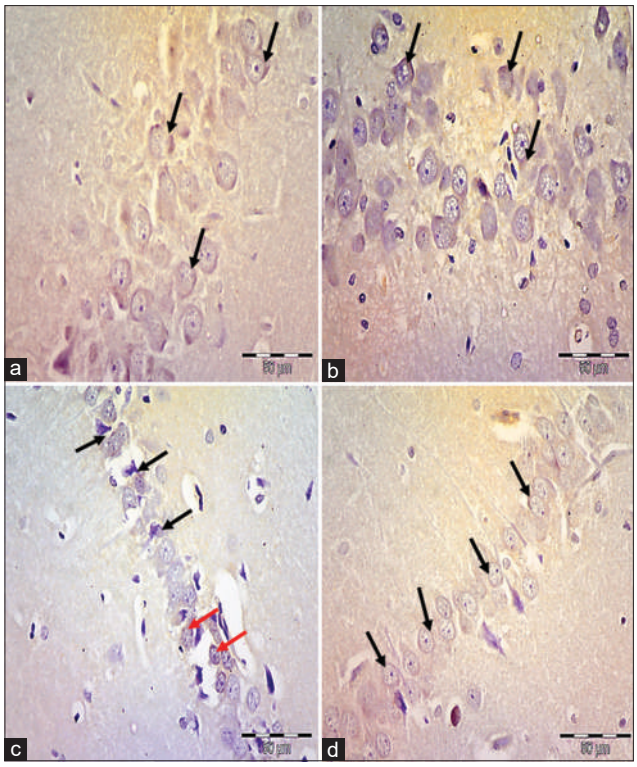

Figure 12: Representative photomicrographs of immunohistochemical staining of brain-derived neurotrophic factor (BDNF) in hippocampi of all experimental groups. (a) The control group and (b) The melatonin-treated group showing positive cytoplasmic expression in many pyramidal neurons (arrows). (c) The monosodium glutamate (MSG)-treated group showing many pyramidal neurons with negative cytoplasmic immunoexpression (black arrows) and few neurons with faint expression (red arrows). (d) The MSG- and melatonin-treated group reveals pyramidal neurons with mild cytoplasmic expression (arrows). Scale bar: 50 μm (BDNF immunostaining, ×400)

free glutamate preventing overstimulation of glutamatergic receptors, thus, preventing glutamate excitotoxicity and subsequent neuronal damage;[32] thus, they are vulnerable to toxic effects of glutamate.[38]

In the current research, levels of Nrf2 and HO-1, immunoreactivity in the MSG-treated group was elevated as the rise in Nrf2 induces HO-1 expression in intracellular levels which has anti-inflammatory property.[39] However, the immunoexpression of Nrf2 and HO-1 was significantly down regulated in response to melatonin therapy.

The primary oxidative stress route involves Nrf2. When body cells are exposed to excessive amounts of oxidative stress, the Nrf2 signaling pathway is activated to detoxify cellular-free radicals and inhibit neuroinflammation[40] which leads to the synthesis of several antioxidant enzymes that reduce the generation of ROS and prevent cell damage.[41]

Under normal circumstances, Nrf2 is degraded in the cytoplasm when the Kelch-like ECH-associated protein 1 (Keap1) attaches to it.[42] Increased oxidative stress in cells causes Nrf2 to separate from from Keap1.

The free-released Nrf2 from the cytoplasm is translocated to the nucleus. This allows the Nrf2 to combine with antioxidant response elements within the nucleus. According to Chen *et al*.[43] this combination upregulates HO-1.

HO-1 has a major role in organ protection against ROS-induced cell damage.[44] In the current research, a light microscopic analysis of hippocampal sections stained with NF-kβ and TNF-α revealed negative cytoplasmic immune staining reaction in the melatonin and control groups while, the MSG-treated group demonstrated strong cytoplasmic immune staining reaction.

These findings are in accordance with Mamun *et al*.[45] who stated that NF-κB contributes to neurodevelopmental brain injury and the consequent cognitive function decline. It has also been shown to generate inflammatory cytokines, such as TNF-α. Furthermore, TNF-α triggers inflammatory process through many methods.[46] As it interacts with a variety of cytokines and chemokines, leading to formation of excess ROS thus elevated TNF-α may indicate inflammation.[47]

A recent study indicated that using melatonin inhibited the activation of gliosis and other inflammatory mediators, such as TNF-α and COX-2.[48]

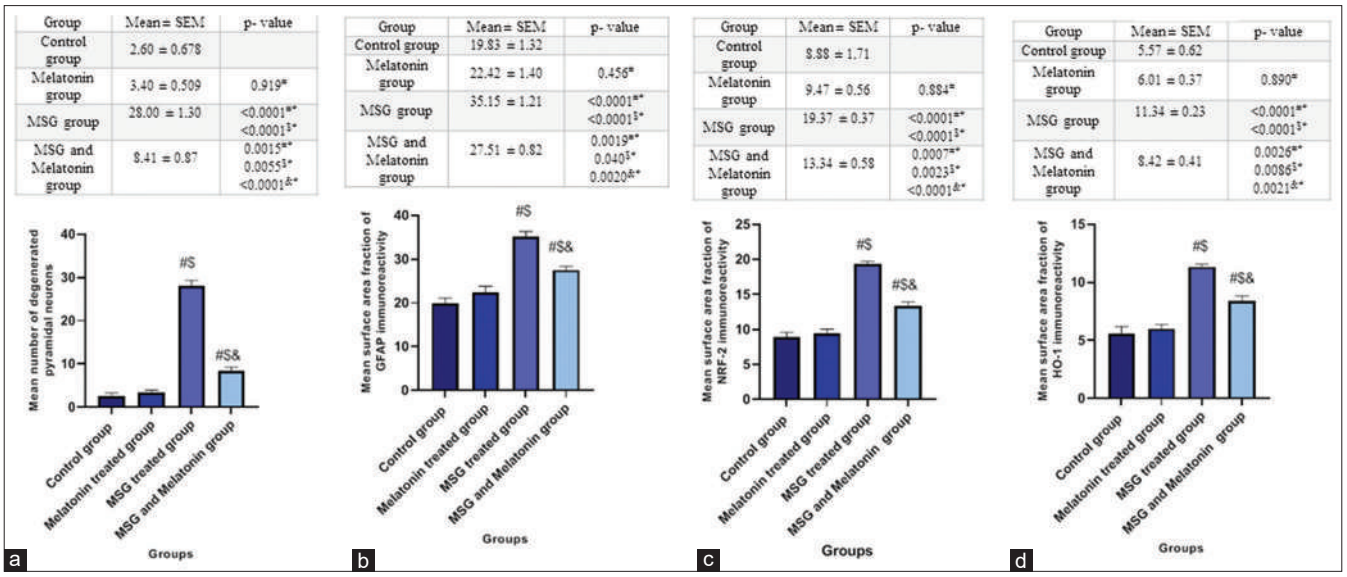

Histogram 2: The mean area fraction (%) of (a) mean number of degenerated pyramidal neurons (b) GFAB immune-positive cells, (c) NRF-2 immune-positive cells, and (d) HO-1 immune-positive cells in the studied groups (*n* = 8) #versus C-group, $versus melatonin group, &versus monosodium glutamate group, **P* < 0.05 is significant. using one-way ANOVA followed by Tukey-Kramer *post hoc* test using one-way ANOVA followed by Tukey-Kramer *post hoc* test

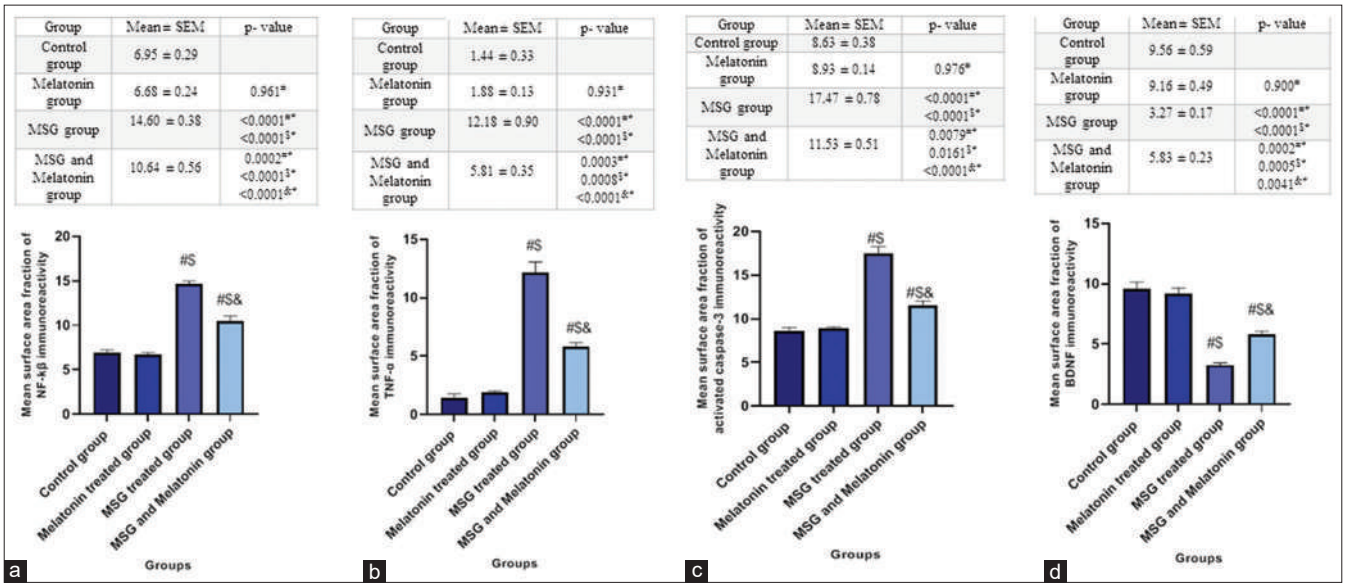

Histogram 3: (a) The mean area fraction (%) of (a) NF-kβ immune-positive cells, (b) tumor necrosis factor-α immune-positive cells, (c) activated caspase-3 immune-positive cells, and (d) BDNF immune-positive cells in the studied groups (*n* = 8) #versus C-group, $versus melatonin group, &versus monosodium glutamate group, **P* < 0.05 is significant. using one-way ANOVA followed by Tukey-Kramer *post hoc* test using one-way ANOVA followed by Tukey-Kramer *post hoc* test

However, melatonin's capacity to inhibit NF-κB may contribute to the decreased GFAP level. According to Bae *et al*.,[49] NF-κB can stimulate GFAP expression in human astroglial cells as it has a binding site in the human GFAP gene.

In the current research, a light microscopic analysis of hippocampal sections stained with caspase-3 revealed a slight cytoplasmic immune staining reaction in the melatonin and control groups while, the MSG-treated group demonstrated a high-positive cytoplasmic and nuclear immune staining reaction.

The MSG group treated with melatonin displayed a moderate cytoplasmic immune staining reaction.

Gudiño-Cabrera *et al*.[35] reported that MSG administration resulted in evident neuronal apoptosis in CA1 and CA3 hippocampal areas with subsequent cognitive impairment.

The increased expression of caspase-3 protein in the hippocampus of MSG-administered rat animals in the current research can explain the histopathological changes observed in brain tissues of the MSG-treated group in the current research in the of the pyramidal cell loss and neuronal degeneration.

MSG-induced apoptotic changes may be due to oxidative stress[50] with subsequent disruption of the mitochondrial inner transmembrane potential,[51] leading to release of different pro-apoptotic factors including cytochrome c and AIF.[52] Translocation of cytochrome c to the cytoplasm promotes caspase-9 and caspase-3 activation, while AIF translocation induces apoptosis in a caspase-independent way.[53] Also Al-Otaibi *et al*.[31] reported that in all tissues treated with MSG there was nuclear pyknosis and this may be due to DNA damage that resulted in cell death.

Generation of ROS can induce a signaling pathway leading to programmed cell death.[54]

In the current research, we observed that melatonin treatment prevented apoptosis in the hippocampal sections stained with caspase-3. These findings can be explained by the down regulation of apoptotic Bax proteins and upregulation of antiapoptotic Bcl2 family proteins exerted by melatonin thus suppressing apoptosis. In addition, it has been demonstrated that melatonin plays a significant role in maintaining mitochondrial homeostasis. This prevents Cyt. C release and subsequent activation of caspase-3. These effects prevent apoptosis and neurodegeneration.[55]

BDNF has been critically implicated in cognitive functions and commonly associated with neurogenesis and neuroprotection.[56] In the current research, degenerative changes detected in hippocampal zones of MSG-treated group, were confirmed by statistical significant decrease in BDNF immunoexpression compared to other groups.

As MSG-treated group showed negative cytoplasmic immunoexpression and few neurons with faint expression. Decreased levels of BDNF in the hippocampus in the current research are in consistent with Gürgen *et al*.[1] who reported that MSG administration resulted in decrease levels of BDNF in cerebral cortex, hippocampus and the whole brain. Also Pringle *et al*.[57] indicated that pretreatment with BDNF reduced the neuronal damage caused by oxygen and glucose deprivation in organotypic hippocampal cultures. On the other hand results by Viana Borges *et al*.[58] reported increased BDNF immunoexpression in brain of mice exposed to social isolation.

The morphometric results of the current research support these immunohistochemical findings, as the mean area fraction of GFAB, Nrf2, HO-1, NF-kβ, TNF-α, and caspase cells showed a significant increase in MSG-treated group compared to other groups and a significant decrease in melatonin-treated group. On the other hand, the mean area fraction of BDNF showed a significant decrease in MSG-treated group compared to other groups and a significant increase in melatonin-treated group.

The current research showed that MSG from MSG administration in adult rats for 14 days resulted in increased MDA tissue levels, immunoexpression of caspase-3, NF-κB, and pro-inflammatory cytokines, including TNF-α, indicating the existence of neuroinflammation, oxidative stress, apoptosis, and degeneration of neuronal cells induced by MSG in rats. These findings are in accordance with Radogna *et al*.[59]

Therefore, the use of antioxidants and anti-inflammatory agent is an important issue in inhibiting neuronal damage. The current research showed that melatonin significantly increased SOD level as well as decreased MDA level. Furthermore, melatonin impact extended beyond its antioxidant capacity by its modulatory effects on Nrf2 and HO-1 to involve suppression of neuroinflammation and apoptosis, these effects were verified by a significant decrease in the hippocampal immunoreactivity of NF-kβ, TNF-α and activated caspase 3 level; hence, it reduced neuroinflammation and maintained neuronal survival.

Interestingly, the complexity of melatonin's function varies depending on the stage of inflammation. It appears to have a temporary pro-inflammatory effect during the early stages of inflammation. However, it appears to have anti-inflammatory properties when chronic inflammation is present.[60]

Because of its anti-inflammatory and antioxidant properties, melatonin preserves glial function, which is why its treatment decreased GFAB immunoexpression. These results support those of Gao *et al*.,[61] who noted that melatonin lowers microglial inflammation by creating a network of anti-inflammatory interactions in a variety of ways.

The current study's findings demonstrate the neuroprotective benefits of melatonin, a naturally occurring antioxidant that restores normal redox activity and improves cells regeneration.

By increasing the production of antioxidant enzymes and preserving the function of the mitochondrial electron transport chain, melatonin reduces ROS leakage and has antioxidant effects. In addition, melatonin's nonreceptor-mediated action makes it a potent free-radical scavenger. Melatonin, its metabolites, and free radicals interact in a very effective sequential manner to create a potent antioxidant cascade.[16]

By reducing oxidative damage to brain lipids, alleviating secondary cerebral energy failure, and increasing antioxidant enzymes, melatonin inhibits neuronal apoptosis and the ensuing neurological impairment that follows free radical noxious events.[62]

Melatonin is a remarkable, versatile pleiotropic agent due to its potent antioxidant, anti-inflammatory, and anti-apoptotic qualities.

Financial support and sponsorship

Nil.

Conflicts of interest

There are no conflicts of interest.

References

1. Gürgen SG, Sayın O, Çeti NF, Sarsmaz HY, Yazıcı GN, Umur N, *et al.* The effect of monosodium glutamate on neuronal signaling molecules in the hippocampus and the neuroprotective effects of omega-3 fatty acids. ACS Chem Neurosci 2021;12:3028-37.
2. Chakraborty SP. Patho-physiological and toxicological aspects of monosodium glutamate. Toxicol Mech Methods 2019;29:389-96.
3. Yap HM, Lye KL, Tan LT. Comprehensive insight of neurodegenerative diseases and the role of neurotoxin agents glutamate. Prog Microbes Mol Biol 2020;3:1-9.
4. Park CH, Choi SH, Piao Y, Kim S, Lee YJ, Kim HS, *et al.* Glutamate and aspartate impair memory retention and damage hypothalamic neurons in adult mice. Toxicol Lett 2000;115:117-25.
5. Maragakis NJ, Rothstein JD. Glutamate transporters in neurologic disease. Arch Neurol 2001;58:365-70.
6. Freeman M. Reconsidering the effects of monosodium glutamate: A literature review. J Am Acad Nurse Pract 2006;18:482-6.
7. Muddapu VR, Dharshini SA, Chakravarthy VS, Gromiha MM. Neurodegenerative diseases – Is metabolic deficiency the root cause? Front Neurosci 2020;14:213.
8. Prinsen H, de Graaf RA, Mason GF, Pelletier D, Juchem C. Reproducibility measurement of glutathione, GABA, and glutamate: Towards *in vivo* neurochemical profiling of multiple sclerosis with MR spectroscopy at 7T. J Magn Reson Imaging 2017;45:187-98.
9. Hajihasani MM, Soheili V, Zirak MR, Sahebkar A, Shakeri A. Natural products as safeguards against monosodium glutamate-induced toxicity. Iran J Basic Med Sci 2020;23:416-30.
10. Dief AE, Kamha ES, Baraka AM, Elshorbagy AK. Monosodium glutamate neurotoxicity increases beta amyloid in the rat hippocampus: A potential role for cyclic AMP protein kinase. Neurotoxicology 2014;42:76-82.
11. Ito R, Lee AC. The role of the hippocampus in approach-avoidance conflict decision-making: Evidence from rodent and human studies. Behav Brain Res 2016;313:345-57.
12. Alsemeh AE, Ibrahim AA, Mohammed HO. Structural and behavioural changes in rat hippocampus induced by methotrexate and the potential ameliorative effect of alpha lipoic acid. Egypt J Histol 2020;43:301-24.
13. Meng X, Li Y, Li S, Zhou Y, Gan RY, Xu DP, *et al.* Dietary sources and bioactivities of melatonin. Nutrients 2017;9:367.
14. Yu GM, Kubota H, Okita M, Maeda T. The anti-inflammatory and antioxidant effects of melatonin on LPS-stimulated bovine mammary epithelial cells. PLoS One 2017;12:e0178525.
15. Esposito E, Cuzzocrea S. Antiinflammatory activity of melatonin in central nervous system. Curr Neuropharmacol 2010;8:228-42.
16. Reiter RJ, Mayo JC, Tan DX, Sainz RM, Alatorre-Jimenez M, Qin L. Melatonin as an antioxidant: Under promises but over delivers. J Pineal Res 2016;61:253-78.
17. Tarocco A, Caroccia N, Morciano G, Wieckowski MR, Ancora G, Garani G, *et al.* Melatonin as a master regulator of cell death and inflammation: Molecular mechanisms and clinical implications for newborn care. Cell Death Dis 2019;10:317.
18. Buege JA, Aust SD. Microsomal lipid peroxidation. Methods Enzymol 1978;52:302-10.
19. Suvarna KS, Layton C, Bancroft JD. Bancroft's Theory and Practice of Histological Techniques. Philadelphia: Elsevier Health Sciences; 2018.
20. Maae E, Nielsen M, Steffensen KD, Jakobsen EH, Jakobsen A, Sørensen FB. Estimation of immunohistochemical expression of VEGF in ductal carcinomas of the breast. J Histochem Cytochem 2011;59:750-60.
21. Singh K, Pushpa A. Alteration in some antioxidant enzymes in cardiac tissue upon monosodium glutamate [MSG] administration to adult male mice. Indian J Clin Biochem 2005;20:43-6.
22. Ito K, Hayashi H. Fermentation-based production of MSG: Challenges and future prospects. J Indus Microbiol Biotech 2019;46:215-25.
23. Brazão V, Santello FH, Filipin Mdel V, Azevedo AP, Toldo MP, de Morais FR, *et al.* Immunoregulatory actions of melatonin and zinc during chronic *Trypanosoma cruzi* infection. J Pineal Res 2015;58:210-8.
24. López-Pérez SJ, Ureña-Guerrero ME, Morales-Villagrán A. Monosodium glutamate neonatal treatment as a seizure and excitotoxic model. Brain Res 2010;1317:246-56.
25. Bera T, Kar S, Yadav P, Mukherjee P, Yadav S, Joshi B. Effects of monosodium glutamate on human health: A systematic review. World J Pharm Sci 2017;5:139-144.
26. Earnheart JC, Schweizer C, Crestani F, Iwasato T, Itohara S, Mohler H, *et al.* GABAergic control of adult hippocampal neurogenesis in relation to behavior indicative of trait anxiety and depression states. J Neurosci 2007;27:3845-54.
27. Swamy AH, Patel NL, Gadad PC, Koti BC, Patel UM, Thippeswamy AH, *et al.* Neuroprotective activity of *Pongamia pinnata* in monosodium glutamate-induced neurotoxicity in rats. Indian J Pharm Sci 2013;75:657-63.
28. Farombi EO, Onyema OO. Monosodium glutamate-induced oxidative damage and genotoxicity in the rat: Modulatory role of Vitamin C, Vitamin E and quercetin. Hum Exp Toxicol 2006;25:251-9.
29. Slopovsky J, Kucharska J, Obertova J, Mego M, Kalavska K, Cingelova S, *et al.* Plasma thiobarbituric acid reactive substances predicts survival in chemotherapy naïve patients with metastatic urothelial carcinoma. Transl Oncol 2021;14:100890.
30. Salim S. Oxidative stress and the central nervous system. J Pharmacol Exp Ther 2017;360:201-5.
31. Al-Otaibi AM, Emam NM, Elabd HK, Esmail NI. Toxicity of monosodium glutamate intake on different tissues induced oxidative stress. A review. J Med Life Sci 2022;4:68-81.
32. Onaolapo OJ, Onaolapo AY, Akanmu MA, Gbola O. Evidence of alterations in brain structure and antioxidant status following 'low-dose' monosodium glutamate ingestion. Pathophysiology 2016;23:147-56.
33. Rycerz K, Krawczyk A, Jaworska-Adamu J, Krawczyk-Marc I. Effects of monosodium glutamate treatment on calretinin-immunoreactive neurons in hippocampus of postnatal rats. Folia Histochem Cytobiol 2014;52:281-8.
34. Zhang S, Wu M, Peng C, Zhao G, Gu R. GFAP expression in injured astrocytes in rats. Exp Ther Med 2017;14:1905-8.
35. Gudiño-Cabrera G, Ureña-Guerrero ME, Rivera-Cervantes MC, Feria-Velasco AI, Beas-Zárate C. Excitotoxicity triggered by neonatal monosodium glutamate treatment and blood-brain barrier function. Arch Med Res 2014;45:653-9.
36. Martínez-Contreras A, Huerta M, Lopez-Perez S, García-Estrada J, Luquín S, Beas Zárate C. Astrocytic and microglia cells reactivity induced by neonatal administration of glutamate in cerebral cortex of the adult rats. J Neurosci Res 2002;67:200-10.
37. Hazzaa SM, Abdelaziz SA, Abd Eldaim MA, Abdel-Daim MM, Elgarawany GE. Neuroprotective potential of *Allium sativum* against monosodium glutamate-induced excitotoxicity: Impact on short-term memory, gliosis, and oxidative stress. Nutrients 2020;12:1028.
38. Ota Y, Zanetti AT, Hallock RM. The role of astrocytes in the regulation of synaptic plasticity and memory formation. Neural Plast 2013;2013:185463.

39. Ahmed SM, Luo L, Namani A, Wang XJ, Tang X. Nrf2 signaling pathway: Pivotal roles in inflammation. Biochim Biophys Acta Mol Basis Dis 2017;1863:585-97.
40. Ngo V, Duennwald ML. Nrf2 and oxidative stress: A general overview of mechanisms and implications in human disease. Antioxidants (Basel) 2022;11:2345.
41. Dinkova-Kostova AT, Kostov RV, Canning P. Keap1, the cysteine-based mammalian intracellular sensor for electrophiles and oxidants. Arch Biochem Biophys 2017;617:84-93.
42. Tian W, Rojo de la Vega M, Schmidlin CJ, Ooi A, Zhang DD. Kelch-like ECH-associated protein 1 (KEAP1) differentially regulates nuclear factor erythroid-2-related factors 1 and 2 (NRF1 and NRF2). J Biol Chem 2018;293:2029-40.
43. Chen C, Pung D, Leong V, Hebbar V, Shen G, Nair S, *et al.* Induction of detoxifying enzymes by garlic organosulfur compounds through transcription factor Nrf2: Effect of chemical structure and stress signals. Free Radic Biol Med 2004;37:1578-90.
44. Das BN, Kim YW, Keum YS. Mechanisms of Nrf2/Keap1-dependent phase II cytoprotective and detoxifying gene expression and potential cellular targets of chemopreventive isothiocyanates. Oxid Med Cell Longev 2013;2013:839409.
45. Mamun AA, Shao C, Geng P, Wang S, Xiao J. Polyphenols targeting NF-κB pathway in neurological disorders: What we know so far? Int J Biol Sci 2024;20:1332-55.
46. Koh WU, Kim J, Lee J, Song GW, Hwang GS, Tak E, *et al.* Remote ischemic preconditioning and diazoxide protect from hepatic ischemic reperfusion injury by inhibiting HMGB1-induced TLR4/MyD88/NF-κB signaling. Int J Mol Sci 2019;20:5899.
47. Kadkhodaee M, Mikaeili S, Zahmatkesh M, Golab F, Seifi B, Arab HA, *et al.* Alteration of renal functional, oxidative stress and inflammatory indices following hepatic ischemia-reperfusion. Gen Physiol Biophys 2012;31:195-202.
48. Maqbool A, Lattke M, Wirth T, Baumann B. Sustained, neuron-specific IKK/NF-κB activation generates a selective neuroinflammatory response promoting local neurodegeneration with aging. Mol Neurodegener 2013;8:40.
49. Bae MK, Kim SR, Lee HJ, Wee HJ, Yoo MA, Ock Oh S, *et al.* Aspirin-induced blockade of NF-kappaB activity restrains up-regulation of glial fibrillary acidic protein in human astroglial cells. Biochim Biophys Acta 2006;1763:282-9.
50. Hashem HE, El-Din Safwat MD, Algaidi S. The effect of monosodium glutamate on the cerebellar cortex of male albino rats and the protective role of Vitamin C (histological and immunohistochemical study). J Mol Histol 2012;43:179-86.
51. Kanki R, Nakamizo T, Yamashita H, Kihara T, Sawada H, Uemura K, *et al.* Effects of mitochondrial dysfunction on glutamate receptor-mediated neurotoxicity in cultured rat spinal motor neurons. Brain Res 2004;1015:73-81.
52. Desagher S, Martinou JC. Mitochondria as the central control point of apoptosis. Trends Cell Biol 2000;10:369-77.
53. Mathew S, Keerikkattil J. Activation of cell death mediated by the crosstalk between caspase-3 and apoptosis inducing factor in the brainstem upon exposure to monosodium glutamate and corticosterone. FASEB J 2021;35. doi: 10.1096/fasebj.2021.35.S1.03922
54. Pulawski W, Ghoshdastider U, Andrisano V, Filipek S. Ubiquitous amyloids. Appl Biochem Biotechnol 2012;166:1626-43.
55. Xu S, Pi H, Zhang L, Zhang N, Li Y, Zhang H, *et al.* Melatonin prevents abnormal mitochondrial dynamics resulting from the neurotoxicity of cadmium by blocking calcium-dependent translocation of Drp1 to the mitochondria. J Pineal Res 2016;60:291-302.
56. Zhang H, Han Y, Zhang L, Jia X, Niu Q. The GSK-3β/β-catenin signaling-mediated brain-derived neurotrophic factor pathway is involved in aluminum-induced impairment of hippocampal LTP *in vivo*. Biol Trace Elem Res 2021;199:4635-45.
57. Pringle AK, Sundstrom LE, Wilde GJ, Williams LR, Iannotti F. Brain-derived neurotrophic factor, but not neurotrophin-3, prevents ischaemia-induced neuronal cell death in organotypic rat hippocampal slice cultures. Neurosci Lett 1996;211:203-6.
58. Viana Borges J, Souza de Freitas B, Antoniazzi V, de Souza Dos Santos C, Vedovelli K, Naziaseno Pires V, *et al.* Social isolation and social support at adulthood affect epigenetic mechanisms, brain-derived neurotrophic factor levels and behavior of chronically stressed rats. Behav Brain Res 2019;366:36-44.
59. Radogna F, Diederich M, Ghibelli L. Melatonin: A pleiotropic molecule regulating inflammation. Biochem Pharmacol 2010;80:1844-52.
60. Cho JH, Bhutani S, Kim CH, Irwin MR. Anti-inflammatory effects of melatonin: A systematic review and meta-analysis of clinical trials. Brain Behav Immun 2021;93:245-53.
61. Gao J, Su G, Liu J, Zhang J, Zhou J, Liu X, *et al.* Mechanisms of inhibition of excessive microglial activation by melatonin. J Mol Neurosci 2020;70:1229-36.
62. Miller SL, Yan EB, Castillo-Meléndez M, Jenkin G, Walker DW. Melatonin provides neuroprotection in the late-gestation fetal sheep brain in response to umbilical cord occlusion. Dev Neurosci 2005;27:200-10.

Original Article

Morphological Study of Hepatic Variations in the Cadaveric Specimens with Its Clinical and Surgical Implications

Abstract

Purpose: The liver, as the second largest organ in the body, plays a crucial role in interpreting hepatic segments and locating liver lesions. Its rare morphological variations are of significant interest. This study aims to evaluate these variations in cadaveric livers, providing crucial insights for surgeons and clinicians in ruling out pathologies in imaging studies and planning surgeries involving the hepatobiliary system. **Materials and Methods:** Fifty formalin-fixed liver specimens of unknown age and gender were used in our study. The morphological variations were observed in the cadaveric livers, and the results were tabulated. **Results:** Out of 50 cadaveric livers, morphological variations were noted in 26 livers. These variations, such as agenesis and hypoplasia of the left lobe, accessory lobe, accessory fissures, umbilical fissure variations, and short gallbladder, have practical implications for surgical planning and clinical diagnosis. Understanding these variations is crucial for effective surgical outcomes and preventing operative complications. **Conclusions:** As surgical procedures like laparoscopy continue to advance, the need for precise knowledge about hepatic variations becomes increasingly urgent. This knowledge is beneficial but essential for surgeons and physicians, ensuring good surgical outcomes, effective clinical diagnosis, and preventing operative complications.

Keywords: *Accessory fissure, accessory lobe of the liver, agenesis, elongation of left lobe of the liver, pons hepatis*

C. Regina[1], J. Kalaivannan[1], J. L. Joeimon[2], K. Santhini Arulselvi[1], R. Jenisha Elizabeth[1]

[1]Department of Anatomy and Pathology, Vinayaka Mission Medical College and Hospital, Karaikal, Vinayaka Mission's Research Foundation, Salem, [2]Department of Hepatology, Institute of Hepatobiliary Sciences, Madras Medical College, Chennai, India

Introduction

The liver, the second largest wedge-shaped gland of the human body, is anatomically divided into two lobes, the right lobe (RL) and the left lobe (LL), based on the attachments of peritoneal ligaments. In addition, two other lobes, the quadrate and the caudate lobe, are separated by the porta hepatis.[1] Liver anomalies can be either congenital or acquired. Congenital malformations include agenesis, aplasia, and hypoplastic lobes, while acquired causes are variations induced by other organs.[2] It is important to note that not all anomalies are congenital, and they must be differentiated from other clinical conditions like liver atrophy caused by cirrhosis, segmental resection, malnutrition, portal vein, and biliary obstruction.[3]

With a wide range of morphological changes, hepatic variations can be classified into anomalies due to defective and excessive development.[4] Defective hepatic development may be associated with malformations of other organs such as diaphragmatic and ligamentous anomalies, and excessive development leads to accessory lobe (AL) formation, which is more prone to torsion.[5,6] In addition to major hepatic fissures, incomplete fissures may be recognized as accessory fissures (AFs), which help interpret lobar anatomy and localize the lesions.[7]

Clinically, liver anatomy can be delineated based on the external morphology (external anatomy) and the other by its vascular and biliary architecture (vascular anatomy). For precise localization of the hepatic lesions and to perform liver resection, the surgeons must be aware of both external and functional variations.[4] With increased demand for laparoscopic procedures and better surgical outcomes, precise knowledge about external hepatic variations is essential.[2] Advanced imaging modalities are valuable in detecting hepatic abnormalities, but detailed macroscopic studies on cadaveric livers still play a crucial role. Many of the variations observed in cadaveric specimens have

How to cite this article: Regina C, Kalaivannan J, Joeimon JL, Arulselvi KS, Elizabeth RJ. Morphological study of hepatic variations in the cadaveric specimens with its clinical and surgical implications. J Anat Soc India 2025;74:124-32.

Article Info

Received: 07 October 2024
Accepted: 15 February 2025
Available online: 30 June 2025

Address for correspondence:
Dr. C. Regina,
Assistant Professor, Department of Anatomy, Vinayaka Mission Medical College and Hospital, Karaikal - 609 609.
Keezhakasakudimedu, Kottucherry (P.O), Pondicherry.
Vinayaka Mission Research Foundation (VMRF), Salem, India.
E-mail: chinnarajaregina@gmail.com

Access this article online

Website: https://journals.lww.com/joai
DOI: 10.4103/jasi.jasi_162_24
Quick Response Code:

provided insights into specific responses to therapies for liver disease. This study aims to understand these morphological variations further, which can aid surgeons and physicians in diagnosing and planning surgeries such as laparoscopic evacuation and thermal ablation of the tumor involving the hepatobiliary system.[8]

Objectives of the study

1. To evaluate the morphological variations of the human cadaveric liver
2. To categorize the hepatic variations according to Netter's classification.

Materials and Methods

Our study was a descriptive one, conducted in the Department of Anatomy after obtaining ethical clearance from the Institutional Ethical Committee, Vinayaka Missions Medical College and Hospital, Karaikal (approval no is IEC/VMMCH/2024/APR/89). We included 50 formalin-fixed livers belonging to adults of unknown age and gender, collected over a 5-year period. Livers with evident pathological conditions, damage, surgical resections, and metastatic disease were excluded from the study. We measured the gross morphology of the RL and LL using inch tape, and the results were tabulated. We also observed and photographed other morphological variations such as agenesis, hypoplastic LL, appendix of the liver, elongation of the LL, AL, AF, and pons hepatis and calculated their frequency. Furthermore, we categorized the morphological variations of the liver based on Netter's classification. It is important to note that the frequency of morphological hepatic variations lacks statistical analysis in this study, which would have served as a basis for comparison with the studied samples.

Results and Observations

- Total cadaveric livers obtained in our study – 50 specimens
- The average width of RL – 8.62 cm (Range – 7.0 to 15.5 cm), and the LL of the liver – 4.06 cm (Range – 2.5 to 8.5 cm).

The morphological hepatic variations were observed, and the results are documented and expressed in percentages in Table 1. As depicted in Figures 1 and 2, agenesis and hypoplastic LL were seen in 8% and 4%, and elongation of the LL and the appendix of the liver was noted in 12% and 14% of the cadaveric specimens. In our study, we have observed variant shapes of the elongated LL (2 – spatula shape, 2 – leaf-like, 1 – truncated pyramid, and 1 – linguiform). The various shapes of extension of the LL were measured using inch tape, as mentioned in Figure 3. The various parameters of the elongated LL, such as length and breadth, were recorded by locating arbitrary points, and the results are tabulated in Table 2. The length was measured at three points: from the apex of the LL to the left lip of the fissure for ligamentum teres hepatis, from the apex to the left lip of the fissure for ligamentum venosum, and from the apex to the tuber omentale. The breadth was measured near the base, middle, and at the apex of the elongated LL.

Table 1: Results of morphological variations of liver in our present study

Morphological variations	Number of specimens (50), frequency (%)
Agenesis of LL	4 (8)
Hypoplasia of LL	2 (4)
Elongation of LL	6 (12)
Appendix of liver	7 (14)
AL	3 (6)
Rectangular shape CL	16 (32)
Pyriform shape CL	4 (8)
Irregular shape CL	3 (6)
Bicornuate CL	6 (12)
Hypoplastic CL	1 (2)
Quadrangular shape QL	12 (24)
Triangle shape QL	8 (16)
Rectangle shape QL	5 (10)
Absent QL	1 (2)
Bilobed QL	2 (4)
Hypoplastic QL	1 (2)
AF	13 (26)
Umbilical fissure variations	9 (18)
Costal cleft with deep impression	6 (12)
Diaphragmatic groove	3 (6)
Short GB	2 (4)

LL: Left lobe, CL: Caudate lobe, QL: Quadrate lobe, AL: Accessory lobe, AF: Accessory fissure, GB: Gallbladder

Figure 1: Morphological variations showing agenesis of the left lobe and hypoplastic left lobe of the liver

The AL was observed in 6% of the specimens. Out of three specimens, one case had two slight AL arising from the quadrate lobe, and in the other two cases, it arose from the caudate lobe, as mentioned in Figure 4. The morphological variations of the caudate and quadrate lobe are depicted

in Figure 5. Variant shapes of caudate lobe were documented; the most common encountered in our study were rectangular (32%), pyriform (8%), irregular (6%), and hypoplastic (2%). Similarly, the most common shapes of quadrate lobes were quadrangular (24%), followed by triangles (16%), rectangles (10%), and hypoplastic (2%). We have observed six cases of bicornuate caudate lobe, an AF dividing the lower end of the caudate lobe into two lobes. A bilobed quadrate lobe was observed in two specimens, formed by a complete horizontal fissure dividing it into two lobes. The caudate lobe was present in a single liver with an absent caudate process, and a prominent papillary process and absent quadrate lobe were observed in one specimen.

AFs were noted in 26% of the cadaveric livers, as shown in Figure 6. The proportion of AFs was higher on the RL than on the LL of the liver. Coastal cleft with deep impressions was seen in 12%, diaphragmatic grooves in 6%, and short gallbladder (GB) in 6% of the cadaveric livers. The umbilical fissure variations were observed in 18% of the specimens, as shown in Figure 7. Based on Netter's classification, Type 1 (normal) was observed in 22 (48%) specimens, Type 2 was very small LL with deep coastal impressions seen in 8 (16%), Type 3 was complete atrophy of the LL seen in 4 (8%), Type 4 was transverse saddle-like liver with relatively large LL seen in 10%, Type 5 was tongue-like process in LL seen in 6 (12%), and Type 7 was diaphragmatic grooves seen in 3 (6%) of the specimens. No liver with deep renal impression (Type 6) was observed in our study. The various livers belonging to various types based on Netter's classification are depicted in Figure 8.

Discussion

Among all digestive organs, the liver is the first to start its organogenesis during the 3rd week of the embryonic period and proliferates in later life. Due to its complex development, liver anomalies are thought to be rare, and it has been associated with other organ abnormalities.[3] The liver primordium develops as a hepatic diverticulum from the ventral and caudal part of the foregut. It consists of rapidly proliferating cells and starts invading the septum transversum.[9] Under the influence of molecular signals BMP (Bone morphogenic protein), FGF2 (Fibroblast growth factor), and HNF 3, 4 (Hepatocyte nuclear transcription factors), cells from septum transversum induce hepatic segmentation, invade the surrounding mesenchyme

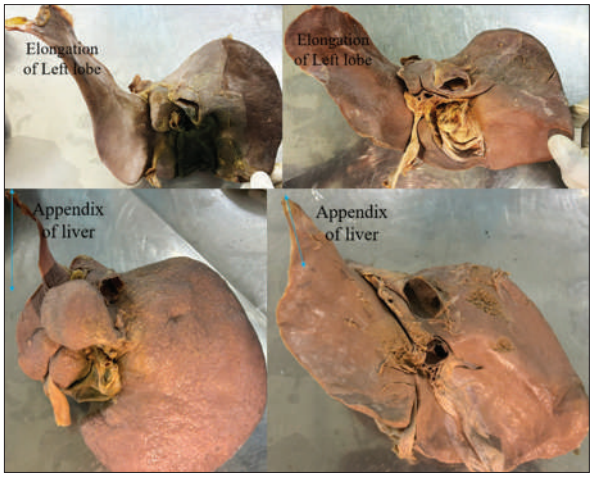

Figure 2: Morphological variations showing elongation of the left lobe and appendix of the liver

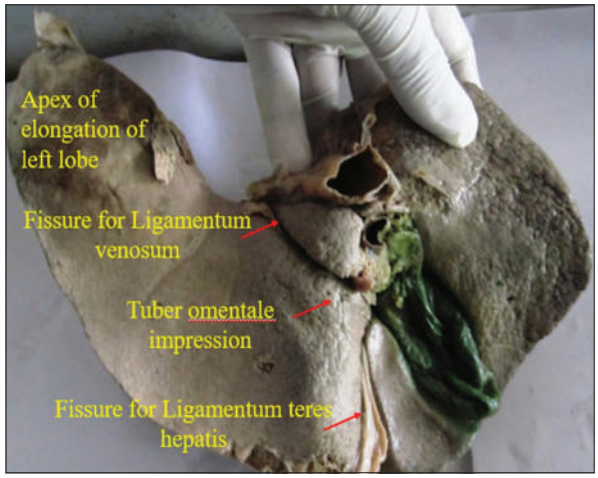

Figure 3: Measurements of elongation of the left lobe of the liver

Table 2: Measurements of elongation of left lobe liver in our present study

Measurements	Abnormal liver 1 (linguiform)	Abnormal liver 2 (leaf like)	Abnormal liver 3 (spatular)	Abnormal liver 4 (pyramid)
Length (cm)				
From upper end of ligamentum venosum till apex of lingual extension	12	9	10	9.5
From lower end of ligamentum teres hepatis till apex of lingual extension	20	15	18.5	16.5
From tuber omentale till apex of lingual extension	14	12	11.5	11
Breadth (cm)				
Base	2	7	7	7
Middle	1	5	5.5	3.5
Apex	1	3.5	5	2.5

to achieve complete hepatic growth.[10] In the initial period, both liver lobes proliferated and were almost equal in size due to abundant oxygenated blood from the umbilical vein. In later pregnancy, some of the hepatocytes degenerate due to decreased nutritional and oxygen supply, which could be the reason for the size reduction, particularly affecting the left lobe.[9]

Morphological anomalies related to defective development of the liver

Agenesis of the liver is a rare congenital disorder defined as the absence of hepatic tissue to the right or left of the fossa of the GB. It was first observed by Arnold–Ashley in 1932, and the incidence has been reported as 0.005%.[11] The hypoplastic lobe of the liver is another rare congenital anomaly. Usually, it is noted accidentally during surgery, at autopsy or during imaging of other organs.[12] Previous studies have reported that the LL is more commonly involved than the RL in both conditions.[13] The standard hepatic segments involved in both conditions are IV in the LL and V and VIII in the RL. Many researchers have observed similar findings in cadaveric specimens and imaging studies, and the results are compared with our present study in Tables 3 and 4.

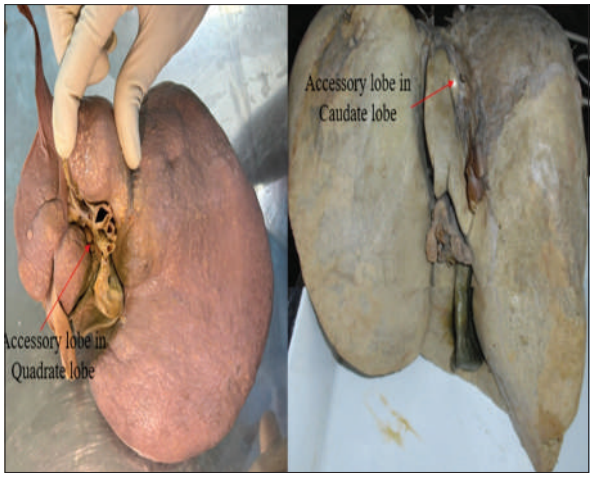

Figure 4: Morphological variations showing accessory lobe of the liver

The congenital cause of agenesis and hypoplasia of the liver lobe is due to umbilical vein anomaly, portal venous thrombosis, and reciprocating error between the primitive diaphragm and the endodermal diverticulum.[16] Patients with these anomalies are clinically asymptomatic with normal function, and the diagnostic clue in both conditions was the absence of liver tissue with invisible hepatic artery, portal veins, and intrahepatic ducts.[15] If left unnoticed, it may lead to complications such as cholecystitis, gastric volvulus, portal hypertension, and Budd–Chiari syndrome.[12,17] Therefore, presurgical knowledge of such anatomical variations is necessary for surgical planning to avoid fatal surgical complications.[17]

Elongation of the LL is defined as extending beyond the left side of the stomach or reaching the spleen. It has to be differentiated from the appendix of the liver, a fibrous

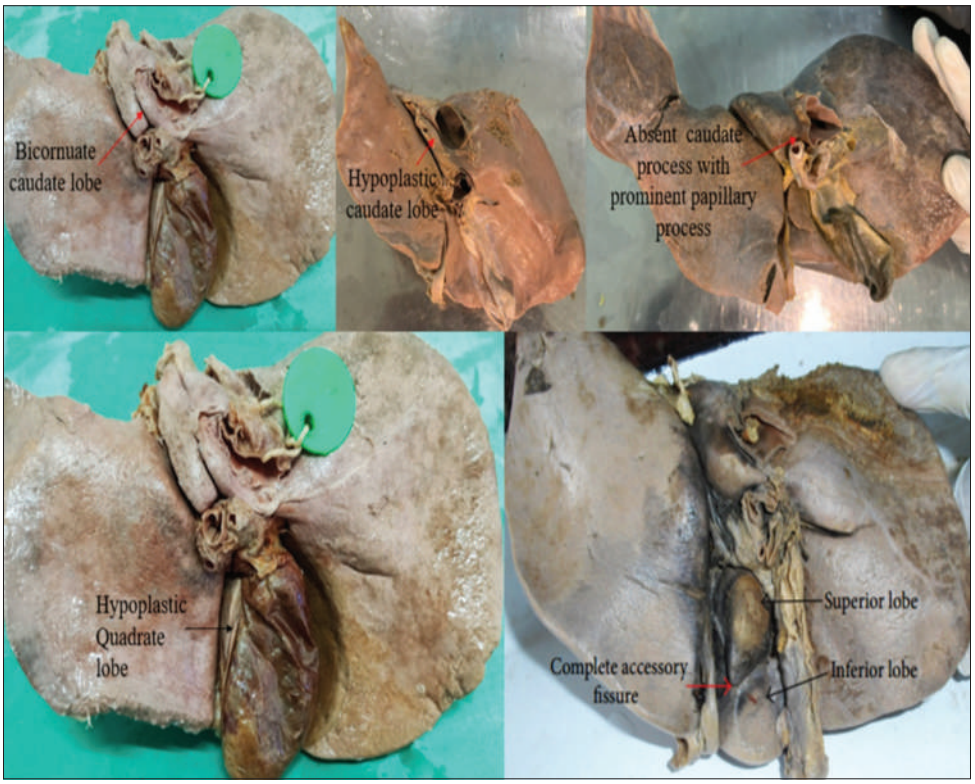

Figure 5: Morphological variations of the caudate lobe and quadrate lobe of the liver

Figure 6: Morphological variations showing accessory fissures, costal cleft, diaphragmatic groove, and short gallbladder

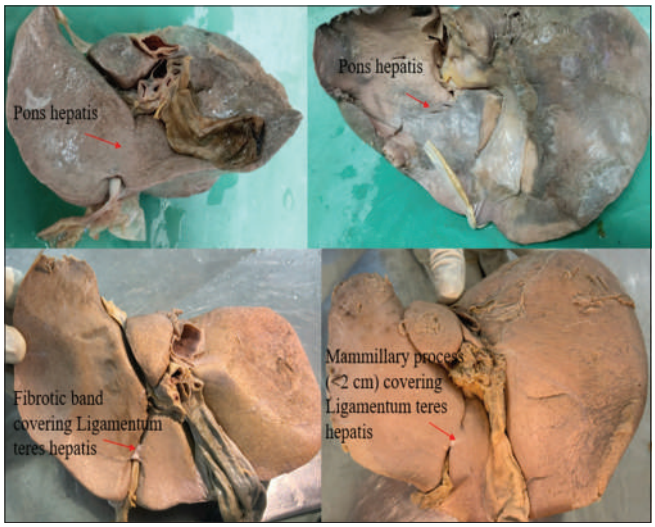

Figure 7: Morphological variations showing abnormalities in fissure for ligamentum teres hepatis

band arising from the left end of the LL, and often appears to be an embryological remnant.[18] Many researchers have reported various shapes on the elongated LL,[19] and the comparative prevalence with other studies is discussed in Table 5. Patients with elongation of the LL may be asymptomatic or may present with pressure symptoms such as epigastric or abdominal pain. It is often undetectable in ultrasonography (USG) while scanning below the xiphoid region, and the presence of gas in the digestive tract often

Table 3: Incidence of agenesis of the left lobe liver among various studies

Studies	Variations observed
Belton and VanZandt, 1983[13]	Two cases of agenesis of LL. Out of two, one is seen accidentally during cholecystectomy surgery and the other one observed during USG of the abdomen
Kanwal and Akhtar, 2021[14]	Single case of agenesis of LL with ectopic GB in CT
Khade and Shah, 2017[15]	One in cadaveric specimen. USG of 400 cases shows, agenesis of LL in 12 cases, absent posterior and anterior segment of right lobe in 12 cases each and complete absence of right lobe in one case
Ceravolo *et al*., 2017[16]	Single case in MRI
Present study, 2024	Four in cadaveric specimens

LL: Left lobe, MRI: Magnetic resonance imaging, CT: Computed tomography, USG: Ultrasonography, GB: Gallbladder

Table 4: Incidence of hypoplasia of left lobe liver among various studies

Studies	Variations observed
Shankar and Kulkarni, 2016[3]	One in cadaveric specimen
Vinnakota and Jayasree, 2013[7]	Two in cadaveric specimens
Ormeci *et al*., 2016[12]	Single case in CT
Singh, 2013[17]	One in cadaveric specimen
Present study, 2024	Two in cadaveric specimens

CT: Computed tomography

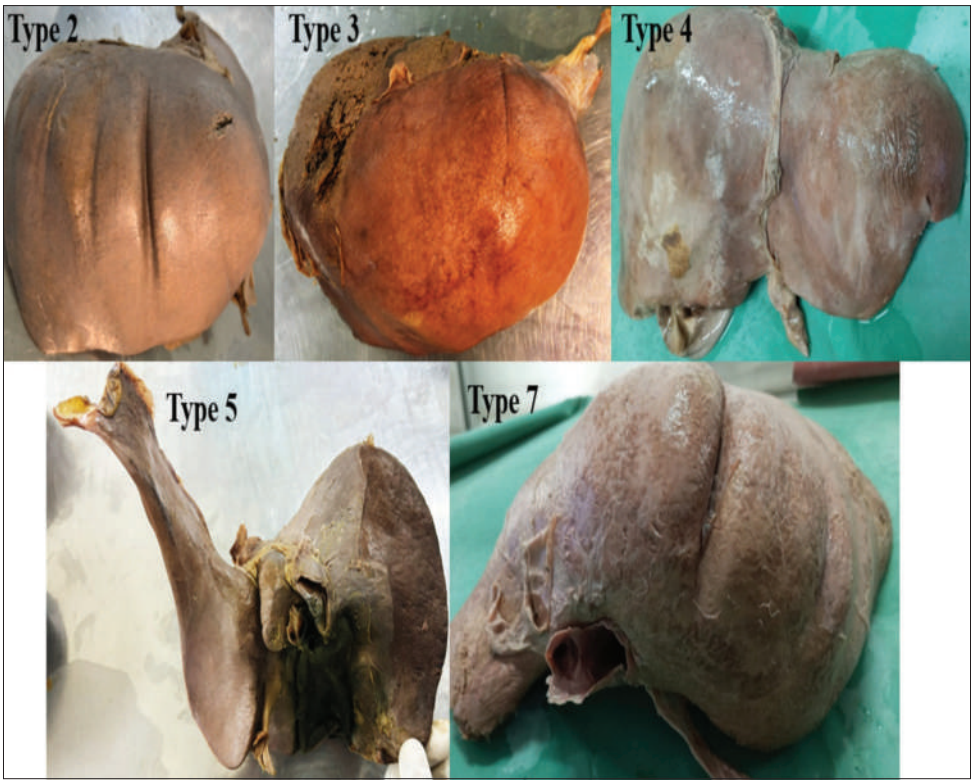

Figure 8: Morphological variations of the liver categorized according to Netter's classification

Table 5: Prevalence of elongation of left lobe and appendix of the liver among various studies

	Number of cases	Frequencies (%)
Nagato *et al*., 2011[2]	13/61	21.31% of elongation of LL liver
Joshi *et al*., 2017[18]	7/80	Elongation of LL - 8.75%
	22/80	Appendix liver - 27.5%
Arya *et al*., 2015[19]	9/60	15% of elongation of LL liver
Patel *et al*., 2014[20]	14/61	28% of elongation of LL liver
Present study, 2024	6/50	Elongation of LL - 12% (2 - spatular, 2 - leaf like, 1 - truncated pyramid, 1 - linguiform)
	7/50	Appendix liver - 14%

LL: Left lobe

facilitates better imaging of the elongated LL.[18] In some cases, it may often be misdiagnosed as focal lesions such as subcapsular splenic hematoma, hydatid cyst, and sarcoma of the liver on radiographic images due to its migration into the left upper quadrant.[2,19] Color Doppler imaging is the best imaging modality to rule out the elongation of the hepatic lobe before proceeding with any therapeutic and diagnostic procedures.[20]

Morphological anomalies related to excessive development of the liver

Excessive development of the liver leads to AL formation. It is a separate lobe attached to the liver by hepatic tissue, mesentery, or a stalk.[20] The embryological reason could be an error in the segmentation of the hepatic bud or the persistent proliferation of mesodermal septa during the 3rd month of the intrauterine life.[9] It more frequently arises from the RL and projects in different directions.[5] The most common AL is Riedel's lobe, which is an inferior extension of the RL of the liver toward the right iliac fossa. It was considered the first anatomical variant of the liver and rarely produces symptoms.[6] Many investigators have documented AL; the results are tabulated in Table 6.

Clinically, it has surgical and radiological importance due to its smaller size and connection through stalk or vascular pedicle. Patients with AL are asymptomatic, and sometimes, it may be misdiagnosed as lymph nodes in radiological images owing to their small size.[21] AL has vascular structures such as portal vein, hepatic artery, and bile duct for its viability. Accidental removal of the AL during surgeries may result in profuse bleeding due to damage to the vascular pedicle.[22] The clinical presentation of AL mainly depends on complications such as torsion, traumatic rupture, and infarction. Torsion is an emergency condition often present with stomach aches due to vascular obstruction, ischemia, and bleeding, which requires surgical interventions as early as possible. Computed tomography, magnetic resonance imaging, or USG have made a diagnosis of AL.[21,23]

The caudate and quadrate lobes are part of the RL of the liver. According to the Couinaud classification, it

is considered an independent segment. Anatomically, the quadrate lobe belongs to the RL of the liver, but functionally, it is dependent on the LL. Many morphological variations were observed on both lobes, but very few investigators have documented them.[4,18] The results of caudate and quadrate lobe variations among various studies are compared in Table 7. The most commonly reported

Table 6: Prevalence of accessory lobe of the liver among various studies

	Number of cases	Frequencies (%)
Sambhav *et al*., 2023[4]	AL on QL - 2/40	5
Baruah and Choudhury, 2016[6]	AL on LL - 1/30	3.33
Vinnakota and Jayasree, 2013[7]	AL in RL - 2/58	3.5
	AL in LL - 1/58	1.7
	AL in CL - 3/58	5.2
	AL in QL - 4/58	6.9
Nayak *et al*., 2013[23]	5/55	9.09
Present study 2024	AL in CL - 2/50	4
	AL in QL - 1/50	2

QL: Quadrate lobe, CL: Caudate lobe, LL: Left lobe, RL: Right lobe, AL: Accessory lobe

Table 7: Prevalence of Caudate and Quadrate lobe variations in our present study and in other studies

	Number of cases	Frequencies (%)
	CL variations	
Sambhav *et al*., 2023[4]	Rectangular shape – 16/40	40
	Pyriform shape – 5/40	12.5
	Irregular shape – 3/40	7.5
	Inverted pyriform shape – 4/40	10
	Bicornuate CL – 6/40	15
	Hypoplastic CL – 6/40	15
	Prominent papillary process – 7/40	17.5
	Absent caudate process – 1/40	2.5
Present study 2024	Rectangular shape – 16/50	32
	Pyriform shape – 4/50	8
	Irregular shape – 3/50	6
	Bicornuate CL – 6/50	12
	Hypoplastic CL – 1/50	2
	Absent caudate process with prominent papillary process – 1/50	2
	QL variations	
Sambhav *et al*., 2023[4]	Quadrangular shape – 10/40	25
	Triangle shape – 7/40	17.5
	Rectangle shape – 6/40	15
	Bilobed QL – 2/40	5
	Absent QL – 1/40	2.5
Present study, 2024	Quadrangular shape – 12/50	24
	Triangle shape – 8/50	16
	Rectangle shape – 5/50	10
	Bilobed QL – 2/50	4
	Hypoplastic QL – 1/50	2
	Absent QL – 1/50	2

CL: Caudate lobe, QL: Quadrate lobe

caudate lobe shape is rectangular, followed by a pyriform shape, which coincides with our present study. Similarly, the most familiar quadrate lobe shapes were quadrangular, followed by triangular and rectangular, which coincides with our study results. We have seen one specimen with an absent quadrate lobe (2%), which was noted similarly by Sambhav *et al*. in 2.5% and Joshi *et al*. in 4% of the specimens.[4,18] Patients with hepatobiliary carcinoma have been treated with hepatectomy along with resection of the caudate lobe, which yields better surgical outcomes.[2] Clinically, a variant caudate and quadrate lobe could be a diagnostic sign of cirrhosis.[4]

Most of the fissures on the hepatic surface formed during the prenatal period disappear through the process of liver development. However, in some places, it may persist on abnormal sites, which may be recognized as an AF. It mainly occurs due to the inward folding of the peritoneum on the undersurface of the liver.[9] In our study, 13 cadaveric livers show the presence of AF, most commonly seen on the caudate and RL and less on the LL and quadrate lobe, as mentioned in Figure 6. The umbilical fissure, also called "fissure for ligamentum teres hepatis," is present on the inferior surface of the liver. It is a normal fissure extending from the liver's inferior border to the porta hepatis's left margin.[1] Many researchers have documented the umbilical fissure variations. Cawich *et al*., in 2021, proposed four types of morphological classification of umbilical fissure variations as follows:[24]

Type 1 – Normal umbilical fissure
Type 2 – Closure of umbilical fissure by fibrotic band in anterior, middle, and posterior part
Type 3 – Closure of umbilical fissure by mammillary (<2 cm length) and lingual process (>2 cm length)
Type 4 – Pons hepatis closed and open type.

In the closed type of pons hepatis, the umbilical fissure is entirely covered by hepatic parenchyma, converting it into a tunnel. In the open type, it is partially covered by hepatic tissue. In our study results, we observed nine cases of umbilical fissure variations, out of which four cases with pons hepatis (closed type), four with the mammillary process, and one with the fibrotic band covering the middle-third of the umbilical fissure.

Another AF is a diaphragmatic groove called "Zhan's groove." It is seen on the hepatic surface due to pressure exerted from the ribs and diaphragm on the uneven growth of hepatic parenchyma.[4] Three specimens showed deep diaphragmatic grooves on the superior liver surface (Netter's Type 7), one of which was more remarkable and prominent, as shown in Figure 6. In elderly patients, these fissures may appear scalloped or lobular, which could be mistaken for macronodular liver in cirrhosis.[19] Recent studies on corrosion casting have suggested that the presence of sulci provides a landmark for portal fissures between adjacent portal territories.[25] The results of all

AFs obtained in our study compared with other studies are documented in Table 8.

Clinically, the presence of AF would serve as a landmark for surgeons when planning for liver resections. Imaging techniques may often misdiagnose because any pulmonary lesions or ascitic fluid may extend through the diaphragm and peritoneum and often present as focal lesions such as liver abscess, metastasis of tumor cells, or intrahepatic hematoma.[7,20,26] During laparoscopic procedures, surgeons often grab the ligamentum teres hepatis with the instruments to manipulate the liver. Hence, the variant umbilical fissure may be hazardous to the surgeons, which leads to damage to hepatic parenchyma by shear stress, resulting in catastrophic bleeding.[24]

Table 8: Prevalence of accessory fissure in present study and in other studies

	Number of cases	Percentage
Nagato *et al*., 2011[2]	Diaphragmatic groove – 4/61	6.56
	Costal cleft – 5/61	8.19
Sambhav *et al*., 2023[4]	AF on RL – 29/40	72.5
	AF on LL – 12/40	30
	AF in CL – 23/40	57.5
	AF in QL – 7/40	17.5
	Diaphragmatic grooves – 3/40	7.5
	Pons hepatis – 3/40	7.5
Nayak, 2013[8]	Short GB – 10/55	18.18
Cawich *et al*., 2021[24]	Umbilical fissure variations – 38/69	55.1
	Type 2	1.5
	Type 3	20.3
	Type 4	33.3
Mamatha *et al*., 2014[26]	AF on right and LL – 5/50	10
	AF in CL – 6/50	12
	AF in QL – 5/50	10
	Diaphragmatic grooves – 6/50	12
	Short GB – 10/55	2
Present study, 2024	AF on RL – 6/50	12
	AF on LL – 2/50	4
	AF in CL – 7/50	14
	AF in QL – 3/50	6
	Costal cleft – 6/50	12
	Diaphragmatic grooves – 3/50	9
	Short GB– 3/50	6
	Umbilical fissure variations – 9/50	18
	Type 2 – 1	2
	Type 3 – 4	8
	Type 4 – 4	8

AF: Accessory fissure, CL: Caudate lobe, QL: Quadrate lobe, LL: Left lobe, RL: Right lobe, GB: Gallbladder

Anatomically, the GB is present on the inferior surface of the RL. The fundus of GB produces a cystic notch on the inferior border of the liver, but in our study, GB was short in two specimens and limited within the GB fossa, as shown in Figure 6. Short GB could be due to abnormal peritoneal folds like cystohepatocolic folds, and it is often misdiagnosed in imaging studies and during laparoscopic surgeries.[8,26] Only a few investigators have reported similar findings, and the results are mentioned in Table 8. According to Netter's classification, this study presents cadaveric livers with all types except Type 6. The results obtained in our study are compared with other studies and documented in Table 9. The primary reason for the hepatic variations is disproportionate development, which leads to misrecognition of the pathologies and adverse surgical outcomes.[4,27]

Limitations of the study

Since the descriptive study was conducted in cadaveric specimens of unknown age and gender, hepatic variations could not be statistically analyzed to substantiate the findings. For better surgical outcomes of hepatic pathologies, the author would like to propose a study in future with a large number of specimens on its descriptive and functional anatomy.

Conclusions

The current study has documented variant morphological changes in the liver, which would contribute to the evolving document and also be helpful for anatomists and surgeons. These variations are quite common and are asymptomatic unless; it is diagnosed incidentally during radiologic

Table 9: Comparison of morphological variations of the liver in various studies based on Netter's classification[27]

Types	Gross variations	Nagato *et al*.[2] *n*=61 (%)	Sambhav *et al*., 2023[4] *n*=40 (%)	Sangeetha and Kumar[28] *n*=50 (%)	Present study *n*=50 (%)
Type 1	Normal	52.46	55	66.9	48
Type 2	Very small LL with deep costal impressions	8.19	10	7	16
Type 3	Complete atrophy of LL	1.64	-	3	8
Type 4	Transverse saddle-like liver with relatively large LL	6.56	17.5	7.10	10
Type 5	Tongue-like process in LL	21.31	2.5	9	12
Type 6	Very deep renal impression and corset constriction	9.84	7.5	6	-
Type 7	Diaphragmatic grooves	-	7.5	-	9

LL: Left lobe

imaging and surgery. Preoperative diagnosis of hepatic variants would be helpful for surgeons and radiologists for misleading diagnoses and in planning hepatobiliary surgeries and portosystemic anastomosis. Whenever there are variations in the liver, it is essential to examine other adjacent organs as it is associated with clinical conditions such as gastric volvulus, diaphragmatic abnormalities, and portal hypertension.

Acknowledgments

The researchers acknowledge the professors of the Department of Anatomy, VMMC and H, Karaikal, for briefly reviewing this manuscript. The authors sincerely thank those who donated their bodies to science so that anatomical research could be performed. The results from such research can potentially increase humankind's overall knowledge, which can then improve patient care. Therefore, these donors and their families deserve our highest gratitude.

Financial support and sponsorship

Nil.

Conflicts of interest

There are no conflicts of interest.

References

1. Standring S. Gray's Anatomy. The Anatomical Basis of Clinical Practice. 41st ed. UK: Elsevier; 2016. p. 1052-3, 1160-3.
2. Nagato AC, Silva MA, Trajano ET, Alves JN, Bandeira AC, Ferreira TA, *et al.* Quantitative and morphological analyses of different types of human liver. J Morphological Sci 2011;28:275-9.
3. Shankar VV, Kulkarni R. Hypoplastic left lobe of the liver. Int J Anat Res 2016;4:1958-60.
4. Sambhav K, Krishna H, Dixit SG, Ghatak S. Morphological study of variations of the human cadaveric liver and its clinical implications. Cureus 2023;15:e35507.
5. Carrabetta S, Piombo A, Podestà R, Auriati L. Torsion and infarction of accessory liver lobe in young man. Surgery 2009;145:448-9.
6. Baruah P, Choudhury PR. Anomalies of liver morphology: A study on cadaveric liver. Int J Anat Res 2016;4:3284-8.
7. Vinnakota S, Jayasree N. A new insight into the morphology of the human liver: A cadaveric study. ISRN Anat 2013;2013:689564.
8. Nayak BS. A study on the anomalies of liver in the South Indian cadavers. Int J Morphol 2013;31:658-61.
9. Gary CS, Steven BB, Philip RB, Philippa H, Francis W. Larsen's Human Embryology. 5th ed. Philadelphia: Elsevier; 2015. p. 350-2.
10. Bezerra JA. Hepatocytes and endothelial cells: Joining forces to conquer development. Pediatr Res 2002;51:413.
11. Merrill GG. Complete absence of the left lobe of the liver. Arch Pathol (Chic) 1946;42:232.
12. Ormeci T, Erdogan ST, Ormeci A, Aygun C. A rare congenital liver anomaly: Hypoplasia of left hepatic lobe. J Pak Med Assoc 2016;66:1662-4.
13. Belton RL, VanZandt TF. Congenital absence of the left lobe of the liver: A radiologic diagnosis. Radiology 1983;147:184.
14. Kanwal R 3rd, Akhtar S. Left hepatic lobe agenesis with ectopic gallbladder. Cureus 2021;13:e16131.
15. Khade A, Shah M. Lobes and segment anomalies of the liver. Glob J Res Anal 2016;6:273-4.
16. Ceravolo I, Guerrieri D, De Vargas Macciucca M, De Cristofaro F, Panzironi G. MRI rare finding: Absence of the left liver lobe. Eur J Radiol Open 2017;4:50-2.
17. Singh R. Hypoplastic left lobe of liver with accessory caudate lobe. Case Rep Med 2013;2013:604513.
18. Joshi SS, Valimbe N, Joshi SD. Morphological variations of left lobe of liver. Int J Comtemp Med Res 2017;4:1956-8.
19. Arya RS, Arya RC, Kumar A, Basan K, Singh B, Jangde S. Study of cadaveric liver lobe anomaly. Indian J Clin Anat Physiol 2015;2:212-5.
20. Patel J, Gosai PP, Desai JN, Bhojak NR, Ram SH. Morphological and quantitative analysis of human liver-a cadaveric study. Natl J Integr Res Med 2014;5:82-5.
21. Pujari BD, Deodhare SG. Symptomatic accessory lobe of liver with a review of the literature. Postgrad Med J 1976;52:234-6.
22. Jambhekar K, Pandey T, Kaushik C, Shah HR. Intermittent torsion of accessory hepatic lobe: An unusual cause of recurrent right upper quadrant pain. Indian J Radiol Imaging 2010;20:135-7.
23. Nayak SB, Kumar N, Sirasanagandla SR, Shetty SD. A mini accessory liver lobe in the fissure for ligamentum teres and its clinical significance: A case report. J Clin Diagn Res 2013;7:2573-4.
24. Cawich SO, Gardner MT, Shetty R, Lodenquai P, Ramkissoon S, Ho P, *et al.* Clinically oriented classification of anatomic variants of the umbilical fissure for ligamentum teres in the human liver. Cureus 2021;13:e15460.
25. Macchi V, Porzionato A, Parenti A, Macchi C, Newell R, De Caro R. Main accessory sulcus of the liver. Clin Anat 2005;18:39-45.
26. Mamatha Y, Murthy CK, Prakash BA. Study on morphological surface variations in human liver. Int J Health Sci Res 2014;4:97-102.
27. Netter FH. Atlas of Human Anatomy. 2nd ed. New York: Guilford Press; 2000.
28. Sangeetha A, Kumar SN. Morphological variations of the liver and its applied significance: A cadaveric study. J Datta Meghe Inst Med Sci Univ 2021;16:303-6.

Original Article

Cultural Considerations in Rhinoplasty: Assessing the Importance of Esthetic Nasal Parameters in the Indian Context

Shehzeen Afaq, S. K. Jain, Nidhi Sharma[1], Sonika Sharma

Department of Anatomy, TMMC and RC, Moradabad, [1]Department of Anatomy, Kalyan Singh Medical College, Bulandshahr, Uttar Pradesh, India

Abstract

Background: The nose is one of the most important feature of the face and greatly influences its esthetics. To have a successful rhinoplasty, it is essential to have extensive knowledge of nasal anatomy and facial esthetic standards. This is because any unfavorable look, whether before or following the surgery, may attract unwanted gazes. On the other hand, two-dimensional (2D) photogrammetry has replaced the direct anthropometric technique for nasal analysis, but its accuracy and reliability are still unknown. This investigation seeks to evaluate the consistency among raters in 2D photogrammetry and to scrutinize both its reliability and precision compared to direct measurements. **Materials and Methods:** This cross-sectional study was done in the Department of Anatomy at Teerthanker Mahaveer Medical College in Moradabad for 1 year. This study included 640 volunteers (320 males and 320 females) across all six zones of the Indian population: SPSS v25 was used for evaluating the data, and a significance threshold of $P < 0.05$ was deployed to establish the level of statistical significance. **Results:** Males and females differed significantly in all nasal measurements using the direct approach, except nasal bridge length. However, when employing 2D indirect photogrammetry, anatomical nose width, and nasal bridge length did not display significant variations. Among the eight parameters examined, five nasal metrics exhibited a strong level of concordance, including nose height, morphological nose width, alar length, nasal tip protrusion, and nasal index. On the other hand, nasal bridge length and columella length showed a reasonable level of reliability in both methods. **Conclusion:** This research implies that nasal traits can differ among ethnicities and potentially affecting perceptions or evaluations. Furthermore, it is crucial to recognize that nasal metrics may vary not only among diverse ethnic groups but also within distinct regions of India, as well as between genders. The results of this research also suggested that 2D photogrammetry proves to be a reliable substitute for the direct method.

Keywords: *Facial analysis, nasal anthropometry, photogrammetry, rhinoplasty, two-dimensional anthropometry*

Introduction

In the world of plastic surgery, creativity plays a pivotal role.[1] Surgeons often need to overcome uncommon hurdles that demand unconventional thinking to attain optimal results.[1] The field of plastic and reconstructive surgery thrives on a diverse range of technologies, pioneering techniques, and meticulous planning, especially in the nuanced domain of facial anthropometry.[2] Reconstructive surgeons may accomplish spectacular results in facial anthropometry by integrating multiple aspects such as technological advances, diverse techniques, innovative adaptations, and strategic planning, thereby improving patients' aesthetics as well as their quality of life.[2]

Rhinoplasty is still considered one of the most prevalent cosmetic surgical procedures throughout the world, with its favorable results reliant on careful preparation before surgery and intraoperative execution.[3] For this procedure, the precise evaluation of nasal measurements and dimensions, previously obtained by direct physical measurements, remains extremely important.[3]

Two-dimensional (2D) photogrammetry has recently evolved as a noninvasive technique, particularly in the realm of facial anthropometry.[4] In the context of faces, this noninvasive method offers an efficient way to obtain multiple facial images from different angles and then, using specialized software (Digimizer and Crisalix) to reconstruct a theer-dimensional (3D) model, analyze various features such

How to cite this article: Afaq S, Jain SK, Sharma N, Sharma S. Cultural considerations in rhinoplasty: Assessing the importance of esthetic nasal parameters in the Indian context. J Anat Soc India 2025;74:133-40.

Article Info

Received: 13 August 2024
Revised: 11 December 2024
Accepted: 19 February 2025
Available online: 30 June 2025

Address for correspondence:
Ms. Shehzeen Afaq, Department of Anatomy, TMMC and RC, Moradabad, Uttar Pradesh, India.
E-mail: shehzeenafaq@gmail.com

Access this article online

Website: https://journals.lww.com/joai

DOI: 10.4103/jasi.jasi_122_24

Quick Response Code:

as symmetry, distances, angles, and proportions to extract specific measurements and data.[4] This method made facial anthropometry more accessible, allowing researchers and practitioners to obtain valuable data without the need for invasive procedures. The 2D approach offers several substantial advantages in the healthcare and medical domains as under:[4]

- Increased patient comfort: This approach provides a noninvasive and pleasant means of retrieving data, which may enhance the entire experience without requiring patients to endure intrusive treatments
- Reduced measurement variability: It can help reduce the variability in measurements compared to manual methods. Human error can lead to inconsistencies in manual methods, whereas proper calibration and execution of photogrammetry ensures more precise and consistent results
- Digital record-keeping: Photogrammetry makes patient data easily accessible for future reference.

However, there has not yet been extensive research on the accuracy of 2D photography in relation to rhinoplasty. In the context of rhinoplasty, assessing the validity and precision of 2D photogrammetry compared to direct measuring methods may provide significant findings for the plastic surgery fraternity. To close this gap, this study will compare the accuracy and reliability of 2D photogrammetry against direct measuring methods for determining nasal measurements for rhinoplasty.

Materials and Methods

This descriptive cross-sectional study took place at the Department of Anatomy in the Teerthanker Mahaveer Medical College and Research Centre in Moradabad, Uttar Pradesh, India. This study, conducted from January 2023 to January 2024, involved 640 participants from six different Indian zones, with 320 males and 320 females, using a cross-sectional research formula ($n = Z\ P\ [100 - P]/E$) to ensure a representative sample size. The study involved individuals from six distinct Indian zones: East, West, North, South, North-East, and Central. The study included healthy Indian subjects aged 18–25.[3] Those having a history of facial plastic surgery,[5] intellectual disability,[5] congenital craniofacial abnormality,[6] significant damage,[5] and mixed-ethnic background were excluded from the research.[3] The study was approved by the Institutional Ethical Committee (Ref. no. TMU/IEC/20-21/103) at TMMC and RC, with informed consent from each subject, following the 1975 Helsinki Declaration's ethical guidelines. Eight nasal dimensions (nose height, anatomical nose width [ANW], morphological nose width [MNW], columella length, nasal bridge length, alar length, nasal tip protrusion, and nasal index) were measured, and calculated by two different approaches: Direct and 2D Indirect.

Direct method

We acquired written agreement before measurements and allayed any lingering doubts by thoroughly explaining the measuring procedure to the participants. Participants were required to maintain a neutral head posture (Frankfurt plane) and facial expressions while measuring anatomical landmarks using a surgical skin pencil and caliper, with average readings considered to be accurate [Figure 1].[7]

2D indirect photogrammetry

A 24.2-megapixel Digital single-lens reflex camera was utilized by the department's photography section to take pictures in well-lit conditions. We captured the photos with the head positioned in the Frank Furt plane and aligned with the reference scale. We scrutinized the images for flaws such as misorientation, distortion, or imaging artifacts. We saved the JPEG files and sent them to the Digimizer Image Analysis programme (Version 5.7.5), MedCalc Software Ltd. Acacialaan 22 8400 Ostend, Belgium (MedCalc Software's VAT registration number is BE 0809 344 640). This software is incredibly user-friendly and versatile for facial image analysis [Figures 2 and 3].[8]

Statistical analysis

We used SPSS version 25 for analysis ((IBM 2009), Chicago, United States), evaluating data homogeneity using Shapiro–Wilk and Kolmogorov–Smirnov tests. A normal distribution implies no variables deviating from the normalcy assumption. We assessed the descriptive statistics of facial parameters using mean and standard deviation, an unpaired *t*-test for sexual dimorphism, and an intra class correlation coefficient (ICC)[4] test to evaluate the reliability of the 2D method against the direct method. The International Chirurgical Correlation (ICC) measures the reliability of measurements from the same group to observations from other groups, with a range of 0–1, ([<0.4: poor reliability], [0.4–0.75: moderate reliability], and [≥0.75: excellent reliability]) allowing researchers to assess data trustworthiness and make

Figure 1: Direct anthropometry

informed decisions about measurement quality. For further assessment, we used another geographical representation (Bland–Altman analysis)[9] and regression analysis[9] to assess the agreement between the two methods. In this method, we plotted the measurement difference (on the Y-axis) obtained by two methods against the average (on the X-axis) of against the average of the two measurements. For every statistical analysis, the threshold of significance for statistical purposes was established at $P < 0.005$.

Results

The mean nasal length in females was 4.1 ± 0.54 and 4.06 ± 0.55 cm by direct and indirect method, respectively. The other measurements were ANW 2.87 ± 0.19 and 2.79 ± 0.23 cm, MNW 3 ± 0.23 and 3.09 ± 0.23 cm, columellar length 0.98 ± 0.21 and 1 ± 0.2 cm, nasal bridge length 4.07 ± 0.38 and 4.12 ± 0.39 cm, alar length 3.2 ± 0.7 and 3.20 ± 0.72 cm, nasal tip protrusion 0.79 ± 0.17 and 0.79 ± 0.18 cm, and nasal index 69.9 ± 10.2 and 70.59 ± 10.8 by both the methods, respectively, as shown in Table 1.

The mean nasal length in males was 4.5 ± 0.43 and 4.16 ± 0.37 cm by direct and indirect method, respectively. The other measurements were ANW 3.01 ± 0.29 and 3.1 ± 0.24 cm, MNW 3.2 ± 0.3 and 3.1 ± 0.24 cm, columellar length 1.2 ± 0.21 and 1.10 ± 0.17 cm, nasal bridge length 4.06 ± 0.4 and 3.6 ± 0.38 cm, alar length 2.9 ± 0.37 and 2.8 ± 0.39 cm, nasal tip protrusion 0.7 ± 0.08 and 0.69 ± 0.11 cm, and nasal inde × 79 ± 11.3 and 76.05 ± 8.8 by both the methods, respectively, as shown in Table 1.

Using both approaches, the mean values for the eight nasal dimensions above showed a substantial difference between males and females. All nasal metrics, except for nasal bridge length, demonstrated significant differences between males and females when measured using the direct technique; however, when measured using 2D indirect photogrammetry, ANW and nasal bridge length did not exhibit significant differences, as shown in Table 2.

Table 3 presents the intraclass correlation coefficient, in both genders. To find out how reliable 2D photogrammetry is in comparison to the direct approach and what the standard deviation of differences has, a reliability evaluation was carried out. ICC values for eight nasal dimensions varied from 0.65 to 0.99 in males and 0.63 to 0.96 in females. The highest ICC score was noted for alar length ([ICC: 0.99, 95% confidence interval [CI]: 0.98–0.99 in male] and [ICC: 0.96, 95% CI: 0.82–0.88 in female]) followed by nasal tip protrusion ([ICC: 0.99, 95% CI: 0.98–0.99 in male] and [ICC: 0.97, 95% CI: 0.92–0.98 in female]) and minimum score of

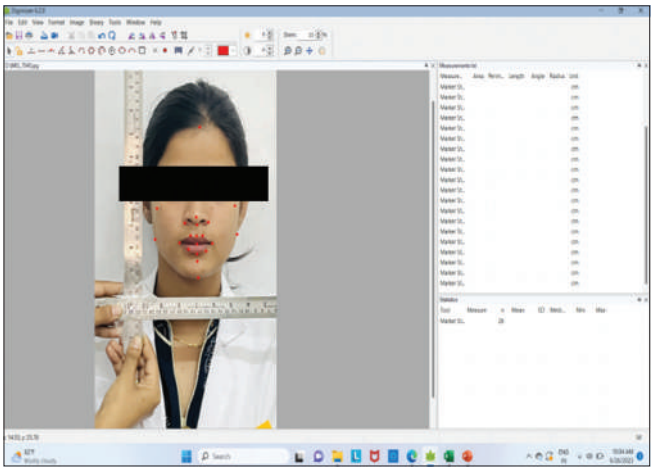

Figure 2: Indirect anthropometry (frontal view)

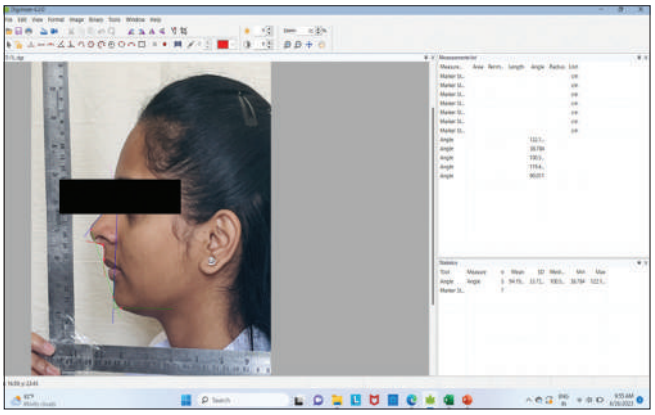

Figure 3: Indirect anthropometry (lateral view)

Table 1: Descriptive statistics of nasal parameters for each gender by both approaches

Parameters	Measurements of nasal parameters (mean±SD)			
	Male		Female	
	Direct method	Indirect method	Direct method	Indirect method
Nose height	4.5±0.43	4.16±0.37	4.1±0.54	4.06±0.55
Anatomical nose width	3.01±0.29	3.1±0.24	2.87±0.19	2.79±0.23
Morphological nose width	3.2±0.3	3.1±0.24	3±0.23	3.09±0.23
Columella length	1.2±0.21	1.10±0.17	0.98±0.21	1±0.2
Nasal bridge length	4.06±0.4	3.6±0.38	4.07±0.38	4.12±0.39
Alar length	2.9±0.37	2.8±0.39	3.2±0.7	3.20±0.72
Nasal tip protrusion	0.7±0.08	0.69±0.11	0.79±0.17	0.79±0.18
Nasal index	79±11.3	76.05±8.8	69.9±10.2	70.59±10.8

SD: Standard deviation

ICC was found in nasal bridge length ([ICC: 0.69, 95% CI: 0.62–0.86 in male] and [ICC: 0.63, 95% CI: 0.58–0.95 in female]). All eight nasal parameters either show moderate reliability or excellent reliability of 2D photometry against the direct measurements.

We used Bland–Altman scatter plots to graphically show all of the nasal characteristics to provide further assurance. In this scatter plot, there were 2-axis, y-axis showed the mean difference between the two approaches, whereas x-axis showed the mean of the two approaches. Out of eight, five nasal parameters displayed a high degree of agreement between the parameters, i.e. nose height, MNW, alar length, nasal tip protrusion, nasal index and ANW, columella length, and nasal bridge length showed moderate reliability in two approaches as shown in Graphs 1-8.

We used another statistical approach for the confirmation of the reliability test was regression analysis as shown in Table 4. In this analysis, we found the same *P* values of *t*-test and analysis of variance test, which confirmed there is reliability between direct and indirect anthropometry.

Table 2: Depiction of the sexual dimorphism in nasal parameters by both approaches

Parameters	Direct method		2D-indirect method	
	t	*P*	*t*	*P*
Nose height	−2.7	<0.05	−3.3	<0.05
Anatomical nose width	2.5	<0.05	0.4	>0.05
Morphological nose width	4.27	<0.05	1.17	<0.05
Columella length	2.35	<0.05	−0.58	<0.05
Nasal bridge length	−0.046	>0.05	−6.9	>0.05
Alar length	−3.02	<0.05	−3.3	<0.05
Nasal tip protrusion	−3.13	<0.05	0.28	<0.05
Nasal index	4.6	<0.05	3.01	<0.05

2D: Two-dimensional

Discussion

A descriptive cross-sectional study was conducted among 640 normal, healthy subjects from six demographic zones of the Indian population for the screening of nasal parameters. As everyone knows, India has a diverse population of many ethnicities and cultures; thus, we included representatives from each of the six zones.

Furthermore, the primary idea underlying this research was to determine whether nasal characteristics differed between India's zones, we might accurately represent the entirety of the Indian population by amassing data from every zone. Our university serves a significant number of students with diverse cultural backgrounds from various regions of India. When performing procedures, such as rhinoplasty, facial plastic surgeons assess patients' appearances using measurements and facial surface anthropometric parameters.

Table 3: Intra-class correlation coefficient values for accuracy of two-dimensional method against direct method in both gender

Parameters	Male		Female	
	Intra class correlation coefficient	95% CI (lower to upper bound)	Intra class correlation coefficient	95% CI (lower to upper bound)
Nose height	0.97	0.93–0.99	0.96	0.96–0.99
Anatomical nose width	0.65	0.71–0.92	0.64	0.72–0.96
Morphological nose width	0.91	0.86–0.96	0.93	0.82–0.97
Columella length	0.86	0.84–0.98	0.84	0.80–0.96
Nasal bridge length	0.69	0.62–0.86	0.63	0.58–0.95
Alar length	0.99	0.98–0.99	0.96	0.82–0.88
Nasal tip protrusion	0.99	0.98–0.99	0.97	0.92–0.98
Nasal index	0.97	0.95–0.98	0.96	0.94–0.97

CI: Confidence interval

Table 4: Regression analysis for methods accuracy in both gender

Parameters	Male						Female					
	Regression		ANOVA		*t*-test		Regression		ANOVA		*t*-test	
	R	R^2	*F*	Significant	*t*	Significant	*R*	R^2	*F*	Significant	*t*	Significant
Nose height	0.24	0.059	3.61	0.062	1.9	0.062	0.26	0.046	3.64	0.064	1.21	0.064
Anatomical nose width	0.25	0.064	3.95	0.05	1.98	0.05	0.29	0.078	3.0	0.04	1.18	0.04
Morphological nose width	0.43	0.188	13.39	0.001	3.66	0.001	0.38	0.178	14.39	0.007	4.67	0.007
Columella length	0.198	0.039	2.36	0.13	1.53	0.13	0.19	0.029	3.16	0.13	1.77	0.13
Nasal bridge length	0.054	0.003	0.172	0.68	0.41	0.68	0.064	0.001	0.182	0.59	0.24	0.59
Alar length	0.051	0.003	1.49	0.701	−0.38	0.701	0.059	0.006	1.5	0.601	0.29	0.601
Nasal tip protrusion	0.28	0.08	5.15	0.027	−2.27	0.027	0.35	0.09	5.0	0.017	−2.14	0.017
Nasal index	0.41	0.16	11.7	0.001	3.43	0.001	0.40	0.15	12.9	0.009	3.19	0.009

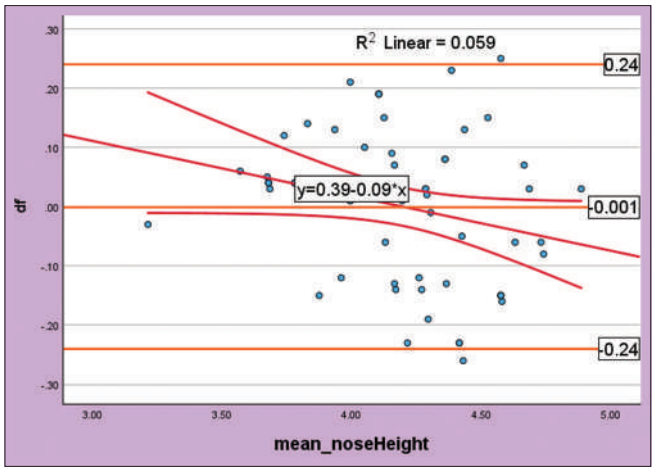

Graph 1: Bland altman analysis plot (BAA) plot for nose height by direct and indirect method

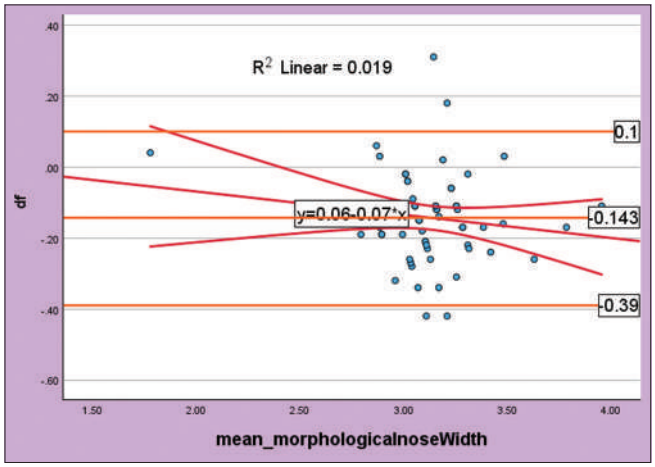

Graph 3: Bland altman analysis plot (BAA) plot for morphological nose width by direct and indirect method

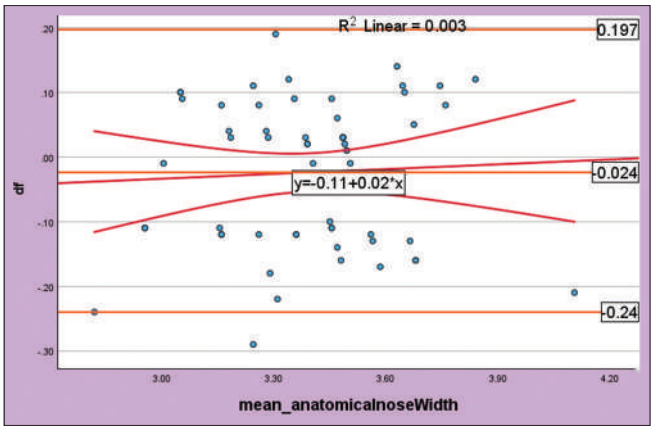

Graph 2: Bland altman analysis plot (BAA) plot for anatomical nose width by direct and indirect method

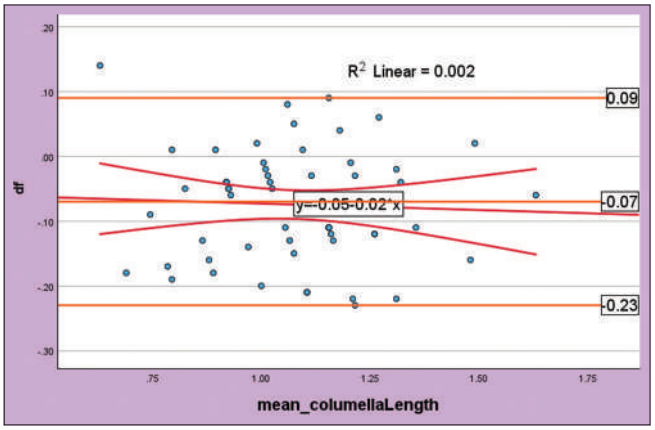

Graph 4: Bland altman analysis plot (BAA) plot for columella length by direct and indirect method

Rhinoplasty is a type of face surgery where the intention is to preserve or restore nasal function and support while achieving esthetic harmony with the adjacent facial characteristics.[10] By one's personality and lifestyle, the nose has varying degrees of significance in terms of facial aesthetics.[10] Nonetheless, the nose contributes significantly to the harmonious and balanced appearance of the face, which might influence how people view beauty in general.[10] The nose is a focus point on the face because its position is positioned in the center. Its dimensions, form, and ratios can have a big impact on the face's overall harmony and equilibrium.[10] Furthermore, it is a crucial component of a beautiful and natural human face. Rhinoplasty can be done for therapeutic reasons to address breathing issues or anomalies in the nose, or it may be performed for cosmetic purposes to enhance the nose's look by reshaping. The exact number of rhinoplasty surgeries carried out year in India may change based on a variety of variables, such as a need for cosmetic surgery, the procedure's attractiveness to a range of demographics, developments in technological advances, and macroeconomic considerations.[3]

Face analysis is the initial stage in planning a surgical procedure and is essential to the formulation of an appropriate treatment strategy for operations involving cosmetic or reconstructive surgical procedures.[11] It is critical to comprehend the patient's nasal deviations from the standard to attain a satisfactory outcome.[11] There are differences in physical characteristics of African, Caucasian, and Asian population, and of course, within each of these groups. Thus, it is not appropriate to compare the "ethnic" nose using data from Caucasians.

So for this, this is the largest research, to the best of our knowledge, which includes subjects from various zones of India and measurements taken by two methods to check the accuracy and reliability of two-dimensional indirect photogrammetry against direct anthropometry. We analyzed eight nasal parameters in frontal and lateral views. From the results of the present study, it was clear that males had greater nasal parameters than females.

In the present study, we found that the mean nasal length in males was 4.5 ± 0.43 and 4.16 ± 0.37 cm by direct and indirect methods, respectively. The mean nasal length in females was 4.1 ± 0.54 and 4.06 ± 0.55 cm by both methods. Parab and Khan[3] conducted research on nasal parameters of the Indian population, and they found mean values

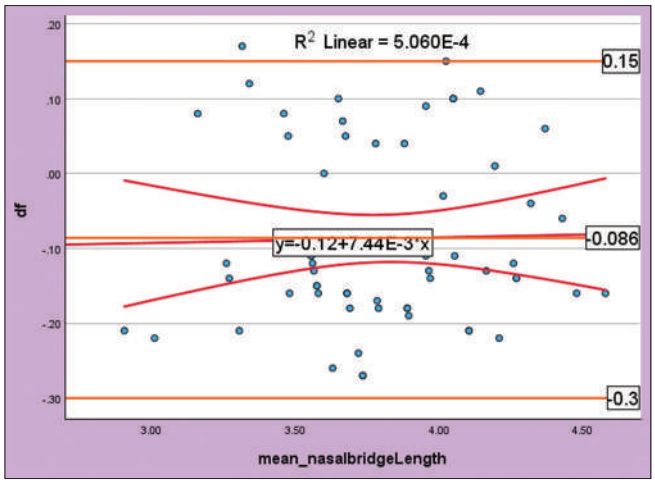

Graph 5: Bland altman analysis plot (BAA) plot for nasal bridge length by direct and indirect method

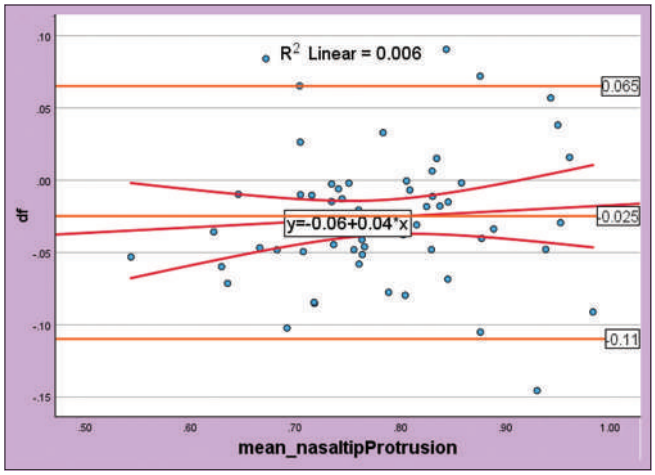

Graph 7: Bland altman analysis plot (BAA) plot for nasal tip protrusion by direct and indirect method

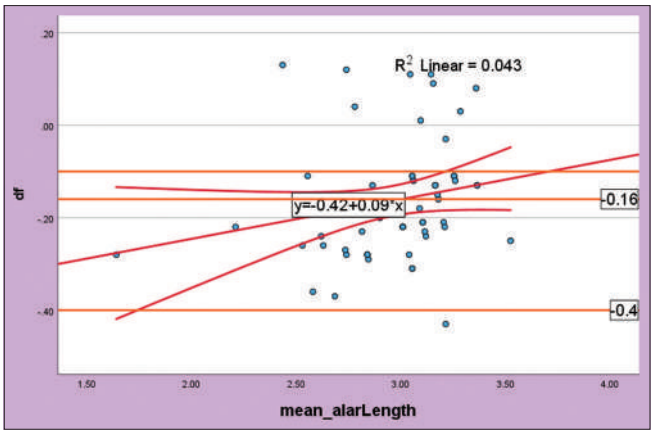

Graph 6: Bland altman analysis plot (BAA) plot for alar length by direct and indirect method

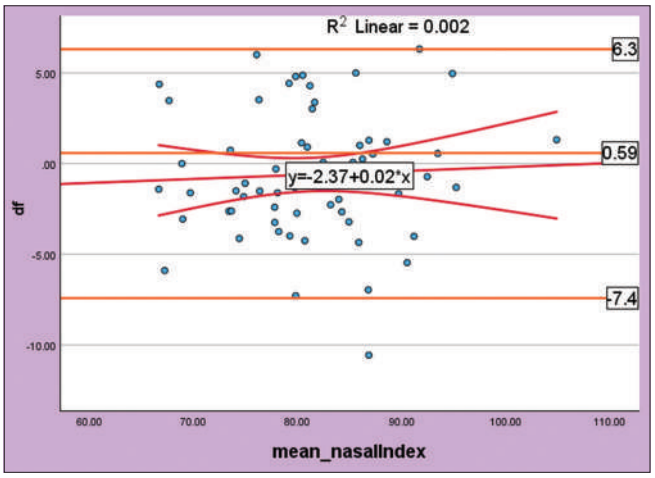

Graph 8: Bland altman analysis plot (BAA) plot for nasal index by direct and indirect method

of nasal length in males 4.43 ± 0.45 cm and in females 4.13 ± 0.45 cm. Aung *et al*.[12] carried out a study on nasal anthropometry in Chinese population with the help of laser scanning technique, and they found 5.35 cm mean value of nasal length. A similar study was conducted by Ofodile and Bokhari[13] in Caucasian population, they got the mean values of nasal length 5.3 cm, which was exactly similar to the previous study. Some other studies showed the mean values of nasal length in different population, such as Afro-American mean values (5.24 cm),[3] Turkish population, the mean value was 5.69 cm,[14] white northern Italian (5.43 cm),[15] and Afro Indian mean values was 5.47 cm).[16] The findings of our study showed that Indian population have a small nasal length as compared to other population.

In the current study, nose width in males was 3.2 ± 0.3 and 3.1 ± 0.24 cm, and in females was MNW 3 ± 0.23 and 3.09 ± 0.23 cm, by both the methods. Parab and Khan[3] research showed that the mean nasal length in males was 3.79 ± 0.29 and in females was 3.57 ± 0.41. The findings of our study coincide with the findings of Parab *et al*.[3] study.

According to our study, columellar length in males was 1.2 ± 0.21 and 1.10 ± 0.17 cm, and in females was 0.98 ± 0.21 and 1 ± 0.2 cm by both approaches. Mehta and Srivastava[10] did the study on the Indian population of different zones, and they found 0.94 ± 0.2 cm mean values of columellar length in both sexes of Indian population. Our study is coinciding the mean values of their study.

In the current study, nasal bridge length in males was 4.06 ± 0.4 and 3.6 ± 0.38 cm, and in females was 4.07 ± 0.38 and 4.12 ± 0.39 cm. Mehta and Srivastava[10] found the 4.39 ± 0.5 cm mean values of both genders.

The nasal index in males was 79 ± 11.3 and 76.05 ± 8.8 and in females was 69.9 ± 10.2 and 70.59 ± 10.8. Mehta and Srivastava[10] found 73.27 in males and 72.35 in females. Patil *et al*.[17] conducted a research on the south Indian population and found the values of nasal index in males was 84.91 and in females was 67.75. Porter and Olson[18] conducted research on African American women and found the values of nasal index 79.7. Chhabra *et al*.[19] did the research the north Indian population, and got the values 77.39 in males and 72.28 in females.

Our values of the nasal index lie between 70 and 84.9, which comes under the category of mesorrhine,[20] consequently, we concluded that it is evident that Indian nasal parameters are distinct from those of Africans, Asians, Caucasians, and other ethnic population.

Consequently, we conclude that Indian nasal parameters must be perceived differently from those of Caucasians, Orientals, and African populations. The face architecture of individuals from various parts of this nation varies from one another. To provide patients outcomes that complement other face characteristics, suitable changes must be made during nose operations based on the varying racial descents of the patients. By recognizing and respecting these differences, should be a significant consideration in plastic surgery, as different ethnic groups may have distinct nasal features, and nasal parameters may vary among different regions within India itself. Consequently, in nose surgeries, it is imperative to tailor the procedures to each patient's racial background to ensure that the outcomes harmonize with their unique facial characteristics. This approach emphasizes how important it is for medical professionals to provide individualized, culturally sensitive treatment.

On the other hand, this research is also assessed the reliability and accuracy of 2D indirect method against the direct method, which is already considered as the gold standard technique. Our study revealed that measurements of nasal dimensions, including nose height, ANW, MNW, columella length, nasal bridge length, alar length, nasal tip protrusion, and nasal index, were examined. Among the eight parameters examined, five nasal measurements demonstrated a high level of agreement between the approaches, namely nose height, MNW, alar length, nasal tip protrusion, and nasal index. However, columella length and nasal bridge length displayed moderate reliability across both approaches. Therefore, only six of the eight nasal dimensions can be reliably and accurately measured using 2D photogrammetry. However, the remaining two parameters exhibited moderate reliability and a level of agreement between the methods. The moderate reliability may be attributed to factors such as image distortion and resolution.[21] In addition, the demographics of the study participants could have contributed to this outcome. More importantly, potential errors might have arisen from measuring columellar length using lateral view photographs.

The 2D photogrammetric method has been widely applied in research both nationally and internationally.[22,23] However, there is limited research and certain constraints in studies that compare 2D photogrammetry with direct measurement. Furthermore, current research exhibits conflicting findings on this matter. Some researchers showed that, for numerous facial dimensions, 2D photogrammetry is less precise compared to direct and 3D measurement methods, whereas the other two studies concluded that 2D photogrammetry aligns closely with direct measurement.[24-26]

Our research introduces novelty by employing three methods to assess the reliability of the 2D method: ICC, Bland–Altman analysis, and regression analysis. These statistical approaches are widely recognized for evaluating reliability. Both agreement and reliability parameters are pivotal in evaluating the quality of the method employed, and our study uniquely combines these three statistical parameters, which are not taken into consideration in previous studies to validate.

It is worth noting that a method's reliability is only beneficial if it also demonstrates good agreement, and conversely, good agreement is not useful if the method lacks reliability.

Nevertheless, drawbacks of the 2D indirect approach encompass measurement errors stemming from subjective analysis, variations in head orientation, magnification discrepancies, parallax effects, and lighting inconsistencies. However, the uniqueness of our study lies in the comprehensive validation analysis conducted to verify the outcomes derived from 2D photogrammetry against the established gold standard method.

We recognize certain limitations in our study. First, direct measurements were conducted by a single observer, preventing the calculation of reliability for this method, unlike the 2D photogrammetry measurements. However, we maintain that any measurement errors in the direct measurement process were minimal due to the training. The research is limited by its exclusion of 3D photogrammetry, a method known for its enhanced accuracy in facial dimension measurement. Finally, future research endeavors should aim to integrate various measurement approaches, including direct, 2D indirect, and 3D technologies.

Conclusion

The study concludes that Indian nasal parameters are likely perceived differently compared to those of Caucasian, Oriental, and African populations. This suggests that nasal features may vary across ethnic groups, influencing how they are perceived or judged. In addition, it is important to note that nasal parameters may vary not only between different ethnicities but also within different regions of India. This highlights the need for tailored approaches in cosmetic procedures to ensure culturally sensitive and aesthetically appropriate outcomes. On the other hand, the findings of this study indicate that 2D photogrammetry emerges as a dependable alternative to the direct method. It offers cost-effectiveness, noninvasiveness, time efficiency, reduced operator dependence, and avoids direct patient contact.

Acknowledgment

I would like to show my gratitude to the Department of Anatomy, TMMC and RC, Moradabad, Uttar Pradesh, India, for all the technical and nontechnical support.

Financial support and sponsorship

Nil.

Conflicts of interest

There are no conflicts of interest.

References

1. Nguyen A, Duong D, O'Sullivan P. Overlapping worlds of art and plastic surgery: Developing a concept model and its implications in surgical education. Global Surg Educ 2023;2:9.
2. Bouguila J, Khochtali H. Facial plastic surgery and face recognition algorithms: Interaction and challenges. A scoping review and future directions. J Stomatol Oral Maxillofac Surg 2020;121:696-703.
3. Parab SR, Khan MM. Do aesthetic average nasal parameters matter for rhinoplasty in India? Indian J Otolaryngol Head Neck Surg 2019;71:2011-8.
4. Lim YC, Abdul Shakor AS, Shaharudin R. Reliability and accuracy of 2D photogrammetry: A comparison with direct measurement. Front Public Health 2021;9:813058.
5. Negi G, Ponnada S, Aravind NK, Chitra P. Photogrammetric correlation of face with frontal radiographs and direct measurements. J Clin Diagn Res 2017;11:C79-83.
6. Elsamny TA, Rabie AN, Abdelhamid AN, Sobhi EA. Anthropometric analysis of the external nose of the Egyptian males. Aesthetic Plast Surg 2018;42:1343-56.
7. Ogodescu E, Popa M, Luca M, Igna A, Miron M, Martha K, *et al*. Updating standards of facial growth in Romanian children and adolescents using the anthropometric method-A pilot study. Int J Environ Res Public Health 2021;18:5288.
8. Shah R, Nair R. Comparative evaluation of facial attractiveness by laypersons in terms of facial proportions and equate it's deviation from divine proportions – A photographic study. J Oral Biol Craniofac Res 2022;12:492-9.
9. Doğan NÖ. Bland-Altman analysis: A paradigm to understand correlation and agreement. Turk J Emerg Med 2018;18:139-41.
10. Mehta N, Srivastava RK. The Indian nose: An anthropometric analysis. J Plast Reconstr Aesthet Surg 2017;70:1472-82.
11. Parsa S, Basagaoglu B, Mackley K, Aitson P, Kenkel J, Amirlak B. Current and future photography techniques in aesthetic surgery. Aesthet Surg J Open Forum 2022;4:ojab050.
12. Aung SC, Foo CL, Lee ST. Three dimensional laser scan assessment of the oriental nose with a new classification of oriental nasal types. Br J Plast Surg 2000;53:109-16.
13. Ofodile FA, Bokhari F. The African-American nose: Part II. Ann Plast Surg 1995;34:123-9.
14. Uzun A, Akbas H, Bilgic S, Emirzeoglu M, Bostanci O, Sahin B, *et al.* The average values of the nasal anthropometric measurements in 108 young Turkish males. Auris Nasus Larynx 2006;33:31-5.
15. Ferrario VF, Sforza C, Poggio CE, Schmitz JH. Three-dimensional study of growth and development of the nose. Cleft Palate Craniofac J 1997;34:309-17.
16. Ofodile FA, Bokhari FJ, Ellis C. The black American nose. Ann Plast Surg 1993;31:209-18.
17. Patil GV, Shishirkumar, Apoorva D, Thejeshwari. Study of nasal index in South Indian population. Int J Curr Res 2014:6;8163-4.
18. Porter JP, Olson KL. Analysis of the African American female nose. Plast Reconstr Surg 2003;111:620-6.
19. Chhabra N, Bedi M, Patnaik VV. Anthropometric study of the nose of 600 North Indian adults (a study done for forensic identification). Natl J Integr Res Med 2012;3:62-8.
20. Omotoso DR, Adagbonyin O, Bienonwu E, Uwagbor V. Anthropometric evaluation of nasal height, nasal breadth and nasal index among bini children in Southern Nigeria. Int J Anat Res 2019;7:6896-900.
21. Kashmoola S, Ariff TM, Wahab BA. Utilization of 2D photography for acquisition of facial anthropometry. Esteem Acad J 2020;16:27-37.
22. El Minawi H, El Saloussy Y, Sabry M, Wahdan W, El Sharkawy O. Facial anthropometry and analysis in Egyptian women. Plast Reconstr Surg Glob Open 2022;10:e4333.
23. Burusapat C, Lekdaeng P. What is the most beautiful facial proportion in the 21st century? Comparative study among miss universe, miss universe Thailand, neoclassical canons, and facial golden ratios. Plast Reconstr Surg Glob Open 2019;7:e2044.
24. Ghoddousi H, Edler R, Haers P, Wertheim D, Greenhill D. Comparison of three methods of facial measurement. Int J Oral Maxillofac Surg 2007;36:250-8.
25. Kook MS, Jung S, Park HJ, Oh HK, Ryu SY, Cho JH, *et al*. A comparison study of different facial soft tissue analysis methods. J Craniomaxillofac Surg 2014;42:648-56.
26. Dindaroğlu F, Kutlu P, Duran GS, Görgülü S, Aslan E. Accuracy and reliability of 3D stereophotogrammetry: A comparison to direct anthropometry and 2D photogrammetry. Angle Orthod 2016;86:487-94.

Original Article

Retroaortic Renal Vein Variations and Hematuria: An Anatomical and Clinical Analysis

Abstract

Background: The retroaortic left renal vein (RV) is an anatomical variant in which the left RV runs between the aorta and the vertebrae and drains into the inferior vena cava. **Aims and Objective:** This study aims to investigate the potential relationship between retroaortic renal vein (RARV) morphology and hematuria. **Materials and Methods:** Abdominal computed tomography images of 371 individuals were analyzed. The frequency and types of RARV variations were assessed and compared between patients ages 10–90 years with and without hematuria. Morphometric measurements, angles, and vertebral levels of RARV types were also analyzed. **Results:** Contrary to previous studies, no clinically significant relationship was found between RARV and hematuria. The most common RARV variation observed was Type 2, differing from the literature, which frequently cites Type 1 as the most prevalent. The Type 2 variation was the most commonly observed in both females and males, typically located at the L2–L3 vertebral level. Despite similar compression observations in individuals with and without hematuria, no direct association with hematuria was identified. The correlation analysis revealed a statistically significant positive correlation between hematuria classification based on urinary erythrocyte ratio and the ratios of diameters of the RARV at the retroaortic level and the middle of the RV. **Conclusion:** The study underscores the importance of recognizing RARV variations, especially Type 2, during abdominal examinations to prevent complications during retroperitoneal or renal interventions. Although a direct relationship between RARV and hematuria was not established, the findings contribute to understanding the anatomical and clinical significance of RARV variations.

Keywords: *Computed tomography, hematuria, renal veins*

Hadi Sasani, Mazhar Ozkan[1], Gara Dilanli, Hakan Hamdi Çelik[2]

Departments of Radiology, and [1]Anatomy, Faculty of Medicine, Tekirdağ Namık Kemal University, Tekirdağ, [2]Department of Anatomy, Faculty of Medicine, Hacettepe University, Ankara, Türkiye

Introduction

The kidneys play a crucial role in the blood filtration process due to their functions related to the removal of waste products from the blood. This makes the vascular structures of these organs particularly significant and susceptible to various anatomical variations. A significant proportion of these variations are observed in the venous structures,[1] with the retroaortic renal vein (RARV) being a relatively more encountered anomaly.[2] This vein, which drains the left kidney and traverses behind the abdominal aorta (AA), represents a frequent variation within the renal venous system.[3] Although these anatomical anomalies are predominantly asymptomatic, they can occasionally be associated with clinical manifestations such as abdominal pain and hematuria.[4,5]

Hematuria, defined as blood in the urine, can arise from various etiologies, including urinary tract infections, renal stones, and neoplastic conditions.[6] A review of the existing literature, which is designed to help summarize the extensive body of scientific research, suggests a potential association between RARV and the occurrence of hematuria.[2,5,7] It is posited that the presence of a RARV could alter renal hemodynamics or contribute to venous hypertension, thereby leading to hematuria.[8] Despite these suggestions, comprehensive analyses investigating this relationship remain limited. Understanding this potential link is essential for urologists and radiologists in diagnosing and managing patients with unexplained hematuria. This relationship is crucial for clinicians, as it can influence diagnostic approaches, treatment strategies, and patient outcomes.[9-11]

This study aims to investigate the intricate interplay between RARV variations and hematuria. The anatomical features of RARV and its prevalence in society are investigated, and its relationship with the incidence of

How to cite this article: Sasani H, Ozkan M, Dilanli G, Çelik HH. Retroaortic renal vein variations and hematuria: An anatomical and clinical analysis. J Anat Soc India 2025;74:141-5.

Article Info

Received: 27 December 2024
Accepted: 19 February 2025
Available online: 30 June 2025

Address for correspondence:
Dr. Hadi Sasani, Department of Radiology, Faculty of Medicine, Tekirdag Namik Kemal University, Tekirdag 59030, Turkey.
E-mail: hsasani@nku.edu.tr

Access this article online

Website: https://journals.lww.com/joai

DOI: 10.4103/jasi.jasi_201_24

Quick Response Code:

hematuria is evaluated. In addition, diagnostic methods, management considerations, and clinical implications associated with this intriguing anatomical variant are discussed.

Materials and Methods

Study design

This is a retrospective cross-sectional study. In accordance with the ethical standards of the responsible committee on human experimentation (institutional or regional) and with the Helsinki Declaration of 1975, as revised in 2013, the local Ethics Committee approved the study protocol (No: 2024.40.03.04, Date: March 26, 2024). Informed consent was obtained from the patients before the study.

Patient population

This study was carried out as a retrospective analysis of computed tomography (CT) images of 371 patients (182 controls and 189 hematuria cases) between the ages of 10 and 90 years, hospitalized at the hospital between March 2017 and February 2024.

Data acquisition

CT acquisitions were performed on 128 row multidetector CT device (Aquilion™ Prime, Canon Medical Systems).

Scanning protocol

CT scanning parameters were as follows for each protocol: 100–250 mAs modulated by personal body mass index dose; 100–140 kV tube voltage, 0.5 mm × 80 collimation, 0.35 s gantry rotation time, 0.813 pitch factor, slice thickness 1 mm and slice interval 0.8 mm. For intravenous bolus injection of non-ionic contrast material (300 mg/100 mL, iohexol, Opaxol®; Opakim Medical Products), a mechanical injector was used at a flow rate of 4.5–5.0 mL/s.

Noncontrast and contrast-enhanced CT examinations of the whole abdomen of optimum quality and selected RARV were included in the study.

Classification

RARV was categorized into four types according to the classification: Type I drains into IVC at normal position, type II drains at a lower level of IVC, type III drains into circumaortic renal vein (CARV), and type IV drains much lower into the left common iliac vein[11,12] [Figure 1].

Image assessment

The images were evaluated by two radiologists (11 years of experience, resident physician) and one anatomist (6 years of experience).

Morphometric parameters such as renal and RARV localization, variation type [Figure 2], length, compression status, diameters of the RARV at the retroaortic level (RtAo) and in the middle of the left renal vein (RV), RtAo/AA [Figure 3] ratio were recorded on the Sectra 7.0 workstation (Sectra AB, Linköping, Sweden).

The presence of CARV status, the diameter of the CARV at the aorticomesenteric level, and the ratio of the diameter of the middle portion of the native left RV to the RV at the aorticomesenteric level were also noted.

The vertebral level of RARV in sagittal plan CT images was recorded. The drainage angle of RARV with the inferior vena cava (IVC) was measured [Figure 4].

Statistical analysis

A statistical package program (SPSS (2008) Statistical Package for Social Sciences Program. Version 17 for Windows, SPSS Inc., Chicago) was used in analyzing data. Normality tests (Shapiro–Wilk/Kolmogorov–Smirnov) were performed to evaluate whether the data were normally distributed. Descriptive tests were used for demographic data (age, gender, height, body mass index, etc.). In the comparison of the groups, a parametric test (independent sample *t*-test) was applied to the data showing normal distribution, and a non-parametric test (Kruskal–Wallis test) was applied to the data not showing normal distribution. The Chi-square test was used in the evaluation of

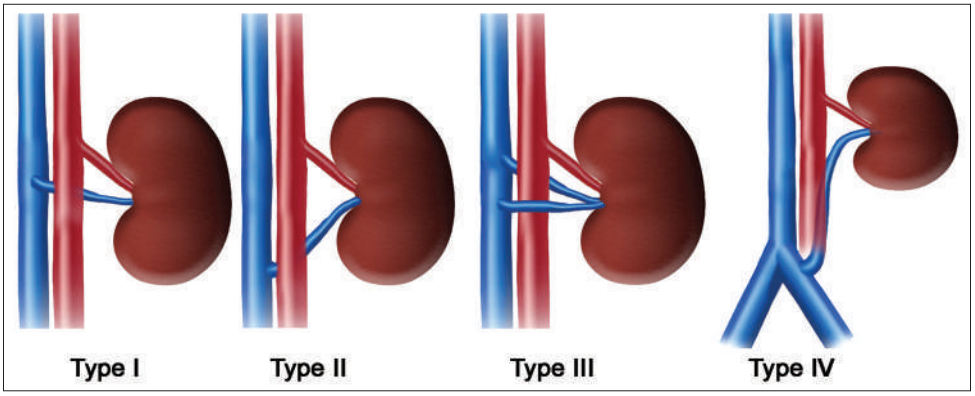

Figure 1: Retroaortic renal vein classification

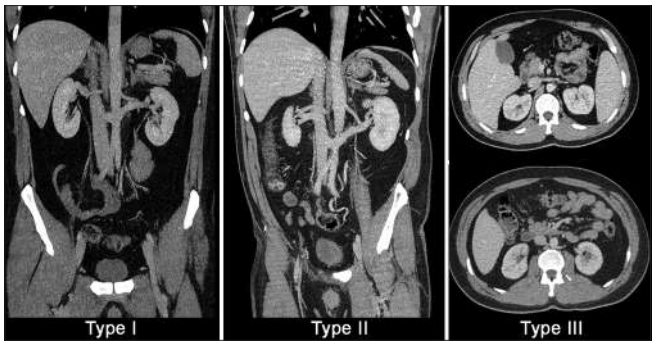

Figure 2: Retroaortic renal vein classification on computed tomography images

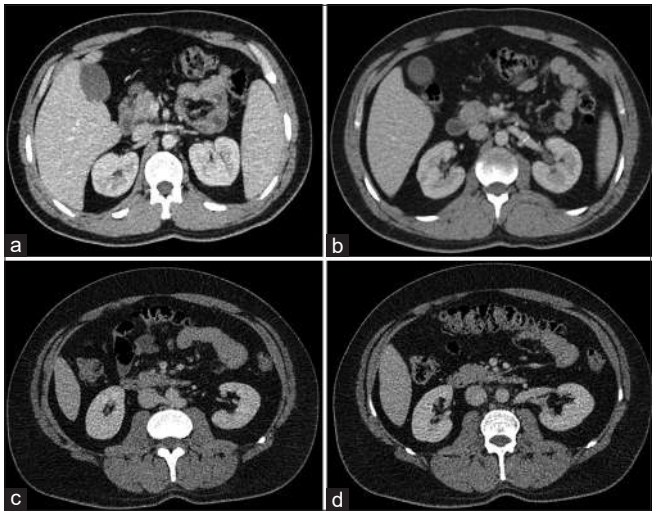

Figure 3: Morphometric measurements of renal vein of retroaortic renal vein (RARV): (a) measurement of the native renal vein at the aorticomesenteric level and (b) measurement from the middle part (yellow arrows), (c) RARV at the retroaortic level and (d) RARV measurement of the middle part (green arrows)

Figure 4: (a) Angle measurement at the level where retroaortic renal vein (RARV) drains into the inferior vena cava, (b) RARV vertebral level (blue arrowheads)

categorical data and Pearson/Spearman Rho test was used in correlation analysis. The statistical significance level was accepted as $P < 0.05$.

Results

In a total of 371 patients, females predominated over males (51.1% in the control group $n = 93$, and 51.3% in the hematuria group $n = 97$). The most common RARV variation type was found to be Type II, and the most common vertebral level was L2–L3 in both groups. Although asymptomatic, RARV compression was detected more in the control group than in the hematuria group (55.5%), and no direct association with hematuria was found. Summary of data in study groups [Table 1] and the morphology of RARV [Table 2] are described.

The study analyzed the distribution of control and hematuria groups among individuals aged 10–79 years, based on gender. Results showed the age range of 50–59 accounted for the majority of cases in both the control and hematuria groups, with males ($n = 21$) constituting the majority of cases. A large number of cases across all hematuric categories were observed in females ($n = 18$) between the ages of 40 and 49 years. The study highlights the importance of understanding age-specific health outcomes.

The analysis revealed a significant relationship between RARV variations and angulation, with Type I and Type II ($P < 0.001$) and Type III ($P < 0.001$), while Type II and Type III did not ($P = 0.581$).

Discussion

This study investigated the potential relationship between hematuria and RARV morphology by analyzing the abdominal CT images of 371 individuals. Contrary to previous studies, no clinically significant relationship was found between RARV and hematuria. In addition, in terms of the frequency of RARV types, our findings differed from the literature, with Type 2 being the most common.

In the literature, there are few comprehensive studies on RARV and it has been observed that only a few cases have been presented.[12-15] The current study was very beneficial in terms of the number of individuals included.

CT imaging is quite useful to assess patients quickly with detail.[12] The classification of RARV by Karkos *et al*. was anatomical, whereas the current study is based on radiological findings from CT images. Moreover, for the first time in the literature, the study examined the angle and vertebral level differences between RARV types in addition to morphometric measurements.[9]

In the current study, the Type 2 RARV variation was the most commonly observed in both females and males, with the most frequent location being at the L2–L3 vertebral level. The primary aim of our study, which was to determine a direct relationship between RARV variation and hematuria, was not achieved.

Type 2, the most common observed variation, is known for its lower level of drainage into the IVC compared to the normal left RV. Contrary to our findings, Nam *et al*. reported that Type 1 was more common.[16]

There are numerous studies in the literature regarding the clinical significance of RARV, citing conditions such as abdominal pain, thrombosis, venous hypertension, varicocele, and hematuria.[8,16-21] Due to the midline position of the AA and developmental changes in venous structures, variations can occur in the drainage of organs on the left side of the abdomen into the IVC. Identifying these clinically significant variations is crucial as it can aid in correlating clinical symptoms and prevent hemorrhage and severe kidney damage during surgery.

During early embryonic development, the initial venous channels undergo several stages of remodeling. As the embryo grows, the postcardinal veins are supplemented by longitudinal vascular channels, including the subcardinal, supracardinal, azygos line, subcentral, and precostal veins. These channels anastomose with the posterior cardinal system and each other, with the subcardinal veins primarily draining the developing mesonephros. Before the renal vessels reach their final form, a circumaortic renal venous ring, or "renal collar," exists around the aorta. This collar is formed by anastomoses between subcardinal veins, supracardinal veins, and supracardinal-subcardinal anastomoses. Normally, the dorsal part of the renal collar degenerates, leaving the ventral vessel as the RV. However, sometimes, the post-aortic part of the renal collar persists, leading to numerous variations in the number, orifices, and main tributaries of the RVs.[22]

Table 1: Summary of data in study groups

	Control (*n*=182), *n* (%)	Hematuria (*n*=189), *n* (%)
Gender		
Male	89 (48.9)	92 (48.7)
Female	93 (51.1)	97 (51.3)
Type of RARV		
Type I	41 (22.5)	42 (22.2)
Type II	123 (67.6)	119 (63)
Type III	18 (9.9)	28 (14.8)
Circumaortic formation		
Yes	18 (9.9)	28 (14.8%)
No	164 (90.1)	161 (85.2%)
RARV level		
L1	0	1 (0.5)
L1–L2	5 (2.7)	10 (5.3)
L2	53 (29.1)	42 (22.2)
L2–L3	63 (34.6)	59 (31.2)
L3	51 (28)	69 (36.5)
L3–L4	7 (3.8)	6 (3.2)
L4	3 (1.6)	2 (1.1)
Compression		
Yes	101 (55.5)	94 (49.7)
No	81 (44.5)	95 (50.3)

RARV: Retroaortic renal vein

In the current study, when comparing the presence of hematuria between males and females, it was found that females had a statistically higher incidence of hematuria compared to males (P = 0.024). This finding is consistent with previous studies.[2] Furthermore, approximately 10% of the control group and 15% of the hematuria group exhibited cases of CARV. Resorlu *et al*.[2] found no association between retroaortic and CARV and hematuria in their study.

Understanding the anomalies of the renal vascular structure during renal surgery is crucial for the success of the surgery and the prevention of complications.[23] Increased pressure in the RV can affect kidney functions and lead to microscopic hematuria. Our study examined the relationship between RARV, which can be compressed between the aorta and vertebra (referred to as posterior nutcracker syndrome), and hematuria. Despite similar observations of compression in individuals with (n = 95) and without (n = 101) hematuria, no direct association with hematuria was found. The literature indicates that Nutcracker syndrome must cause approximately fourfold compression to affect nephrological functions.[24,25]

Correlation analysis of hematuria classification based on urinary erythrocyte ratio revealed a statistically significant positive correlation with the RtAo and middle RARV ratios (P = 0.015 and P = 0.023, respectively). It

Table 2: Retroaortic renal vein morphology in the study groups

Parameters	Control (*n*=182)	Case (*n*=189)	*P*
Angle	73.79±18.43	72.31±19.80	0.417
Length	67.96±13.17	69.82±12.62	0.372
Diameter of RetAo	5.22±2.23	5.66±2.42	0.087
Diameter of RARV at mid-level	9.46±2.35	9.52±2.55	0.942
Diameter of AA	16.37±3.96	16.33±4.53	0.958
Ratio middle/RetAoV	2.16±1.09	1.99±1.10	0.050
Diameter of native RV at AoMes level in CARV (mm)	5.06±2.30 (*n*=17)	6.22±2.25 (*n*=26)	0.160
Mid-portion diameter of native RV in CARV (mm)	8.04±2.70 (*n*=17)	8.08±1.55 (*n*=26)	0.921

RV: Renal vein, RARV: Retroaortic RV, RetAo: RARV at retroaortic level, AA: abdominal aorta, AoMes: Aorticomesenteric level, CARV: Ccircumaortic RV

is believed that this relationship could be supported by previous study results and used to explain the association between RARV and hematuria. The absence of a significant relationship in our study suggests that the presence of RARV alone may not be a sufficient cause of hematuria. This finding is crucial for clinicians, as it emphasizes the need to consider other etiological factors when diagnosing and managing hematuria. While anatomical variations like RARV should still be recognized and documented, the current results imply that their clinical impact on hematuria may be limited.

A major strength of our study is the large sample size, which enhances the reliability and generalizability of our findings. In addition, the use of abdominal CT scans provided high-resolution imaging, allowing for accurate identification of RARV and other anatomical features. However, this study also has limitations. The retrospective design may introduce selection bias, and the reliance on CT scans means that functional assessments of renal hemodynamics were not performed. Future studies incorporating functional imaging techniques or prospective designs could provide further insights into this relationship.

Conclusion

RARV variations are generally asymptomatic venous anomalies. Despite the numerous studies associating these variations, which are anatomically predisposed to entrapment, with hematuria, there was no direct relationship at the current study. In addition, contrary to existing literature, this study demonstrated that Type 2 was the most common type of RARV variation. Thus, attention to this variation during abdominal examinations is important to prevent possible complications that may arise during retroperitoneal or renal interventions.

Availability of data and materials

Patient data were obtained from the hospital data system.

Financial support and sponsorship

Nil.

Conflicts of interest

There are no conflicts of interest.

References

1. Hostiuc S, Rusu MC, Negoi I, Dorobanțu B, Grigoriu M. Anatomical variants of renal veins: A meta-analysis of prevalence. Sci Rep 2019;9:10802.
2. Resorlu M, Sariyildirim A, Resorlu B, Sancak EB, Uysal F, Adam G, *et al.* Association of congenital left renal vein anomalies and unexplained hematuria: Multidetector computed tomography findings. Urol Int 2015;94:177-80.
3. Hoeltl W, Hruby W, Aharinejad S. Renal vein anatomy and its implications for retroperitoneal surgery. J Urol 1990;143:1108-14.
4. Chen Y, Xing J, Liu F. Left renal vein transposition is effective for posterior nutcracker syndrome. Int J Clin Exp Med 2014;7:5925-7.
5. Fujishima Y, Watanabe K, Tabira Y, Iwanaga J, Odo Y, Saga T, *et al*. A retroaortic left renal vein in a female cadaver. Kurume Med J 2018;64:103-7.
6. Horie S, Ito S, Okada H, Kikuchi H, Narita I, Nishiyama T, *et al.* Japanese guidelines of the management of hematuria 2013. Clin Exp Nephrol 2014;18:679-89.
7. Zhang L, Qing L, Mingxing X, Jing W, Li Z, Yao D, *et al.* Clinical value of ultrasonography in the diagnosis of left renal vein behind abdominal aorta. J Chin Physician 2021;12:502-5.
8. Powell CR, Schwartz BF, Stoney RJ, Stoller ML. Gross hematuria secondary to renal vein hypertension from unilateral retroperitoneal fibrosis. Urology 2000;55:436.
9. Karkos CD, Bruce IA, Thomson GJ, Lambert ME. Retroaortic left renal vein and its implications in abdominal aortic surgery. Ann Vasc Surg 2001;15:703-8.
10. Idhrees M, Velayudhan B. Retroaortic left renal vein in open thoracoabdominal aneurysm repair: A modified approach. Eur J Cardiothorac Surg 2022;62:ezac452.
11. Krastev N, Tivcheva Y, Malinova L, Jelev L. Retroaortic left renal vein: A clinically significant vascular variation with suggestion of a practical typological scheme. Anatomy 2022;16:41-5.
12. Karaman B, Koplay M, Ozturk E, Basekim CC, Ogul H, Mutlu H, *et al.* Retroaortic left renal vein: Multidetector computed tomography angiography findings and its clinical importance. Acta Radiol 2007;48:355-60.
13. Yeşildağ A, Adanir E, Köroğlu M, Baykal B, Oyar O, Gülsoy UK. Incidence of left renal vein anomalies in routine abdominal CT scans. Tani Girisim Radyol 2004;10:140-3.
14. Hsieh C, Tiao W, Chou Y, Tiu C. Retroaortic left renal vein: Three case reports. J Med Ultrasound 2012;20:115-8.
15. Mohammadi S, Gholami Farashah M, Frounchi N, Shoorei H, Shariat M. Retro aortic left renal vein: A case report and brief literature of review. Open Access J Surg 2018;8:555744.
16. Nam JK, Park SW, Lee SD, Chung MK. The clinical significance of a retroaortic left renal vein. Korean J Urol 2010;51:276-80.
17. Gibo M, Onitsuka H. Retroaortic left renal vein with renal vein hypertension causing hematuria. Clin Imaging 1998;22:422-4.
18. Arslan H, Etlik O, Ceylan K, Temizoz O, Harman M, Kavan M. Incidence of retro-aortic left renal vein and its relationship with varicocele. Eur Radiol 2005;15:1717-20.
19. Mendizábal S, Román E, Serrano A, Berbel O, Simón J. Left renal vein hypertension syndrome. Nefrologia 2005;25:141-6.
20. Allam SR, Livingston TS, Kalaria V, Diaz-Calderon W, Pumphrey JA, Patel L, *et al.* Posterior nutcracker syndrome: An infrequent cause of hematuria. Kidney Int 2014;85:985-6.
21. Dhandhalya C, Chudasama S, Patel R. Retro aortic left renal vein with advanced rcc: A case report with literature review. Int J Sci Res 2023;12:22-3.
22. Haładaj R, Polguj M, Wysiadecki G, Żytkowski A, Topol M. Circumaortic left renal vein (circumaortic renal collar) associated with the presence of vascular anomalies: A case series and review of literature. Folia Morphol (Warsz) 2019;78:437-43.
23. Bialek EJ, Malkowski B. Unusual drainage of the bifurcated left renal vein into a dilated lumbar azygos vein and inferior vena cava. Vasc Endovascular Surg 2019;53:585-8.
24. Dunphy L, Penna M, Tam E, El-Kafsi J. Left renal vein entrapment syndrome: Nutcracker syndrome! BMJ Case Rep 2019;12:e230877.
25. Fontanella G, Borrelli S, Dello Iacono U, Brogna B. Imaging of Type I Retroaortic Left Renal Vein and Nutcracker Syndrome. Preprints. [doi:10.20944/preprints202201.0190.v1]

Original Article

Morphometry of Zygomatic Bone with Topographic Variations of Zygomaticofacial and Zygomaticotemporal Foramina: An Observational Study

Prenika Shangloo, Midhat Syed[1], Heena Raina[2], Sangeeta Gupta[2]

Department of Anatomy, Governement Medical College, Jammu University, [2]Department of Anatomy, Governement Medical College, Jammu, [1]Department of Anatomy, SKIMS, Srinagar, Jammu and Kashmir, India

Abstract

Background: With hiking incidence of road traffic accidents and associated midfacial trauma, craniofacial neonatal malformations, and increasing demand for cosmesis, the frequency of facial surgeries is increasing day by day and the principal focus is on the facial dissection of the zygomatic bone. Like other bones, this bone is also liable to have anatomical variations. Thus, the current study was designed to delineate morphometric parameters for designing more apt zygomatic implants to maintain the integrity of zygomatic complex and restore a normal facial contour in cases of complex and comminuted fractures of zygomatic bone moreover, during the surgical approach, the knowledge of the topography of zygomaticofacial and zygomaticotemporal foramina can be utilized to preserve the sensory nerves and giving the regional anesthetic block as well. **Materials and Methods:** Eighty bones, including zygomatic bones of human dry skulls and individual zygomatic bones (both sides) of unknown age and sex, were included in the current observational analysis; these bones were obtained from the bone bank of post graduate department of anatomy. The morphometry of the zygomatic bone and the topography of zygomaticofacial and zygomaticotemporal foramina were studied, and measurements were noted and analyzed. **Results:** The dimensions, i.e., width and length of bone, were higher on the right side as compared to the left side with a statistically nonsignificant difference. Type I bone was most frequent on the left side and type II was most frequent on the right side. Topographically, zygomaticofacial foramina were located near the orbital margin as compared to the jugal point with insignificant *P* values. Similarly, the zygomaticotemporal foramina were largely located on the temporal surface of the bone with an average distance of 4.72 ± 2.79 mm on the right side and 4.36 ± 3.67 mm on the left side from the jugal point. **Conclusions:** The outcome of the current analysis concluded that all dimensions of zygomatic bone were slightly more on the right side as compared to the left side and type I bone was frequently present on the left side, whereas on the right side type-II bone was more frequent and foramen was frequently found near the orbital margin. Hence, it is evident that anatomical variations can be exhibited by the zygomatic bone, so it is advisable for surgeons to consider all the parameters of zygomatic bone while choosing the implants and improve the surgical success. Moreover, awareness of these variations should be taken into consideration while conducting various surgical procedures pertaining to the midfacial region.

Keywords: *Malar bone, zygomatic bone, zygomaticofacial foramina, zygomaticotemporal foramina*

Introduction

Cheekbone prominence forms a characteristic feature of every individual and is produced by the zygomatic complex contributed by the zygomatic bone itself; the malar process and zygomatic process of the temporal bone.[1] The zygoma is an irregular bone with three surfaces, three processes, and five borders. It occupies the upper and medial section of the facial part of the skull[2,3] [Figure 1]. It is located at the junction between the temporal bone, orbital wall, and tooth-bearing snout of the maxilla. The facial skeleton, the zygomatic bone in particular, is designed as such to bear the pull and friction created by the masticatory muscles and transmit these forces from the maxilla to other facial bones and also supports critical muscles such as the masseter and zygomaticus major.[4]

Apart from playing an important role in the esthetic appearance of a person, the zygomatic bone is also associated with important nerves which come out through various foramina of the bone. Amongst these nerves, the most important ones are the branches from the maxillary division of the trigeminal nerve. These nerves, along with

How to cite this article: Shangloo P, Syed M, Raina H, Gupta S. Morphometry of zygomatic bone with topographic variations of zygomaticofacial and zygomaticotemporal foramina: An observational study. J Anat Soc India 2025;74:146-51.

Article Info

Received: 17 February 2025
Revised: 10 April 2025
Accepted: 13 April 2025
Available online: 30 June 2025

Address for correspondence:
Dr. Prenika Shangloo, Department of Anatomy, Governement Medical College, Jammu, Jammu and Kashmir, India.
E-mail: prenika1982@gmail.com

Access this article online

Website: https://journals.lww.com/joai
DOI: 10.4103/jasi.jasi_32_25
Quick Response Code:

Figure 1: Showing the parts of the zygomatic bone with various processes and zygomaticofacial foramina depicted by arrow

the corresponding vessels, take exit through the foramina of their corresponding name, i.e., zygomaticofacial foramen and zygomaticotemporal foramen, respectively.[5] Due to the clear association of these nerves with the zygomatic arch complex, these nerves are easily liable to trauma whenever midfacial injuries are there. Moreover, these nerves are also used for the regional block for the surgeries of the face and orbit. Apart from the variability in the existence of these foramina, anatomical variations are documented regarding the position, frequency, and contents of these foramina and these dissimilarities are not only interindividual but also can be noticed in the same person when both sides are compared. In addition, awareness regarding these anatomical variations in the frequency and location of the zygomatic foramina is important for having command in surgeries involving malar bones.[6]

Since bones forming the zygomatic complex are thin, these bones can fracture easily with minimal force and are accompanied by injury to the adjacent sensory as well as motor nerves. A substantial functional and cosmetic morbidity is associated with zygomatic complex fractures. Fractures with functional or esthetic impairments often require surgical management, which may result in various unwanted outcomes such as paraesthesia and ipsilateral palsy of the face.[7] Fractures of the zygomatico maxillary complex or zygomatic arch can often lead to unsightly deformities of the face and functional issues, including trismus, enophthalmos, diplopia, and paraesthesia of the infraorbital nerve. A broad spectrum for the management of such zygomatic complex fractures is available ranging from simple observation to open reduction with internal fixation depending on the severity and degree of pathology associated with the fracture. Hence, repositioning of the malar bone to its exact site and in apt size is critical and that should be dealt with great precision and care.[8]

During the last few decades, road traffic accident have been on a rampant rise. Data shows that across our state only about 893 people were killed and 8469 people were injured during the year 2023 associated with an increase in facial injuries hence, leading to rising incidence of maxillofacial surgeries; to perform such kind of asthetic surgeries the surgeon should be well verse with the morphometric variations observed in the bones of facial region as well as the topography of various foramina existing in the same. There are a number of studies depicting the morphometry of zygomatic bone and the topographic variations in the zygomaticofacial and zygomaticotemporal foramina; however comprehensive similar studies do exist in the Indian subcontinent but there are scanty data available in the north zone of the country. Furthermore, the comprehensive details and accurate data pertaining to various landmarks, foramina, and the morphometry of the zygomatic bones are also important for the three-dimensional (3D) reconstruction and printing of the facial morphology as well as for the resident teaching programs.[9] Hence, it was planned to design a study to estimate the morphometric variations of the zygomatic bone and the topographic variations of the zygomaticofacial and zygomaticotemporal foramina of the bone.

Materials and Methods

Study design

This was an observational analysis conducted on 80 bones, including zygomatic bones of a human dry skull about 60 in number and individual zygomatic bones (both sides) about 20 in number, procured from the bone bank of a tertiary care teaching hospital. The study protocol was verified and approved by the Institutional Ethical Committee (IEC/GMC/2022/1030).

Sample size estimation

G * power 3.1.9.7 software (Heinrich- Heine- Universitat Dusseldorf, Dusseldorf, Germany) was used to determine the sample size and a *t*-test with two independent mean differences was selected for assessment. The minimum sample size estimated for this study was 21 for each group and the power used was 0.95 with an effect size of 0.5 and the probability for α-error was 0.05. In this study, the sample size taken was 40 bones in each group, i.e., right and left side bones.

Inclusion and exclusion criteria

The bones of adult human beings of unknown sex and age were included in the study and they all were dry and macerated, completely ossified, complete in all respects, and without any gross abnormality so that they could give the correct morphometry and were cleaned thoroughly before commencement of the measurements. All the deformed, broken, and incomplete bones were excluded from the study.

The morphometric measurements of these bones [Figure 2] and the topography of zygomaticofacial [Figure 3] and

Figure 2: Showing the morphometric measurements of the zygomatic bone

Figure 3: Showing variable topographic position of the zygomaticofacial foramina three being present on the body of zygomatic bone near the jugal point and one is located near the frontozygomatic suture

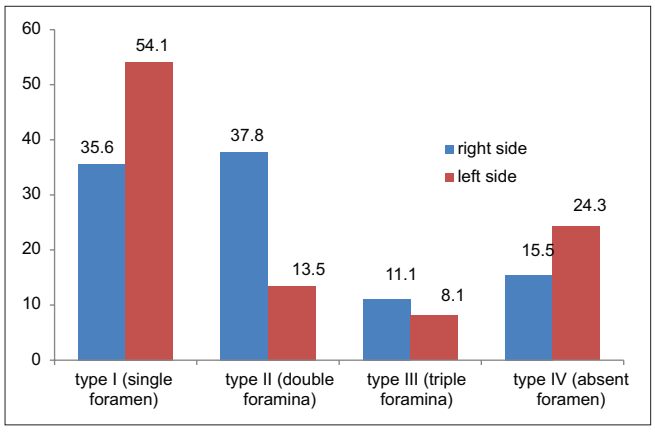

Figure 4: Bar graph showing the distribution of various types of zygomatic bones in study sample

zygomaticotemporal foramina were studied and noted. Various parameters studied were the length and width of the zygomatic bone along with the topography of the zygomaticofacial and zygomaticotemporal foramina.

The length of the zygomatic bone was measured from the zygomatico maxillary suture to the temporo zygomatic suture and the width of the zygomatic bone was measured from the orbital margin to the posteroinferior border.[10,11] Regarding the topography of the zygomaticofacial foramen, first, they were identified with the help of the probe, and then, the distance of the foramen was measured from the orbital margin as well as from the jugal point (the point where frontal and temporal processes of zygomatic bone are joined).[5,12,13] Similarly, the topography of the zygomaticotemporal foramen was also noted by first identifying the foramina with the help of the probe, and then the distance of the foramen was measured from the posterosuperior border of the frontal process of the zygomatic bone.

Data analysis

All the parameters were measured with the help of sliding vernier calipers, averaged out and the data thus gathered were subjected to standard analytical tests (*t*-test) using IBM SPSS version 26 (IBM corp., Armonk, New York) statistical software. The results were interpreted in the form of maximum and minimum values along with mean ± standard deviation. The independent *t*-test was used to assess the significant differences in means between the right and left sides.

Results

The data obtained from the measurements of the zygomatic bone in aforementioned study inferred that the mean width of the bone on the left side stood out to be 12.9 ± 2.36 mm with a range of 8–18 mm, whereas on the right side, it was slightly higher as compared to the left side with mean width falling at 13.34 ± 2.97 mm with statistically nonsignificant $P = 0.48$ [Table 1].

Further, marginally, the mean length of the bone on the right side was more, which stood out to be 38.41 mm with a standard deviation of ± 3.83 and a range of 25–46 mm as compared to the left side, which was 38.25 mm with a standard deviation of 3.31 and range of 32–46 mm with statistically nonsignificant $P = 0.848$ [Table 2].

In addition, while looking for the existence and number of the zygomaticofacial foramina on the zygomatic bone, it was noticed that single foramen (type I) was present in 35.6% of bones and 54.1% of bones on the right and left sides, respectively, type II bone with double foramina was more common on the right side with 37.8% prevalence and 13.5% prevalence on the left side, on the contrary prevalence of type III (with triple foramina) and type IV (absent foramina) was much less. On the right side, type III was found in 11.1% of the bones, whereas it was present in 8.1% on the left side. However, absent foramina (type IV bone) were observed in 15.5% on the right side, whereas on the left side, it was 24.3%. On concluding the observations, it was summarized

Table 1: Comparison of the width of the zygomatic bone on both sides

Width	Minimum (mm)	Maximum (mm)	Mean±SD	*P*	*t*
Left	8	18	12.91±2.36	0.48	0.706
Right	9	20	13.34±2.97		

SD: Standard deviation

Table 2: Comparison of linear measurements of zygomatic bone on the right and left side

Length	Minimum (mm)	Maximum (mm)	Mean±SD	*P*	*t*
Left	32	46	38.25±3.31	0.848	0.192
Right	25	46	38.41±3.83		

SD: Standard deviation

Table 3: Frequency of the incidence of zygomaticofacial foramina and accordingly the zygomatic bones are classified as type I with single foramina, type II with double foramina, type III with triple foramina, and type IV with absent foramen

Type of bone	Right side (%)	Left side (%)	Total (%)
Type I (single foramen)	35.6	54.1	89.7
Type II (double foramina)	37.8	13.5	51.3
Type III (triple foramina)	11.1	8.1	19.2
Type IV (absent foramen)	15.5	24.3	39.8
Total	100	100	200

Table 4: The distance of zygomaticofacial foramina from the orbital and jugal point on the right and left side

Parameters	Right side (mm)	Left side (mm)	*P*	*t*
Distance from orbital margin	4.74±3.65	4.06±3.46	0.396	0.854
Distance from jugal point	7.61±4.22	6.69±5.41	0.388	0.868

SD: Standard deviation

Table 5: The distance of zygomaticotemporal foramina from the jugal point on the right and left side

Parameters	Right side (mm)	Left side (mm)	*P*	*t*
Distance from jugal point	4.72±2.79	4.36±3.67	0.428	0.346

that the most prevalent bone type was type I, with only single foramina on the left side, whereas on the right side, the most common type was type II [Table 3 and Figure 4].

Broadly, the topographical location of the zygomaticofacial foramina on the right side was 4.74 ± 3.46 mm from the orbital margin, whereas on the left side, it was 4.06 ± 3.46 mm with a $P = 0.396$. On the other hand, the distance of zygomaticofacial foramina from the jugal point on the right side was 7.61 ± 4.22, whereas on the left side, it was 6.69 ± 5.41 mm with $P = 0.388$ [Table 4].

Considering the topographical location of the zygomaticotemporal foramina, it was observed that all the foramina were located on the temporal surface of the zygomatic bone and the foramina were positioned near the jugal point on the left side with an average distance of 4.36 ± 3.67 mm, whereas on the right side it was 4.72 ± 2.79 mm with $P = 0.428$ and $t = 0.346$ [Table 5].

Discussion

Aforementioned study was conducted on 80 zygomatic bones, which were obtained from the bone bank of the tertiary care teaching hospital. Various parameters under study, namely length and width of the bone, frequency, and topography of the zygomaticofacial and zygomaticotemporal foramina, the distance of zygomaticofacial foramina from the orbital margin and jugal point, and distance of zygomaticotemporal foramina from the jugal point, were measured and noted.

The results were statistically tabulated and it was inferred that the zygomatic bone was wider on the right side with a mean value of 13.34 ± 2.97 mm as compared to the left side, which was 12.91 ± 2.36 mm. Similarly, the variation in the length of bone on both sides was also reported in the aforementioned study with slightly more dimensions on the right side, i.e., 38.41 ± 3.83 mm, as compared to the left side, which was 38.25 ± 3.31 mm. These parameters when compared bilaterally, showed a statistically insignificant relation. Such bilateral variations of the data in length and width of the zygomatic bone were also reported by Kim *et al*.,[10] Krishnan and Thenmohzi.[11]

Further, the bones were classified as type I, type II, type III, and type IV depending upon the number of zygomaticofacial foramina present. The most common type of bone present on the left side was type I (single foramen) with 54.1% incidence, whereas on the right side type II (double foramina) bone was the most common type with 37.8% incidence, type III was the least prevalent type of bone on both right (11.1%) and left sides (8.1%), and type IV (absent foramen) bone ranked 3rd in the occurrence on both sides. A similar type of classification of the zygomatic bone was also given by Nteli Chatzioglou *et al*.[5] but they classified the zygomatic bones into six types and concluded that the most common type was type I (single foramen) and type II (double foramina), whereas Senthil Kumar and Kesavi[12] have classified the bones into five types and declared that most common type was type I on the both right and left sides and Ferro *et al*.[14] also classified the bones into five types and concluded that the most common type was type I (single foramen), i.e., 49.8% irrespective of the side. Loukas *et al*. also classified the bones in a similar fashion and inferred that type I bone was most frequent in occurrence.[15] However, Mangal *et al*.,[6] Aksu *et al*.,[16] Lone *et al*.,[17] Del Neri *et al*.,[18] and Hwang *et al*.[19] did not classify the bones into any types and made the same conclusion that the most common type of bone

was with single foramen with 44.9%, 44.4%, 67.14%, 44%, and 50.9% occurrence, respectively. Deana and Alves also quoted single zygomaticofacial foramen as the most frequent type, and precisely, sex were an important factor in determining the frequency and location of the foramen.[20] In addition, Sharma also summarized the results of the study as the bones with single and double zygomaticofacial foramina were the most frequent types of bones, and triple and quadruple foramina were less frequently seen.[21]

Regarding the topographic location of the zygomaticofacial foramina, it was observed that the foramina were located closer to the orbital margin on both the right and left sides as compared to the jugal point and the distance from the orbital margin was 4.74 ± 3.65 mm and 4.06 ± 3.46 mm on right and left side, respectively. Nteli Chatzioglou *et al*.,[5] Senthil Kumar and Kesavi,[12] and Aksu *et al*.[16] also established similar findings regarding the topography of zygomaticofacial foramina; however, the interval between the orbital margin and the zygomaticofacial foramen was 6.67 ± 3.27 mm; 6.8 and 6.9 mm on the right and left sides and 5.94 ± 1.43 mm, respectively, which was slightly more as compared to the observations finalized in the current study. Furthermore, Kim *et al*.[10] reported only the presence of zygomaticofacial foramina on the body , frontal process and at the junction of the body and frontal process without signifying the topographical variations of these foramina. However, Kawata *et al*.[22] considered the jugale-zygomaxillare line as the reference standard and reported that all the foramina were located above this reference line in contrast to all the scientific data cited in the present study. Furthermore, Ferro *et al*. used some distinct landmarks to locate the zygomaticofacial foramina.[14] Lone *et al*. estimated the location of zygomaticofacial foramen from the frontozygomatic suture, zygomaticomaxillary suture, and the orbital margin and concluded that the measurements were more on the right side as compared to the left side.[17] Hwang *et al*. also delineated the distance of the zygomaticofacial foramen from the zygomatic suture and the orbital rim, which stood out to be 24.4 mm and 7.61 mm, respectively, which was slightly more as reported in the present study.[19] Deana and Alves in distinction commented that there was no difference in the distance between the orbital cavity and the zygomaticofacial foramen when both sides were taken into consideration.[20]

While considering the topographic location of zygomaticotemporal foramina in the present study, the results concluded that all the foramina were located on the lateral surface of the malar bone with an average distance from jugal point 4.36 ± 3.67 mm and 4.72 ± 22.79 mm on the left and right sides, respectively. However, Siddiqui *et al*. also studied the location of zygomaticotemporal foramina and inferred that 4.5% of the zygomaticotemporal foramina were located on the lateral surface of the bone, 0.5% were lying superior to zygomaticofacial foramina and 0.5% of the foramina were present in duplication, but no mention was made regarding the distance of foramina from various anatomical landmarks of the bone.[13] Iwanaga *et al*. traced the intraorbital path of the zygomaticotemporal nerve along with the lacrimal nerve but did not comment on the location of zygomaticotemporal foramina.[23] Kim *et al*. also observed only the number of zygomaticotemporal foramina and classified the bones according to the number but did not give any data regarding the location of the foramina of the bone.[10] In distinction to present inference, Loukas *et al*. reported only the frequency of the zygomaticotemporal foramina.[15]

Conclusions

With an increasing incidence of midfacial surgeries, it is the need of the hour that the morphometric and topographic data pertaining to zygomatic bone complex must be available for various ethnic groups so that it becomes easy for the surgeons to perform surgeries, nerve blocks, and other procedures and they must be made aware of the anatomical variations of the bones, nerves, and foramina present in the midfacial region. The results of this study, when summarized, inferred that all the dimensions of zygomatic bone were slightly more on the right side as compared to the left side and on the left side, the most frequent bone type observed was type I, whereas on the right side type II bone was more frequent and foramen was frequently found near the orbital margin. However, data pertaining to the topographic location of zygomaticotemporal foramina are deficient; so it is advisable to conduct more such studies and identify various anatomical variations for the same. Hence, it is evident that anatomical variations can be present in this bone so the surgeons should take into consideration all the parameters to choose the implants and improve the surgical success. Moreover, precise awareness of these variables will be helpful for surgeons for various surgical procedures to be carried out in the midfacial region, 3D printing of zygomatic bones, and designing of grafts for implantation. Besides, it is also recommended that further studies should be organized to look into the sexual differences pertaining to the zygomatic bone.

Acknowledgments

We, the authors, sincerely bow our head as a mark of gratitude for those who donated their bodies for the research work to be undertaken in the field of anatomy. Their untold contribution to the mankind by becoming part of scientific research is incomparable. The conclusions of such studies are going to help to reduce suffering and improve the patient management. Thus, these donors and their families need to acknowledged for this great act of selflessness and the mankind shall always remain indebted to them.[24]

Financial support and sponsorship

Nil.

Conflicts of interest

There are no conflicts of interest.

References

1. Furst IM, Austin P, Pharoah M, Mahoney J. The use of computed tomography to define zygomatic complex position. J Oral Maxillofac Surg 2001;59:647-54.
2. Scheuer L, Black S. The head, neck and dentition. In: Developmental Juvenile Osteology. London: Academic Press; 2000. p. 36-170.
3. Nikolova S, Toneva D, Georgiev, I. A case of bipartite zygomatic bone. Eur J Forensic Sci 2017;4:1. [doi: org/10.5455/ejfs.238160].
4. Wang Q, Dechow PC. Divided zygomatic bone in primates with implications of skull morphology and biomechanics. Anat Rec (Hoboken) 2016;299:1801-29.
5. Nteli Chatzioglou G, Sağlam L, Çandir BN, Yiğit M, Gayretli Ö. Anatomical variations of the zygomaticofacial foramen and its related canal through the zygomatico-orbital and zygomaticotemporal foramina in dry human skulls. Surg Radiol Anat 2024;46:33-40.
6. Mangal A, Choudhry R, Tuli A, Choudhry S, Choudhry R, Khera V. Incidence and morphological study of zygomaticofacial and zygomatico-orbital foramina in dry adult human skulls: The non-metrical variants. Surg Radiol Anat 2004;26:96-9.
7. Morgan BD, Madan DK, Bergerot JP. Fractures of the middle third of the face – A review of 300 cases. Br J Plast Surg 1972;25:147-51.
8. Bergeron JM, Raggio BS. Zygomatic arch fracture. In: StatPearls. Treasure Island (FL): StatPearls Publishing; 2024. Available from: https://www.ncbi.nlm.nih.gov/books/NBK549898/. [Last updated on 2024 Jan 26].
9. Chaudhary B, Anand U, Kumar V, Agarwal P, Kumar P, Priyadarshi RN. Feasibility and adaptation of three- dimensional model for surgical planning and training: A pilot study. Natl J Clin Anat 2021;10:220-5.
10. Kim HJ, Paik DJ, Choi BY, Chung MS, Han SH, Hwang YI, *et al*. Measurements of the zygomatic bones and morphology of the zygomaticofacial and zygomaticotemporal foramina in Korean. Korean J Phys Anthropol 1997;10:225-34.
11. Krishnan P, Thenmohzi MS. Estimation of dimensions of zygomatic arch in human dry skull. Int J Res Trends Innov 2020;5:58-9.
12. Senthil Kumar S, Kesavi D. Incidence and location of zygomaticofacial foramen in adult human skulls. Int J Med Res Health Sci 2014;3:80-3.
13. Siddiqui HF, Konschake M, Ottone NE, Olewnik Ł, Iwanaga J, Aysenne A, *et al*. A marginal process of the zygomatic bone predicts a lateral exit of the zygomaticotemporal nerve: An anatomical study with application to surgery around the midface. Clin Anat 2023;36:708-14.
14. Ferro A, Basyuni S, Brassett C, Santhanam V. Study of anatomical variations of the zygomaticofacial foramen and calculation of reliable reference points for operation. Br J Oral Maxillofac Surg 2017;55:1035-41.
15. Loukas M, Owens DG, Tubbs RS, Spentzouris G, Elochukwu A, Jordan R. Zygomaticofacial, zygomaticoorbital and zygomaticotemporal foramina: Anatomical study. Anat Sci Int 2008;83:77-82.
16. Aksu F, Ceri NG, Arman C, Zeybek FG, Tetik S. Location and incidence of the zygomaticofacial foramen: An anatomic study. Clin Anat 2009;22:559-62.
17. Lone M, Telang A, Rajgopal L, Bhuiyan PS. Location and incidence of the zygomatico-facial foramen in dry human skulls: An anatomical study. J Anat Soc India 2016;65:164-6.
18. Del Neri NB, Araujo-Pires AC, Andreo JC, Rubira-Bullen IR, Ferreira Júnior O. Zygomaticofacial foramen location accuracy and reliability in cone-beam computed tomography. Acta Odontol Scand 2014;72:157-60.
19. Hwang SH, Jin S, Hwang K. Location of the zygomaticofacial foramen related to malar reduction. J Craniofac Surg 2007;18:872-4.
20. Deana NF, Alves N. Frequency and location of the zygomaticofacial foramen and its clinical importance in the placement of zygomatic implants. Surg Radiol Anat 2020;42:823-30.
21. Singroha R, Verma U, Rathee SK, Agrawal S. A study on incidence of zygomaticofacial foramen in dried human skulls of North Indian population. Int J Adv Res 2024. p. 391-396. Available from: www.journalijar.com. [Last accessed on 2024 Dec 25].
22. Kawata K, Ide Y, Sunohara M. Anatomical study of the zygomaticofacial foramen and zygomatic canals communicating with the zygomaticofacial foramen for zygomatic implant treatment: A cadaver study with micro-computed tomography analysis. Anat Cell Biol 2024;57:204-12.
23. Iwanaga J, Wilson C, Watanabe K, Oskouian RJ, Tubbs RS. Anatomical study of the zygomaticotemporal branch inside the orbit. Cureus 2017;9:e1727.
24. Iwanaga J, Singh V, Ohtsuka A, Hwang Y, Kim HJ, Moryś J, *et al.* Acknowledging the use of human cadaveric tissues in research papers: Recommendations from anatomical journal editors. Clin Anat 2021;34:2-4.

Original Article

Septal Aperture of the Humerus: A Morpho-anatomical Variation with Clinical Significance

Dragana Radošević, Milica Vuletić, Stefan Dimić, Dušica Marić, Nikola Vučinić, Zorka Drvendžija, Radmila Peric[1]

Department of Anatomy, Medical Faculty, University of Novi Sad, [1]Department of Radiology, Center of Radiology, Clinical Center of Vojvodina, Medical Faculty, University of Novi Sad, Novi Sad, Serbia

Abstract

Introduction: In the distal end of the humerus, between the coronoid and olecranon fossae, there is a bony plate with different thicknesses and transparency. There may be an opening that represents an anatomical variation with significant implications for surgical and radiological practice. **Aim:** The aim of this study was to examine the incidence, morphological characteristics, and morphometric relationships of the septal aperture (SA)/transparent septum (TS) to the adjacent structures and present their clinical implication. **Materials and Methods:** The study included 80 humeri. Morphometric measurements (dimensions and position of the aperture) were performed in the ImageJ (version 150i) program. The presence and number of SAs were detected by inspection. Humeri without aperture were exposed to a beam of light to determine the degree of septum transparency. **Results:** The SA was found on 12 humeri (15%), and 25 humeri had a TS (31.25%). The most common shape was circular (50%), and oval and irregular types were also observed. A cribriform shape (17%) was detected in the group of transparent septa. The vertical and horizontal diameters were 4.06 mm and 6.59 mm, and the area was 26.12 mm^2. The SA is located 28.10 mm from the lateral and 24.81 mm from the medial epicondyle. No statistically significant difference was observed between the left and right humeri. **Conclusion:** This research provides important insights for surgical treatment of the lower segment of the humerus and in radiology to distinguish it from osteolytic and cystic lesions.

Keywords: *Clinical significance, humerus, morphometric analysis, septal aperture*

Introduction

The olecranon and coronoid fossae in the distal end of the humerus are most often separated by a bony plate with different thicknesses. This thin and transparent plate is known as the supratrochlear septum. The synovial sheet of the articular capsule of the elbow joint covers it.[1] The septum can be perforated or transformed into an opening when described as a morpho-anatomical variation with anthropological and clinical importance. In the literature, this opening is called differently (septal aperture [SA], olecranon aperture, supratrochlear foramen, intercondylar foramen, etc.).[1-5] We will use SA in this research. The incidence of SA varies from 0.3% to 58%, being diverse among different ethnic groups.[6,7]

According to Hirsh, in the olecranon area, a thin bony plate is present until the 7th year of life, after which the bone partition is gradually absorbed and an SA is formed.[7] However, cases of SA have also been reported in younger children.[8] A SA occurs during adolescence or, more often, in adulthood due to incomplete bone ossification, an increase in the intralamellar space, and gradual absorption of the bone septum.[9] A detailed review of the literature showed that the SA was first described by Meckel back in 1825 and was subsequently studied by other researchers in many animals (hyenas, dogs, and cattle).[10,11] Charles Darwin considered this aperture in humans to be one of the phylogenetic characteristics that evolutionarily link humans to primates.[12] Vascular structures usually do not pass through it, which is why recent studies suggest that the term aperture should be used instead of opening for this variation.[13,14]

Different theories about the SA etiology have been proposed, based on mechanical influences and metabolic and genetic factors, but no theory has yet been accepted as definitive. The formation of the SA may be related to changes at the level of the T-box gene, which encodes the synthesis of proteins responsible for the postnatal development of the upper limbs.[15]

How to cite this article: Radošević D, Vuletić M, Dimić S, Marić D, Vučinić N, Drvendžija Z, *et al*. Septal aperture of the humerus: A morpho-anatomical variation with clinical significance. J Anat Soc India 2025;74:152-8.

Article Info

Received: 13 January 2025
Revised: 27 January 2025
Accepted: 13 April 2025
Available online: 30 June 2025

Address for correspondence:
Dr. Dragana Radošević, Department of Anatomy, Medical Faculty, University of Novi Sad, Hajduk Veljkova Street No. 3, Novi Sad, Serbia. E-mail: dragana.radosevic@mf.uns.ac.rs

Access this article online

Website: https://journals.lww.com/joai

DOI: 10.4103/jasi.jasi_10_25

Quick Response Code:

According to the mechanical theory, the SA is formed by the gradual atrophy of the bony plate of the elbow fossa due to repetitive bending and stretching movements in the elbow joint, i.e. during intense physical activities when the elasticity of the bone changes ("robustness theory").[4]

Supracondylar fractures are the most common fractures in the pediatric population and are most often treated by intramedullary fixation through the medial and lateral epicondyles.[16,17] The success of this procedure, among other things, depends on the anatomical characteristics of the distal end of the humerus. It has been noted that the intramedullary canal is narrower in the humeri with an SA, which may compromise the fixator placement's success.[15] Furthermore, during the radiological evaluation of changes in the distal part of the humerus, an SA can be misinterpreted as an osteolytic lesion or cyst.[18]

Due to all of the above, the present research aimed to examine the frequency and morphometric characteristics (shape and dimensions) and more precisely determine the position of the SA on the humeri in the Serbian population. We highlight the clinical importance of results, which may be beneficial to orthopedists and radiologists.

Materials and Methods

The study was conducted at the Department of Anatomy, Faculty of Medicine, University of Novi Sad. The Ethics Committee approved the research (decision number 01-39/269). This investigation involved precise measurements on dry adult bones of unknown gender and age. The examination included a total of 80 humeri from the osteology collection of the Department of Anatomy of the Faculty of Medicine in Novi Sad (38 of the left side and 42 of the right side). The same researcher performed all measurements, ensuring consistency and accuracy.

The humeri were photographed by the Olympus SP-560UZ digital camera with 18x optical zoom from a fixed distance. All calculations were performed in ImageJ's image processing program (version 150i).

The analysis first involved the observation of the distal ends of the humeri, after which those humeri with a SA [Figure 1a] were first separated as the SA group. The humerus that did not have an aperture was exposed to a beam of light directed from behind to the front, in the region of the ulnar fossa, to note the transparency of the septum. Humeri with transparent septum [TS; a bone plate that lets light through, Figure 1b] formed the TS group of humeri. In contrast, if light did not pass through the distal ends of the humeri [Figure 1c], an opaque septum was recorded (OS group). In this way, groups with SA and TS were further morphometrically analyzed. All three types are also shown radiologically for a more detailed presentation and understanding of the types [Figure 2].

Furthermore, by visualizing the shape of the SA and the TS, several observed morphological types were identified and described, as shown in Figures 1 and 2. Their frequency is graphically represented.

Morphometric analysis

The measurement and calculation of the dimensions of the SA/TS included the following parameters [Figure 3]:

vd, the vertical diameter of the SA/TS

hd, the horizontal diameter of the SA/TS

A, area of the SA/TS

Measurement and calculation of parameters that describe the position of the SA and TS to the surrounding anatomical structures on the distal end of the humerus:

oe-le, the distance of the outer edge (oe) of the SA/TS from the most prominent point of the lateral epicondyle (le) of the humerus

ie-me, the distance of the inner edge of the examined SA/TS from the most prominent point of the medial epicondyle (me) of the humerus

le-th, the distance of the lower edge of the SA/septum from the lower edge of the trochlea humeri (th)

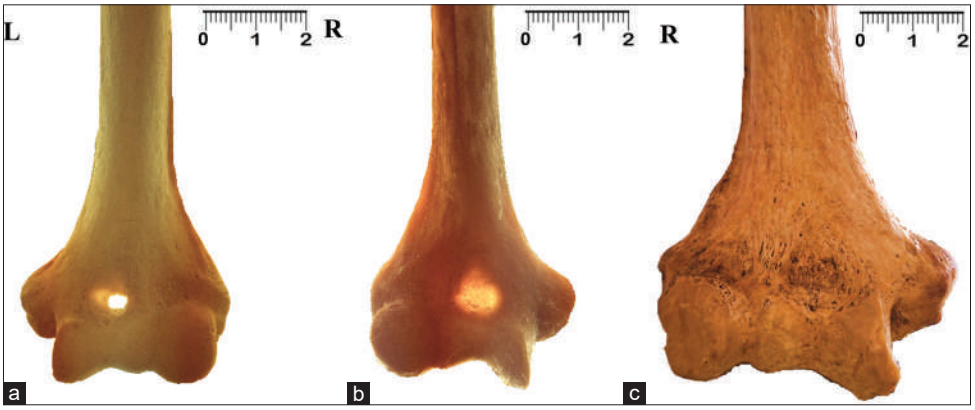

Figure 1: View of the septal aperture (a), transparent septum (b), and opaque septum (c) on the distal ends of the examined humeri

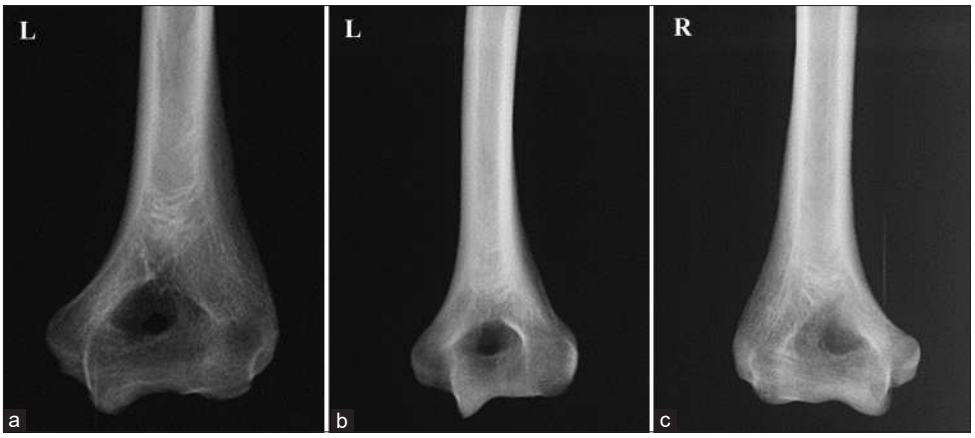

Figure 2: Anteroposterior radiographic view of septal aperture (a), transparent septum (b), and opaque septum (c)

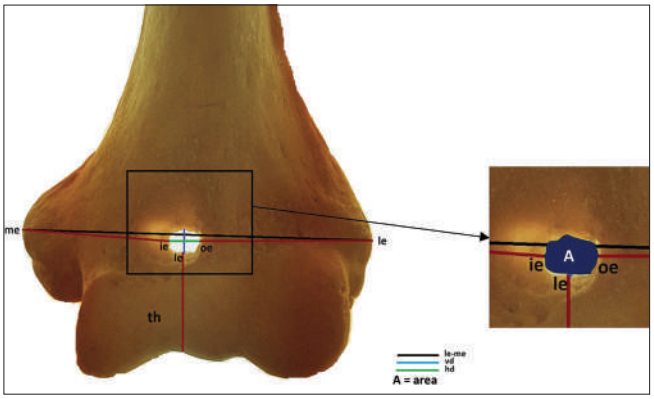

Figure 3: Presentation of the parameters of the morphometric analysis of the septal aperture (SA) on the distal end of the examined humeri: le-me, the distance between the humerus's most prominent point of the lateral epicondyle (le) and the most prominent point of the medial epicondyle (me); vd, the vertical diameter of the SA/transparent septum (TS); hd, the horizontal diameter of the SA/TS

le-me, the distance between the humerus's most prominent point of the lateral epicondyle (le) and the most prominent point of the medial epicondyle (me).

The statistical analysis of the obtained data was performed in the program GraphPad Prism software 10.0.0, Dotmatics, Boston, Massachusetts. The results are presented as descriptive statistics parameters (mean value [$\bar{x}$], standard deviation, and minimum and maximum value [Min–Max]). Student's *t*-test was used to determine the difference between groups. A statistically significant difference was considered if $P < 0.05$.

Results

As part of the descriptive analysis of the distal ends of the examined 80 humeri, 12 bones (15%) with a SA were found, while a TS was found on 25 humeri (31.25%). The remaining part of the examined sample (53.75%) belonged to the group that has an opaque septum [Table 1]. The frequency of the SA was equally present on the left and right humeri, while the TS was minimally more frequent on the left side (13 vs. 12 bones).

By analyzing the shape of the SA and the TS, we noted several morphological types. A round, oval, and irregular SA type was observed [Figure 4]. In addition, a cribriform TS (consisted of several smaller openings through which light passed) was also seen [Figure 4].

Graphs 1 and 2, respectively, show the percentage representation of certain types of SA and TS. The most common is the round type of SA (50%), followed by the oval shape with 33% representation, while the least common is the irregular aperture (17%). In the group of humeri with a TS, the round and oval type are equally represented (28%) [Graph 2].

The results of the statistical analysis of the descriptive parameters that describe the size and distance of the aperture/septum from the surrounding anatomical structures are shown in Table 2. The average value of the vertical diameter was 4.06 mm, and the horizontal diameter was 5.59 mm. SAs and transparent septa have an average surface area of 26.12 mm^2. The distance of the opening/septum from the outer epicondyle is 28.10 mm, and from the inner, 24.81 mm. The lower edge of the SA is 16.25 mm away from the trochlea. The inner and outer epicondyles are 59.62 mm apart.

Table 3 shows the descriptive statistics analysis of the parameters that define the dimensions of SAs and transparent septa and their comparison in relation to the side of the body. No statistically significant difference was found between the measured parameters of the left and right humeri [Table 3].

Table 4 shows the parameters of SAs and transparent septa that describe their distance from the surrounding anatomical structures (internal and external epicondyle and trochlea) on the distal edge of the humerus. No statistically significant difference in the values of the measured parameters between the left and right humeri was found [Table 4].

Discussion

Bony anatomical variations, a subject of extensive research, have practical implications for the successful

Table 1: Frequency of the presence of a septal opening, transparent, and opaque septum in the entire examined sample and in relation to the side of the body

	Total (*n*=80), *n* (%)	Left (*n*=38), *n* (%)	Right (*n*=42), *n* (%)
SA	12 (15)	6 (50)	6 (50)
TS	25 (31.25)	13 (52)	12 (48)
OS	43 (53.75)	19 (44.18)	21 (55.81)

SA: Septal aperture, TS: Transparent septum, OS: Opaque septum

Table 2: Results of descriptive analysis of morphometric parameters of humerus with septal aperture and humerus with transparent septum together (*n*=37)

Parameters	x̄±SD	Minimum–maximum
vd (mm)	4.06±1.28	0.56–6.32
hd (mm)	6.59±2.90	0.85–14.10
Area (mm^2)	26.12±21.33	0.24–12.15
oe-le (mm)	28.10±3.56	21.72–36.50
ie-me (mm)	24.81±3.48	18.10–30.31
le-th (mm)	16.25±1.89	13.41–21.50
le-me (mm)	59.62±6.37	47.12–75.34

vd: Vertical diameter, hd: Horizontal diameter, oe-le: Distance of the outer edge (oe) of SA from the lateral epicondyle (le), ie-me: Distance of the inner edge (ie) of SA from the medial epicondyle (me), le-th: Distance of the lower edge (le) of SA from the trochlea (th), le-me: Distance between the lateral epicondyle (le) and medial epicondyle (me), SD: Standard deviation

implementation of diagnostic and therapeutic procedures.[19-21] The incidence of confirmed SA in studies conducted on different populations varies widely from 0.3% to 58%. Our research, revealing a frequency of 15%, aligns with the results of other European studies [Table 5]. Notably, the lowest incidence was reported in the work of Papaloucas *et al*. (0.3%),[22] while the highest values were reported in Americans, 58%,[7] and Australians, 46.5%.[8] These findings have practical implications for diagnostics, engaging us in the potential applications of this research.

The incidence of an SA is differs among different ethnicities, ranging from 0.3% to 58%.[18,23,24] Anthropological studies reported that America has the highest incidence of SA (58%),[7,18,24] while Europeans have the lowest frequency of 11%.[14,24] It is also stated that people who have an SA on the distal end of the humerus show excessive extension in the elbow joint.[23,24]

Our study did not show differences in the incidence of SA in relation to the side of the body. It was found that their representation was equal in our examined sample (50%). An equal representation of apertures in relation to the side of the body was also published by Silva *et al*. (27.9% and 27.8%),[25] as well as Singhal and Rao (27.9% and 27.8%).[12] However, published results in many studies have shown that the SA is more frequent on females' left side of the body.[2,18,26-28] One of the theories that explains the mechanism of SA is the theory of the elasticity of the

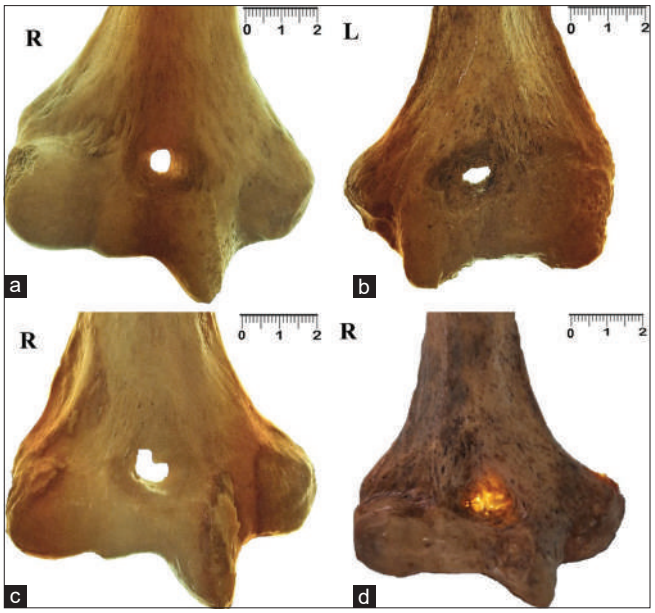

Figure 4: Different types of septal aperture: Circular (a), oval (b), irregular (c), and cribriform type of transparent septum (d)

humerus and hyperextension in the elbow joint. The theory of elasticity explains that the humerus on the nondominant side of the body is more likely to have an SA because the bones on the dominant side of the body are more rigid and less elastic.[2,7,10,29] Hyperextension of the joints is a consequence of the increased elasticity of collagen fibers, and this phenomenon is more common in women,[22] so this can explain the higher incidence of SA on the female humerus.

Through a descriptive analysis of the shape of the SA, we determined that the most common type is round (50%), then oval (33%), and the least common is an opening of irregular shape (17%). The results obtained in our study are similar to the published data of other studies, which also showed that the most common is the circular SA.[18,23] However, numerous studies state that the oval type of opening is most often present on the investigated lower ends of the humerus and with different percentages of representation – Naqshi *et al*. (90.9%),[30] Silva *et al*. (39%),[25] and Mallikarjun *et al*. (43.75%).[31]

In this study, the frequency of the TA is higher than the SA (31.25%). The results of other published studies are different [Table 5], and it can be assumed that the formation of a TS is multifactorial with racial and ethnic heterogeneity. Regarding the shape of the TA, the round and oval morphological types are equally present in our research (28%). In this group of humerus, we found a lattice septum (4 humeri). A triangular[3,13] and kidney-shaped septum was found in other studies.[2,13] The formation of a different TA and the SA shape most likely reflects the degree of bone degradation, which supports the mechanical theory explaining the opening. Namely, the size of the olecranon and coronoid process of the ulna

affects the intensity of pressure in the area of the ulnar fossa during flexion and extension of the elbow joint. The septal opening forms from front to back.[32] Repeated elbow joint movements can gradually cause atrophy of the TS, leading progressively to the development of the septal opening in that place. Therefore, it can be assumed that TA is a vulnerable part of the bone, probably leading to aperture formation.

Descriptive analysis of the morphometric parameters of all examined humerus together (with SA and TS) showed that the average value of vd was 4.06 mm, and hd was 6.59 mm. Similar results were obtained in the research of Erdogmus (4.04 mm and 5.63 mm),[29] and slightly lower values were published in the study by Kundalić *et al*. (3.33 mm and 5.25 mm),[3] which was produced on the territory of Serbia. Analyzing the hd of septal openings and transparent septa, our results and those of other studies show some variation. In this study, the mean value of hd is 6.92 mm on the left side and 6.51 mm on the right side. Similar values of this parameter were obtained by the authors from India (6.50 mm),[28] as well as by Nayak *et al*. (6.55 mm).[23]

On the contrary, some anthropological studies have reported slightly lower values for the horizontal diameter. Silva *et al*. found a value of 4.85 mm on the right side,[25] Kundalić *et al*. reported 5.25 mm,[3] and Li *et al*. found 4.47 mm on the left side and 3.26 mm on the right side.[33] Our study, however, did not established a statistically significant difference in the horizontal diameter between the two sides of the body. However, the literature states that the horizontal diameter of the opening is larger on the left humerus.[29,33] The mean value of the surface of the septal openings and transparent septa on the left side was 26.16 mm^2, while on the right side, it was slightly higher at 27.02 mm^2 without a statistically significant difference (P = 0.80). The values of the area of the septal openings in the study by Silva *et al*. are 19.91 mm^2 on the left and 19.63 mm^2 on the right side of the body.[25] Slightly lower values of this parameter are found in a study conducted in China, where the mean value of the opening surface on the left side was 13.10 mm^2 and on the right side, 18.43 mm^2.[33] The observed heterogeneity in dimensions supports that the size of the septal opening is different in members of other populations, and the processes of migration and colonization of people in certain countries can influence it.

By analyzing the parameters of the opening and septum distance from the surrounding bony structures, we aimed to define their localization more precisely. The septal opening/septum is located 28.10 mm from the external

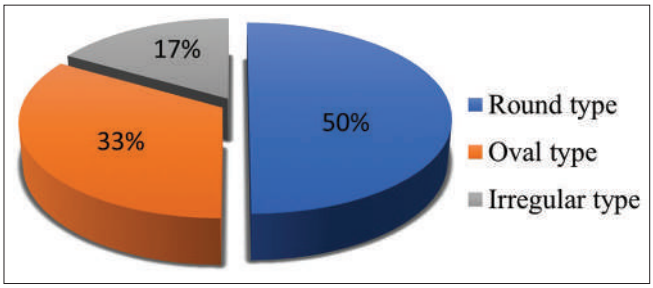

Graph 1: Types of septal apertures in the examined sample

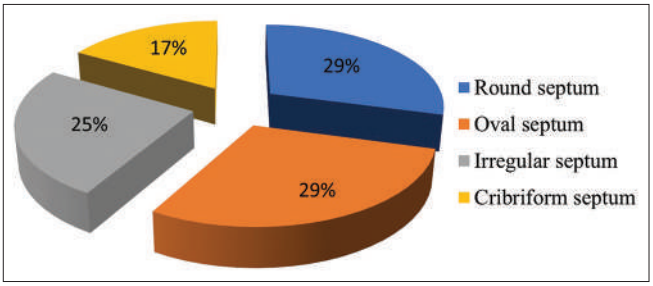

Graph 2: Types of transparent septum in the examined sample

Table 3: Descriptive statistics parameters of septal aperture and transparent septum dimensions and comparison of left and right humerus

Parameters	Left (n=19)		Right (n=18)		P
	x̄±SD	Minimum–maximum	x̄±SD	Minimum–maximum	
hd (mm)	6.92±2.52	2.14–11.58	6.51±3.13	0.85–14.1	0.66
vd (mm)	4.10±1.16	1.92–6.01	3.85±1.43	0.56–6.32	0.49
Area (mm^2)	26.16±12.72	7.43–46.52	27.02±27.78	0.24–12.15	0.80

vd: vertical diameter, hd: horizontal diameter, SD: Standard deviation

Table 4: Distance parameters of septal openings and transparent septa in relation to the surrounding bony structures

Parameters	Left (n=19)		Right (n=18)		P
	x̄±SD	Minimum–maximum	x̄±SD	Minimum–maximum	
oe–le (mm)	28.25±4.14	23.22–36.50	28.01±3.02	21.72–32.51	0.83
ie–le (mm)	24.11±3.64	18.15–29.87	25.54±3.24	18.17–30.31	0.21
le–th (mm)	16.15±1.88	13.54–20.36	16.36±1.95	13.41–21.50	0.74
le–me (mm)	59.25±7.30	47.12–75.34	60.02±5.41	47.83–70.63	0.72

oe-le: Distance of the outer edge (oe) of SA from the lateral epicondyle (le), ie-me: Distance of the inner edge (ie) of SA from the medial epicondyle (me), le-th: Distance of the lower edge (le) of SA from the trochlea (th), le-me: Distance between the lateral epicondyle (le) and medial epicondyle (me), SD: Standard deviation

Table 5: Incidence of septal aperture and transparent septum in different populations

Research	Population	Incidence of SA (%)	Incidence TS (%)
Papaloucas *et al*.[22]	Greece	0.3	/
Myszka[4]	Poland	7.5	/
Kundalić *et al*.[3]	Serbia	10	67.1
Ndou *et al*.[18]	Europe	16	32.5
Silva *et al*.[25]	Brazil	19.8	78
Bradshaw *et al*.[26]	Portugal	16.83	21.6
Mathew *et al*.[2]	India	24.5	56.96
Mallikarjun *et al*.[31]	India	32	28.5
Hrdlicka[8]	Australia	46.5	/
Hirsh[7]	America	58	/
Current study	Serbia	15	31.25

SA: Septal aperture, TS: Transparent septum

epicondyle, 24.81 mm in relation to the inner epicondyle, and 16.25 mm away from the lower edge of the trochlea of the humerus. Literature data also suggest that the septal opening is positioned closer to the medial epicondyle,[3,23,29] although a statistically significant difference was not confirmed in all studies. By observing the values of the calculated parameters in relation to the side of the body, we calculated that the septal opening/septum is 28.25 mm away from the external epicondyle on the left side or 28.01 mm on the right side of the body. These parameters for the internal epicondyle are 24.11 mm on the left and 25.54 mm on the right humerus. Our data are consistent with the research of Lalita *et al*. (24.97 mm on the left and 25.12 mm on the right humerus)[13] and Mathew *et al*. (24.91 mm on the left and 24.39 mm on the right humerus).[2] The mean value of the le-th parameter in our study was 16.15 mm on the left and 16.36 mm on the right humerus. In relation to our results, similar and slightly lower values were found in the study by Mathew *et al*. (14.41 mm)[2] and Lalita *et al*. (14.97 mm on the right side and 15.07 mm on the left humerus).[13] In our research, no statistically significant difference was found in relation to the side of the body when observing the parameters of the distance of the opening and the septum from the surrounding bony structures. Indeed, some constitutional differences exist in relation to the side of the body. Still, it can also be assumed that the lack of statistical significance is due to the small sample in our research. It is also observed that research conducted in different parts of the world yields results with noticeable discrepancies, which the constitutional differences of certain ethnic species can explain.

Supracondylar fractures account for about 75% of all injuries in the pediatric age group.[34] One of the most common causes of this type of fracture is a fall on an outstretched arm when the distal segment of the shoulder is displaced backward. In such injuries, intramedullary fixation is usually indicated as a surgical treatment. It has been shown that a septal opening is associated with a narrowed intramedullary canal, making it difficult to treat the fracture and adequately place the fixator. The width of the intramedullary canal is statistically significantly smaller in the humerus with a septal opening, so preoperative preparation is essential in the case of a septal opening to achieve the desired precision of intramedullary fixation.[16,24] The septal opening is essential in interpreting radiological findings of the upper extremity. If they are present, a septal opening or a TS can give a wrong radiological assessment regarding an osteolytic lesion, i.e. a cyst at the observed site.[18,35]

Limitations

It is important to acknowledge the limitations of our research. The small sample size may have affected the statistical significance of our findings. Additionally, as this study was performed on dry bones, we could not analyze the potential effect of aging on the occurrence and morphometry of SA. Equally, we were unable to determine the handedness, a factor that could significantly contribute to the robusticity hypothesis.

Conclusion

There is still a need for consensus on whether the term "aperture" or "opening" is more appropriate to describe the communication between the olecranon and coronoid fossa. This communication is known to be a pathway for vascular structures. However, it is important to note that most studies that have analyzed the distal end of the humerus were conducted on dry bones, from which the soft tissues were removed. Therefore, it is not certain whether the vascular elements actually passed through this opening.

This study significantly enhances our understanding of the detailed morphometry and anatomical localization of SA in Serbians, highlighting the diversity in their morphological forms. By precisely defining the position and size of the SA, we provide a valuable resource for clinicians, enabling them to more effectively conduct diagnostic and therapeutic procedures. However, it is crucial to emphasize the need for ongoing research, particularly in the area of soft-tissue analysis, to fully comprehend the impact of these anatomical variations on the development of SA. Anthropological research on bone variations is essential for a comprehensive understanding of the anatomical structures of the human body. We stress the importance of conducting similar studies on other populations to provide a global perspective on this important anatomical variation.

Financial support and sponsorship

Nil.

Conflicts of interest

There are no conflicts of interest.

References

1. Shivaleela C, Afroze KH, Lakshmiprabha S. An osteological study of supratrochlear foramen of humerus of South Indian population with reference to anatomical and clinical implications. Anat Cell Biol 2016;49:249-53.
2. Mathew AJ, Gopidas GS, Sukumaran TT. A study of the supratrochlear foramen of the humerus: Anatomical and clinical perspective. J Clin Diagn Res 2016;10:C05-8.
3. Kundalić B, Marković B, Mitković M, Ugrenović S, Jovanović I, Čukuranović-Kokoris J, *et al.* Olecranon aperure of the humerus – A morphometrical study. Serb Arch of Med (Serbian Archives of Medicine) 2021;149:328-33.
4. Myszka A. Septal aperture aetiology: Still more questions than answers. Folia Morphol (Warsz) 2015;74:219-24.
5. Baker SA, Boyd A, Anderson S, Kelly AP, Garcia G, Campbell AL. Analysis of humeral septal apertures in forensic and archaeological samples. Forensic Sci Int Rep 2022;5:100273.
6. Chagas CA, Gutfiten-Schlesinger G, Leite TF, Pires LA, Silva JG. Anatomical and radiological aspects of the supratrochlear foramen in Brazilians. J Clin Diagn Res 2016;10:C10-3.
7. Hirsh IS. The supratrochlear foramen; clinical and anthropological considerations. Am J Surg 1927;2:500-5.
8. Hrdlicka A. The humerus: Septal apertures. Antropology 1932;10:31-96.
9. Morton SH, Crysler WE. Osteochondritis dissecans of the supratrochlear septum. J Bone Joint Surg 1945;27:12-24.
10. Benfer RA, Tappen NC. The occurrence of the septal perforation of the humerus in three non humen primates species. Am J Phys Anthropol 1968;29:19-28.
11. Haziroglu RM, Ozer M. A supratrochlear foramen in the humerus of cattle. Anat Histol Embryol 1990;19:106-8.
12. Singhal S, Rao V. Supratrochlear foramen of the humerus. Anat Sci Int 2007;82:105-7.
13. Lalita BT, Francis MY, Balaji K, Raghunath G, Kumaresan M. A comprehensive study on supratrochlear foramen of human humerus and its clinical significance – A review. Biomed Pharmacol J 2021;14:1197-207.
14. Pires LA, Leite TF, Fonseca Junior A, Babinski MA, Chagas CA. The olecranon aperture of the humerus: A meta-analysis with anthropological and clinical discussion. Homo 2019;70:75-84.
15. Govoni KE, Linares GR, Chen ST, Pourteymoor S, Mohan S. T-box 3 negatively regulates osteoblast differentiation by inhibiting expression of osterix and runx 2. J Cell Biochem 2009;106:482-90.
16. Paraskevas GK, Papaziogas B, Tzacveas A, Giaglis G, Kitsoulis P, Natsis K. The supratrochlear foramen of the humerus and its relation to the medullary canal: A potencial surgical aplication. Med Sci Monit 2010;16:119-23.
17. Higuchi DH, de Oliveira GA, Alves JP, Lebedenco L, Dobashi ET. Supracondylar fractures in children: A systematic review of treatment options. Acta Ortop Bras 2024;32:e278420.
18. Ndou R, Smith P, Gemell R, Mohatla O. The supratrochlear foramen of the humerus in a South African dry bone sample. Clin Anat 2013;26:870-4.
19. Magcaba N, Olojede SO, Lawal SK, Rennie C, Azu OO, Naidu EC. Morphology and morphometry of the anterior clinoid process in a select South African population. J Anat Soc India 2024;73:167-71.
20. Mudhol RS, Narahari S, Havaldar RR. Morphological and anthropometrical features of human ear ossicles. A 1 – Year cadaveric observational study. J Anat Soc India 2022;71:88-92.
21. Prashanth KU, Pai MM, Murlimanju BV, Prabhu LV, Prameela MD. Estimation of humerus length by measuring the dimensions of its lower fragments. J Anat Soc India 2021;70:209-15.
22. Papaloucas C, Papaloucas M, Stergiulas A. Rare cases of humerus apertures in Greeks. Trends Med Res 2011;6:178-83.
23. Nayak SR, Das S, Krishnamurthy A, Prabhu LV, Potu BK. Supratrochlear foramen of the humerus: An anatomico – Radiological study with clinical implication. Upsala J Med Sci 2009;114:90-4.
24. De Wilde V, De Maeseneer M, Lenchik L, Van Roy P, Beeckman P, Osteaux M. Normal osseous variants presenting as cystic or lucent areas on radiography and CT imaging: A pictorial overview. Eur J Radiol 2004;51:77-84.
25. Silva FA, Silva TS, Souza PR, Reis RS, Ferreira MR, Magalhães CP. Morphological and morphometric study of the supratrochlear foramen. J Morphol Sci 2018;35:54-7.
26. Bradshaw R, Elipoulos C, Borrini M. Septal aperture of the humerus: Etiology an frequency rates in two European population. Anat Rec (Hoboken) 2020;303:1821-30.
27. Raghavendra K, Reddy AK, Shirol VS, Dixit D, Desai SP. Morphometric analysis of septal aperture in humerus. Int J Med Res Health Sci 2014;3:269-72.
28. Krishnamurthy A, Yelicharla AR, Takkalapalli A, Munishamappa V, Bovinndala B, Chandramohan M. Supratrochlear foramen of humerus: A morphometric study. Int J Biol Med Res 2011;2:829-31.
29. Erdogmus S. The importance of the supratrochlear foramen of the humerus in humans: An anatomical study. Med Sci Monit 2014;20:2643-50.
30. Naqshi BF, Shah AB, Gupta S. Olecranon fossa in humeri of North Indian population of Jammu- a morphometric study. Int J Med Sci Public Health 2018;6:250-3.
31. Mallikarjun M, Reveendra Patil GT, Solomon Krupanidhi U. Morphological study of supratrochlear foramen in adult dry humerus bones. Int J Anat Res 2020;8:7604-8.
32. Mays S. Septal aperture of the humerus in a mediaeval human skeletal population. Am J Phys Anthropol 2008;136:432-40.
33. Li J, Mao Q, Li W, Li X. An anatomical study of the supratrochlear foramen of the Jining population. Turk J Med Sci 2015;45:1369-73.
34. Houshian S, Mehdi B, Larsen MS. The epidemiology of elbow fracture in children: Analysis of 355 fractures, with special reference to supracondylar humerus fractures. J Orthop Sci 2001;6:312-5.
35. Tiwari V, Ali FB, Patra A, Dhiman A, Sharma SK. The conundrum of olecranon aperture and its relation to the distal end of the humerus in a modern Indian population: An anatomical and surgical perspective. Morphologie 2023;107:199-206.

Original Article

The Prevalence of Gantzer's Muscle in the Israeli Population: A Cadaver-based Anatomical Study

Bahaa M. Medlej[1,2], Tomer Keidan[3,4], Amir Oron[3,4]

[1]Department of Anatomy and Anthropology, Sackler Faculty of Medicine, Tel Aviv University, Tel Aviv, [3]Department of Orthopedic Surgery, Kaplan Medical Center, Rehovot, Israel affiliated to the Faculty of Medicine, The Hebrew University, Jerusalem, Israel, [2]Department of Anatomy, Arab American University, Ramallah, Palestine

Abstract

Introduction: The Gantzer muscle (GM) is an anatomical variant of the human upper extremity. Its two bellies – the accessory muscle of the flexor digitorum profundus (AFDP) and the accessory flexor policis longus (AFPL) have been described in several populations. Despite the GM's commonality, little consideration has been given to its origin, possible function, or clinical significance. Our study aimed to assess the prevalence of the GM in the local population of Israel, to characterize it demographically, and to define side preference if present. **Materials and Methods:** We examined cadavers of individuals of Israeli nationality (n = 88, n = 49 females; n = 39 males; all >60 years old). Our study was performed at the Department of Anatomy and Anthropology, Sackler School of Medicine, Tel Aviv University. **Results:** Gantzer's muscle (either AFDP or AFPL or both) was present in 61 out of 88 cadavers (69.3%). Prevalence of the AFPL was 60.2%, found in 53 out of 88 cadavers dissected. In 34.1% of cadavers, the muscle was present bilaterally. Among the unilateral cases (n = 23), prevalence was the same for the right and left sides (χ^2 =1.087, df = 1, P = 0.297). **Conclusions:** Our findings demonstrate a high prevalence of Gantzer's muscle in the Israeli population. We found at least one of the accessory muscles in 69.3% of cadavers assessed. The course of the GM most commonly found was as an accessory muscle inserted into the flexor pollicis longus (FPL) tendon; thus, we believe the GM may contribute to the precision of function of the thumb as a fine tuner to FPL muscle function.

Keywords: *Accessory muscles, evolution of the human forearm, flexor digitorum profundus, flexor pollicis longus, Gantzer's muscles, human evolution, tendinous connection, variation*

Introduction

The Gantzer muscle (GM) was first mentioned in 1813 by Gantzer *et al.*[10] (Hacettepe Üniversitesi. Anatomi Anabilim Dali. and MATHEW, 2014) and later described as two separate accessory muscles connecting the superficial layer of the anterior compartment to the deep layer in the human forearm (*Anatomy Atlases: Illustrated Encyclopedia of Human Anatomic Variation: Opus I: Muscular System: Alphabetical Listing of Muscles*, no date).[2] The muscle was described in accordance with its course, either as the accessory muscle of the flexor digitorum profundus (AFDP) or the accessory muscle of the flexor pollicis longus (AFPL) (Jones *et al.*, 1997a).[11] Modern medical literature refers to the GM mostly as a syndrome-promoting culprit in medical cases, as this muscle has been suggested as a possible cause for anterior interosseous nerve (AIN) syndrome[6,26,31] (Tabib W1, Aboufarah F, 2001; Degreef and Smet, 2004; and Zdilla *et al.*, 2019). Little consideration has been given to its role in human manual activities or to its possible role as a donor in cases of upper extremity injuries or neuropathies.

In numerous anatomical studies performed in the past several decades, at least one of the bellies of the GM was found in 33.3% to 89.3%[4,15,22] (Mahakkanukrauh *et al.*, 2004; Caetano *et al.*, 2015; and Roy *et al.*, 2015). Prevalence in males and females was found to be similar (Jones *et al.*, 1997a), while a prevalence nearing 50% has been demonstrated in several diverse cohorts including Caucasian, Korean, Thai, and Ashkenazi Jews (AL-QATTAN, 1996; SHIRALI *et al.*, 1998; Potu *et al.*, 2007; and Caetano *et al.*, 2015).[1,3,4,21]

The two distinct muscle bellies of the GM originate from the coronoid process of the Ulna (Malar, 2012), from the medial humeral epicondyle, or from the flexor digitorum superficialis (FDS) muscle fibers (Chakravarthi, 2013).[5] The GM

How to cite this article: Medlej BM, Keidan T, Oron A. The prevalence of Gantzer's muscle in the Israeli population: A cadaver-based anatomical study. J Anat Soc India 2025;74:159-63.

Article Info

Received: 06 October 2021
Revised: 18 January 2023
Accepted: 23 March 2023
Available online: 30 June 2025

Address for correspondence:
Dr. Amir Oron,
Chief of Hand Surgery and Microsurgery, Department of Orthopedic Surgery, Kaplan Medical Center, Rehovot, Israel.
E-mail: amiroronmd@gmail.com

Access this article online

Website: https://journals.lww.com/joai
DOI: 10.4103/jasi.jasi_170_21
Quick Response Code:

insertion is either at the flexor pollicis longus (FPL) tendon or one of the flexor digitorum profundus (FDP) tendons (Chakravarthi, 2013).[5] The GM is usually found in close proximity to the median nerve and its main branch, the AIN[1,12,15,17,20,23] (Mangini, 1960; AL-QATTAN, 1996; Jones *et al.*, 1997a; SHIRALI *et al.*, 1998; Oh, Chung and Koh, 2000; Mahakkanukrauh *et al.*, 2004; and Pai *et al.*, 2008) which in the majority of cases serves as the nerve supply for this muscle (DELLON and MACKINNON, 1987).[7] Occasionally, the GM receives its innervation directly from the trunk of the median nerve[11-13] (Jones *et al.*, 1997b, 1997a; Chakravarthi, 2013; Lasch, Nazer, and Bartholdy, 2018), though dual innervation from both the AIN and the median nerve has been described (Jones *et al.*, 1997a).[11] The GM blood supply comes mainly from the ulnar artery, nourishing both heads while blood supply from the recurrent ulnar artery, median artery, and anterior interosseous artery are less frequent (Jones *et al.*, 1997b).[12]

The study of muscle variation is of clinical importance as it may assist physicians in reaching accurate diagnosis and treatment of various upper limb neuropathies (Chakravarthi, 2013).[5] It may also provide opportunities for nerve and tendon transfer and grafting: a recent study performed at our institution found that the average distance of the GM nerve origin from the ulnar nerve was small enough to allow use of the GM nerve as a donor in cases of neuropathy or trauma to the upper extremity, a process described previously using the terminal AIN to the pronator quadratus (Dunn *et al.*, 2019).[9] Nevertheless, the GM is currently found mainly incidentally during procedures[3] (Andring, Kennedy, and Iannuzzi, 2018), imaging studies[14] (López Milena *et al.*, 2001), or routine anatomical dissections of the upper extremity[11,18,28] (Jones *et al.*, 1997a; Thejodhar, Potu and Vasavi, 2008; and Naveen *et al.*, 2011). Despite its seeming prevalence, it has not been systematically reported or described.

Our study aims to assess the prevalence of GM in the local population of Israel, to characterize it demographically, and to seek for side preference.

Materials and Methods

Our sample included cadavers of elderly Israeli individuals (n = 88, n = 49 females; n = 39 males; all >60 years old) from the Department of Anatomy and Anthropology, Sackler School of Medicine, Tel Aviv University. The right and left forearms of each cadaver were carefully dissected to detect any accessory muscle of the flexor pollicis longus (AFPL) and accessory muscle of the flexor digitorum profundus (AFDP) muscles [Figure 1a and b].

First, the skin was flayed to reveal the anterior compartment of the forearm. Next, the superficial muscles were cut and reflected, exposing the deep compartment. Finally, the AFPL and AFDP were carefully separated from the FPL and FDP, respectively, to expose the origin, insertion, and location of each muscle [Figure 2].

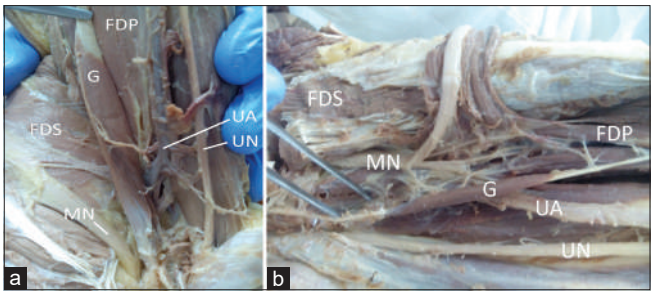

Figure 1: (a) Flexor pollicis longus accessory head variant: (b) flexor digitorum profundus accessory head variant: G: Gantzer's muscle, FDP: Flexor digitorum profundus, FDS: Flexor digitorum superficialis, MN: Median nerve, UA: Ulnar artery, UN: Ulnar nerve

Statistical analysis

Prevalence of GM was calculated using the Chi-square test, using the SPSS 220.0 software (IBM Inc. Armonk, New York, USA). Associations between categorical data including a differentiation as to sex were conducted using the Chi-square test and Fisher's exact test.

Results

Prevalence of Gantzer's muscles

One of the two bellies of the GM was present in 61 out of 88 cadavers (69.3%). The prevalence of AFPL was the highest (60.2%), found in 53 out of 88 cadavers dissected [Table 1]. In 34.1% of cadavers, the muscle was present bilaterally. Among the unilateral cases (n = 23), the prevalence was the same for right and left (χ^2 = 1.087, df = 1, P = 0.297, Table 1].

The prevalence of the AFDP was lower (20.5%) as the muscle was found in only 18 cadavers [Table 1]. Fisher's exact test for side distribution (n = 11) was not significant [χ^2 = 2.273, df = 1, P = 0.132, Table 1].

In 10 cases (11.4%), both AFPL and AFDP heads were found on at least one side, yet there was no significant association between the presence of the two muscles (χ^2 = 0.206, P = 0.650).

Demographics: sex distribution

The presence of at least one AFPL muscle was similar in males and in females [61.5% and 59.2%, respectively, χ^2 = 0.050, P = 0.823, Table 2]. However, there was a significant association between the right–left distribution of the muscle and sex [Fisher's exact test, χ^2 =5.891, P = 0.049, Figure 3]. There were significantly more male cadavers, in which the muscle was present in the right forearm (41.7% vs. 13.8% in females), whereas in females, the muscle was more common on the left side (24.1% vs. 8.3% in males).

The presence of at least one AFDP muscle was similar in males and in females [17.9% and 22.4%, respectively,

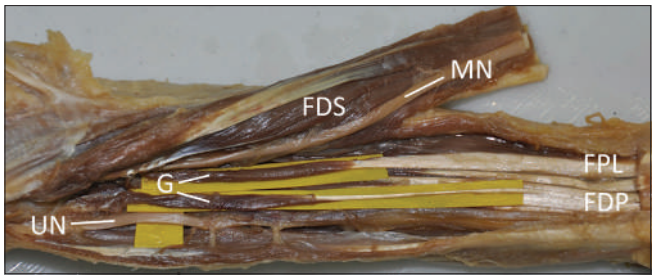

Figure 2: Both flexor pollicis longus and flexor digitorum profundus accessory heads combined: GM: Gantzer muscle, FDP: Flexor digitorum profundus, FDS: Flexor digitorum superficialis, FPL: Flexor pollicis longus, MN: Median nerve, UN: Ulnar nerve

χ^2 = 0.270, P = 0.603, Table 3]. Notice that among the unilateral cases and similarly to the distribution of the ADPL, the frequency of the AFDP on the left side was greater in females (12.2% vs. 5.1% in males). However, our sample was too small to determine if this finding was significant.

Topographic anatomy

In all cases, AFPL originated from the common flexor tendon and medial epicondyle and inserted into the distal third of the FPL muscle. The AFDP had the same origin as the AFPL and was inserted into the FDP tendon to the second or third digits. Topographically, the AFPL was located between the FDP and the FDS funneled obliquely from the posterior third of the flexor policies longus to the medial epicondyle. In the proximal third of the forearm, the median nerve was found between the FDS and AFPL.

Discussion

The prevalence of Gantzer's muscles

Numerous studies have found a high prevalence of GMs in various populations[11,20,30] (Jones *et al.*, 1997a; Pai *et al.*, 2008; and Yang *et al.*, 2017) [Table 4]. Similarly, there are many case reports where the muscle was found incidentally, indicating that it is commonly present (Jones, Abrahams, and Sañudo, 1997; López Milena *et al.*, 2001; Potu *et al.*, 2007; Malar, 2012; and Lasch, Nazer, and Bartholdy, 2018).[12,13,14,16,19,21]

Our data are represented as the prevalence of the GM in the Israeli population per individual cadaver rather than the number of forearms dissected. Our main interest was to follow the evolution of the forearm muscles and their function as it was inferred from the GM shape and topography. We used the data reported by previous authors to recalculate the total frequency of GM appearances and obtain the prevalence per individual cadaver [Table 4]. We stipulate that a better understanding of the prevalence and morphology of the GM will prove useful for clinicians wishing to utilize it for grafting or physicians treating patients with AIN syndrome.

Our findings demonstrate a high prevalence of Gantzer's muscles in the Israeli population. We found at least one of the accessory muscles in 69.3% of 88 cadavers. In comparison to the literature, Pai *et al.* (Pai *et al.*, 2008) [20] found that 66.6% of their 63 cadavers presented

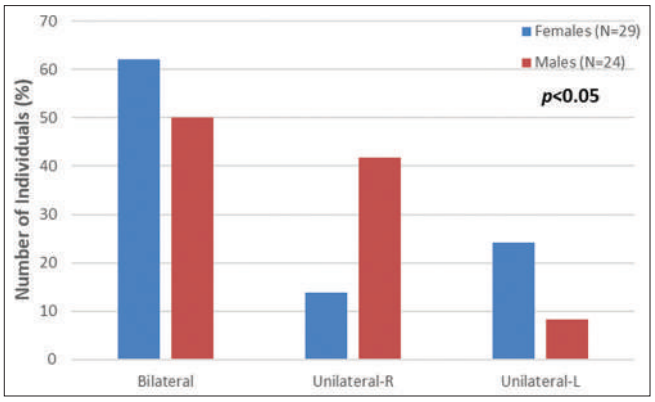

Figure 3: Distribution of the accessory flexor policis longus muscle in males and females by side

Table 1: Prevalence of the accessory flexor pollicis longus and the accessory flexor digitorum profundus muscles

Findings	Frequency (n=88)	Prevalence (%)
AFPL		
Bilateral	30	34.1
Unilateral		
Right	14	15.9
Left	9	10.2
Total	53	60.2
AFDP		
Bilateral	7	8.0
Unilateral		
Right	3	3.4
Left	8	9.1
Total	18	20.5

AFPL: Accessory muscle of the flexor pollicis longus, AFDP: Accessory muscle of the flexor digitorum profundus

Table 2: Prevalence of accessory flexor pollicis longus muscle by sex

Presence	Females (n=49), n (%)	Males (n=39), n (%)
Bilateral	18 (36.7)	12 (30.8)
Unilateral-R	4 (8.2)	10 (25.6)
Unilateral-L	7 (14.3)	2 (5.1)
Yes (total)	29 (59.2)	24 (61.5)
No	20 (40.8)	15 (38.5)

Table 3: Prevalence of accessory flexor digitorum profundus muscle by sex

Presence	Females (n=49), n (%)	Males (n=39)
Bilateral	4 (8.2)	3 (7.7)
Unilateral-R	1 (2.0)	2 (5.1)
Unilateral-L	6 (12.2)	2 (5.1)
Yes (total)	11 (22.4)	7 (17.9)
No	38 (77.6)	32 (82.1)

Table 4: Prevalence of Gantzer muscle s by ethnicity

Author	Ethnical group	Study population and sex (*n*)	Percentage prevalence (*n/N* cadavers)	Side distribution
Yang *et al*., 2017	Korean	37 cadavers (73 upper limbs)	81.0 (30/37)	Bilateral: 5 Unilateral right: 14 unilateral left: 11
Current study	Caucasian (Israeli-Jewish)	88 cadavers 176 forearms	69.3 (61/88)	Bilateral Unilateral right Unilateral left
Pai *et al*., 2008	South India	63 cadavers 126 upper limbs Not specified	66.6	Not specified
Uyaroglu *et al*., 2006 (Uyaroglu, Kayalioglu and Erturk, 2006)[29]	Turkish	26 cadavers 52 upper limbs Not specified	65.3 (17/26)	Bilateral: 10 Unilateral: 7
Johns *et al*., 1997	Not specified	40 cadavers 22 males 18 females	60.0 (24/40)	Bilateral: 14 Unilateral right: 6 Unilateral left: 2
Dellon and Makinnon, 1987	Not specified	31 cadavers	45.1 (14/31)	Not specified
Tamang *et al*., 2013	Not specified	30 cadavers 20 males 10 females	43.3 (13/30)	Bilateral: 2 Unilateral right: 7 Unilateral left: 4
Chakravarthi KK, 2013	Not specified	54 upper limbs	72.0	Not specified

with at least one AFPL or AFDP. Jones *et al*.[11] (Jones *et al.*, 1997a) found a frequency of GMs in 60% of their sample. Moreover, Yang *et al*.[30] (Yang *et al.*, 2017) reported a frequency of 47.95% (35 out of 73) of upper limbs dissected and detailed that five were bilateral and 25 unilateral; therefore, their true prevalence was 81.0% when cadaver prevalence is assessed.

Tamang *et al*.[27] (Tamang *et al.*, 2013) found a lower prevalence of GM instances (43.3%). Among 30 dissected cadavers, in their study, 15 instances of AFPL muscle were found. In two, the muscle appeared bilaterally (6.67%); in seven cadavers, it was present only in the left forearm (23.3%), and in four cadavers, it was present on the right side (13.3%). Similar findings were presented by Dellon and Mackinnon (DELLON and MACKINNON, 1987), who found GMs in 14 out of 31 cadavers dissected (45.1%).

Chakravarthi *et al*.[5] (Chakravarthi, 2013) found the muscle in 72.2% of 54 upper limbs dissected. Twenty-three of the GMs were AFPL (42.6%) and 16 were AFDP (29.6%). This study did not mention on which side the GMs occurred.

Jones *et al*.[11] (Jones *et al.*, 1997a) were among the few who published data regarding the distribution of the GMs among males and females, as well as providing data on the side at which it was found. Our study found similar results in terms of side distribution for each sex. Our study did, however, demonstrate differences between sexes in right–left distribution among the unilateral cases.

The appearance of both AFPL and AFDP simultaneously is sparse. We found that only 10% of forearms have both heads, a number slightly higher than the 4.76% described by Pai *et al*.[20] (Pai *et al.*, 2008). The fact that AFDP frequency is much lower than AFPL may indicate a different contribution to hand movement.

Comparative anatomy and evolutionary aspects

Like the findings of Jones, Pai, and others, our study demonstrates that the AFPL is the more frequent among the two bellies of the GM. While the full function of the GM cannot be concluded based on an anatomical study alone, we stipulate that the muscle may contribute to the precision of function of the thumb as a fine tuner to the FPL muscle. This assumption arises due to the GMs course, inserting into the FPL tendon in most cases. The FPL itself is a distinct muscle of the genus *Homo*, which is absent in all other hominoids[25] (Straus, 1942) and is found only in hylobatids. Among non-hominoid primates excluding hylobatids, the FPL is a tendon derived from the FDP and attached to the thumb but not a distinct muscle. Nevertheless, it flexes the thumb in the same manner as the FPL in modern humans[8] (Diogo, Richmond, and Wood, 2012). The GM's high prevalence indicates that its presence is not an anomaly but a distinct unit with unique function.

It has been proposed that the evolutionary advantage of a separate belly in the muscles of the thumb was the dexterity requirements of the Acheulian technology[8,24] (Shrewsbury *et al.*, 2003; Diogo, Richmond, and Wood, 2012). If so, the presence of the accessory muscles of the FPL and FDP might be an autapomorphic trait providing said advantages.

Future research on the exact function of the muscle is needed, as well as further investigation of the right-sided to left-sided distribution among males and females.

Financial support and sponsorship

Nil.

Conflicts of interest

There are no conflicts of interest.

References

1. Al-Qattan MM. Gantzer's muscle. An anatomical study of the accessory head of the flexor pollicis longus muscle. J Hand Surg Br 1996;21:269-70.
2. Bergman RA. Anatomy Atlases: Illustrated Encyclopedia of Human Anatomic Variation: Opus I: Muscular System: Alphabetical Listing of Muscles; 2016.
3. Andring N, Kennedy SA, Iannuzzi NP. Anomalous forearm muscles and their clinical relevance. J Hand Surg Am 2018;43:455-63.
4. Caetano EB, Sabongi JJ, Vieira LÂ, Caetano MF, Moraes DV. Gantzer muscle. An anatomical study. Acta Ortop Bras 2015;23:72-5.
5. Chakravarthi K. Unusual unilateral multiple muscular variations of back of thigh. Ann Med Health Sci Res 2013;3 Suppl 1:S1-2.
6. Degreef I, De Smet L. Anterior interosseous nerve paralysis due to gantzer's muscle. Acta Orthop Belg 2004;70:482-4.
7. Dellon AL, Mackinnon SE. Musculoaponeurotic variations along the course of the median nerve in the proximal forearm. J Hand Surg Br 1987;12:359-63.
8. Diogo R, Richmond BG, Wood B. Evolution and homologies of primate and modern human hand and forearm muscles, with notes on thumb movements and tool use. J Hum Evol 2012;63:64-78.
9. Dunn JC, Gonzalez GA, Fernandez I, Orr JD, Polfer EM, Nesti LJ. Supercharge end-to-side nerve transfer: Systematic review. Hand (N Y) 2021;16:151-6. [doi: 10.1177/1558944719836213].
10. Anabilim Dali RA, Mathew AJ. Hacettepe University, Faculty of Medicine, Department of Anatomy. Int J Anat Var 2014:45-48. Available from: https://www.pulsus.com/scholarly-articles/gantzer-of-flexor-pollicis-longus--a-culprit-in-kilohnevin-syndrome.html.
11. Jones M, Abrahams PH, Sañudo JR, Campillo M. Incidence and morphology of accessory heads of flexor pollicis longus and flexor digitorum profundus (gantzer's muscles). J Anat 1997;191:451-5.
12. Jones M, Abrahams PH, Sañudo JR. Case report: Accessory head of the deep forearm flexors. J Anat 1997;191:313-4.
13. Lasch E, Nazer M, Bartholdy L. Bilateral anatomical variation in the formation of Trunks of the brachial plexus – A case report. J Morphol Sci 2018;35:9-13.
14. López Milena G, Ruiz Santiago F, Chamorro Santos C, Cañadillas Barea L. Forearm soft tissue mass caused by an accessory muscle. Eur Radiol 2001;11:1487-9.
15. Mahakkanukrauh P, Surin P, Ongkana N, Sethadavit M, Vaidhayakarn P. Prevalence of accessory head of flexor pollicis longus muscle and its relation to anterior interosseous nerve in Thai population. Clin Anat 2004;17:631-5.
16. Malar D. Bilateral variation of forearm flexor muscles – A case report and clinical significance. Natl J Clin Anat 2012;1:40-3.
17. Mangini U. Flexor pollicis longus muscle. J Bone Joint Surg 1960;42:467-559.
18. Naveen NS, Murlimanju BV, Kumar V, Pulakunta T, Jeeyar H. Thanatophoric dysplasia: A rare entity. Oman Med J 2011;26:196-7.
19. Oh CS, Chung IH, Koh KS. Anatomical study of the accessory head of the flexor pollicis longus and the anterior interosseous nerve in Asians. Clin Anat 2000;13:434-8.
20. Pai MM, Nayak SR, Krishnamurthy A, Vadgaonkar R, Prabhu LV, Ranade AV, *et al.* The accessory heads of flexor pollicis longus and flexor digitorum profundus: Incidence and morphology. Clin Anat 2008;21:252-8.
21. Potu BK, Gorantla VR, Pulakunta T, Rao MS, Mamatha T, Vollalla VR, *et al.* Accessory head of flexor pollicis longus muscle and its significance in anterior interosseous nerve syndrome: Case report and review. Int J Morphol 2007;25:911-4. [doi: 10.4067/s0717-95022007000400037].
22. Roy J, Henry BM, Pękala PA, Vikse J, Ramakrishnan PK, Walocha JA, *et al.* The prevalence and anatomical characteristics of the accessory head of the flexor pollicis longus muscle: A meta-analysis. PeerJ 2015;3:e1255.
23. Shirali S, Hanson M, Branovacki G, Gonzalez M. The flexor pollicis longus and its relation to the anterior and posterior interosseous nerves. J Hand Surg Br 1998;23:170-2.
24. Shrewsbury MM, Marzke MW, Linscheid RL, Reece SP. Comparative morphology of the pollical distal phalanx. Am J Phys Anthropol 2003;121:30-47.
25. Straus WL. Rudimentary Digits in Primates. Q Rev Biol 1942;17:228-43.
26. Tabib W, Aboufarah F, Asselineau A. Compression of the anterior interosseous nerve by gantzer's muscle. Chir Main 2001;20:241-6.
27. Tamang BK, Sinha P, Sarda RK, Shilal P, Murlimanju BV. Incidence and morphology of accessory head of flexor pollicis longus muscle – An anatomical study. J Evol Med Dent Sci 2013;2:6800-7. Available from: https://go.gale.com/ps/i.do?p=HRCA&sw=w&issn=22784748&v=2.1&it=r&id=GALE%7CA362965748&sid=googleScholar&linkaccess=fulltext. [Last accessed on 2020 Jun 20].
28. Thejodhar P, Potu BK, Vasavi RG. Unusual palmaris longus muscle. Indian J Plast Surg 2008;41:95-6.
29. Uyaroglu FG, Kayalioglu G, Erturk M. Incidence and morphology of the accessory head of the flexor pollicis longus muscle (gantzer`s muscle) in a Turkish population. Neurosciences (Riyadh) 2006;11:171-4.
30. Yang K, Jung SJ, Lee H, Choi IJ, Lee JH. Topographical relations between the gantzer's muscle and neurovascular structures. Surg Radiol Anat 2017;39:843-8.
31. Zdilla MJ, Pacurari P, Celuck TJ, Andrews RC, Lambert HW. A Gantzer muscle arising from the brachialis and flexor digitorum superficialis: Embryological considerations and implications for median nerve entrapment. Anat Sci Int 2019;94:150-3.

Original Article

Comparative Morphology of Papillary Muscles of the Right and Left Atrioventricular Valvular Apparatus of the Human Heart

Adya Priyadarshini, Kaweri Dande, Anita Rani, Jyoti Chopra, Anoop Kumar Verma, Navneet Kumar

Department of Anatomy, King George's Medical University, Lucknow, Uttar Pradesh, India

Abstract

Background: The papillary muscles (PMs) have a significant role in ventricular overextension. The knowledge of variations in the number, shape, and grouping pattern of PM of the right and the left ventricle is useful for the surgeons in dealing with reparative procedures, PM dysfunction, and use of valve homograft for the valve replacement surgeries. Hence, familiarity with the variability of PMs is crucial in guiding surgical interventions and improving the success of various cardiac procedures. **Aims and Objective:** To study the morphology of PMs of the right and left atrioventricular valvular apparatus of the human heart. **Subjects and Methods:** The study was carried out on 100 formalin-fixed hearts of both genders of all ages. PMs were observed on the basis of number, shape, and grouping. **Results:** In the current review, the frequency of PM was found to be between 2 and 4 in both the right and left atrioventricular valves. Three types of shapes of PM were observed, i.e. conical, pyramidal, and broad. Conical-shaped PMs were more frequently present on the left side than on the right side. PMs were also divided on the basis of their grouping pattern. They showed single-, two-, and multiple-head grouping patterns. **Conclusion:** No two-valve complexes have the same architectural arrangement, as each individual's heart seems to be distinct. This highlights the need for conducting future large-scale research across the world to derive a better understanding of morphological variations. This will enable the cardiothoracic surgeons to conduct the surgical procedures according to the unique PM pattern of the individual patient.

Keywords: *Cadaver, heart, morphology, papillary muscle*

Introduction

Valvular heart diseases are quite common and can lead to an increased risk of morbidity and mortality. The atrioventricular valve complex consists of an orifice and its annulus, leaflets, chordae tendineae, and papillary muscles (PMs).[1] Mechanical attributes of atrioventricular valve framework are largely determined by the link between PM and the valve that transmits contractions of the muscle to the valve leaflet. Synchronous contraction of PMs helps prevent atrioventricular leaflet prolapse. Loss of contractility of PM can be caused by its fibrosis, necrosis, or hypoxia.[2] Therefore, valve prolapse can be the result of both PM rupture and its dysfunction.

It is well evident that the right and left compartments of the heart exhibit different hemodynamic properties due to different functional demands. The shape of the PMs has a significant impact on the passage of blood flow through the heart. The conical shape of PMs helps facilitate smooth cardiovascular physiology by minimizing obstruction to blood flow. The chances of ventricular outflow tract obstruction are higher in hypertrophy of fan-shaped PMs and muscles with a broad apex. Increase in the size and in the number of muscles may contribute to the left ventricular outflow tract obstruction, especially when it is accompanied with progression of hypertrophic cardiomyopathy.[3]

As the rate of valvular heart illnesses are rising, aside from translation of radiological pictures, data about the physical varieties of PMs will empower a specialist to reestablish the actual trustworthiness of the atrioventricular valve complex by utilizing different methods like realignment, repositioning, reproduction, and resectioning.[4] Therefore, it is crucial that we know the variations in the normal architecture of PMs of the heart.

Subjects and Methods

After obtaining clearance from the ethical review board of University via Ref. code:

How to cite this article: Priyadarshini A, Dande K, Rani A, Chopra J, Verma AK, Kumar N. Comparative morphology of papillary muscles of the right and left atrioventricular valvular apparatus of the human heart. J Anat Soc India 2025;74:164-8.

Article Info

Received: 15 June 2024
Accepted: 23 May 2025
Available online: 30 June 2025

Address for correspondence:
Dr. Adya Priyadarshini, King George's Medical University, Lucknow, Uttar Pradesh, India.
E-mail: priyadarshini.adya26@gmail.com

Access this article online

Website: https://journals.lww.com/joai

DOI: 10.4103/jasi.jasi_87_24

Quick Response Code:

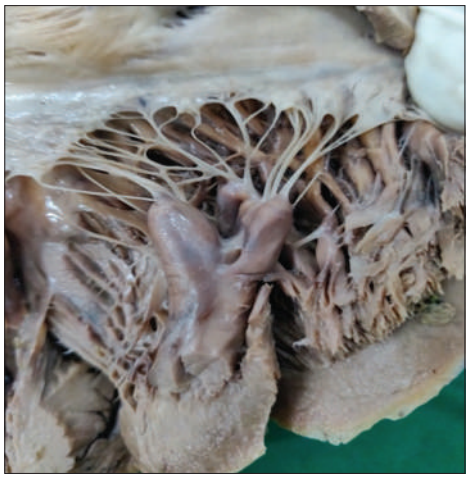

Figure 1: Broad and pyramidal papillary muscle

Figure 2: Conical papillary muscle

Figure 3: Multiple head papillary muscle

Figure 4: Single- and two-head papillary muscle

97th ECM IIB-Thesis/P46 from the ethical review board of institution, 100 human hearts of adult age group, of either sex were procured within 24 h after death, from the Anatomy and Forensic Medicine Department. Hearts with disrupted atrioventricular valves or with abnormal morphology like prolapse or dilatation were discarded. Hearts were either dissected (n = 20) out from cadavers by following the standard dissection steps[5] or retrieved (n = 80) after autopsy. Each heart was numbered and kept in 10% formaldehyde solution for minimum 24 h before observation.

To visualize the PMs of the right atrioventricular valve, the incision was started from the level of entry of the superior vena cava into the right atrium till the level of entry of inferior vena cava into the right atrium.

Along the inferior border of the heart, the second incision was given to the inferior margin of the anterior interventricular groove along the acute margin of the heart. Right to the anterior interventricular groove, the third incision was made. The aall was retracted carefully and the interior was washed under tap water thoroughly to remove the clots and to visualize the PMs [Figures 1-4].[6]

For the left atrioventricular valvular apparatus, another incision was made on the left margin of the heart, which was extended till the apex of the heart to open the left ventricle. The number, shape, and grouping pattern of PMs were studied.

The following observations were made regarding PM:

- Number of PMs: Counted with reference to their attachment to the base
- Shape of PMs
  - Conical base and apex are almost equal in measurement
  - Pyramidal base is comparatively broader than the apex
  - Broad base of the PM is narrow, but apex is quite broad
- Grouping of PM
  - Classical PM consisting of single head
  - Two-head PMs are with single common base but two heads

- Multiple-head PMs are with more than two heads.

Results

Frequency of papillary muscles

Number of well-formed muscles supporting chordae tendinae were not showing any fixed distribution for each AV valve complex. These muscles ranged from 2 to 4 for both AV apparatuses. On the right side, 38% of hearts had two PMs, whereas 9% of hearts exhibited four PMs. Classical description of three PMs of the right side was found only in 53% of samples. In the left side, only 28% of samples exhibited two PMs. In 48% of cases, three PMs were present, and in 24% of cases, four PMs were present.

Shape of papillary muscles

PM showed a few varieties in its shape. It may be conical, pyramidal, or broad shaped [Figure 5]. Each apparatus showed differences in the frequency of PMs according to their shapes. Conical-shaped PMs were observed more frequently in the left side AV apparatus (1.72 ± 0.92) as compared to the right (0.82 ± 0.59). These values were statistically significant too ($P \leq 0.001$). For other two shapes, i.e. pyramidal and broad type, though the mean number was slightly higher on the right side, these values did not show statistically significant association (0.82 ± 0.69 vs. 0.62 ± 0.76; 1.07 ± 0.78 vs. 0.62 ± 0.78).

Grouping of papillary muscles

PMs can additionally be grouped based on the number of their heads. It can be single (classical), double, or multiple [Figure 6]. In the present study, single-headed PMs were significantly higher in the number in the left side as compared to the right. Double- and multiheaded PMs were slightly higher in number on the right side, but we did not find these values as statistically significant [Table 1].

Discussion

The significant result of this study demonstrates that no two PMs out of 100 hearts had the equivalent morphological and morphometric highlights.

Frequency of papillary muscles

It has been cited in the literature that normally, there are 2–3 PMs present in atrioventricular valve. Extended number of papillary strong construction could incite overflowing part obstruction. It is additionally seen to be related with regurgitation. Thus, information on varieties in number of PM might assist us with figuring out the etiology in pathological states.[7]

In Left Atrioventricular Valve (LAVV)

Gray's anatomy[7] stated that there are only two PMs in the left ventricle: one large anterior PM and one small posterior PM. These PMs may vary in length and breadth and may be bifid. Ho's study on the anatomy of the mitral valve mentioned that there are usually groups of PMs arranged fairly close together.[8] Oosthoek *et al*. noted the presence of a third PM,[9] whereas Madu and D'Cruz detected a third accessory PM closer to the apex in uncommon cases.[10] Victor and Nayak found that intragroup interconnections are more frequent than intergroup interconnections, with the later limited to the exchange of a few strands at the level of the chordae tendineae.[4]

In Right Atrioventricular Valve (RAVV)

Harsha and Chandrashekhar found that the number of PMs was present with a frequency of 2–10. Maximum numbers of PMs were 10 seen in only 1% heart and minimum numbers of PMs were 2 seen in 3.1%. Anterior PMs were present in all (100%) hearts. Maximum numbers of muscles observed were three seen in 6.3% and minimum number was 1 seen in 68.8% hearts. Two PMs were seen in the remaining 25% of hearts.

Posterior PMs were seen in 98.95% of hearts. Seven PMs were observed in only 1% of hearts and one PM was seen in 28.1% of hearts.[1]

Shape of papillary muscles

The shape of the PM plays a very crucial role in blood flow mechanism. It has been seen that blood stream is better in atrioventricular valve in cases with tapered and pyramidal shape PM, while there may be an opportunity of deterrent if more number of broad-apexed PMs are available in

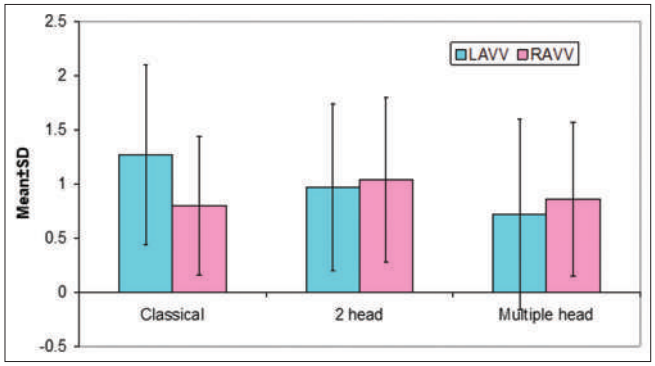

Figure 5: Comparison of number of papillary muscles between the right and left AV

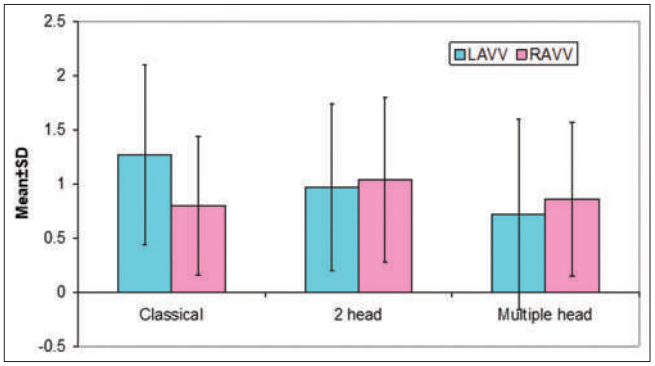

Figure 6: Comparison of papillary muscle between LAVV and RAVV according to grouping

Table 1: Distribution of papillary muscles of atrioventricular valves according to the number of heads

Grouping of PM on the basis of number of heads	Type of AV valve	Mean±SD	Minimum	Maximum	Student's *t*-test
Single	Left	1.27±0.83	0	4.00	*t*=4.506
	Right	0.80±0.64	0	3.00	*P*<0.001
Double	Left	0.97±0.77	0	2.00	*t*=0.645
	Right	1.04±0.76	0	3.00	*P*=0.520
Multiple	Left	0.72±0.88	0	3.00	*t*=1.240
	Right	0.86±0.71	0	2.00	*P*=0.216

AV: Atrioventricular valve, PM: Papillary muscles, SD: Standard deviation

AV valve.[4] As there is association of shape of PM with the normal functioning of the atrioventricular valve, it prompted us to study their morphology and morphometry.

In LAVV

According to Gunnal *et al*., four shapes of PMs were noted, i.e., conical, broad-apexed, pyramidal, and fan shaped. They found that the conical PM was found in 45.51% of cases, broad-apexed was found in 50.48% of cases, pyramidal was found in 26.73% of cases, and fan shaped was found in 12.93% of cases.[4]

In RAVV

According to Hosapatna *et al*., 13 out of 15 hearts had conical-shaped PM, whereas 2 hearts had flat-topped PM.[11]

Grouping of papillary muscles

In LAVV

Muraleedharan and Sailaja noted that group of PM varied from 2 to 4. They observed that two-group PMs were present in 73% of hearts, three-group PMs were present in 23% of hearts, whereas three-group PMs were present in 4% of hearts.[12]

According to Gunnal *et al*., classical PMs were found in 3.44%, 2 groups in 43.11%, 3 group in 31.90%, and 4 groups were found in 21.55% of hearts.[4]

In RAVV

According to Muraleedharan and Sailaja, two-group PMs were present in 16% of hearts and three-group PMs were present in 84% of hearts.[12]

According to Kumar *et al*., the anterior PMs presented 1 head in 27.78% and 2 heads in 25%, while posterior PMs presented 1 head in 27.78% and 2 heads in 25%. All the septal PMs presented with one head. Single anterior PM was found to be 97.22%, while posterior PM was found to be single in 72.28% and double in 27.78. Septal PM was found to be single in 25% of cases and absent in 38.89% of cases.[13]

Conclusion

Our study revealed significant differences in the morphology of papillary muscles[PM] between left atrioventricular valve [LAVV] and right atrioventricular valve[RAVV]. Notably, number of PM in LAVV was significantly higher compared to RAVV. Additionally, conical-shaped PM were more prevalent in LAVV, whereas pyramidal and broad-shaped PM were more common in RAVV, with a significant difference observed for broad-shaped PM. Furthermore, classical grouping of PM was observed in a significantly higher number of LAVV compared to RAVV. These findings highlight the distinct morphological features of PM in LAVV and RAVV.

Acknowledgment

I would like to express my heartfelt gratitude to all those who have contributed to the successful completion of this paper. I am deeply grateful to the Department of Anatomy and the Department of Forensic Medicine and Toxicology, KGMU, Lucknow, for granting me this opportunity. Additionally, I would like to thank my family for their constant support.

Financial support and sponsorship

The study was financially supported by the Department of Anatomy and Forensic Medicine and Toxicology, KGMU.

Conflicts of interest

There are no conflicts of interest.

References

1. Harsha BR, Chandrashekhar KT. Cadaveric study on anterior and posterior papillary muscles of tricuspid valve. Int J Anat Res 2015;3:865-8.
2. Aulakh KK, Saxena AK, Aneja PS, Bansal S. A morphometric study of the papillary muscles of the left ventricles of human cadaveric hearts in North-West population. J Evol Med Dent Sci 2016;5:7344-52.
3. Vadlamani PC, Awari PS. Disparity in morphology of papillary muscles of the mitral valve complex with surgical significance. Int J Anat Res 2020;8:7294-99.
4. Gunnal SA, Wabale RN, Farooqui MS. Morphological variations of papillary muscles in the mitral valve complex in human cadaveric hearts. Singapore Med J 2013;54:44-8.
5. Koshi R. Cunningham's Manual of Practical Anatomy Thorax an Abdomen. 16th ed. Oxford; 2017. p. 26, 57.
6. Udhayakumar S, Yasawardene SG. Aortic annular measurements in fresh post-mortem hearts; a study in Sri Lankans. Ceylon Med J 2015;60:148-51.
7. Shah P, Standring S. Gray's Anatomy- The Anatomical Basis of Clinical Practice. 39th ed. London: Elsevier-Churchill Livingstone; 2005. p. 1006-8.

8. Ho SY. Anatomy of the mitral valve. Heart 2002;88 Suppl 4:v5-10.
9. Oosthoek PW, Wenink AC, Wisse LJ, Gittenberger-de Groot AC. Development of the papillary muscles of the mitral valve: Morphogenetic background of parachute-like asymmetric mitral valves and other mitral valve anomalies. J Thorac Cardiovasc Surg 1998;116:36-46.
10. Madu EC, D'Cruz IA. The vital role of papillary muscles in mitral and ventricular function: Echocardiographic insights. Clin Cardiol 1997;20:93-8.
11. Hosapatna M, Souza AD, Das MA, Supriya, Ankolekar VH, D Souza AH. Morphology of papillary muscles in human adults: A cadaveric study. Ibnosina J Med Biomed Sci 2014;6:168-72.
12. Muraleedharan SS, Sailaja K. A comparative study of number and position of papillary muscles and clinical significance. Int J Anat Res 2018;6:6002-8.
13. Kumar S, Singh KA, Tamang BK. A morphological and morphometric study of right ventricular papillary muscles in North Indian region. Natl J Integr Res Med 2015;6:52-5.

Original Article

Nasofacial Anthropometry and Ethnic Identity in Meghalaya, Northeast India: A Cross-sectional Study

Pranoti Sinha, Suvamoy Chakraborty[1], Manu Coimbatore Balakrishnan[2], Sauradeep Das[2], Shruti Agarwall[2]

[1]Department of Anatomy, PA Sangma International Medical College and Hospital, USTM, Khanapara, [2]Department of Otorhinolaryngology, North Eastern Indira Gandhi Regional Institute of Health and Medical Sciences, Shillong, Meghalaya, India

Abstract

Introduction: Nasofacial anthropometry plays a vital role in identification, racial analysis, reconstructive surgeries, and respirator design. Craniofacial abnormalities are common in the Southeast Asian region. The state of Meghalaya is in Northeast India, with its population different from neighboring states and East Asia. With no previous studies among adults of Meghalaya population, this study was undertaken to analyze the nasofacial anthropometric features. **Materials and Methods:** This cross-sectional study conducted from 2022 to 2023 measured face length (FL), face width (FW), facial Index (FI), nasal length (NL), nasal width (NW), nasal index (NI), philtrum distance (PD), and commissural distance (CD). **Results:** One hundred and four adults from Meghalaya were selected. Khasi, Garo, and Jaintia communities constituted 51 (49%), 27 (26%), and 26 (25%), respectively. The mean ± standard deviation of age was 29.5 ± 8.4 years. The mean FI was 98.13 (hyperleptoprosopic). The common face types were hyperleptoprosopic (52%) and mesoprosopic (20%). Khasi showed leptoprosopic; Garo and Jaintia showed hyperleptoprosopic type. The mean NI was 72.2 (mesorrhine). The common nose types were leptorrhine (46%) and mesorrhine (44%). Khasi and Garo showed mesorrhine, whereas Jaintia showed leptorrhine type. A statistically significant difference was noted between Jaintia and Garo in FL and FI; Jaintia and Khasi in FL, FI, NL, NW, and PD; Garo and Khasi in FL, FI, NL, NW, and PD. **Conclusion:** We believe that our study provides a comprehensive assessment of nasofacial anthropometry in the ethnic adults of Meghalaya, filling a gap in existing research. The identified variations highlight the necessity of population-specific anthropometric standards, particularly in forensic analysis and surgical interventions aimed at preserving ethnic characteristics.

Keywords: *Anthropometry, forensic, nasofacial*

Introduction

Anthropometry is a noninvasive method of measuring the size, composition, and proportion of the human body. It is a universally applicable, inexpensive, and portable method.[1,2] Nasofacial anthropometry measurements are crucial for individual identification, analyzing gender and racial differences, forensic investigations, diagnosing congenital abnormalities, and guiding facial reconstructive surgeries.[3] It is also important when designing masks, respirators, etc.[2] The occurrence of craniofacial dysmorphisms such as hypertelorism, hypotelorism, and frontoethmoidal encephalomeningocele is common among the Southeast Asian population.[4] The state of Meghalaya is in Northeast India, adjacent to the other Southeast Asian countries. Northeast India includes eight different states. Although adjacent, the population differs from other states of Northeast India and neighboring East Asia due to the diverse population from different ethnic backgrounds.[5]

The nasofacial anthropometry differs from one region to another and from one population to another. This mandates for population-based anthropometric standards.[6] The nasofacial anthropometry in the ethnic adult population of Meghalaya was evaluated in this study. No antecedent anthropometry measurements have been performed on the Meghalaya population. The large proportion of the Northeast Indian population has Mongoloid characteristics and hence hyperleptoprosopic characteristics are anticipated.[7]

Aims and objective

Primary objective: To assess the nasofacial anthropometric characteristics of the adult population of Meghalaya.

How to cite this article: Sinha P, Chakraborty S, Balakrishnan MC, Das S, Agarwall S. Nasofacial anthropometry and ethnic identity in Meghalaya, northeast India: A cross-sectional study. J Anat Soc India 2025;74:169-75.

Article Info

Received: 18 June 2024
Accepted: 23 May 2025
Available online: 30 June 2025

Address for correspondence:
Dr. Manu Coimbatore Balakrishnan, Department of Otorhinolaryngology, North Eastern Indira Gandhi Regional Institute of Health and Medical Sciences, Shillong - 793 018, Meghalaya, India.
E-mail: cbalakrishnanmanu@gmail.com

Access this article online

Website: https://journals.lww.com/joai
DOI: 10.4103/jasi.jasi_90_24
Quick Response Code:

Materials and Methods

The institutional ethics committee approval was obtained. The cross-sectional study spanned over 12 months from 2022 to 2023.

Inclusion criteria

1. Healthy adults who belonged to the ethnic population of Meghalaya
2. People above or equal to 18 years of age belonging to both the genders.

Exclusion criteria

1. The Meghalaya nonnative population
2. Presence of any trauma to the face or head
3. Craniofacial anomalies which were grossly detectable
4. Facial or nasal plastic surgery
5. Presence of marriage outside the community in the previous three family generations.

On the basis of the mean nasal index (NI) of 76.27 with a standard deviation (SD) of 7.39 and a precision of 1.5 at a 95% confidence interval, the sample size (N) was calculated to be 93.[2]

$N = Z^{2\alpha} * SD^2/D^2$

where $Z^{2\alpha}$ at 95% confidence interval is 1.96, SD = 7.39, and D = 1.5

$N = 1.96^2 * 7.39^2/1.5^2 = 93$ individuals.

However, a total of 104 individuals were selected by convenient sampling. Spreading calipers were used to measure the anthropometry readings. Various landmarks were used for the face, nose, and orolabial region. Nasion, gnathion, zygions, subnasale, ala of the nose, and angles of the mouth were the landmarks used. The following dimensions were measured. Face length (FL), face width (FW), nasal length (NL), nasal width (NW), philtrum distance (PD), and commissural distance (CD) were measured in centimeters (cm).

FL was measured between nasion and gnathion.

FW was measured between the two zygions.

NL was measured between nasion and subnasal, and NW was measured between the lateral border of both the alas of the nose.

PD was measured from the columella base to the midline depression of the vermillion border.

CD was measured as the distance between the corners of the mouth.

The facial index (FI) was calculated (face length × 100/face width) and the NI was calculated (nasal width × 100/nasal length).

The face shape was classified by Bansiter into the following types: hypereuryprosopic type with FI of ≤79.9, euryprosopic type with FI of 80–84.9, mesoprosopic type with FI of 85–89.9, leptoprosopic type with FI of 90–94.9, and hyperleptoprosopic type with FI of ≥95.[8,9] They were described as very broad face, broad face, round face, long face, and very long face, respectively.

The nose shape was classified by Martin and Sallar into the following types: hyperleptorrhine type with NI of ≤54.9, leptorrhine with NI of 55–69.9, mesorrhine with NI of 70–84.9, platyrrhine with NI of 85–99.9, and hyperplatyrrhine of NI of ≥100.[10,11] They were described as the long narrow nose, moderately narrow nose, moderate size nose, moderately wide nose, and very wide nose, respectively.[11]

Statistical analysis

Data entry was done in Microsoft Excel 2016 (Microsoft Corp., Redmond, Washington, USA). Statistical analysis was performed using Statistical Package for the Social Sciences (SPSS) version 16 (IBM SPSS Statistics, Armonk, New York, USA) to note any differences in the variables. $p \leq 0.05$ in any of the statistical tests was considered statistically significant.

Independent variables: Gender, age, FL, FW, NL, NW, PD, and CD

Dependent variables: FI (prosopic index) and NI.

Results

In our study, 104 participants belonging to the native population of Meghalaya were included. They belonged to the following communities: Khasi, Garo, and Jaintia. They constituted 51 (49%), 27 (26%), and 26 (25%) individuals, respectively. Analysis of variance was performed for all three communities, and subgroup analysis was performed. In our total sample population, the mean ± SD age was 29.5 ± 8.4 years. The mean ± SD of ages was 31.7 ± 9.4 years, 27.2 ± 6.1 years, and 27.5 ± 7.5 years, respectively, for the Khasi, the Garo, and the Jaintia communities.

The different nasofacial anthropometric measurements of our study population are summarized in Table 1. Between the males and females in our study population, a statistically significant difference was noted in FL, FW, and NW. However, between the Khasi community males and females, a statistically significant difference was noted only in NW. Between the male and female population in the Garo and the Jaintia communities, no statistically significant difference was noted.

In our study population, the mean FI was 98.13, implying hyperleptoprosopic face. Except for the Khasi male and female population which showed leptoprosopic face type, the remaining male and female population of Garo and Jaintia showed hyperleptoprosopic face type.

In our study population, the mean NI was 72.2 implying mesorrhine nose. The male and female population of the

Table 1: Summary of Nasofacial anthropometry of the study population

Anthropometric variables (*n*=104)	Total sample population (*N*=104)				Khasi (*n*=51; 49%)			Garo (*n*=27; 26%)			Jaintia (*n*=26; 25%)		
	Total (*n*=104), mean±SD	Male (*n*=34), mean±SD	Female (*n*=70), mean±SD	*p*	Male (*n*=11), mean±SD	Female (*n*=40), mean±SD	*p*	Male (*n*=10), mean±SD	Female (*n*=17), mean±SD	*p*	Male (*n*=13), mean±SD	Female (*n*=13), mean±SD	*p*
FL (cm)	13.03±1.62	13.51±1.53	12.80±1.62	0.036*	12.36±0.92	11.98±0.87	0.212	13.65±1.66	13.25±1.14	0.512	14.69±1.44	14.23±1.90	0.491
FW (cm)	13.35±0.95	13.64±0.96	13.22±0.93	0.032*	13.81±1.29	13.15±1.05	0.080	13.59±0.54	13.55±0.55	0.861	13.57±0.95	12.96±0.85	0.096
FI	98.13±14.70	99.77±15.46	97.34±14.37	0.433	90.25±11.53	91.74±16.80	0.684	100.64±13.67	98.04±10.45	0.610	109.16±16.84	110.29±16.80	0.865
NL (cm)	5.61±0.74	5.79±0.75	5.52±0.72	0.083	5.45±0.52	5.27±0.71	0.428	5.73±0.61	5.85±0.78	0.676	6.04±0.85	6.038±0.52	1.000
NW (cm)	3.98±0.46	4.11±0.40	3.92±0.48	0.050*	4.04±0.35	3.77±0.36	0.030*	4.15±0.58	4.20±0.26	0.788	4.11±0.55	4.11±0.55	1.000
NI	72.2±13.14	72.00±9.65	72.35±14.60	0.901	74.66±8.25	73.44±17.11	0.821	72.76±10.79	72.85±9.42	0.983	69.11±10.81	68.47±9.93	0.875
PD (cm)	2.12±0.51	2.11±0.46	2.13±0.53	0.887	1.88±0.44	1.91±0.37	0.821	2.412±0.64	2.05±0.44	0.129	2.36±0.42	2.42±0.53	0.746
CD (cm)	5.38±0.63	5.45±0.66	5.34±0.62	0.405	5.41±0.49	5.24±0.52	0.231	5.582±0.69	5.3±0.75	0.329	5.61±0.74	5.35±0.77	0.374

*Significant *P* value. FL: Face length, FW: Face width, FI: Facial index, NL: Nasal length, NW: Nasal width, NI: Nasal index, PD: Philtrum distance, CD: Commissural distance

Khasi and the Garo communities showed mesorrhine nose type, whereas the Jaintia community showed leptorrhine nose type. No statistically significant difference was noted in FI and NI between the male and female participants in the total sample population and the subpopulation groups. The minimum and maximum values of FL, FW, FI, NL, NW, and NI in our study population are depicted in Table 2.

The most common face type in our study was hyperleptoprosopic type constituting 52%. It was followed by mesoprosopic type (20%) and euryprosopic type (17%). Leptoprosopic and hypereuryprosopic types constituted only 8% and 3%, respectively.

The most common nose type in our study was leptorrhine type constituting 46%. It was followed by mesorrhine (44%). Platyrrhine, hyperplatyrrhine, and hyperleptorrhine types constituted only 7%, 2%, and 1%, respectively, in our study [Tables 3 and 4].

The distribution of various face types among the Jaintia, Garo, and Khasi communities is depicted in Figure 1. Among the Jaintia, the hyperleptoprosopic type was the most common constituting 73%. Among the Garo, the hyperleptoprosopic type was the most common and it constituted 63%. Among the Khasi, the hyperleptoprosopic type constituted 35% followed by mesoprosopic and euryprosopic types each constituting 27%.

The distribution of different nose types among the three communities is shown in Figure 2. Among the Jaintia, leptorrhine type was the most common type constituting 54%, and among Garo, it constituted 48% to be the common type. In contrast among the Khasi, the mesorrhine type was the most common constituting 51%. It was followed by leptorrhine type constituting 41% [Figures 1 and 2].

The comparison of various anthropometric variables in the ethnic adults of Meghalaya is depicted in Table 5. Between the Jaintia and the Garo communities, a statistically significant difference was noted in FL and FI. Between the Jaintia and Khasi communities, a statistically significant difference was noted in FL, FI, NL, NW, and PD. A statistically significant difference was noted in FL, FI, NL, NW, and PD between Garo and Khasi communities [Table 5].

Discussion

The scientific measurement of the composition, size, and proportion of the human body is anthropometry. It is a noninvasive method and nasofacial anthropometry specifically deals with the dimensions of the nose and face.[2] Nasofacial anthropometry is useful in the identification of an individual, forensic analysis, facial reconstruction, sleep-disordered breathing pathophysiology, nasofacial anomaly quantification, and correction.[2,12]

Table 2: Nasofacial anthropometry of the study population

Parameters	Total (*n*=104)		Jaintia (*N*=26)		Garo (*n*=27)		Khasi (*n*=51)	
	Male (*n*=34)	Female (*n*=70)	Male (*n*=13)	Female (*n*=13)	Male (*n*=10)	Female (*n*=17)	Male (*n*=11)	Female (*n*=40)
FL (cm) (minimum–maximum)	10.50–17.00	10.00–18.00	12.50–17.00	11.50–17.00	12.00–15.00	11.00–18.00	10.50–13.50	10.00–13.00
FW (cm) (minimum–maximum)	11.50–16.00	11.00–15.50	12.00–14.50	12.00–14.50	13.00–14.50	13.00–14.50	11.50–16.00	11.00–15.50
FI (minimum–maximum)	72.41–141.67	74.19–141.67	86.21–141.67	85.19–141.67	82.76–115.38	81.48–138.46	72.41–113.04	74.19–116.36
NL (cm) (minimum–maximum)	4.00–7.00	2.50–7.00	4.00–7.00	5.50–7.00	4.50–7.00	4.50–7.00	5.00–6.50	2.50–6.50
NW (cm) (minimum–maximum)	3.50–5.00	3.00–5.00	3.50–5.00	3.50–5.00	4.00–4.50	3.00–5.00	3.50–4.50	3.00–4.50
NI (minimum–maximum)	50.00–90.91	57.14–160.00	50.00–87.50	57.14–90.91	57.15–88.87	57.14–90.91	58.33–81.81	58.33–160.00

FL: Face length, FW: Face width, FI: Facial index, NL: Nasal length, NW: Nasal width, NI: Nasal index

The importance of nose and face shape beauty has been described from historical times in art, surgery, and anatomy.[10] Nasofacial anthropometry data have been described to be crucial in planning surgeries for cleft lip, nasal correction, and reconstructive septorhinoplasties. The data can be used as objective measures during such reconstructions and avoid vague dysmorphisms like long noses or widely placed eyes.[13] This highlights the need for large population-based measurements for wider application in the medical field.

Sushruta, the renowned ancient Indian surgeon, is widely regarded as the father of rhinoplasty. Given India's vast and diverse population, conducting studies focused exclusively on its demographic variations is imperative for advancing medical and anthropological research. The Indian nose when compared to the European nose is described as being shorter, wider, and less rotated.[14] Kadakia and Saman emphasized the importance of maintaining the unique dimensions of the Indian nose and face, noting that Indian patients prefer to preserve their ethnic identity during facial reconstruction. Surgeons should consider these factors to ensure patient satisfaction and culturally appropriate outcomes.[14]

Correction of craniofacial anomalies in pediatric or adult populations requires achieving dimensions in the near-normal range.[15] This normal range can be derived through such anthropometry studies. The facial anthropometry varies from region to region and from population to population. The role of the same has been described in the evolution and identification of individuals and groups.[8,16] The nose shape is largely dependent on the ethnicity, which in turn is influenced by the habitat's climate. Wider noses are commonly seen in warm and humid places, whereas people in cold and dry places usually have narrow noses.[17] Recently, the importance of NL and NW as good predictors of gender differentiation, especially among the modern human population, has been described.[18] This was similar to our study, in which the NW can differentiate the gender among the study population.

The mean FI of the ethnic adults of the Meghalaya population in our study was of hyperleptoprosopic face type. This was in concordance with our research hypothesis. The subpopulation groups in our study also depicted similar findings. This was in contrast to other reported studies from Kerala and Andhra Pradesh from India, Nepal, Malaysia, and China.[2,6,8,19,20] Similar finding of hyperleptoprosopic face type was seen in a female study population from Iran.[10] Table 6 shows the comparison of the facial indices of various populations.

Although studies on cephalic indices and facial indices from different populations are present, on literature search when the article was prepared, not several regional studies are present on NI [Table 7].

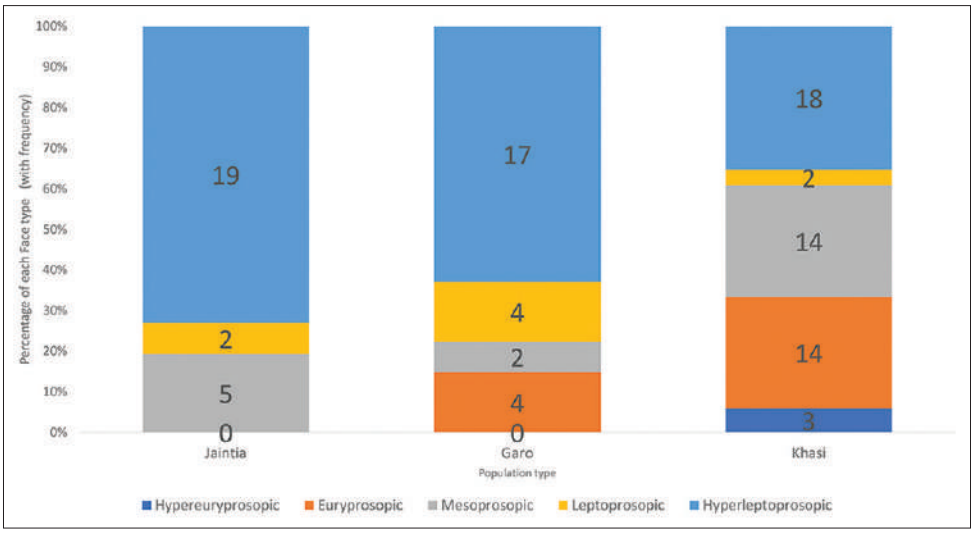

Figure 1: Face type distribution in subpopulation groups

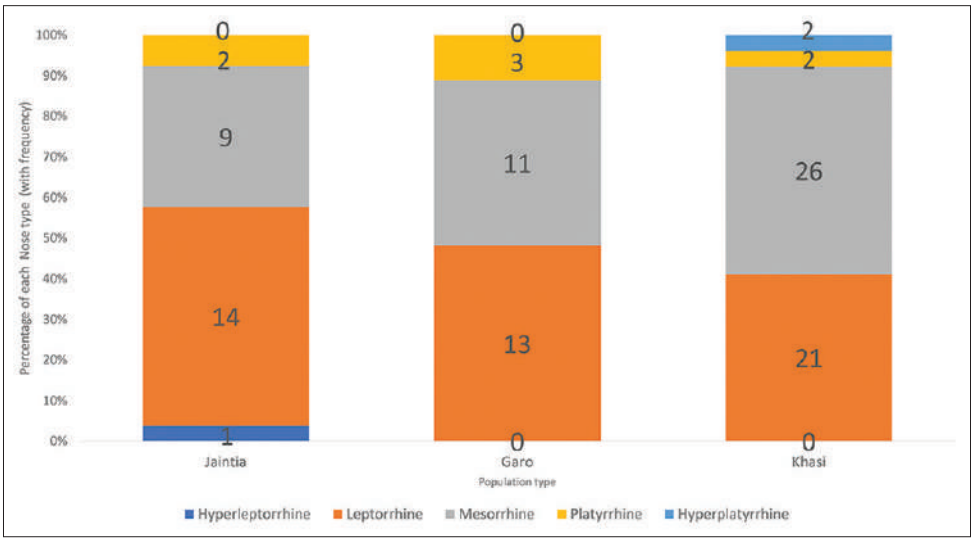

Figure 2: Nose type distribution in subpopulation groups

Table 3: Distribution of face types among the study population

Gender (*N*=104)	Face type, *n* (%)				
	Hypereuryprosopic (*n*=3; 3%)	Euryprosopic (*n*=18; 17%)	Mesoprosopic (*n*=21; 20%)	Leptoprosopic (*n*=8; 8%)	Hyperleptoprosopic (*n*=54; 52%)
Male (*n*=34; 33%)	1 (3)	4 (12)	7 (20)	3 (9)	19 (56)
Female (*n*=70; 67%)	2 (3)	14 (20)	14 (20)	5 (7)	35 (50)

Table 4: Distribution of nose types among the study population

Gender (*N*=104)	Nose type, *n* (%)				
	Hyperleptorrhine (*n*=1; 1%)	Leptorrhine (*n*=48; 46%)	Mesorrhine (*n*=46; 44%), *n* (%	Platyrrhine (*n*=7; 7%)	Hyperplatyrrhine (*n*=2; 2%)
Male (*n*=34; 33%)	1 (3)	12 (35)	19 (56)	2 (6)	0
Female (*n*=70; 67%)	0	36 (51)	27 (39)	5 (7)	2 (3)

Sinha *et al*. studied newborn babies of Sikkimese origin and found the FI to be 100.02 and 97.26, respectively, in the males and females.[3] This was similar to our study, but in contrast to other studies as mentioned in Table 6.

Table 5: Comparison of the Nasofacial anthropometric variables among the ethnic population of Meghalaya

Dependent variable	(I) tribe	(J) tribe	Mean difference (I−J)	SE	*P*
FL (cm)	1	2	0.96154*	0.35241	0.023#
	1	3	2.39683*	0.30906	0.000#
	2	3	1.43529*	0.30525	0.000#
FW (cm)	1	2	−0.30484	0.26370	0.751
	1	3	−0.02293	0.23127	1.000
	2	3	0.28192	0.22841	0.660
FI	1	2	10.04685*	3.50289	0.015#
	1	3	18.30784*	3.07206	0.000#
	2	3	8.26099*	3.03415	0.023#
NL (cm)	1	2	0.26068	0.18638	0.495
	1	3	0.72866*	0.16346	0.000#
	2	3	0.46797*	0.16144	0.014#
NW (cm)	1	2	−0.05128	0.12247	1.000
	1	3	0.28401*	0.10740	0.028#
	2	3	0.33529*	0.10608	0.006#
NI	1	2	−3.99715	3.60308	0.810
	1	3	−4.90742	3.15993	0.371
	2	3	−0.91027	3.12094	1.000
PD (cm)	1	2	0.11453	0.12859	1.000
	1	3	0.48446*	0.11278	0.000#
	2	3	0.36993*	0.11139	0.004#
CD (cm)	1	2	0.00299	0.17458	1.000
	1	3	0.20234	0.15311	0.568
	2	3	0.19935	0.15122	0.571

*Significant mean difference between ethnic communities, #Significant *p* value. 1: Jaintia, 2: Garo, 3: Khasi. FL: Face length, NI: Nasal index, NW: Nasal width, NL: Nasal length, FI: Facial index, FW: Face width, SE: Standard error, PD: Philtrum distance, CD: Commissural distance

The strength of the study is that there are no antecedent nasofacial anthropometry findings on the ethnic adults of Meghalaya. Our conventional noninvasive anthropometry measurement is by a widely available and commonly used tool without the radiation risk or need for expensive gadgets. The authors of the study believe that these data on nasofacial anthropometry can be used for future medical and anthropological use by adding to the pool of regional anthropometry data. The relatively small sample size is a limitation of the study. The authors hence recommend a large sample-sized study on our population to strengthen the results.

Conclusion

Hyperleptoprosopic type was the common face type and leptorrhine type was the common nose type in our study population. We believe that our study provides a comprehensive assessment of nasofacial anthropometry in the ethnic adults of Meghalaya, filling a crucial gap in existing research with insights into the facial and nasal characteristics among the Khasi, the Garo, and the Jaintia communities. The observed variations underscore the importance of population-based anthropometric standards, particularly in surgical interventions preserving ethnic traits and in forensic analysis. However, we recommend further studies with large sample-sized populations to further validate our results. In addition, longitudinal studies could provide insights into the developmental changes in nasofacial morphology among the Meghalaya population.

Acknowledgments

We acknowledge Dr. Bishwajeet Saikia, Department of Anatomy, and Dr. Prachurya Tamuli, post graduate trainee, Department of Otorhinolaryngology, for their support.

Table 6: Comparison of the facial index among various populations

Authors	Population (gender)	Mean FI (face type)	Common face type
Current study	Meghalaya, India (male/female)	99.77/97.34 (hyperleptoprosopic/hyperleptoprosopic)	Hyperleptoprosopic/Hyperleptoprosopic
Muralidhar *et al*. (2021)[6]	Kerala, India (mean value)	94.3 (leptoprosopic)	Leptoprosopic
Ranga and Mallika[20]	South Kerala, India (male/female)	80.13/80.53 (Euryprosopic/euryprosopic)	Leptoprosopic/euryprosopic
Rahimi Jaberi *et al*.[10]	Iran (male/female)	88.40/97.10 (Mesoprosopic/hyperleptoprosopic)	Mesoprosopic/hyperleptoprosopic
Pandeya and Atreya[8]	Nepal (male/female)	89.33/85.80 (Mesoprosopic/mesoprosopic)	Leptoprosopic/mesoprosopic
Kumari *et al*.[19]	Andhra Pradesh, India (male/female)	87.45/82.45 (Mesoprosopic/euryprosopic)	Mesoprosopic/euryprosopic
Wai *et al*. (2015)[2]	Malaysia (male/female)	87.04/90.59 (Mesoprosopic/leptoprosopic)	Leptoprosopic/leptoprosopic
Wai *et al*. (2015)[2]	China (male/female)	85.90/85.40 (Mesoprosopic/mesoprosopic)	Mesoprosopic/mesoprosopic

FI: Facial index

Table 7: Comparison of the Nasal index among various populations

Authors	Population (gender)	Mean NI (nasal type)	Common nose type
Current study	Meghalaya, India (male/female)	72.00/72.35 (Mesorrhine/mesorrhine)	Mesorrhine/leptorrhine
Rahimi Jaberi *et al*.[10]	Iran (male/female)	88.2/93.1 (Platyrrhine/platyrrhine)	Platyrrhine/platyrrhine
Mohammed *et al*.[11]	Northwest Nigeria (male/female)	74.08/69.9 (Mesorrhine/leptorrhine)	Mesorrhine/leptorrhine
Wai *et al*. (2015)[2]	Malaysia (male/female)	80.25/81.77 (Mesorrhine/mesorrhine)	Mesorrhine/mesorrhine
Jagadish *et al*.[15]	Karnataka, India (male/female)	65.39/65.23 (Leptorrhine/leptorrhine)	Leptorrhine/leptorrhine

NI: Nasal index

Financial support and sponsorship

Nil.

Conflicts of interest

There are no conflicts of interest.

References

1. Physical Status: The Use of and Interpretation of Anthropometry, Report of a WHO Expert Committee. Available from: https://www.who.int/publications-detail-redirect/9241208546. [Last accessed on 2023 Dec 24].
2. Wai MM, Thwin SS, Yesmin T, Ahmad A, Adnan AS, Hassan AA, *et al.* Nasofacial anthropometric study among university students of three races in Malaysia. Adv Anat 2015;2015:1-5.
3. Sinha P, Tamang BK, Chakraborty S. Craniofacial anthropometry in newborns of Sikkimese origin. J Laryngol Otol 2014;128:527-30.
4. Chatdokmaiprai C, Kiranantawat K, Lertsithichai P, Taeshineetanakul P. Normative data of the interorbital distance in Thai population. J Craniofac Surg 2018;29:1939-44.
5. Political Map of India. Available from: https://www.surveyofindia.gov.in/pages/political-map-of-india. [Last accessed on 2023 Dec 21].
6. Muralidhar NV, Ranjan A, Jayashankar Rao JS, Sreeshyla HS, Nitin P. Cephalic index, facial index and dental parameters: A correlative study to evaluate their significance in facial reconstruction. J Oral Maxillofac Pathol 2021;25:537-42.
7. Saha K, Bhowmik MK, Bhattacharjee D. Anthropometric measurement of North-East Indian faces for forensic face analysis. In: Muda AK, Choo YH, Abraham A, N. Srihari S, editors. Computational Intelligence in Digital Forensics: Forensic Investigation and Applications Studies in Computational Intelligence. Vol. 555. Cham: Springer International Publishing; 2014. p. 125-44. Available from: https://link.springer.com/10.1007/978-3-319-05885-6_7. [Last accessed on 2021 Oct 12].
8. Pandeya A, Atreya A. Variations in the facial dimensions and face types among the students of a medical college. J Nepal Med Assoc 2018;56:531-4.
9. Williams P, Bannister L, Berry M, Collins P, Dyson M, Dussek J, *et al.* Skeletal system. In: Gray's Anatomy. 38th ed. London: Elbs with Churchill Livingston; 1995. p. 607-12.
10. Rahimi Jaberi K, Kavakebian F, Mojaverrostami S, Najibi A, Safari M, Hassanzadeh G, *et al.* Nasofacial anthropometric study among students of shiraz university of medical sciences, Iran: A population based study. Indian J Otolaryngol Head Neck Surg 2019;71:206-11.
11. Mohammed I, Mokhtari T, Ijaz S, Akanji O, Abdullahi Ngaski A, Milanifard M. Anthropometric study of nasal index in Hausa ethnic population of Northwestern Nigeria. J Contemp Med Sci 2018;4:26-9.
12. Dubey A, Upadhyay S, Mathur S, Kant S, Singh BP, Makwana R. Comparative evaluation of craniofacial anthropometric measurements in Indian adult patients with and without obstructive sleep apnea: A pilot study. J Indian Prosthodont Soc 2015;15:331-6.
13. Doddi NM, Eccles R. The role of anthropometric measurements in nasal surgery and research: A systematic review. Clin Otolaryngol 2010;35:277-83.
14. Kadakia S, Saman M. Anatomic Considerations in Indian Rhinoplasty: Review of Anthropometric Studies. J Oto Rec Surg 2016;2:111.
15. Jagadish Chandra H, Ravi MS, Sharma SM, Rajendra Prasad B. Standards of facial esthetics: An anthropometric study. J Maxillofac Oral Surg 2012;11:384-9.
16. Khatun S. Cephalic index in indigenous tharu community. J Nepal Med Assoc 2018;56:825-9.
17. Dhulqarnain AO, Mokhtari T, Rastegar T, Mohammed I, Ijaz S, Hassanzadeh G. Comparison of nasal index between Northwestern Nigeria and Northern Iranian populations: An anthropometric study. J Maxillofac Oral Surg 2020;19:596-602.
18. Scendoni R, Kelmendi J, Arrais Ribeiro IL, Cingolani M, De Micco F, Cameriere R. Anthropometric analysis of orbital and nasal parameters for sexual dimorphism: New anatomical evidences in the field of personal identification through a retrospective observational study. PLoS One 2023;18:e0284219.
19. Kumari KL, Babu PV, Kumari PK, Nagamani M. A study of cephalic index and facial index in Visakhapatnam, Andhra Pradesh, India. Int J Res Med Sci 2015;3:656-8.
20. Ranga M, Mallika M. Cephalic index and facial index of adults in rural South Kerala, India. Int J Sci Study 2020;8:41-5.

Original Article

Ameliorative Effect of *Moringa oleifera* Leave on the Thickness of Articular Cartilage in Arthritic Rat Model

Abstract

Objective: The objective of this study was to determine the protective effect of *Moringa oleifera* on articular cartilage of formalin-induced arthritis in rats. **Study Design:** The study design was a lab-based experimental study. **Place and Duration of Study:** Department of Anatomy, Islamic International Medical College, Rawalpindi, from September 2020 to September 2021. **Methodology:** A total of 30 mature male albino rats, weighing between 250 and 300 g, were randomly assigned to three separate groups. The sample size for this study was 10. With the exception of animals belonging to Group A, all other animals were administered a subplanter injection of formaldehyde on their right paw on both day 1 and day 3 of the experiment. The rats in Group A and Group B were provided with a standardized diet for rats. During the course of the trial, rats in Group C were administered *Moringa* aqueous extract at a dosage of 500 mg/kg body weight via oral administration for a continuous period of 28 days. Following the conclusion of the experiment, all the animals underwent dissection. The right hind leg was subsequently extracted, processed, and stained using H and E and toluidine blue. This was done to facilitate microscopic assessment of the thickness of both uncalcified and calcified cartilage (CC). The data analysis was conducted using SPSS version 21. **Results:** The administration of *Moringa* aqueous extract through oral means resulted in a noteworthy increase in the thickness of uncalcified cartilage ($P < 0.001$ when comparing different groups). In addition, there was a decrease in the thickness of CC, with Group A measuring 9.26 ± 0.21 µm, Group B measuring 62.92 ± 0.21 µm, and Group C measuring 14.01 ± 0.21 µm ($P < 0.01$). **Conclusion:** *Moringa* leave extract is an effective antiarthritic agent in ameliorating the thickness of articular cartilage thickness in an arthritic rat model.

Keywords: *Articular cartilage, flavonoids, formaldehyde-induced arthritis, Moringa, osteoarthritis*

Ayesha Shahid, Shabana Ali[1], Huma Bennish[2], Tooba Khursheed[3], Maleeha Zafar, Tayyaba Qureshi[1], Numrah Safdar[4], Hassan Mumtaz[5]

Department of Anatomy, HITEC-IMS, Taxila, [1]Department of Anatomy, IIMC, [2]Department of Anatomy, NUST School of Health Sciences, [3]Department of Anatomy, Army Medical College, Rawalpindi, [4]AMR-IPC Program, N.I.H., [5]Department of Public Health, Association for Social Development, Islamabad, Pakistan

Introduction

Osteoarthritis (OA) is a prevalent rheumatic disease that is frequently observed in individuals of advanced age. The prevalence of this condition is 13% in females and 10% in males aged 60 years and older.[1] It is considered to be a leading cause of disability. The phenomenon typically has a positive correlation with age; but it can manifest in individuals of younger age groups as well. Based on a comprehensive analysis, it has been determined that hip and knee OA rank as the eleventh leading contributor to worldwide disability and the thirty-eighth highest in terms of disability-adjusted life years.[2]

The occurrence of OA is associated with the deterioration of cartilage and the remodeling of bone, which is mostly attributed to the active response of inflammatory cells and chondrocytes.[3] The gradual deterioration of articular cartilage results in the manifestation of joint discomfort and impaired joint function. The degradation of collagen and proteoglycans is caused by the release of enzymes from these cells, resulting in cartilage injury.[4] The loss of joint space is a common occurrence. The thickness of articular cartilage is notably reduced, particularly in the uncalcified region. Conversely, the thickness of calcified cartilage (CC) is augmented as a result of the process of calcification occurring at the tidemark. Changes in articular cartilage typically result in subsequent occurrences of subchondral bone sclerosis and the production of osteophytes.[5]

OA can be categorized into primary or idiopathic OA, as well as secondary OA resulting from factors such as trauma, infections, endocrine abnormalities, and

How to cite this article: Shahid A, Ali S, Bennish H, Khursheed T, Zafar M, Qureshi T, *et al.* Ameliorative effect of *Moringa oleifera* leave on the thickness of articular cartilage in arthritic rat model. J Anat Soc India 2025;74:176-81.

Article Info

Received: 26 August 2023
Revised: 16 July 2024
Accepted: 23 May 2025
Available online: 30 June 2025

Address for correspondence:
Dr. Hassan Mumtaz, Association for Social Development, Islamabad, Pakistan.
E-mail: Hassanmumtaz.dr@gmail.com

Access this article online

Website: https://journals.lww.com/joai
DOI: 10.4103/jasi.jasi_91_23

Quick Response Code:

congenital illnesses that disrupt the typical structure and function of articular cartilage. The primary risk variables encompass age, obesity, prior joint injuries, and mechanical factors.[6]

The global adoption and utilization of herbal medicines containing phytonutrients or nutraceuticals is experiencing rapid expansion. In contemporary times, a significant number of individuals are engaging in the consumption of these particular products as a means of managing a wide array of ailments inside various healthcare environments.[7] *Moringa oleifera* (MO), also referred to as the drumstick tree, belongs to the botanical family Moringaceae. The plant in question exhibits a wide distribution over numerous tropical and subtropical nations.[8] MO is considered to be a reliable and credible source for possible compounds that have the potential to improve health. The substance exhibits a diverse range of polyphenols, flavonoids, and antioxidants, which contribute to its notable osteoprotective characteristics.[9]

The existing body of literature has documented the presence of four distinct kinds of flavonoids inside the leaves of MO. The aforementioned compounds include quercetin, kaempferol, isorhamnetin, and apigenin. There is a scarcity of evidence pertaining to the occurrence of myricetin in MO. Flavonoids exhibit robust antioxidant properties, hence facilitating the donation of electrons or hydrogen atoms through metal chelation. The bioflavonoid known as Kaempferol has been observed to have a beneficial impact on OA by inhibiting inflammation in chondrocytes, avoiding apoptosis in osteoblasts, and inhibiting autophagy in osteoclasts while initiating autophagy in osteoblasts. The active treatment agent in OA functions by inhibiting pro-inflammatory mediators such as interleukin-6 (IL-6), IL-18, and IL-17.[10] The compound quercetin effectively hinders the process of programmed cell death, known as apoptosis, in chondrocytes. This inhibition is achieved by decreasing the caspase-3 pathway. In addition, quercetin creates a favorable microenvironment that supports the growth and multiplication of chondrocytes, hence facilitating the repair of cartilage. The intervention has demonstrated efficacy in alleviating joint pain and reducing inflammation often observed in individuals with OA. The intervention leads to an enhancement in muscular strength, hence resulting in improved joint mobility in those affected by OA. The aqueous extract of *Moringa* exhibited the ability to restore cartilage in a rat model with arthritis.[11]

In light of the advantageous impacts of MO, a recent research endeavor was initiated to examine the potential antiarthritic properties of MO leaves in improving the thickness of articular cartilage in a rat model of arthritis.

Methodology

The experiment conducted was laboratory-based, and a nonprobability consecutive sampling technique was employed to choose the sample. The present investigation was conducted at the Department of Anatomy, Islamic International Medical College Rawalpindi, in conjunction with the National Institute of Health (NIH), subsequent to obtaining consent from the Ethics Review Committee (Riphah/IRC/20/243), Islamic International Medical College. The study spanned from September 2020 to September 2021.

The research was conducted using a sample of 30 adult male rats of the Albino Sprague Dawley species, which served as a mammalian model for the investigation. The study comprised adult male rats that were 2 months old and weighed 300 g. Rats weighing <300 g and female rats were excluded from the investigation. The animal care and handling procedures adhered to the rules established by the Ethical Review Committee of the Islamic International Medical College in Rawalpindi.

The MO leaves were thoroughly rinsed with tap water in order to eliminate any potential contaminants and debris. The leaves were subjected to a washing process, followed by drying under shade. Subsequently, the dried leaves were finely ground using a grinder and then passed through a screen to obtain a powdered form. The aqueous extract of the plant was made in our laboratory by combining 100 g of powdered dry leaves with 1000 ml of boiling water and allowing the mixture to steep for a duration of 5 min. The mixture was passed through a sterile filter paper into a sterile tube. A freshly produced aqueous extract, comprising 100 mg of MO per milliliter, was used for each set of trials. Subsequently, the specimen was subjected to refrigeration at a temperature of 4°C for a duration of 6 days. The dried leaf powder of MO was acquired from a reputable local herbal medicinal store.[11]

The rats were housed in cages under the supervision of the Animal House of the NIH, located in Chak Shehzad, Islamabad. A total of 45 rats, each weighing around 300 g, were housed in a controlled environment at a standard temperature of 22°C ± 0.5°C within an air-conditioned room. Subsequently, the rats were transferred to sanitary stainless-steel cages that maintained a 12-h light and dark cycle, accompanied by a humidity level of 50%. The participants were provided with unlimited access to food and water for 7 days to facilitate acclimatization. Each group consisted of 10 male rats.

The experimental design consists of four groups: control Group A, negative control Group B, and two treatment Group C. Group A (referred to as the control group) and Group B (referred to as the negative control group) were administered a regular diet orally for a duration of 28 days. The rats in experimental group C were administered an oral dose of 500 mg/kg of aqueous extract of MO leaves, which was mixed in their diet for a duration of 28 days. Arthritis was produced in all the animals by administering 0.1 ml formaldehyde (2% v/v) into the left hind paw

through subplantar route on both day 1 and day 3 of the experiment, 1 h after oral administration of vehicle/drugs. The gross observation of the right hind paw was conducted on rats belonging to groups A, B, C, and D to document any alterations in joint diameter.

The diameter of the ankle joint was assessed at five-time points (0 days, 7th day, 14th day, 21st day, and 28th day) using Vernier calipers. Initially, the examiner palpated the osseous landmarks located on the medial and lateral aspects of the joint. The medial malleolus of the tibia and the lateral malleolus of the fibula were readily observed, after which the ankle joint was positioned between the two arms of the broader side of the Vernier Caliper.

After a period of 24 h after the last administration of the dose, the rat was subjected to anesthesia using cotton balls soaked in chloroform until it reached a state of unconsciousness, which was considered as the method of euthanasia.

The animals were positioned in a dorsal recumbent posture. The dissection was conducted using sterile equipment. The area of skin on the right hind leg below the knee joint was shaved, and afterward, the right hind limb was excised using a bone cutter in close proximity to the ankle joint. Then, the specimen underwent saline washing and was then preserved in a 10% formalin solution. The decalcification process involved immersing the bone in formic acid for a duration of 10 days. After the process of decalcification, the ankle joints were divided into the frontal plane, resulting in two roughly equivalent sections. The tissue samples were immersed in liquefied paraffin wax for embedding purposes. The blocks underwent sequential sectioning at approximately 200-ml intervals. The specimens were sliced into 5-mm-thick pieces using a microtome in order to facilitate histological examination.

Toluidine blue was used to stain the slide. The thickness of uncalcified cartilage (UCC) and CC was measured by observing all slides under a microscope at a magnification of ×40, using Image J software. A perpendicular line was delineated with respect to the joint surface, and three more lines were drawn in a parallel manner, with each line positioned on each side of the aforementioned perpendicular line.

The measurement for UCC involved assessing the distance from the cartilage surface to the tidemark. Similarly, the measurement for CC involved evaluating the distance from the tidemark to the cement line, which is situated between the subchondral bone and the CC. The thickness of each sample was determined and afterwards verified by doing four measurements for each sample. Data were collected from all the readings.

The data were inputted and analyzed using SPSS version 21, and the outcomes were presented as the mean ± standard deviation. The application of one-way analysis of variance was utilized to compare the means of thickness across the control, negative control, and treatment groups. The intergroup comparisons among groups were conducted using the *post hoc* Tukey's test. A $P \leq 0.05$ was deemed statistically significant.

Results

In the toluidine blue-stained segment of the ankle joint, the average thickness of UCC was measured to be 104um, 23.52um, and 84.67um in control Group A, negative control Group B, and treatment Group C, respectively. Group B had a reduction in cartilage thickness, but Group C demonstrated an increase in cartilage thickness, as shown in Figure 1. Upon doing a comparison of the mean values between Group B and Group C, it was seen that there exists a statistically significant difference in the means, as shown by a $P < 0.01$. A notable distinction was seen between Group A and Groups B and C [Table 1 and Figures 2 and 4].

The average thickness of CC was measured to be 9.26 µm, 62.92 µm, and 14.01 µm in normal control A, negative control B, and treatment Group C, respectively, based on toluidine blue stained sections. The variable exhibited a

Table 1: Mean measurement of uncalcified cartilage thickness among control Group A, negative control Group B, and treatment group C of albino rats by *post hoc* Tukey test

Parameters	Group A, mean±SD	Group B, mean±SD	Group C, mean±SD	*P*
UCT	104.4±0.4	23.52±0.4	84.67±0.4	<0.01
Post-hoc analysis				
Intergroup comparison	B versus A, <0.01	B versus C, <0.01	C versus A, <0.01	

SD: Standard deviation, UCT: Uncalcified cartilage thickness

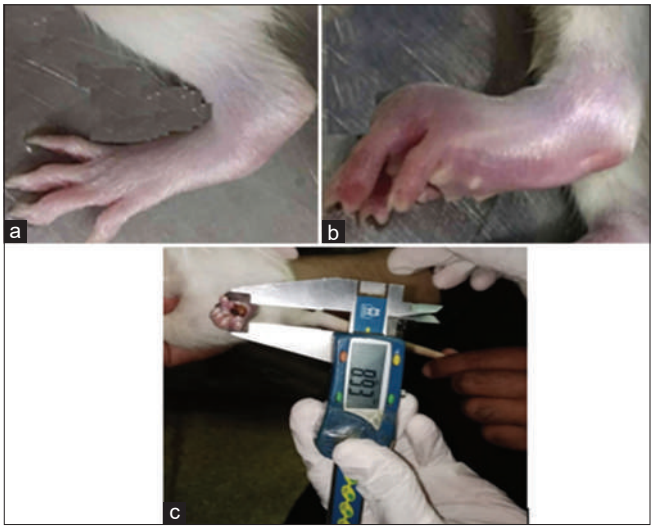

Figure 1: (a) Normal Paw, (b) Inflamed Paw, (c) Measurement of Joint Diameter by Vernier Caliber

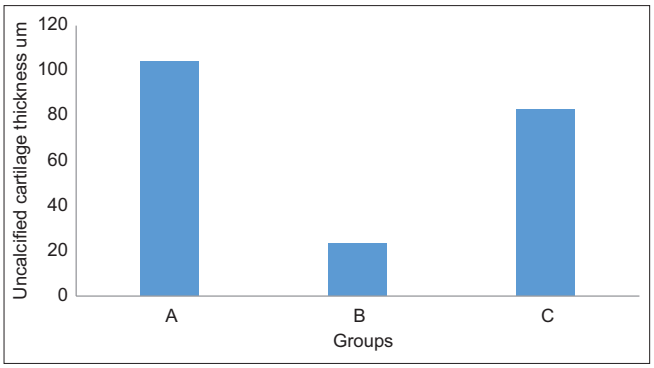

Figure 2: Bar chart showing mean thickness of uncalcified cartilage thickness in control Group A, negative control B, and treatment Group C

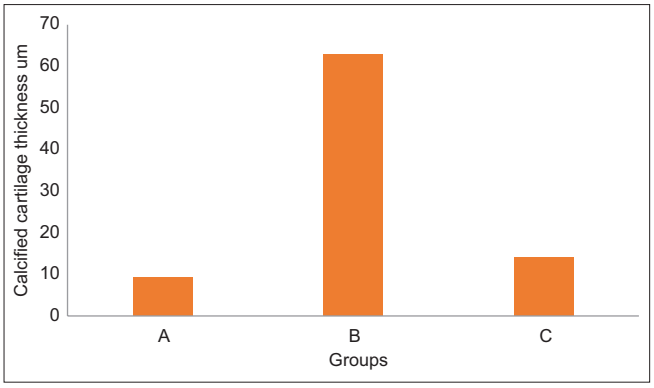

Figure 3: Bar chart showing mean thickness of uncalcified cartilage thickness in control Group A, negative control B, and treatment Group C

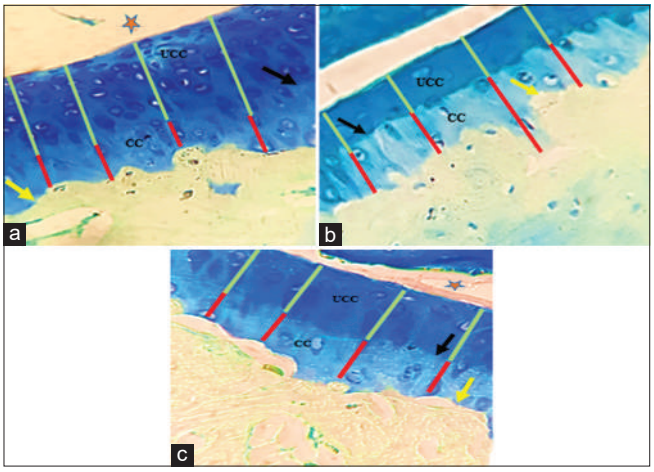

Figure 4: Photomicrograph of coronal section of ankle joint showing uncalcified cartilage (UCC) and calcified cartilage (CC) thickness in control A, negative control B, and treatment group C (toluidine blue stains at 40 × 10×). Straight red lines show CC thickness. Green lines show UCC thickness. Black arrow showed tidemark. Yellow arrow shows the cement line. Star reflected joint space, UCC: Uncalcified cartilage, CC: Calcified cartilage

rise in group B, but it demonstrated a drop-in Group C. Upon doing a comparison of the mean values between Group B and C, it was determined that there exists a significant mean difference, as shown by a $P < 0.01$. Upon comparing the mean values of Group C with the control Group A, it was determined that the mean difference was not statistically significant [Table 2 and Figures 3 and 5].

Table 2: Mean measurement of calcified cartilage thickness among control A, negative control B versus treatment Group C

Parameters	Group A, mean±SD	Group B, mean±SD	Group C, mean±SD	*P*
CCT	9.26±0.21	62.92±0.21	14.01±0.21	<0.01
Post-hoc analysis				
Intergroup comparison	B versus A, <0.01	B versus C, <0.01	C versus A, 0.16	

SD: Standard deviation, CCT: Calcified cartilage thickness

The animals exhibited an increase in joint diameter over the course of the observation period following the administration of a 0.1 ml dose of formaldehyde at a concentration of 2% v/v. The highest degree of joint swelling was noted on day 14, followed by a progressive reduction in swelling, with the exception of the negative control group. The experimental group that served as the negative control exhibited a statistically significant increase in joint diameter throughout the course of the 28-day period. The group that received MO treatment exhibited a reduction in joint swelling between day 14 and day 28. When comparing the mean values, it was seen that the group treated with Moringa had a substantial decrease in joint diameter compared to the group B. The diagram is seen in Figure 5.

Discussion

OA is a degenerative joint condition that commonly affects the joints of the lower limb. It impacts the flexibility of joints, resulting in the experience of pain during motions. The management of OA can be optimized through a comprehensive approach that encompasses lifestyle modifications, pharmacological interventions, and other therapeutic modalities, according to the severity of the condition.[12] The increasing popularity of herbal drugs for the safe and effective management of arthritis can be attributed to the major side effects and high cost associated with pharmaceutical therapy.[13,14]

The utilization of MO leaves has demonstrated effective outcomes in the treatment of various ailments, including diabetes, asthma, paralysis, OA, hypertension, diarrhea, infection, and ulceration. This substance is employed in numerous inflammatory disorders and expedites the wound-healing process.[15] *Mentha officinalis*, commonly known as MO, shares a common characteristic with various other herbal plants in that it possesses flavonoids. The aforementioned flavonoids exhibit potent properties in combating hyperlipidemia, aging, osteoporosis, and inflammation. The mechanism of action of MO involves the reduction of serotonin, histamine, and prostaglandin synthesis, hence exhibiting anti-inflammatory effects.[4,16]

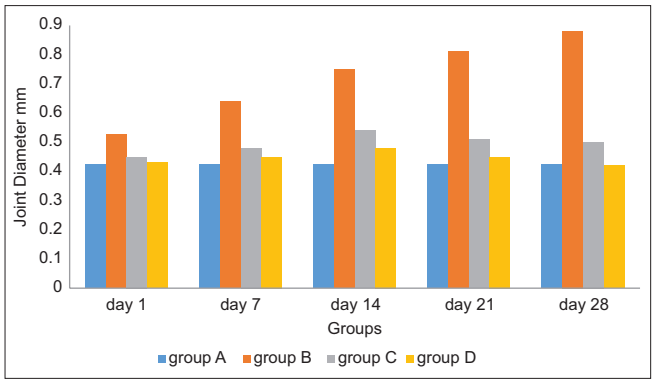

Figure 5: Bar chart showing the joint diameter of negative control and 13 treatment group on day 1, day 7, day 14, day 21 and day 28 of male rats n=10

The scavenging properties of the methanolic and ethanolic leaf extract are specifically directed against superoxyl and peroxyl radicals. The increasing recognition of the anti-inflammatory and antioxidant characteristics of MO has led to its growing reputation as an effective medication for treating arthritis.[17]

In the current investigation, it was observed that the administration of Moringa aqueous extract resulted in a considerable reduction in paw edema and ankle joint diameter in a rat model of arthritis produced by formaldehyde. This finding aligns with a study conducted by Nishat Fatima in 2016, which emphasized the reduction in joint diameter by the administration of *Moringa* extract for 10 days at a dosage of 500 mg/kg.[11] In 2017, Asha Jaja-Chimedza[18] conducted a study examining the impact of *Moringa* seed extract, administered at a dosage of 500 mg/kg, on the reduction of ankle joint diameter in a rat paw edema model produced by carrageenan.

The administration of formaldehyde through subplantar injection resulted in various pathological alterations in the articular cartilage of the ankle joint in rats. The analysis of toluidine-stained sections from the negative control group demonstrated a notable reduction in the thickness of UCC. In the present investigation, the oral administration of *Moringa* extract in Group C was found to considerably enhance the thickness of UCC, as demonstrated in Table 1 and Figure 2.

In a study conducted by Nishat Fatima and Syeda Jabeen Fatima in 2016, the researchers demonstrated the successful regeneration of cartilage in an arthritic rat model after 10 days.[11] In 2018, a study conducted by Amara Saleem shown that the administration of 600 mg/kg of orally administered *Moringa* extract for a duration of 10 days resulted in low inflammation and erosion of epithelial cells in the articular cartilage of arthritic rats.[3] There is a scarcity of data concerning the impact of *Moringa* leaf extract on the quantitative thickness of articular cartilage in an arthritic rat model.[17]

The analysis of sections stained with toluidine blue revealed a distinct boundary between articular cartilage and CC. The thickness of CC exhibited an increase in the negative control group in comparison to the control group, which can be attributed to the calcification process and the irregularity of the tidemark. In our investigation, the oral administration of *Moringa* extract resulted in a reduction in the thickness of the calcified zone. There is currently a lack of information pertaining to the potential antiarthritic effect of *Moringa* extract on micromorphological changes in CC thickness.[18] However, numerous research has demonstrated the anti-inflammatory capabilities of *Moringa* extract. In 2021, Thitiya Luetragoon observed that the utilization of *Moringa* extract resulted in a reduction of oral inflammation and gingivitis. Furthermore, the findings suggested that this extract shown promise in enhancing oral health among individuals who smoke, with noticeable improvements observed within a 4-week timeframe.[19]

In a study conducted by Youjin Kim in 2017, an extract derived from *Moringa* was employed to treat experimental colitis in rats. The findings of this study revealed a downregulation of inflammatory markers, indicating the potential anti-inflammatory properties of the extract.[20] One limitation of this study is the absence of biochemical analysis, such as the measurement of IL-6 and TNF alpha levels, which could have provided additional evidence supporting the antiarthritic efficacy of MO.

Conclusion

MO, was found effective antiarthritic agent in attenuating the thickness of cartilage in arthritic rat models. This study assessed the medicinal properties of MO leaves in an arthritic rat model. The results guide the use of this plant extract as a medicine for the treatment of inflammation associated with OA.

Acknowledgment

We are highly obliged to Riphah International University, Rawalpindi for providing us with immense help and opportunities for carrying out our research. We are also thankful to Dr. Hussain Ali, Scientific Officer, NIH, Islamabad for his immense help in animal handling and housing of animals. We thank Mr. Ijaz Lab technician in NIH, provision and establishing protocols of MDA assay kits.

Financial support and sponsorship

Nil.

Conflicts of interest

There are no conflicts of interest.

References

1. Velikova T, Shumnalieva R, Kalina Darina Kachakova TY, Ivanova-Todorova E, Kyurkchiev D, Monov S. 25-Oh Vitamin D3/D2 levels in osteoarthritis and rheumatoid arthritis patients. Ann Chronic Dis 2017;2:1-5.
2. Liu Q, Wang S, Lin J, Zhang Y. The burden for knee osteoarthritis among Chinese elderly: Estimates from a

nationally representative study. Osteoarthritis Cartilage 2018;26:1636-42.
3. Saleem A, Saleem M, Akhtar MF. Antioxidant, anti-inflammatory and antiarthritic potential of *Moringa oleifera* Lam: An ethnomedicinal plant of *Moringaceae* family. South African J Bot 2020;128:246-56.
4. Zhuang Z, Ye G, Huang B. Kaempferol alleviates the interleukin-1β-induced inflammation in rat osteoarthritis chondrocytes via suppression of NF-κB. Med Sci Monit 2017;23:3925-31.
5. Seidenstuecker M, Watrinet J, Bernstein A, Suedkamp NP, Latorre SH, Maks A, *et al*. Viscoelasticity and histology of the human cartilage in healthy and degenerated conditions of the knee. J Orthop Surg Res 2019;14:256.
6. Kwoh CK. Epidemiology of osteoarthritis. Epidemiol Aging 2012;26:523-36.
7. Szychlinska MA, Imbesi R, Castrogiovanni P, Guglielmino C, Ravalli S, Di Rosa M, *et al*. Assessment of Vitamin D supplementation on articular cartilage morphology in a young healthy sedentary rat model. Nutrients 2019;11:1260.
8. Wong SK, Chin KY, Ima-Nirwana S. The osteoprotective effects of kaempferol: The evidence from *in vivo* and *in vitro* studies. Drug Des Devel Ther 2019;13:3497-514.
9. Dhakar R, Pooniya B, Gupta M, Maurya S, Bairwa N, Sanwarmal V. *Moringa* : The herbal gold to combat malnutrition. Chronicles Young Sci 2011;2:119.
10. Maldini M, Maksoud SA, Natella F, Montoro P, Petretto GL, Foddai M, *et al*. '*Moringa oleifera*: Study of phenolics and glucosinolates by mass spectrometry'. J Mass Spectrom 2014;49:900-10.
11. Fatima N, Fatima SJ. Pharmacological screening for anti-arthritic activity of *Moringa oleifera*. Asian J Pharm Clin Res 2016;9:1-6.
12. Mendoza S, Noa M, Valle M, Mendoza N, Mas R. Effects of D-003 on formaldehyde-induced osteoarthritis in rats. Int J Pharm Sci Rev Res 2012;16:21-4.
13. Loeser RF, Kelley KL, Armstrong A, Collins JA, Diekman BO, Carlson CS. Deletion of JNK enhances senescence in joint tissues and increases the severity of age-related osteoarthritis in mice. Arthritis Rheumatol 2020;72:1679-88.
14. Jönsson T, Eek F, Dell'Isola A, Dahlberg LE, Ekvall Hansson E. The better management of patients with osteoarthritis program: Outcomes after evidence-based education and exercise delivered nationwide in Sweden. PLoS One 2019;14:e0222657.
15. Sujatha BK, Patel P. *Moringa oleifera* – Nature ' s Gold. Imp J Interdiscip Res 2017;3:1175-9.
16. Nasri H, Baradaran A, Shirzad H, Rafieian-Kopaei M. New concepts in nutraceuticals as alternative for pharmaceuticals. Int J Prev Med 2014;5:1487-99.
17. Tshabalala T, Ncube B, Madala NE, Nyakudya TT, Moyo HP, Sibanda M, *et al*. Scribbling the cat: A case of the "miracle" plant, *Moringa oleifera*. Plants 2019;8:1-23.
18. Evans LA, Pitsillides AA. Structural clues to articular calcified cartilage function: A descriptive review of this crucial interface tissue. J Anat 2022;241:875-95.
19. Wadee SA, Sarhat ER, Najim RS. Effect of *Moringa oleifera* extract on serum glucose and interleukin-1, interleukin-2 and tumor necrosis factor α in streptozotocin-induced diabetic rats effect of *Moringa oleifera* extract on serum glucose and interleukin-1, interleukin-2 and tumor necrosi. Tikrit Med J 2018;24:61-8.
20. Kim Y, Wu AG, Jaja-Chimedza A, Graf BL, Waterman C, Verzi MP, *et al*. Isothiocyanate-enriched *Moringa* seed extract alleviates ulcerative colitis symptoms in mice. PLoS One 2017;12:e0184709.

Review Article

Facial Nerve Injury and its Neurosurgical Reanimation

Abstract

The facial Paralysis, also known as a facial nerve palsy, is the inability to move muscles which control facial expressions, viz, blinking, smiling, etc. Facial nerve takes origin from the brainstem, passes through the pontomedullary cistern, the internal acoustic meatus, and the facial canal. It comes out of the skull through the stylomastoid foramen to supply the muscles of facial expression. The facial palsy is common and caused by various factors including stroke, tumor, infections or trauma. The surgical facial reanimation is needed when facial paralysis is chronic and no likelihood of spontaneous recovery. This is often done 12 months of paralysis after proper investigation. The purpose of facial reanimation is to restore the facial movements and symmetry in individuals with facial paralysis so that he/she can have a natural smile and facial expression.

Keywords: *Facial paralysis, surgical reanimation, facial nerve, facial expression, facial canal, brainstem*

Vishram Singh, Rashi Singh[1], Gaurav Singh[2]

Department of Anatomy, Kasturba Medical College, Mangalore, Manipal Academy of Higher Education, Manipal, Karnataka, [1]Department of Pediatric and Preventive Dentistry, Santosh Dental College and Hospital, NCR Delhi, [2]British Medical Journal, Noida, NCR Delhi, India

Introduction

The facial nerve is a 7th cranial nerve having large motor and small sensory roots. Both these roots arise from ventrolateral aspect of the brain stem at pontomedullary junction [Figure 1].[1]

The facial nerve is composed of approximately 10,000 nerve fibers, 7000 of which are myelinated and form motor roots which innervate the muscles of facial expression responsible for wide range of *facial expression* like smile, frowning, closing the eyes, anger , surprise, depression etc. hence the facial nerve is also called the Queen of the face.[2]

The remaining 3000 nerve fibers of the facial nerve are unmyelinated and from small sensory roots (also called nervus inter medius). The nervus intermedius contains two types of fibers:

a. Special sensory fibers to carry taste sensation from anterior 2/3rd of tongue and soft palate
b. Preganglionic parasympathetic motor fibers which provide the secretomotor fibers to the submandibular and sublingual salivary gland, responsible for the production of tears and saliva.

Course/ Segments and Branches

After arising from the ventrolateral of pontomedullar junction, along with 8th cranial nerve passes posteriorly through the subarachnoid space of the cerebello-pentine angle to enter the outer end of the internal acoustic meatus (IAM)/ internal auditor canal (IAC) with 2–8 mm diameter in the temporal bone. It is called the *cisternal segment* of the facial nerve and gives no branch.

At the outer end of IAM, the two components of the facial nerve join to form a single nerve. This part is called as *meatal segment*. It gives no branch thereafter the facial nerve as follows a devious course in the facial canal through the temporal bone. This part of the facial nerve is of great importance to the ENT surgeons [Figure 288 P362 Mc Gregor].

The course of the facial nerve in the facial canal is divided into the following 3 segments (a) Labyrinthine segment, (b) Tympanic segment, and (c) Mastoid segment.

The initial direction of the facial nerve in the facial canal is laterally and slightly forward covered by the superior surface of the petrous part of the temporal bone. In this part, it runs over the junction of the cochlea and vestibule of the bony labyrinth. When it reaches the medial wall of the middle ear, it presents an oval swelling on the nerve called the geniculate ganglion (facial ganglion). This is

How to cite this article: Singh V, Singh R, Singh G. Facial nerve injury and its neurosurgical reanimation. J Anat Soc India 2025;74:182-8.

Article Info

Received: 20 March 2025
Accepted: 20 May 2025
Available online: 30 June 2025

Address for correspondence:
Prof. Vishram Singh, B5/3 Hahnemann Enclave, Plot No. 40, Sector 6, Dwarka Phase – 2, New Delhi - 110 075, India.
E-mail: drvishramsingh@gmail.com

Access this article online

Website: https://journals.lww.com/joai
DOI: 10.4103/jasi.jasi_55_25
Quick Response Code:

called the *labyrinthine segment* of the facial canal. It is about 3–5 mm long and extends from the fundus of IAC to the end of the genicular fossa containing the geniculate ganglion. The geniculate ganglion gives off 3 branches: (a) A Greater petrosal nerve, (b) A small filament to a tympanic branch of the glossopharyngeal nerve to form a lesser petrosal nerve, and (c) a branch to sympathetic plexus around the middle meningeal artery to from external petrosal nerve [Figure 2].[3]

From genu onward, the facial nerve runs horizontally backward in the medial wall of the middle ear (tympanum) in a bony canal below the lateral semicircular canal and above the oval window to reach the posterior wall of the middle ear. Here, it is easily identifiable in the coronal section [Figure 3].

It is called the tympanic segment and is about 8–11 mm long. It gives no branches. As it enters the posterior wall of the middle ear above the bony pyramid, and takes a sharp turn downward (often called, as posterior genu of the facial nerve) and runs in the posterior wall of the middle ear. It is closely related to mastoid anturn and mastoid air cells posteriorly hence facial nerve is vulnerable to injury during surgical procedures in this area. Here, the nerve takes a slight lateral inclination to come near the tympanic membrane to enter the stylomastoid canal. This descending part of the facial nerve is called the *mastoid segment*. It is about 8–14 mm long and gives the following 3 branches:

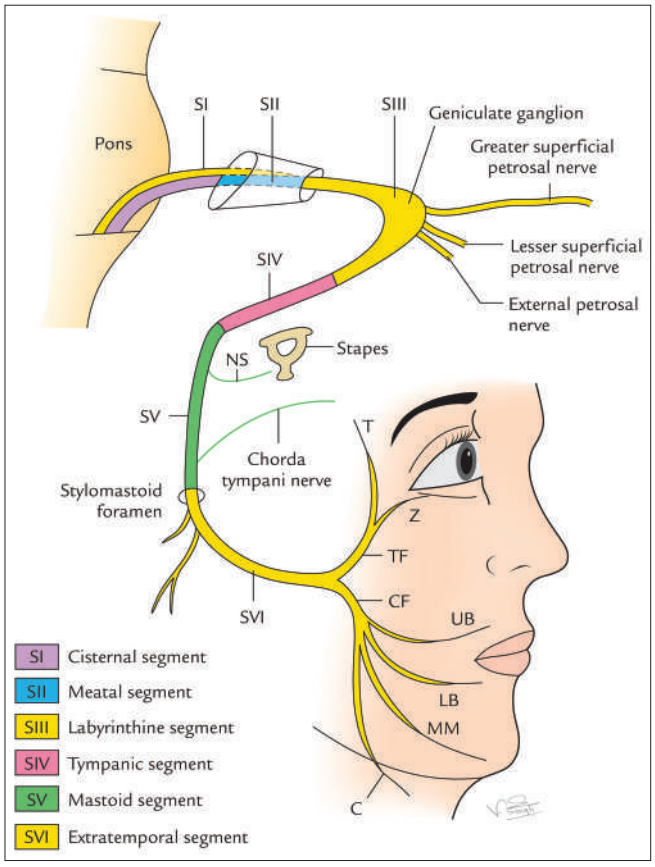

Figure 1: Course, segments and branches of facial nerve NS+ Nerve to stapedius

a. Nerve to stapedius muscle
b. Chorda tympani nerve
c. Sensory branch to auricular branch of vagus. It is given just below the origin of chorda tympani nerve.

The mastoid segment of the facial nerve comes out through the stylomastoid foramen at a point 2.5–4 and deep to the middle of the anterior border of the mastoid process and almost at once enters into the parotid gland. It is called the infratemporal segment of the facial nerve. The extratemporal segment extends from stylomastoid foramen to pes anserinus. The pes anserinus is the point where the facial nerve splits into temperofacial and cervicofacial trunks. It is about 15–20 mm long. Branches of the extratemporal segment segment of the facial nerve:

Before entering into the parotid gland. It gives the following branches

a. Posterior auricular nerve to supply occipitalis muscle
b. Nerve to stylohyoid a long thin twing to supply stylohyoid muscle
c. Nerve to the posterior belly of the digastric muscle.

In the parotid gland

In the parotid gland, the facial nerve lies superficial to the retromandibular vein (In Patey's faciovenous plane) and external carotid artery deep to their planes and soon divides into two divisions.

a. Temparofacial (TF) trunk runs sharply upward and divides into temporal (T) and Zygomatic (Z) branches to supply frontalis and orbicularis oculi, respectively
b. Cervicofacial (CF) trunk continues the course of the parent trunk downward and it gives off the following 3 or 4 branches;
    - Buccal branches: The upper buccal (UB) supply the muscles above the upper lip and the lower branch (LB) supplies the buccinator muscle and muscle below the lower lip
    - Manginal mandibular branch supplies muscles of the lower lip and chin. It runs below the angle of the mandible and ends in the area of the second premolar tooth. Injury of MMB of the facial nerve causes facial asymmetry

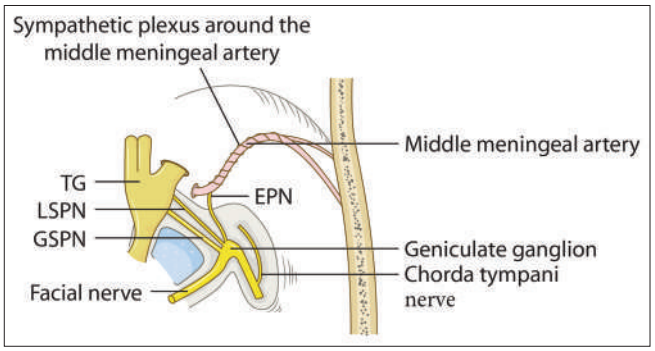

Figure 2: Course and connections of facial nerve in temporal bone. TG = Trigeminal ganglion, LSPN =Lesser superficial petrosal nerve, GSPN= Greater superficial petrosal nerve

- Cervical branch of the facial nerve extends into the upper part of the neck deep to the platysma which it supplies. It lies about 8 mm medial to the angle of the mandible.

The various segments of the facial nerve consisting of lower motor neurons (LMN) along with their location and length are given in Table 1.

Facial paralysis

In facial paralysis, there is inability to move the muscles of face due to facial nerve damage. This leads to loss of various facial expressions, viz. smile, happiness, surprise, contempt, sadness, fear, disgust, anger etc.

Causes of facial paralysis

These are:

- Bell's Palsy
- Fracture base of skull
- Middle ear infection
- Tumours
- Stroke
- Iatrogenic injuries etc.

Out of these causes only Bell's Palsy is discussed in detail as under.[4]

Bell's palsy:

It is most common cause of one sided facial nerve palsy accounting for about 70% cases. It is named after Charles Bell (1774-1842). The exact cause of Bell's palsy is not known, but it is thought to occur due to swelling of nerve in facial canal following an viral infection (Herpes Simplex). The common signs and symptoms are as follows [Figure 4]

- Loss of wrinkles on forehead
- Inability to close eye (Bell's phenomenon present)

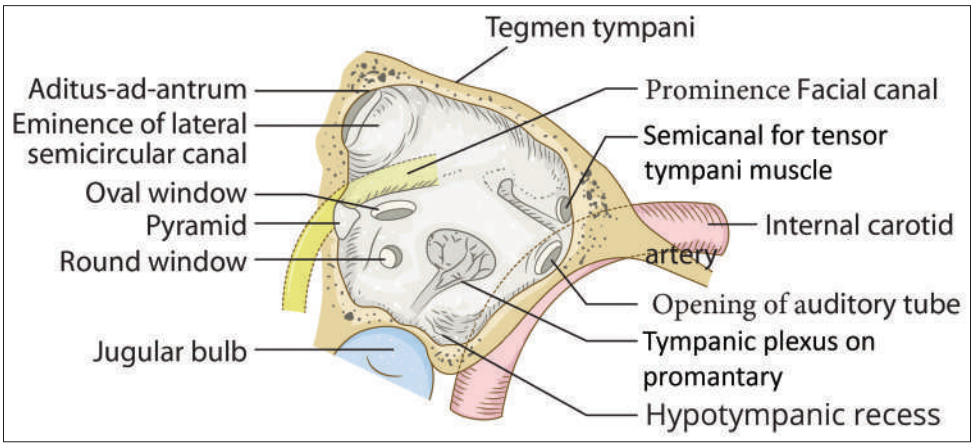

Figure 3: Tympanic cavity and facial canal seen from lateral side

Table 1: Showing segments, location and their branches of facial nerve

Segment	Location	Length (mm)	Branches
Cisternal segment	From brain stem to IAM	5–7	No branches
Meatal segment or canalicular segment	Part of facial nerve that runs through IAM	8	No branches
Labyrinthine segment	From fundus of IAC to distal end of genicular fossa containing geniculate ganglion	3–4	Greater superficial petrosal nerve
			Twing to Jacobson's nerve (external petrosal nerve)
			Twing to sympathetic plex around internal carotid artery
Tympanic segment	From geniculate ganglion to pyramidal eminence	8–11	No branches
Mastoid segment	From pyramidal eminence to stylomastoid foramen	10–14	Nerve to stapedius
			Chorda tympanic nerve
			Communicating branch to auricular branch of vague
Extratemporal segment	From stylomastoid foramen to pes anserinus	15–20	Temporal
			Zygomatic
			Buccal
			Marginal mandibular
			Cervical

IAC: Internal auditor canal, IAM: Internal acoustic meatus

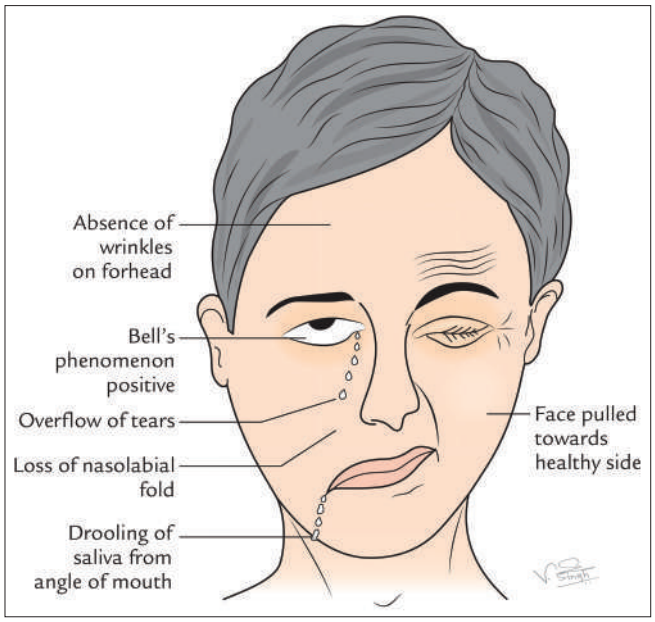

Figure 4: Showing signs and symptoms of Bell's palsy

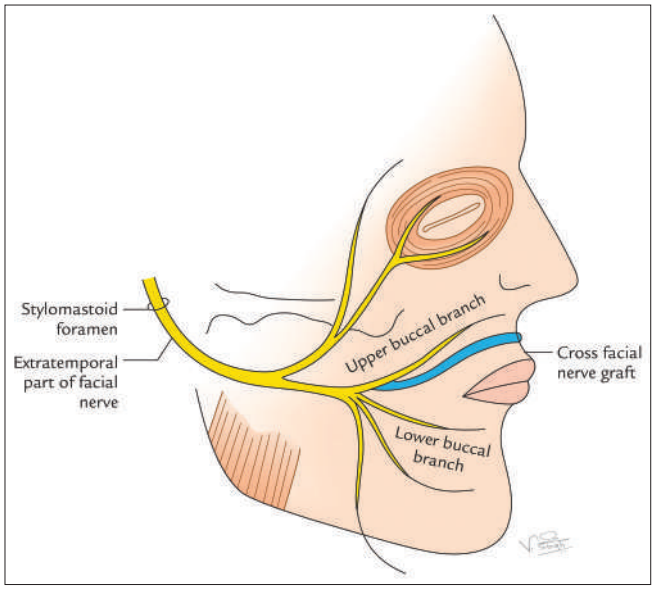

Figure 6: Cross facial nerve grafting

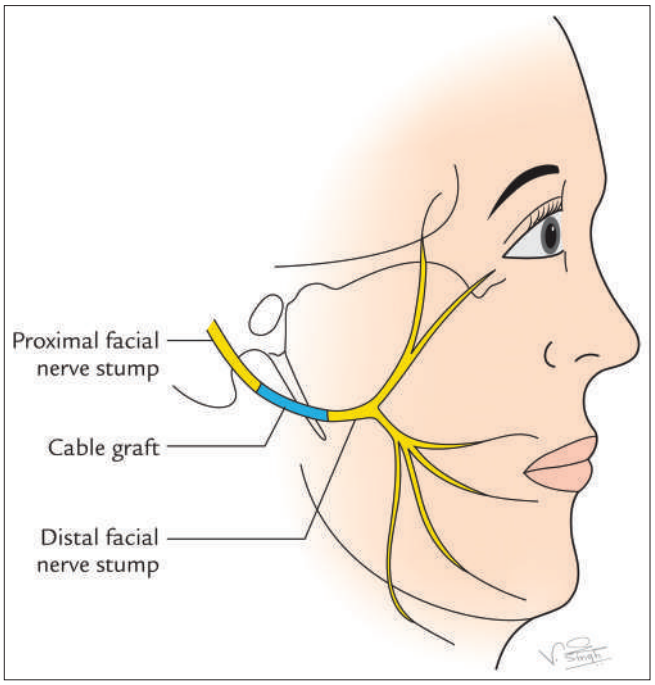

Figure 5: Cable graft

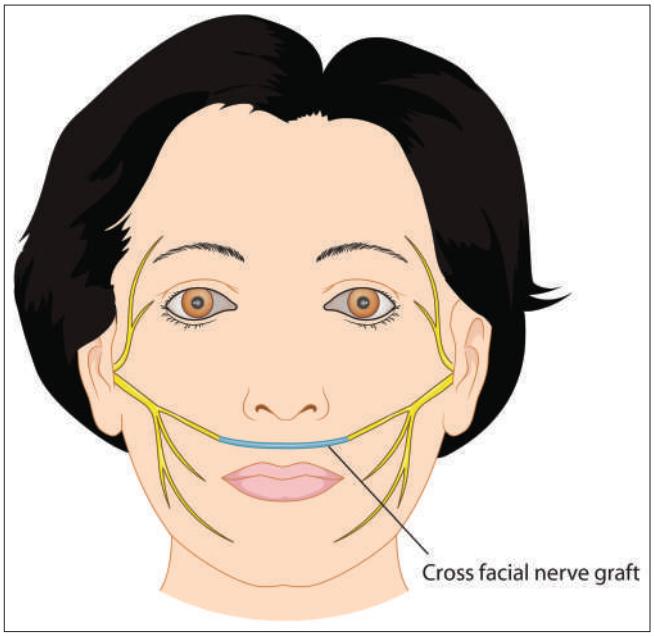

Figure 7: Cross facial nerve graft

- overflow of tears
- Loss of nasolabial fold
- Drooling of saliva
- Inability to laugh.

Some other symptoms other than the paralysis of muscles of face are also seen depending on site of lesions in facial canal as under[4]:

- *Lesion of translabyrinthine part:* will cause loss of lacrimation and disturbance in function of other branches
- *Lesion in the tympanic part* will cause tinnitus (i.e. (Hearing loss)
- *Lesion in the mastoid segment* will cause stapedial reflex leading to hyperacusis (i.e. hearing of loud sounds) and loss of taste sensations in the 2/3rd of the tongue due to involvement of chorda tympani nerve
- *Lesion in the extratemporal part* due to the involvement of pes anserinus and all terminal branches of facial nerve cause paralysis of only muscles of facial expression.

Surgical Reanimation of Facial Paralysis

Facial reanimation surgery is done in grade VI of facial palsy (Hous and Brachman's grading system of facial Palsy

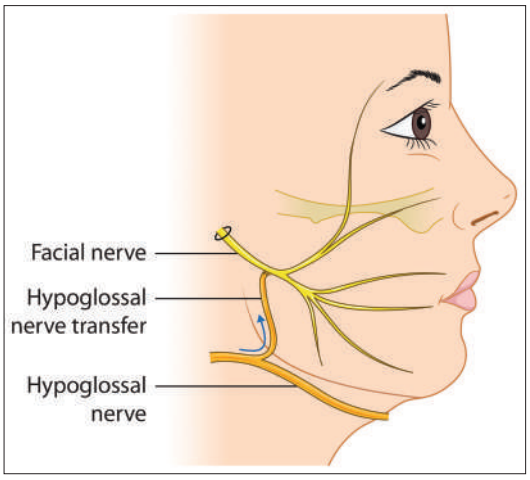

Figure 8: Hypogossal nerve transfer

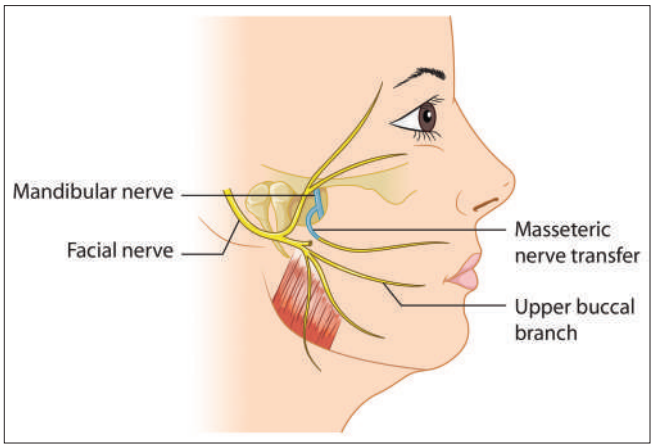

Figure 9: Masseteric nerve transfer

1985).[5] This grade stands for total paralysis, namely, loss of movements, loss of tone, contracture, and spasm of facial muscles. This surgery can help restore symmetry and functions to the face.

The various surgical procedures used to do this are:

a. Neurorrhaphy
b. Facial nerve decompression
c. Interposition nerve grafting, to overcome the gaps
d. Cross-facial nerve grafting (CFNG)
e. Nerve transfers
f. Muscle transposition.

a. *Neurorrhaphy* (End-to-end anastomosis of severed nerve):[6] It is a surgical produce by which two cut end to end of a severed nerve are brought together by end-to-end anastomosis. It is the treatment of choice for facial nerve injury. The functional outcomes are better if the nerve is repaired immediately after injury or within 72 h of injury before completion of Wallerian degeneration and the distance or gap between two cut ends shall be around 2.5 mm to 3.5 but not more than 5 mm for tension-free neurorrhaphy.

The neurorrahaphy is performed under an operating microscope. The sutures should be interrupted and knots should not be overtightend to displaced nerve fascicles.

There are different types of neurorrhaphy, including end-to-end, end-to-side, side-to-side, and laterolateral neurorrhaphy.

When is it should be used?

- When nerve segments can be approximated without tension
- When there is a viable proximal nerve stump
- When there is a small gap between the cut nerve ends.

How it is done?

- The epineurium of the separated nerve ends is sutured together
- Individual fascicles of groups of fascicle endings are sutured together
- The nerve may be stretched to make it more flexible.

N. B. Neurorrhaphy is preferred over nerve grafting.

b. *Facial nerve decompression*:[7] It is a surgical procedure to relieve pressure and reduce compression on the facial nerve by removing a bone that compressing it. It is a treatment option in Bell's palsy where we expect positive outcomes from medical treatment.
The most common site of facial nerve compression is the labyrinthine segment because it lies in the narrowest part of the facial canal with a diameter of <0.7 mm. This segment of nerve runs from the fundus of IAC to the geniculate ganglion.

The other less common sites of facial nerve compression are:

- Middle ear segment by epitympanic cholesteatoma
- At Stylomastoid foramen. It is the most common site of facial nerve compression in children.

In facial nerve decompression, a surgeon removes the bone or growth that is compressing the nerve. It takes about 15 days to recover.

c. *Interposition grafting (Cable graft)*:[8] If the gap between proximal and distal nerve stumps is too long to allow primary neurorrhaphy, an interposition graft or "cable" graft [Figure 5] is used to bridge the distances between two cut ends.

The sensory nerves commonly used for cable grafting are: sural nerve, great auricular nerve, and medial and lateral cuteneus nerves of forearm.

The size length and location of the great auricular nerve are a convenient source for facial nerve repair. Further, this nerve is about 7 cm long and has a diameter of about 1.5 mm.

d. Cross facial nerve graft (CFNG) [Figures 6 and 7]: It is a surgical procedure by which a neurosurgeon transfers nerve activity from the healthy side of the face to the

paralyzed side of the face to reanimate the paralyzed facial muscles.

In this procedure, a neurosurgeon usually harvests the sural nerve and uses it to connect the facial nerves of both sides.

This nerve graft acts as a conduit for nerve fibers of the healthy facial nerve to grow onto the opposite paralyzed side.

The CFNGs can restore spontaneous and natural facial animation and their ability to produce emotionally mediated movements.

The facial muscle movements usually return back 9–12 months after operation.

The above mechanism is based on the fact that there is a general rule in the human body, which dictates that the human body has a surplus ability to perform any given function. For example, we have two lungs, two kidneys, two ovaries, two testes, etc., although one can survive with the functions of just one.

This protective phenomenon called functional reserve also exists in the facial nerve.

There are usually several branches of the facial nerve which can perform any given function such as closing the eyes, smiling, or pursing the lips.[9,10]

e. *Nerve transfers:* It is a surgical procedure, in which a healthy nerve is connected to the damaged facial nerve to restore, facial expression.

The nerve fibers from the donor nerve grow into the damaged facial nerve. As a result, facial muscles are activated allowing the patient to smile, close the lip, or move his/her face in different ways or as per wish.

The nerve transfers are usually done when the proximal facial nerve stump is unavailable, as when nerve injury occurs at the skull base or above.

Nerves which are commonly used for nerve transfer are the hypoglosed nerve and masseteric nerve. The other nerves which can be used for nerve transfer are: the great auricular nerve and spinal accessory nerves.[11]

a. *Hypoglossal nerve transfer [Figure 8]:* In general, the epineurium of hypoglosed nerve is incised and its fascicles are reflected superiorly. Similarly, an epineurial window is made in the facial nerve and 1/3rd to ½ of its fascicles are divided. Now, the fascicles of the hypoglossal nerve are sewen with those of the facial nerve by an end-to-end anastomosis. It is called jump graft.[12]
   - *Masseteric nerve transfer:* The masseteric nerve lies directly deep to the facial nerve, hence easily accessed by the same incision which is used for facial nerve exposure.
     The masseteric nerve is a branch of the anterior division of the mandibular nerve. It emerges at the upper border of the lateral pterygoid and passes laterally through the mandibular notch (sigmoid notch of mandible) to enter deep to the masseter muscle and supply it from its deeper aspect.[13]
     The masseteric nerve contains about 1500 axons which are hereby enough to maintain the tone of masseteric muscle. Hence, masseteric nerve transfer is not very effective. However, the anatomical location of the masseteric nerve makes it ideal for smile rehabilitation.[14]

f. Muscle transposition: It involves moving the healthy fascial muscles to areas affected by paralysis to restore movement and symmetry. It is usually done when nerve regeneration techniques are not feasible. The muscles commonly used for this purpose are temporalis or masseter.

The nerve grafting or nerve transfers techniques are used to connect the transposed muscle to facial nerve or another nerve to restore function.

Sometimes a gracilis muscle from thigh is transferred to the face and innervated by a nerve.

They are commonly done to restore natural smile and facial expression.

Conclusion

Facial nerve injuries pose significant challenges due to their impact on both function and aesthetics. Timely diagnosis and appropriate surgical interventions, such as neurorrhaphy, nerve decompression, interposition grafting, or CFNG, can help restore facial movement and improve patient quality of life. Advances in nerve transfers and muscle transposition techniques have further enhanced the outcomes of facial reanimation procedures.

Looking ahead, continuous research in nerve regeneration and innovative treatment modalities, including bioengineering and neuromodulation, holds promise for further improvements in managing facial paralysis. A multidisciplinary approach combining neurosurgery, otolaryngology, plastic surgery, and rehabilitation remains essential for achieving optimal functional and esthetic results in affected patients.

Financial support and sponsorship

Nil.

Conflicts of interest

There are no conflicts of interest.

References

1. Singh V. Textbook of Clinical Neuroanatomy. 5th ed. New Delhi: Elsevier Pvt. Ltd.; 2004. p. 106-7.
2. Decker GA, Phesne du Plessis DJ. Lee McGregor's Synopsis of Surgical Anatomy. Mumbai: K.M. Verghese Co.; 1995. p. 263-368.

3. National Institute of Health. Available from: https://www.ncbi.nlm.nih.gov. [Last accessed on 2024 Dec 11].
4. Melvin TA, Limb CJ. Overview of facial paralysis: current concepts. Facial plastic surgery. 2008;24:155-63.
5. House JW, Brackmann DE. Facial nerve grading system. Otolaryngol Head Neck Surg 1985;93:146-7.
6. Saha S, Pal S, Sengupta M, Chowdhury K, Saha VP, Mondal L. Identification of facial nerve during parotidectomy: A combined anatomical and surgical study. Indian J Otolaryngol Head Neck Surg 2014;66:63-8.
7. George E, Richie MB, Glastonbury CM. Facial nerve palsy: Clinical practice and cognitive errors. Am J Med 2020;133:1039-44.
8. Spencer CR, Irving RM. Causes and management of facial nerve palsy. Br J Hosp Med (Lond) 2016;77:686-91.
9. Lee EI, Hurvitz KA, Evans GR, Wirth GA. Cross-facial nerve graft: Past and present. J Plast Reconstr Aesthet Surg 2008;61:250-6.
10. Jeong J, Almansoori AA, Park HS, Byun SH, Min SK, Choung HW, *et al.* Per-oral cross-facial sural nerve graft for facial reanimation. Maxillofac Plast Reconstr Surg 2018;40:22.
11. Renkonen S, Sayed F, Keski-Säntti H, Ylä-Kotola T, Bäck L, Suominen S, *et al.* Reconstruction of facial nerve after radical parotidectomy. Acta Otolaryngol 2015;135:1065-9.
12. Jandali D, Revenaugh PC. Facial reanimation: An update on nerve transfers in facial paralysis. Curr Opin Otolaryngol Head Neck Surg 2019;27:231-6.
13. Ryzenman JM, Pensak ML, Tew JM Jr. Facial paralysis and surgical rehabilitation: A quality of life analysis in a cohort of 1,595 patients after acoustic neuroma surgery. Otol Neurotol 2005;26:516-21.
14. Jandali D, Revenaugh PC. Facial reanimation: An update on nerve transfers in facial paralysis. Curr Opin Otolaryngol Head Neck Surg 2019;27:231-6.

The Editorial Process

A manuscript will be reviewed for possible publication with the understanding that it is being submitted to Journal of the Anatomical Society of India alone at that point in time and has not been published anywhere, simultaneously submitted, or already accepted for publication elsewhere. The journal expects that authors would authorize one of them to correspond with the Journal for all matters related to the manuscript. All manuscripts received are duly acknowledged. On submission, editors review all submitted manuscripts initially for suitability for formal review. Manuscripts with insufficient originality, serious scientific or technical flaws, or lack of a significant message are rejected before proceeding for formal peer-review. Manuscripts that are unlikely to be of interest to the Journal of the Anatomical Society of India readers are also liable to be rejected at this stage itself.

Manuscripts that are found suitable for publication in Journal of the Anatomical Society of India are sent to two or more expert reviewers. During submission, the contributor is requested to provide names of two or three qualified reviewers who have had experience in the subject of the submitted manuscript, but this is not mandatory. The reviewers should not be affiliated with the same institutes as the contributor/s. However, the selection of these reviewers is at the sole discretion of the editor. The journal follows a double-blind review process, wherein the reviewers and authors are unaware of each other's identity. Every manuscript is also assigned to a member of the editorial team, who based on the comments from the reviewers takes a final decision on the manuscript. The comments and suggestions (acceptance/ rejection/ amendments in manuscript) received from reviewers are conveyed to the corresponding author. If required, the author is requested to provide a point by point response to reviewers' comments and submit a revised version of the manuscript. This process is repeated till reviewers and editors are satisfied with the manuscript.

Manuscripts accepted for publication are copy edited for grammar, punctuation, print style, and format. Page proofs are sent to the corresponding author. The corresponding author is expected to return the corrected proofs within three days. It may not be possible to incorporate corrections received after that period. The whole process of submission of the manuscript to final decision and sending and receiving proofs is completed online. To achieve faster and greater dissemination of knowledge and information, the journal publishes articles online as 'Ahead of Print' immediately on acceptance.

Clinical trial registry

Journal of the Anatomical Society of India favors registration of clinical trials and is a signatory to the Statement on publishing clinical trials in Indian biomedical journals. Journal of the Anatomical Society of India would publish clinical trials that have been registered with a clinical trial registry that allows free online access to public. Registration in the following trial registers is acceptable: http://www.ctri.in/; http://www.actr.org.au/; http://www.clinicaltrials.gov/; http://isrctn.org/; http://www.trialregister.nl/trialreg/index.asp; and http://www.umin.ac.jp/ctr. This is applicable to clinical trials that have begun enrollment of subjects in or after June 2008. Clinical trials that have commenced enrollment of subjects prior to June 2008 would be considered for publication in Journal of the Anatomical Society of India only if they have been registered retrospectively with clinical trial registry that allows unhindered online access to public without charging any fees.

Authorship Criteria

Authorship credit should be based only on substantial contributions to each of the three components mentioned below:

1. Concept and design of study or acquisition of data or analysis and interpretation of data;
2. Drafting the article or revising it critically for important intellectual content; and
3. Final approval of the version to be published.

Participation solely in the acquisition of funding or the collection of data does not justify authorship. General supervision of the research group is not sufficient for authorship. Each contributor should have participated sufficiently in the work to take public responsibility for appropriate portions of the content of the manuscript. The order of naming the contributors should be based on the relative contribution of the contributor towards the study and writing the manuscript. Once submitted the order cannot be changed without written consent of all the contributors. The journal prescribes a maximum number of authors for manuscripts depending upon the type of manuscript, its scope and number of institutions involved (vide infra). The authors should provide a justification, if the number of authors exceeds these limits.

Contribution Details

Contributors should provide a description of contributions made by each of them towards the manuscript. Description should be divided in following categories, as applicable: concept, design, definition of intellectual content, literature search, clinical studies, experimental studies, data acquisition, data analysis, statistical analysis, manuscript preparation, manuscript editing and manuscript review. Authors' contributions will be printed along with the article. One or more author should take responsibility for the integrity of the work as a whole from inception to published article and should be designated as 'guarantor'.

Conflicts of Interest/ Competing Interests

All authors of must disclose any and all conflicts of interest they may have with publication of the manuscript or an institution or product that is mentioned in the manuscript and/or is important to the outcome of the study presented. Authors should also disclose conflict of interest with products that compete with those mentioned in their manuscript.

Submission of Manuscripts

All manuscripts must be submitted on-line through the website https://review.jow.medknow.com/jasi. First time users will have to register at this site. Registration is free but mandatory. Registered authors can keep track of their articles after logging into the site using their user name and password.

- If you experience any problems, please contact the editorial office by e-mail at editor@jasi.org.in

The submitted manuscripts that are not as per the "Instructions to Authors" would be returned to the authors for technical correction, before they undergo editorial/ peer-review. Generally, the manuscript should be submitted in the form of two separate files:

[1] Title Page/First Page File/covering letter:

This file should provide

1. The type of manuscript (original article, case report, review article, Letter to editor, Images, etc.) title of the manuscript, running title, names of all authors/ contributors (with their highest academic degrees, designation and affiliations) and name(s) of department(s) and/ or institution(s) to which the work should be credited, . All information which can reveal your identity should be here. Use text/rtf/doc files. Do not zip the files.
2. The total number of pages, total number of photographs and word counts separately for abstract and for the text (excluding the references, tables and abstract), word counts for introduction + discussion in case of an original article;
3. Source(s) of support in the form of grants, equipment, drugs, or all of these;
4. Acknowledgement, if any. One or more statements should specify 1) contributions that need acknowledging but do not justify authorship, such as general support by a departmental chair; 2) acknowledgments of technical help; and 3) acknowledgments of financial and material support, which should specify the nature of the support. This should be included in the title page of the manuscript and not in the main article file.
5. If the manuscript was presented as part at a meeting, the organization, place, and exact date on which it was read. A full statement to the editor about all submissions and previous reports that might be regarded as redundant publication of the same or very similar work. Any such work should be referred to specifically, and referenced in the new paper. Copies of such material should be included with the submitted paper, to help the editor decide how to handle the matter.
6. Registration number in case of a clinical trial and where it is registered (name of the registry and its URL)
7. Conflicts of Interest of each author/ contributor. A statement of financial or other relationships that might lead to a conflict of interest, if that information is not included in the manuscript itself or in an authors' form
8. Criteria for inclusion in the authors'/ contributors' list
9. A statement that the manuscript has been read and approved by all the authors, that the requirements for authorship as stated earlier in this document have been met, and that each author believes that the manuscript represents honest work, if that information is not provided in another form (see below); and
10. The name, address, e-mail, and telephone number of the corresponding author, who is responsible for communicating with the other authors about revisions and final approval of the proofs, if that information is not included on the manuscript itself.

[2] Blinded Article file: The main text of the article, beginning from Abstract till References (including tables) should be in this file. The file must not contain any mention of the authors' names or initials or the institution at which the study was done or acknowledgements. Page headers/ running title can include the title but not the authors' names. Manuscripts not in compliance with the Journal's blinding policy will be returned to the corresponding author. Use rtf/doc files. Do not zip the files. **Limit the file size to 1 MB.** Do not incorporate images in the file. If file size is large, graphs can be submitted as images separately without incorporating them in the article file to reduce the size of the file. The pages should be numbered consecutively, beginning with the first page of the blinded article file.

[3] Images: Submit good quality color images. **Each image should be less than 2 MB in size.** Size of the image can be reduced by decreasing the actual height and width of the images (keep up to 1600 x 1200 pixels or 5-6 inches). Images can be submitted as jpeg files. Do not zip the files. Legends for the figures/images should be included at the end of the article file.

[4] The contributors' / copyright transfer form (template provided below) has to be submitted in original with the signatures of all the contributors within two weeks of submission via courier, fax or email as a scanned image. Print ready hard copies of the images (one set) or digital images should be sent to the journal office at the time of submitting revised manuscript. High resolution images (up to 5 MB each) can be sent by email.

Contributors' form / copyright transfer form can be submitted online from the authors' area on https://review.jow.medknow.com/jasi.

Preparation of Manuscripts

Manuscripts must be prepared in accordance with "Uniform requirements for Manuscripts submitted to Biomedical Journals" developed by the International Committee of Medical Journal Editors (October 2008). The uniform requirements and specific requirement of Journal of the Anatomical Society of India are summarized below. Before submitting a manuscript, contributors are requested to check for the latest instructions available. Instructions are also available from the website of the journal (www.jasi.org.in) and from the manuscript submission site https://review.jow.medknow.com/jasi.

Journal of the Anatomical Society of India accepts manuscripts written in American English.

Copies of any permission(s)

It is the responsibility of authors/ contributors to obtain permissions for reproducing any copyrighted material. A copy of the permission obtained must accompany the manuscript. Copies of any and all published articles or other manuscripts in preparation or submitted elsewhere that are related to the manuscript must also accompany the manuscript.

Types of Manuscripts

Original articles:

These include randomized controlled trials, intervention studies, studies of screening and diagnostic test, outcome studies, cost effectiveness analyses, case-control series, and surveys with high response rate. The text of original articles amounting to up to 3000 words (excluding Abstract, references and Tables) should be divided into sections with the headings Abstract, Key-words, Introduction, Material and Methods, Results, Discussion and Conclusion, References, Tables and Figure legends.

An abstract should be in a structured format under following heads: **Introduction, Material and Methods, Results,** and **Discussion and Conclusion.**

Introduction: State the purpose and summarize the rationale for the study or observation.

Material and Methods: It should include and describe the following aspects:

Ethics: When reporting studies on human beings, indicate whether the procedures followed were in accordance with the ethical standards of the responsible committee on human experimentation (institutional or regional) and with the Helsinki Declaration of 1975, as revised in 2000 (available at http://www.wma.net/e/policy/17-c_e.html). For prospective studies involving human participants, authors are expected to mention about approval of (regional/ national/ institutional or independent Ethics Committee or Review Board, obtaining informed consent from adult research participants and obtaining assent for children aged over 7 years participating in the trial. The age beyond which assent would be required could vary as per regional and/ or national guidelines. Ensure confidentiality of subjects by desisting from mentioning participants' names, initials or hospital numbers, especially in illustrative material. When reporting experiments on animals, indicate whether the institution's or a national research council's guide for, or any national law on the care and use of laboratory animals was followed. Evidence for approval by a local Ethics Committee (for both human as well as animal studies) must be supplied by the authors on demand. Animal experimental procedures should be as humane as possible and the details of anesthetics and analgesics used should be clearly stated. The ethical standards of experiments must be in accordance with the guidelines provided by the CPCSEA and World Medical Association Declaration of Helsinki on Ethical Principles for Medical Research Involving Humans for studies involving experimental animals and human beings, respectively). The journal will not consider any paper which is ethically unacceptable. A statement on ethics committee permission and ethical practices must be included in all research articles under the 'Materials and Methods' section.

Study design:

Selection and Description of Participants: Describe your selection of the observational or experimental participants (patients or laboratory animals, including controls) clearly, including eligibility and exclusion criteria and a description of the source population. *Technical information*: Identify the methods, apparatus (give the manufacturer›s name and address in parentheses), and procedures in sufficient detail to allow other workers to reproduce the results. Give references to established methods, including statistical methods (see below); provide references and brief descriptions for methods that have been published but are not well known; describe new or substantially modified methods, give reasons for using them, and evaluate their limitations. Identify precisely all drugs and chemicals used, including generic name(s), dose(s), and route(s) of administration.

Reports of randomized clinical trials should present information on all major study elements, including the protocol, assignment of interventions (methods of randomization, concealment of allocation to treatment groups), and the method of masking (blinding), based on the CONSORT Statement (http://www.consort-statement.org).

Reporting Guidelines for Specific Study Designs

Initiative	Type of Study	Source
CONSORT	Randomized controlled trials	http://www.consort-statement.org
STARD	Studies of diagnostic accuracy	http://www.consort-statement.org/stardstatement.htm
QUOROM	Systematic reviews and meta-analyses	http://www.consort- statement.org/Initiatives/MOOSE/moose.pdf statement.org/Initiatives/MOOSE/moose.pdf
STROBE	Observational studies in epidemiology	http://www.strobe-statement.org
MOOSE	Meta-analyses of observational studies in epidemiology	http://www.consort- statement.org/Initiatives/MOOSE/moose.pdf

Statistics: Whenever possible quantify findings and present them with appropriate indicators of measurement error or uncertainty (such as confidence intervals). Authors should report losses to observation (such as, dropouts from a clinical trial). When data are summarized in the Results section, specify the statistical methods used to analyze them. Avoid non-technical uses of technical terms in statistics, such as 'random' (which implies a randomizing device), 'normal', 'significant', 'correlations', and 'sample'. Define statistical terms, abbreviations, and most symbols. Specify the computer software used. Use upper italics (*P* 0.048). For all *P* values include the exact value and not less than 0.05 or 0.001. Mean differences in continuous variables, proportions in categorical variables and relative risks including odds ratios and hazard ratios should be accompanied by their confidence intervals.

Results: Present your results in a logical sequence in the text, tables, and illustrations, giving the main or most important findings first. Do not repeat in the text all the data in the tables or illustrations; emphasize or summarize only important observations. Extra- or supplementary materials and technical detail can be placed in an appendix where it will be accessible but will not interrupt the flow of the text; alternatively, it can be published only in the electronic version of the journal.

When data are summarized in the Results section, give numeric results not only as derivatives (for example, percentages) but also as the absolute numbers from which the derivatives were calculated, and specify the statistical methods used to analyze them. Restrict tables and figures to those needed to explain the argument of the paper and to assess its support. Use graphs as an alternative to tables with many entries; do not duplicate data in graphs and tables. Where scientifically appropriate, analyses of the data by variables such as age and sex should be included.

Discussion: Include summary of *key findings* (primary outcome measures, secondary outcome measures, results as they relate to a prior hypothesis); *Strengths and limitations* of the study (study question, study design, data collection, analysis and interpretation); *Interpretation and implications* in the context of the totality of evidence (is there a systematic review to refer to, if not, could one be reasonably done here and now?, what this study adds to the available evidence, effects on patient care and health policy, possible mechanisms); *Controversies* raised by this study; and *Future research directions* (for this particular research collaboration, underlying mechanisms, clinical research).

Do not repeat in detail data or other material given in the Introduction or the Results section. In particular, contributors should avoid making statements on economic benefits and costs unless their manuscript includes economic data and analyses. Avoid claiming priority and alluding to work that has not been completed. New hypotheses may be stated if needed, however they should be clearly labeled as such. About 30 references can be included. These articles generally should not have more than six authors.

Review Articles:

These are comprehensive review articles on topics related to various fields of Anatomy. The entire manuscript should not exceed 7000 words with no more than 50 references and two authors. Following types of articles can be submitted under this category:

- Newer techniques of dissection and histology
- New methodology in Medical Education
- Review of a current concept

Please note that generally review articles are by invitation only. But unsolicited review articles will be considered for publication on merit basis.

Case reports:

New, interesting and rare cases can be reported. They should be unique, describing a great diagnostic or therapeutic challenge and providing a learning point for the readers. Cases with clinical significance or implications will be given priority. These communications could be of up to 1000 words (excluding Abstract and references) and should have the following headings: Abstract (unstructured), Key-words, Introduction, Case report, Discussion and Conclusion, Reference, Tables and Legends in that order.

The manuscript could be of up to 1000 words (excluding references and abstract) and could be supported with up to 10 references. Case Reports could be authored by up to four authors.

Letter to the Editor:

These should be short and decisive observations. They should preferably be related to articles previously published in the Journal or views expressed in the journal. They should not be preliminary observations that need a later

paper for validation. The letter could have up to 500 words and 5 references. It could be generally authored by not more than four authors.

Book Review: This consists of a critical appraisal of selected books on Anatomy. Potential authors or publishers may submit books, as well as a list of suggested reviewers, to the editorial office. The author/publisher has to pay INR 10,000 per book review.

Other:

Editorial, Guest Editorial, Commentary and Opinion are solicited by the editorial board.

References

References should be *numbered* consecutively in the order in which they are first mentioned in the text (not in alphabetic order). Identify references *in text*, tables, and legends by Arabic numerals in superscript with square bracket after the punctuation *marks. References cited only* in tables or figure legends should be numbered in accordance with the sequence established by the first identification in the text of the particular table or figure. Use the style of the examples below, which are based on the formats used by the NLM *in Index Medicus*. The titles of journals *should be abbreviated* according to the style used in Index Medicus. Use complete name of the journal for non-indexed journals. Avoid using abstracts as references. Information from manuscripts submitted but not accepted should be cited in the text as "unpublished observations" with written permission from the source. Avoid citing a "personal communication" unless it provides essential information not available from a public source, in which case the name of the person and date of communication should be cited in parentheses in the text. The commonly cited types of references are shown here, for other types of references such as newspaper items please refer to ICMJE Guidelines (http://www.icmje.org or http://www.nlm.nih.gov/bsd/uniform_requirements.html).

Articles in Journals

1. Standard journal article (for up to six authors): Parija S C, Ravinder PT, Shariff M. Detection of hydatid antigen in the fluid samples from hydatid cysts by co-agglutination. Trans. R.Soc. Trop. Med. Hyg.1996; 90:255–256.
2. Standard journal article (for more than six authors): List the first six contributors followed by *et al*.

Roddy P, Goiri J, Flevaud L, Palma PP, Morote S, Lima N. *et al*., Field Evaluation of a Rapid Immunochromatographic Assay for Detection of Trypanosoma cruzi Infection by Use of Whole Blood. J. Clin. Microbiol. 2008; 46: 2022-2027.

3. Volume with supplement: Otranto D, Capelli G, Genchi C: Changing distribution patterns of canine vector borne diseases in Italy: leishmaniosis vs. dirofilariosis. Parasites & Vectors 2009; Suppl 1:S2.

Books and Other Monographs

1. Personal author(s): Parija SC. Textbook of Medical Parasitology. 3rd ed. All India Publishers and Distributors. 2008.
2. Editor(s), compiler(s) as author: Garcia LS, Filarial Nematodes In: Garcia LS (editor) Diagnostic Medical Parasitology ASM press Washington DC 2007: pp 319-356.
3. Chapter in a book: Nesheim M C. Ascariasis and human nutrition. In Ascariasis and its prevention and control, D. W. T. Crompton, M. C. Nesbemi, and Z. S. Pawlowski (eds.). Taylor and Francis,London, U.K.1989, pp. 87–100.

Electronic Sources as reference

Journal article on the Internet: Parija SC, Khairnar K. Detection of excretory *Entamoeba histolytica* DNA in the urine, and detection of *E. histolytica* DNA and lectin antigen in the liver abscess pus for the diagnosis of amoebic liver abscess. *BMC Microbiology* 2007, **7**:41. doi:10.1186/1471-2180-7-41. http://www.biomedcentral.com/1471-2180/7/41

Tables

- Tables should be self-explanatory and should not duplicate textual material.
- Tables with more than 10 columns and 25 rows are not acceptable.
- Number tables, in Arabic numerals, consecutively in the order of their first citation in the text and supply a brief title for each.
- Place explanatory matter in footnotes, not in the heading.
- Explain in footnotes all non-standard abbreviations that are used in each table.
- Obtain permission for all fully borrowed, adapted, and modified tables and provide a credit line in the footnote.
- For footnotes use the following symbols, in this sequence: *, †, ‡, §, ‖,¶ , **, ††, ‡‡
- Tables with their legends should be provided at the end of the text after the references. The tables along with their number should be cited at the relevant place in the text

Illustrations (Figures)

- Upload the images in JPEG format. The file size should be within 1024 kb in size while uploading.
- Figures should be numbered consecutively according to the order in which they have been first cited in the text.
- Labels, numbers, and symbols should be clear and of uniform size. The lettering for figures should be large enough to be legible after reduction to fit the width of a printed column.
- Symbols, arrows, or letters used in photomicrographs

should contrast with the background and should be marked neatly with transfer type or by tissue overlay and not by pen.
- Titles and detailed explanations belong in the legends for illustrations not on the illustrations themselves.
- When graphs, scatter-grams or histograms are submitted the numerical data on which they are based should also be supplied.
- The photographs and figures should be trimmed to remove all the unwanted areas.
- If photographs of individuals are used, their pictures must be accompanied by written permission to use the photograph.
- If a figure has been published elsewhere, acknowledge the original source and submit written permission from the copyright holder to reproduce the material. A credit line should appear in the legend for such figures.
- Legends for illustrations: Type or print out legends (maximum 40 words, excluding the credit line) for illustrations using double spacing, with Arabic numerals corresponding to the illustrations. When symbols, arrows, numbers, or letters are used to identify parts of the illustrations, identify and explain each one in the legend. Explain the internal scale (magnification) and identify the method of staining in photomicrographs.
- Final figures for print production: Send sharp, glossy, un-mounted, color photographic prints, with height of 4 inches and width of 6 inches at the time of submitting the revised manuscript. Print outs of digital photographs are not acceptable. If digital images are the only source of images, ensure that the image has minimum resolution of 300 dpi or 1800 x 1600 pixels in TIFF format. Send the images on a CD. Each figure should have a label pasted (avoid use of liquid gum for pasting) on its back indicating the number of the figure, the running title, top of the figure and the legends of the figure. Do not write the contributor/s' name/s. Do not write on the back of figures, scratch, or mark them by using paper clips.
- The Journal reserves the right to crop, rotate, reduce, or enlarge the photographs to an acceptable size.

Protection of Patients' Rights to Privacy

Identifying information should not be published in written descriptions, photographs, sonograms, CT scans, etc., and pedigrees unless the information is essential for scientific purposes and the patient (or parent or guardian, wherever applicable) gives informed consent for publication. Authors should remove patients' names from figures unless they have obtained informed consent from the patients. The journal abides by ICMJE guidelines:

1. Authors, not the journals nor the publisher, need to obtain the patient consent form before the publication and have the form properly archived. The consent forms are not to be uploaded with the cover letter or sent through email to editorial or publisher offices.
2. If the manuscript contains patient images that preclude anonymity, or a description that has obvious indication to the identity of the patient, a statement about obtaining informed patient consent should be indicated in the manuscript.

Sending a revised manuscript

The revised version of the manuscript should be submitted online in a manner similar to that used for submission of the manuscript for the first time. However, there is no need to submit the "First Page" or "Covering Letter" file while submitting a revised version. When submitting a revised manuscript, contributors are requested to include, the 'referees' remarks along with point to point clarification at the beginning in the revised file itself. In addition, they are expected to mark the changes as underlined or colored text in the article.

Reprints and proofs

Journal provides no free printed reprints. Authors can purchase reprints, payment for which should be done at the time of submitting the proofs.

Publication schedule

The journal publishes articles on its website immediately on acceptance and follows a 'continuous publication' schedule. Articles are compiled in issues for 'print on demand' quarterly.

Copyrights

Checklist

Covering letter

- Signed by all contributors
- Previous publication / presentations mentioned
- Source of funding mentioned
- Conflicts of interest disclosed

Authors

- Last name and given name provided along with Middle name initials (where applicable)
- Author for correspondence, with e-mail address provided
- Number of contributors restricted as per the instructions
- Identity not revealed in paper except title page (e.g. name of the institute in Methods, citing previous study as 'our study', names on figure labels, name of institute in photographs, etc.)

Presentation and format

- Double spacing
- Margins 2.5 cm from all four sides
- Page numbers included at bottom
- Title page contains all the desired information
- Running title provided (not more than 50 characters)
- Abstract page contains the full title of the manuscript
- Abstract provided (structured abstract of 250 words for original articles, unstructured abstracts of about 150 words for all other manuscripts excluding letters to the Editor)
- Key words provided (three or more)
- Introduction of 75-100 words
- Headings in title case (not ALL CAPITALS)
- The references cited in the text should be after punctuation marks, in superscript with square bracket.
- References according to the journal's instructions, punctuation marks checked
- Send the article file without 'Track Changes'

Language and grammar

- Uniformly American English
- Write the full term for each abbreviation at its first use in the title, abstract, keywords and text separately unless it is a standard unit of measure. Numerals from 1 to 10 spelt out
- Numerals at the beginning of the sentence spelt out
- Check the manuscript for spelling, grammar and punctuation errors
- If a brand name is cited, supply the manufacturer's name and address (city and state/country).
- Species names should be in italics

Tables and figures

- No repetition of data in tables and graphs and in text
- Actual numbers from which graphs drawn, provided
- Figures necessary and of good quality (colour)
- Table and figure numbers in Arabic letters (not Roman)
- Labels pasted on back of the photographs (no names written)
- Figure legends provided (not more than 40 words)
- Patients' privacy maintained (if not permission taken)
- Credit note for borrowed figures/tables provided
- Write the full term for each abbreviation used in the table as a footnote

Journal of
The Anatomical Society of India

Salient Features:

- Publishes research articles related to all aspects of Anatomy and Allied medical/surgical sciences.
- Pre-Publication Peer Review and Post-Publication Peer Review
- Online Manuscript Submission System
- Selection of articles on the basis of MRS system
- Eminent academicians across the globe as the Editorial board members
- Electronic Table of Contents alerts
- Available in both online and print form.

The journal is registered with the following abstracting partners:
Baidu Scholar, CNKI (China National Knowledge Infrastructure), EBSCO Publishing's Electronic Databases, Ex Libris – Primo Central, Google Scholar, Hinari, Infotrieve, Netherlands ISSN center, ProQuest, TdNet, Wanfang Data

The journal is indexed with, or included in, the following:
SCOPUS, Science Citation Index Expanded, IndMed, MedInd, Scimago Journal Ranking, Emerging Sources Citation Index.

Impact Factor® as reported in the 2024 Journal Citation Reports® (Clarivate Analytics, 2025): 0.2

Editorial Office:
Dr. Vishram Singh, Editor-in-Chief, JASI
B5/3 Hahnemann Enclave, Plot No. 40, Sector 6,
Dwarka Phase – 2, New Delhi - 110 075, India.
Email: editorjasi@gmail.com
(O) | Website: www.asiindia.in

The journal is owned and run by The Anatomical Society of India